
# Applications of Fluorescent Displacement-Based Sensors for Monitoring Time-Resolved Changes in Analyte Concentrations

by

**Mara Florea**

A thesis submitted in partial fulfillment
of the requirements for the degree of

**Doctor of Philosophy**
**in Chemistry**

Thesis Committee

**Prof. Dr. Werner M. Nau**
Jacobs University Bremen

**Prof. Dr. Thomas C. Nugent**
Jacobs University Bremen

**Dr. Andreas Hennig**
BAM Federal Institute for
Materials Research and Testing

Date of Defense: November, 3rd 2011

Jacobs University Bremen

School of Engineering and Science

*To my dear Mother (Mami)*

# TABLE OF CONTENTS

# ABSTRACT

The present doctoral thesis describes the development of novel fluorescence-based sensors for real-time monitoring of analyte concentration changes. Water-soluble macrocycles, such as cyclodextrins, calixarenes, cyclophanes, and cucurbiturils, and their ability to encapsulate biologically and environmentally relevant analytes, as well as fluorescent dyes are the basis of such sensing systems.

The first part of the thesis focuses on cucurbiturils, known as highly symmetric, rigid, pumpkin-shaped macrocycles with two carbonyl-lined portals and a hydrophobic cavity. Herein, the reversible encapsulation of neutral guests, such as volatile hydrocarbons by cucurbiturils has been investigated using a fluorescent indicator displacement approach. Measurements in salt-free aqueous solution have disclosed a surprisingly strong (binding constants up to $10^7$ $M^{-1}$) and highly selective binding towards the investigated hydrocarbons (differentiation of alkanes from alkenes, isoalkanes from *n*-alkanes, and *cis*- from *trans*-alkenes), contrasting the common conception of cucurbiturils as cation receptors.

The second part of the thesis relates to the area of enzyme assay design, which allows real-time monitoring of analyte changes during biochemical transformations. The first introduced assay exploits the use of anion-receptor macrocycles, for following ATP dephosphorylation *via* a fluorescence-based supramolecular tandem assay. The methodology has been also exploited to screen for activators of the model enzyme employed, potato apyrase, as well as to monitor the dephosphorylation of other nucleotides. The second assay, also performed in accordance with the supramolecular tandem strategy, enables a label-free, continuous monitoring of histone tail peptide methylation in homogeneous solution. The third project employs nuclear magnetic resonance spectroscopy for experimental testing of molecules with inhibitory potential against L-aspartate-α-decarboxylase, an enzyme known for its critical role in the growth of microorganisms, such as *Mycobacterium tuberculosis*.

# ACKNOWLEDGEMENTS

First of all, I would like to convey my gratitude and appreciation towards my academic supervisor, Prof. Dr. Werner Nau, whose scientific insights have always inspired and helped me, particularly in the most challenging moments of my research work. He taught me that giving up is never a solution, that hard work is always rewarding, and that working with people requires a lot of patience. I thank him for always having his office door open for me, regardless of his extremely full schedule. Above all, I thank him for standing by me in good and bad times during my studies and for being my constant support throughout the years.

I would like to express my gratitude towards former and present members of the Nau group for valuable knowledge, good mood, and making our laboratory a great place to be in. Among the people I closely worked with, I would like to mention Dr. Andreas Hennig, for his guidance and for introducing me to the area of enzyme assays, which became one of my most beloved research topics. I am very thankful to Ms. Alexandra I. Lazar, who synthesized the anchor dye, NAS-P, which was implemented for hydrocarbon sensing, Mr. Khaleel I. Assaf and Prof. Dieter Klapstein for computational calculations, and Ms. Lora Angelova for preliminary experiments involving phosphatases. I thank Dr. David M. Bailey, Dr. Maik Jacob, and Dipl.-Chem. Thomas Schwarzlose for help with matters outside the main project. I would like to acknowledge Ms. María José Gonzáles-Álvarez and Dr. Ana Rei for their contributions to the development of the supramolecular tandem assay for methyltransferases, as well as Prof. Albert Jeltsch and Dr. Srikanth Kudithipudi for providing us with the model enzyme, Dim-5 and help with conducting mass spectrometry experiments. I am thankful to Prof. Dr. Kunchithapadam Swaminathan and Ms. Reetu Sharma, who initiated the project for inhibitors screening against L-aspartate-α-decarboxylase.

I am thankful to Prof. Dr. Werner M. Nau, Prof. Dr. Thomas C. Nugent, and Dr. Andreas Hennig for being part of the examination committee and their effort and time dedicated to reviewing my thesis.

Financial help is gratefully acknowledged from the Fonds der Chemischen Industrie, which provided me not only with a PhD stipend, but also with a great opportunity to attend many scientific meetings and conferences worldwide, Jacobs University Bremen, for constant support along the years, and the Robert-Bosch foundation, as well as the GDCh for generous travel support.

Finally, I would like to particularly thank the most important three women in my life, who have constantly supported me with their love and inspired me with their strength: my mother, Otilia, and my two cousins, Oana and Carmen. I am thankful to Upakul for his support, optimism, and efforts to cheer me up even in stressful times, as well as to my dear friend Lisa for her patience and continuous motivation. I also would like to mention Mrs. Marie-Rose Clerc and Mrs. Maria Nincu for their help and faith they have had in me.

# LIST OF PUBLICATIONS

**1.** M. Florea, S. Kudithipudi, A. Rei, M. José Gonzáles-Álvarez, A. Jeltsch, W. M. Nau, "A Fluorescence-Based Supramolecular Tandem Assay for Monitoring Lysine Methyltransferase Activity in Homogeneous Solution", *Chem. Eur. J.* **2012**, *18*, in press.

**2.** M. Florea and W. M. Nau, "Strong Binding of Hydrocarbons to Cucurbituril Probed by Fluorescent Dye Displacement: A Supramolecular Gas-Sensing Ensemble", *Angew. Chem.* **2011**, *123*, 9510-9514; *Angew. Chem. Int. Ed.* **2011**, *50*, 9338-9342. (Featured in ChemViews Magazine)

**3.** W. M. Nau, M. Florea, K. I. Assaf, "Deep Inside Cucurbiturils: Physical Properties, Binding Preferences, and Volumes of their Inner Cavity", *Isr. J. Chem.* **2011**, *51*, 559-577.

**4.** M. Florea and W. M. Nau, "Implementation of Anion-Receptor Macrocycles in Supramolecular Tandem Assays for Enzymes Involving Nucleotides as Substrates, Products, and Cofactors", *Org. Biomol. Chem.* **2010**, *8*, 1033-1039.

**5.** W. M. Nau, M. Florea, H. Sahoo, H. Bakirci, A. Hennig, D. M. Bailey, "Nano-TRF und Tandem Assays für HTS und Multiparameteranalytik" in: "Multiparameteranalytik – Methoden, Applikationen, Perspektiven", K. Conrad, W. Lehmann, U. Sack, U. Schedler, Eds., Pabst Verlag, Lengerich, **2008**, 147-162.

**6.** H. Sahoo, A. Hennig, M. Florea, D. Roth, T. Enderle, W. M. Nau, "Single-Label Assays for Tyrosine Phosphorylation using Nanosecond Time-Resolved Fluorescence Detection", *J. Am. Chem. Soc.* **2007**, *129*, 15927-15934.

**7.** A. Hennig, M. Florea, D. Roth, T. Enderle, W. M. Nau, "Design of Peptide Substrates for Nanosecond Time-Resolved Fluorescence Assays of Proteases: 2,3-Diazabicyclo[2.2.2]oct-2-ene as a Noninvasive Fluorophore", *Anal. Biochem.* **2007**, *360*, 255-265.

## IN PREPARATION:

**8.** M. Florea, K. I. Assaf, D. Klapstein, W. M. Nau, "An Experimental and Computational Investigation of the Hydrophobic Effect Driving Host-Guest Complexation with Cucurbiturils", in preparation.

**9.** R. Sharma, M. Florea, W. M. Nau, K. Swaminathan, "An Exploratory Screening for Inhibitors Against *Mycobacterium tuberculosis* L-aspartate-α-decarboxylase", in preparation.

# PARTICIPATION IN SCIENTIFIC CONFERENCES

## ORAL CONTRIBUTIONS:

11/2011 Falling Walls – The International Conference on Future Breakthroughs in Science and Society, Berlin, Germany. Talk entitled: "Breaking the Wall of Sensing What We Need"

05/2011 MoLife Research Center Retreat, Seefeld, Germany. Talk entitled: "Supramolecular Tandem Enzyme Assays: Monitoring Enzymatic Activity Using Macrocycle-Encapsulated Fluorescent Dyes"

01/2011 NanoFun Center and Nanomol Graduate Retreat, Clausthal-Zellerfeld, Germany. Talk entitled: "Gas Sensing Made Supramolecular"

07/2009 1st International Conference on Cucurbiturils (ICCB), Pohang, Korea. Talk on "Selective Gas Binding with Cucurbit[6]uril"

## POSTER CONTRIBUTIONS:

06/2011 2nd International Conference on Cucurbiturils (ICCB), Cambridge, UK. M. Florea and W. M. Nau, "Strong Binding of Hydrocarbons to Cucurbiturils in Aqueous Solution Probed by Fluorescent Dye Displacement: A Supramolecular Gas-Sensing Ensemble"

09/2010 22. Lecture Conference on Photochemistry, Erlangen, Germany. M. Florea and W. M. Nau, "Supramolecular Cucurbituril-Fluorescent Dye Complexes for Selective Gas Sensing of Light Hydrocarbons"

08/2010 3rd EuCheMS Chemistry Congress, Nürnberg, Germany. M. Florea and W. M. Nau, "Supramolecular Cucurbituril-Fluorescent Dye

Complexes for Selective Gas Sensing of Light Hydrocarbons”

07/2010 XXIII IUPAC Symposium on Photochemistry, Ferrara, Italy. M. Florea and W. M. Nau, “Supramolecular Cucurbituril-Fluorescent Dye Complexes for Selective Gas Sensing of Light Hydrocarbons”

02/2010 Central European Conference on Photochemistry (CECP), Bad Hofgastein, Austria. M. Florea and W. M. Nau, “Supramolecular Cucurbituril-Fluorescent Dye Complexes for Selective Gas Sensing of Light Hydrocarbons”

08/2009 XXIV International Conference on Photochemistry, Toledo, Spain. M. Florea and W. M. Nau, “A Novel Fluorescence-Based Supramolecular Tandem Assay for Monitoring ATP Depletion by Potato Apyrase”

07/2009 10$^{th}$ International Conference on Calixarenes, Seoul, Korea. M. Florea and W. M. Nau, “Selective Gas Binding with Cucurbit[6]uril”

07/2009 1$^{st}$ International Conference on Cucurbiturils (ICCB), Pohang, Korea. M. Florea and W. M. Nau “Selective Gas Binding with Cucurbit[6]uril”

06/2009 IV International Symposium on Macrocyclic & Supramolecular Chemistry (ISMSC), Maastricht, the Netherlands. M. Florea and W. M. Nau, “A Novel Fluorescence-Based Supramolecular Tandem Assay for Monitoring ATP Depletion by Potato Apyrase”

10/2008 21. Vortragstagung der Fachgruppe Photochemie, Bielefeld, Germany. M. Florea and W. M. Nau, “A Novel Fluorescence-Based Supramolecular Tandem Assay for Monitoring ATP Depletion by Potato Apyrase”

08/2007 Calix2007, 9$^{th}$ International Conference on Calixarene Chemistry and the “Workshop on Cucurbit[n]uril Molecular Containers”, College

Park, MD, USA. M. Florea and W. M. Nau “Supramolecular Tandem Assays for ATP-Dependent Enzymes”

01/2007 Bremen Molecular and Marine Biology (BMMB) Meeting, Bremen, Germany. M. Florea, A. Hennig, W. M. Nau “Nanosecond Time-Resolved Fluorescent Protease and Phosphatase Assays”

# SUMMARY

The goal of this PhD thesis is the development of novel applications involving fluorescence-based sensors for real-time monitoring of analyte concentration changes. The work conducted is at the interphase between supramolecular and physical-organic chemistry. Throughout my studies, I have been involved in working with water-soluble macrocycles such as calixarenes, cyclodextrins, cyclophanes, and particularly cucurbiturils (introduced in Chapter 1). The interactions of these supramolecular hosts with fluorescent dyes have been investigated. While we have been interested in the characterization, design, and understanding of the properties belonging to these supramolecular assemblies, practical applications were also envisaged. To this end, inspired by the indicator displacement strategy, I was able to implement such host/dye reporter pairs as highly sensitive fluorescence-based sensors for the real-time detection of biologically and environmentally relevant analytes and their changes in concentration.

Chapter 2 focuses on the use of cucurbit[*n*]urils, CB*n*, and their potential for encapsulating, sensing, and selectively binding neutral guests, particularly volatile hydrocarbons. We believe that the study is of fundamental interest in order to understand the solvophobic forces for driving host-guest complexation. This aspect has been particularly intriguing given that CB*n* have always been perceived as cation-receptor macrocycles. The peculiar properties of the CB*n* inner cavity and the hydrophobic driving force governing their complexation with neutral guests have been explored (Section 2.1 and Appendix 5). In Section 2.2 an innovative fluorescence-based approach for sensitive detection of hydrocarbons relying on the indicator displacement strategy from CB*n* is described (Appendix 6). The sensitivity of the system allows measurements in salt-free aqueous solution, which disclosed a surprisingly strong and selective binding, surpassing those reported for other receptors. The fluorescence detection allowed for the first time a continuous monitoring of hydrocarbon encapsulation *via* displacement.

The projects described in Chapter 3 are focused on monitoring changes in concentrations of analytes during biochemical transformations, a second area of

interest that originated during my BSc and MSc studies (Appendix 1-3). During my PhD, I developed three different enzyme assays, out of which two were designed using the supramolecular tandem assay strategy.

First, I have developed a substrate-selective tandem assay for ATP-dependent enzymes. This project has been a continuation of my MSc studies and been finalized and published during my PhD time (Appendix 4). The study deals with following ATP consumption by dephosphorylation caused by an enzyme called potato apyrase. This particular assignment also allowed the implementation of anion-receptor macrocycles, namely an amino-derivative of γ-cyclodextrin and a cyclophane, into the tandem assay methodology. In addition to enzymatic conversion monitoring, the assay has been implemented for screening of activators and it was transferred to other nucleotides.

The second assay was designed for Dim-5 from *Neurospora crassa*. This is a histone lysine methyltransferase, which specifically trimethylates K9 of the histone H3 tail and which was provided to us as part of a collaboration with the Jeltsch research group at Jacobs University Bremen. Assays for this enzyme were previously restricted to the use of radioactive labels or more laborious techniques. By means of the developed product-selective tandem assay, its activity can be followed in a continuous and label-free fashion. Additionally, its functionality was also illustrated by performing inhibition studies, rendering it suitable for future screenings.

The third project focuses on the conversion of aspartic acid to β-alanine, which is carried out by L-aspartate-α-decarboxylase and which was part of a joint project with the National University of Singapore. The purpose of the study has been a systematic screening for inhibitors against L-aspartate-α-decarboxylase, which has a crucial role for the virulence and persistence of the bacterial agent causing tuberculosis, *Mycobacterium tuberculosis*. Unlike the previous two enzyme assays, the enzymatic transformation, namely the depletion of aspartic acid and concomitant formation of β-alanine was followed using nuclear magnetic resonance (NMR) spectroscopy. The inhibitory effect of several known as well as novel inhibitors identified *via* bioinformatics could be conveniently established by NMR studies.

# CHAPTER 1

## *– Introduction –*

## 1.1 SUPRAMOLECULAR CHEMISTRY

Today, we are privileged to witness a multitude of scientific and technological advancements. Nonetheless, scientists across the world still face many challenges for a complete understanding of matter, its properties, and behavior. In order to advance successfully in science, proper communication and interdisciplinarity are crucial criteria. The latter attribute has awoken my interest towards supramolecular chemistry, which I believe is one of the most dynamic areas in research with impact on analytical chemistry, biochemistry, nanotechnology, environmental and material sciences. In fact, two famous statements have highlighted this synergism. In 1959, when discussing the top-down approach Richard P. Feynman said the legendary sentence that "*there is plenty of room at the bottom*"; a few years later, Jean-Marie Lehn, when referring to the bottom-up approach replied: "*there is even more room at the top*".

Supramolecular chemistry emerged in the 1980's, following the pioneering work of Pedersen, Cram, and Lehn (Figure 1.1.1).[1-3] The Nobel Prize for the work within the supramolecular chemistry field in 1987 has tremendously fueled the area. In fact, in the editorial of this year's first issue of *Angewandte Chemie International Edition*, entitled "25 Years Full of Chemical Discovery", François Diderich pointed out that currently one third of all publications in the leading chemical journals deal with supramolecular systems.[4] By definition, supramolecular assemblies are held together by intermolecular interactions such as electrostatic and hydrophobic forces, hydrogen bonding, cation-π, charge-dipole interactions, or π-π stacking.[5] These noncovalent, reversible, and highly dynamic forces have been recognized and addressed when characterizing chemical and particularly biological systems, for instance DNA helix formation, antigen-antibody binding, or the highly specific recognition properties of enzymatic pockets as docking sites.

Much of the research in the field has been in fact stimulated by biological systems and numerous supramolecular systems have been explored in an effort to mimic nature's molecular recognition phenomena. A large variety of fascinating molecular receptors, or supramolecular hosts, have emerged, with unique inner-phase properties. Many host molecules were designed such that they are able to recognize substrates or guest molecules, by means of noncovalent forces, in order

to form discrete entities. Host-guest complexes are representations of prototypal supramolecular architectures, which after Pederson's metal ions encapsulation by crown ethers,[1] opened vast territories. Inclusion of smaller molecules into container compounds does not only afford fundamental insight into the intermolecular forces governing complexation, but also opens new horizons to a myriad of practical applications ranging from analyte sensing to drug delivery, and to the design of synthetic enzymes.


**Figure 1.1.1** Cover picture in *Angewandte Chemie International Edition* with the occasion of the special topical issue on Supramolecular Chemistry. The image illustrates an example of molecular self-organization based on the work of J.-M. Lehn, which is similar to the DNA helix formation. Double-helical complexes called helicates, form spontaneously from penta(bipyridine) ligands and $Cu^{+}$ ions in solution.

One specific area where principles of supramolecular chemistry have become popular is that of analyte sensing. Particularly, host-guest complexes involving chromogenic or fluorogenic guests incorporated into supramolecular structures, sensitive to external stimuli such as pH, metal ions, and particularly organic or biomolecular analytes, are of immediate relevance towards practical applications.[6-8] Traditionally, a functional chemosensor needs to contain a binding site for the analyte, which in biochemical applications is very often an

antibody, whereas in supramolecular chemistry this is frequently an acyclic synthetic receptor or a macrocycle. The presence and ideally the quantity of an analyte upon binding are usually detected *via* signal transduction obtained from the signaling unit, which may be, for example, a fluorophore or a radiotracer. Important to note is that while the signaling probe is the vehicle carrying the signal enabling the human eye to get a closer peak into the molecular world, the sensing process takes place at the receptor level; the properties of the latter, such as its sensitivity and selectivity, are essential for the formation of an ensemble with the analyte of interest.

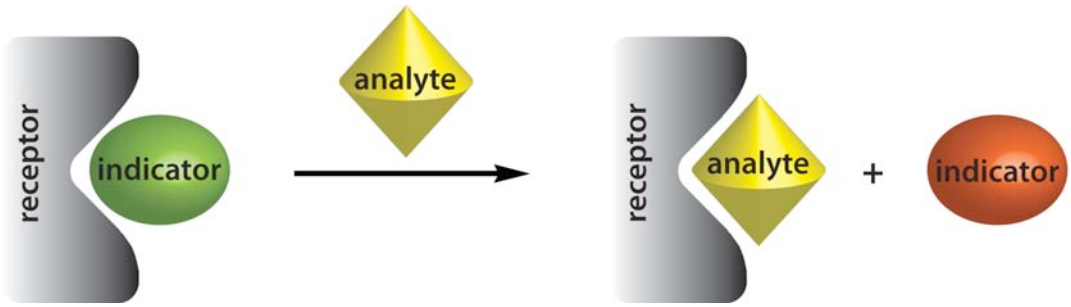


**Scheme 1.2.1** The indicator displacement assay principle.

## 1.2 INDICATOR DISPLACEMENT ASSAYS

Among the plethora of techniques developed for detection of analytes at certain concentrations, a novel and convenient approach has emerged in recent years known as *indicator displacement assay*. The main idea is based on a competition between the indicator and the analyte of interest for the binding site. Upon addition of the analyte, the indicator is being displaced from the binding pocket, causing a signal change, such as in color or fluorescence (Scheme 1.2.1). Early reports where the indicator displacement technique has been employed refer to the sensing of acetylcholine by a resorcinol-based calixarene,[9] and calix[*n*]arenes, in general.[10] The area of indicator displacement assays was soon after conceptualized by Anslyn,[7,11] and became a benchmark for sensor design due to aspects such as: *i*) a simplification of the system's architecture and synthesis, since it does not require covalent tethering of the signaling unit and the receptor; *ii*) it offers a large variety of options when choosing a receptor; *iii*) it allows the use of multiple indicators, even when in combination with one single

host; *iv*) the same receptor/indicator can be employed for the detection of several structurally related analytes; *v*) it is suitable to be used in homogeneous systems. In combination with recognition arrays, the indicator displacement method offers an incredible number of applications for sensing of various analytes, ranging from enantiomeric excess determination of amino acids,[12] to peptide recognition patterns,[13,14] to the detection of explosives,[15] and complex media ingredients.[16-18]

The basic signaling mechanism of indicator displacement assays has been, and still is, abundantly employed in biochemical antibody-based immunoassays. Here, the labeled antigen, which is meant to generate the transduction signal, is being competitively displaced by the untagged antigen-containing analyte. Radioactive and fluorescent labels are known to be the most sensitive ones for the design of such assays.[19-21] For instance, sensitive detection of insulin using radioimmunoassays revolutionized the field of endocrinology, which was acknowledged with the Nobel Prize in 1977.[22] Alternatively, immunoassays have also been developed using fluorescently labeled antigens.[19,23] Despite their extremely high sensitivity, immunoassays pose certain drawbacks, as they remain to be highly expensive; moreover, in order to achieve their well-known high specificity, antibodies need to be expressed for each and every analyte. They also require multiple steps, such as washing and separation, which makes them not only unsuitable for homogeneous measurements, but also less practical for industrial applications where large libraries of analytes need to be screened.

An abundant number of synthetic receptors have been designed and used in combination with fluorogenic and chromogenic probes, predominantly for molecular recognition of anionic analytes. Receptors from the Anslyn group are mainly based on a 1,3,5-trisubstituted-2,4,6-triethylbenzene scaffold incorporating guanidinium and boronic acid moieties as binding sites. A few examples from the large array of anionic species identified are citrate, commonly found in soft drinks,[16] tartrate,[17] an ingredient of grapes and wines, and gallate,[11] found in Scotch whiskies. Phosphates, for instance inositol-1,4,5-triphosphate,[11] or gluconic acid, which has been used for the detection of glucose oxidase activity, were detected in a similar manner.[18] A large variety of receptors incorporating metal ions have also been constructed,[11] particularly for the binding of negatively

charged amino acids, such as glutamate[24] and aspartate,[25] as well as carbonate.[26]

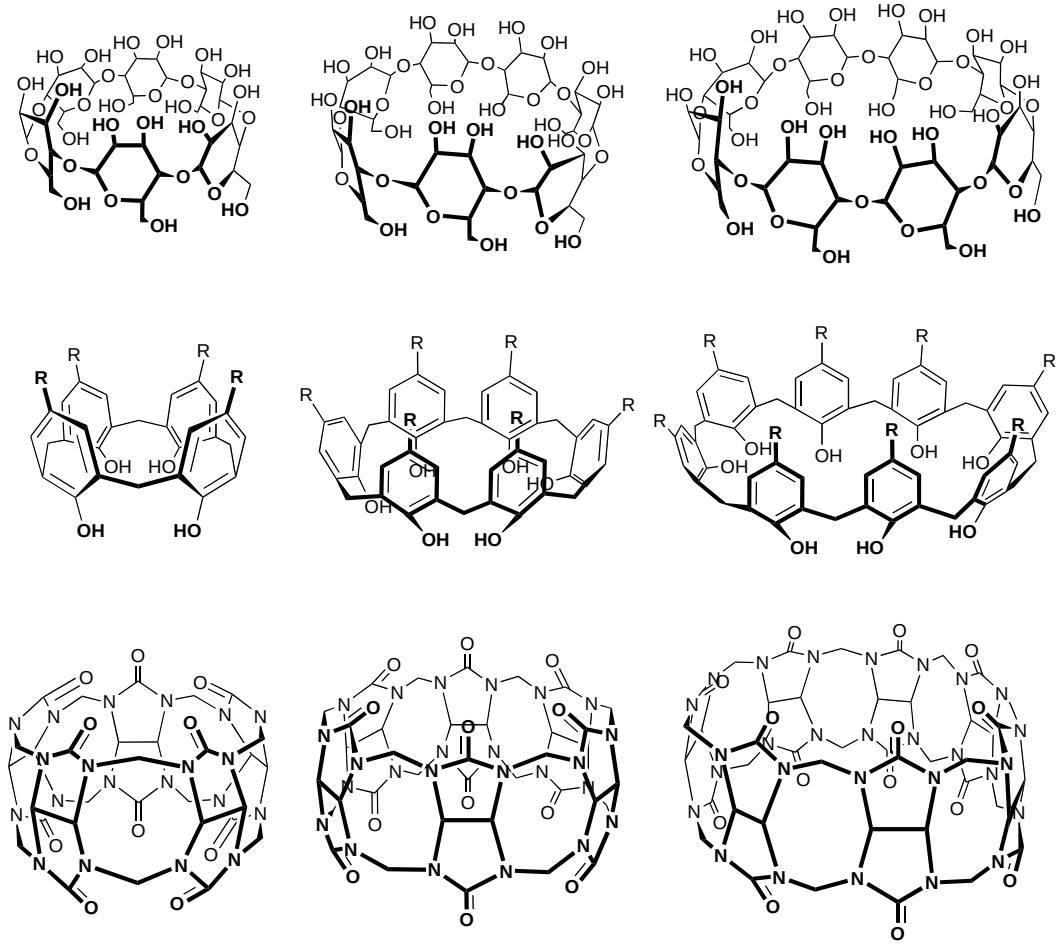

**Scheme 1.3.1** Water-soluble macrocyclic host molecules, from top to bottom and from left to right: cyclodextrins (α, β, γ), calix[*n*]arenes (*n* = 4, 6, 8, and R = $SO_3^-$, for the most common water-soluble ones), and cucurbit[*n*]urils (*n* = 5, 6, 7).

## 1.3 INDICATOR DISPLACEMENT ASSAYS WITH MACROCYCLIC RECEPTORS

Alternatively, the use of macrocycles for sensing applications has become very attractive due to the ability of these host molecules to form supramolecular complexes with smaller guest molecules, including fluorescent probes. Generally, macrocycles are cyclic oligomers with a well-defined size and shape. Since most of them possess an inner cavity, macrocycles are considered to be molecular containers of nanoscale dimensions.[27] Given the interest in environmentally and

biologically relevant sensing applications, an emphasis has been placed on water-soluble macrocycles. The most common ones in this context are cyclodextrins, calix[*n*]arenes, and cucurbit[*n*]urils (Scheme 1.3.1). These three classes of molecular containers have been part of the present work and their properties have been exploited in combination with fluorescent probes for the development of sensors able to monitor time-resolved changes of analyte concentrations.

Cyclodextrins (CDs) are naturally occurring host molecules, while cucurbit[*n*]urils (CB*n*) and calix[*n*]arenes (CX*n*) are synthetically obtained. Structurally, CDs are composed of glycopyranose blocks joined by acetal linkages and they are commonly available in three sizes (α-, β-, and γ-CD), corresponding to the number of α-D-glucose units they possess (6, 7, or 8, respectively). CB*n* macrocycles were initially discovered around 1900 by Behrend,[28] but they were structurally and mechanistically characterized only much later by Mock.[29] They are pumpkin-shaped, highly rigid macrocycles, obtained by acid-catalyzed condensation of glycoluril with formaldehyde and are nowadays available in different sizes (*n* = 5-8 and 10),[30-33] depending on the number of glycoluril units they contain. The volumes of their inner cavities range from 68 $Å^3$ for CB5 to 691 $Å^3$ for CB10,[34] allowing guests of different sizes to be encapsulated. The CB homologues, however, present striking differences regarding their aqueous solubility, with the even-numbered ones displaying a low water solubility.[35] CX*n* hosts are probably after CDs the most common class of macrocycles. In contrast to CDs and CB*n*, CX*n* are characterized as highly electron-rich species, incorporating aryl groups in their structure. Additionally, their structural flexibility allows them to adopt different conformations in solution, which, however, may be synthetically controlled by the appended groups on their rims.[36] CX*n* macrocycles are also commonly available in different sizes (e.g., CX4, CX5, CX6, with CX4 being the most common one) and the sulfonated ones introduced by Shinkai display a high water solubility.[37]

All three classes of macrocycles possess a hydrophobic cavity reminiscent of an enzymatic pocket, which combined with the aqueous solubility further highlights the enzyme-mimetic potential of water-soluble supramolecular hosts. Their hydrophobic interior allows them to include neutral guests or nonpolar organic residues via hydrophobic interactions. Additionally, the unique structural

differences of these macrocycles play a major role in their host-guest chemistry providing them with highly specific means of interaction, which result in very different complexation behaviors. Native and chemically modified CDs[38,39] are generally perceived as being able to encapsulate neutral or anionic guests. Their high water-solubility, wide availability, and inexpensive scale-up possibilities have made CDs the macrocycles of choice for industrial applications.[40-42] CX*n* with charged functional groups, such as sulfonato or trimethylammonium moieties, render them not only soluble in aqueous solution, but also practical for the binding of both cationic and anionic analytes.[43,44] Unlike CDs and CX*n*, which can be synthetically tailored for binding different classes of guests, functionalization of CB*n* has remained a challenge, with few exceptions.[45-47] Their inherent cation-receptor properties arise from the two carbonyl-laced portals, which establish natural docking sites for positively charged guests, either inorganic ones or ammonium-based organic ones.[35,48-51]

One of the most prominent photophysical alterations caused by the encapsulation of a dye by a macrocycle is its fluorescence intensity. The inclusion effects are generally attributed to one or a combination of the following factors: *i*) relocation of the fluorophore into the more hydrophobic environment provided by the host cavity;[52,53] *ii*) geometrical confinement of the dye, which limits its rotational and vibrational freedom;[54,55] and *iii*) protection from external quenchers, such as the solvent or oxygen, offered by the walls of the host.[33,56] Conversely, decomplexation of the dye from the macrocycle reverses these alterations, which from a practical point of view can be induced by the addition of an analyte causing dye displacement. The regeneration of the dye fluorescence can be accurately monitored and sensing systems can be established this way according to the indicator displacement principle (Scheme 1.2.1 and 1.3.2). In this case the receptor is represented by a macrocycle, which determines the selectivity and sensitivity towards the investigated analytes. The photophysical properties of the fluorescent dye, or the indicator, allow for signaling of the analyte binding, either through a fluorescence increase (switch-ON response, taking place in those cases when the dye is quenched upon inclusion complex formation) or decrease (switch-OFF, taking place when the dye undergoes fluorescence enhancement upon complexation with the host).

A large variety of water-soluble fluorescent dyes exist and their combination with macrocycles has been recently reviewed.[57] Among them, the dyes exhibiting strong fluorescence and absorbing light at long wavelengths are particularly desirable for sensing applications.

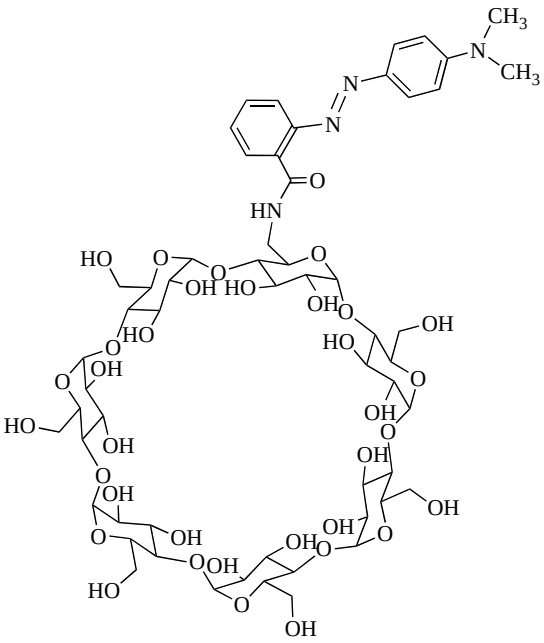

**Figure 1.3.1.** The first combination between a macrocycle (β-cyclodextrin) and an indicator dye (methyl red), covalently attached to each other, for selective sensing of analytes (in this case adamantane carboxylic acid) *via* the indicator displacement strategy.[58]

One of the original indicator displacement sensor studies involving macrocycles is that of Ueno and coworkers where the indicator, methyl red, a known pH indicator dye, has been attached to a β-cyclodextrin wall.[58] Addition of the guest, in this case adamantane carboxylic acid induces a displacement or relocation of the dye from the macrocyclic cavity to the bulk solvent, signaling the analyte. This example has further inspired the design of similar covalently linked macrocycle/dye sensing systems.[59] The covalent tethering of a macrocycle to a fluorophore is advantageous for the fact that due to the local proximity, a high concentration of the complex is insured. This may be particularly relevant under conditions where concentrations cannot be perfectly adjusted, for instance when working with biological samples, such as tissues or cells. However, several

obstacles are associated with this approach such as laborious synthetic methods and limitations with respect to the variation of the indicator.

The drawbacks of the covalent tethering approach have been overcome by the use of intermolecular macrocycle/dye assemblies (Scheme 1.3.2). Not only does this eliminate the need for an additional covalent bond, but access to a large variety of available fluorescent dyes is also permitted. The latter allows the desired "tuning" for the envisaged applications, such as the choice of a dye corresponding to a switch-ON or switch-OFF response. An additional benefit is also the ability to adjust the concentrations of macrocyle and dye so that the affinity range of a particular analyte is matched. An important principle for setting up convenient indicator displacement assays is that the affinity product defined as binding constant *times* concentration should be approximately the same for the dye and the analyte.[43]

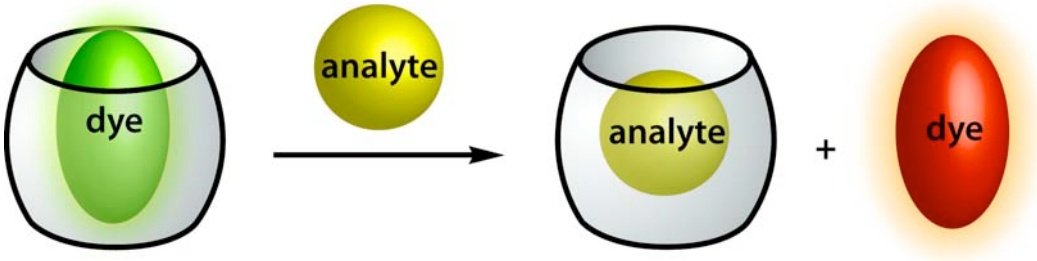


**Scheme 1.3.2**. Indicator displacement assay for sensing of analytes using a macrocycle/dye reporter pair.

The use of macrocycles for the recognition of cationic analytes using the indicator displacement strategy is best illustrated by calixarenes and resorcinarenes, which have been explored for the sensing of bioanalytes, particularly neurotransmitters of the choline and carnitine type. The first system reported to detect acetylcholine employed a resorcinol-based calixarene in combination with a pyrene N-alkylpyridinium dye.[9] However, the strongly alkaline organic conditions were only remedied later by cyano substitution of the host.[60] Shinkai introduced the use of *p*-sulfonato calix[*n*]arenes for detection of acetylcholine near neutral pH.[10] Unfortunately, the fluorophore of choice at that time, the same pyrene-appended pyridinium required alcoholic solution in order to avoid aggregation. Operational systems at physiological pH using fully water-

soluble reporter pairs have emerged only recently (Scheme 1.3.3).[43,61-63] Larger CX*n* have been alternatively used in combination with bulkier fluorescent guests, such as Rhodamine B,[64] at the expense of lower binding affinities.

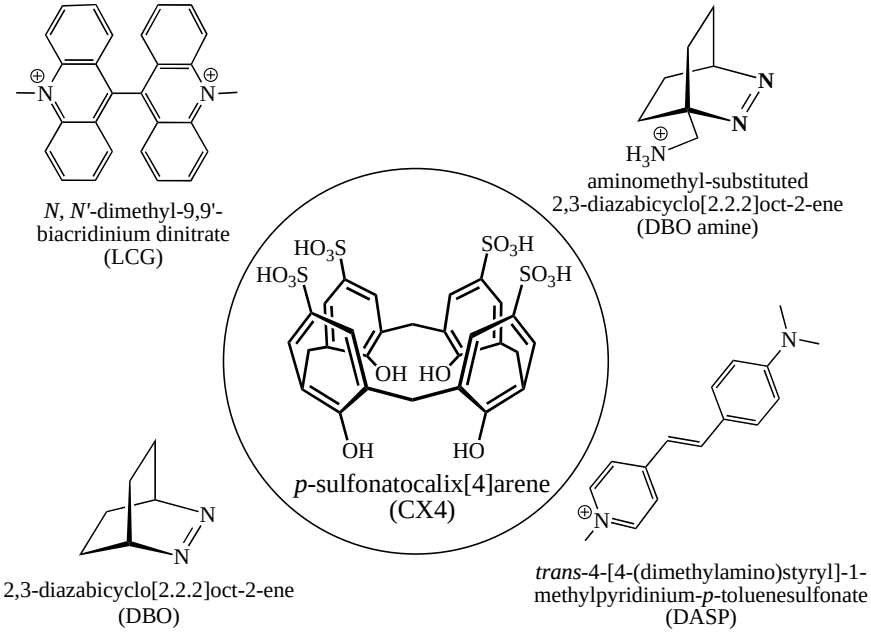


**Scheme 1.3.3.** Fluorescent dyes investigated in combination with *p*-sulfonatocalix[4]arene (CX4) suitable for acetylcholine detection in aqueous solution.

Prime examples related to molecular recognition of anionic analytes are nucleotides and DNA. Several reporter pairs comprised of anion-receptor macrocycles and negatively charged fluorescent dyes,[44,65-68] such as 8-hydroxy-1,3,6-pyrene trisulfonate (HPTS) or fluorescein, have been reported. The supramolecular hosts are either of the cyclophane type (Scheme 1.3.4, **1**, **2**, and **3**) or of the CX type (Scheme 1.3.4, **4** and **5**). In all cases, nucleotide binding is thought to involve synergistic effects of electrostatic interactions, H-bonding, and π-π stacking. In addition to bioanalytes, halide anions also represent prime targets for sensing, but their recognition in aqueous solution remains a great challenge.[69] An example for selective recognition of fluoride in MeCN or $CH_2Cl_2$ is the use of calix[4]pyrrole, **6** coupled with 4-nitrophenolate for colorimetric detection.[70]

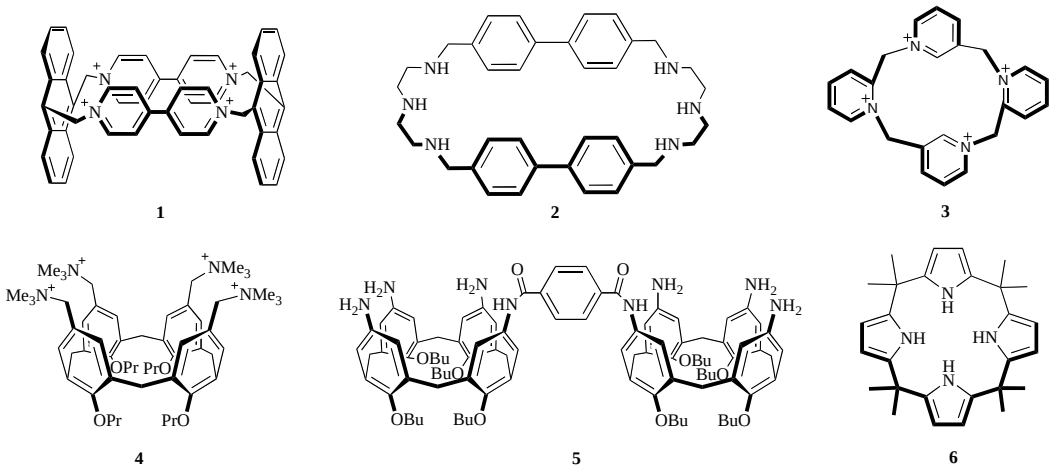


**Scheme 1.3.4.** Macrocycles with anion-receptor properties employed for sensing *via* indicator displacement assays. They were used for recognition of nucleotides (**1**, **2**, **3**, **4**), DNA (**5**), and fluoride (**6**).

Fluorescence-based displacement assays using CB*n* have been inaugurated only recently,[55] opening an extraordinary number of applications for this class of macrocycles. The first fluorescent dye implemented for this type of sensing principle has been Dapoxyl, which upon inclusion with CB7 undergoes a fluorescence enhancement factor of up to 200.[55] Note that in addition to polarity and confinement effects, which are the typical rationale for inclusion effects in the case of CDs and CX*n*, encapsulation of fluorophores with CB*n* is also influenced by charge-dipole interactions. It has already been recognized that these interactions are responsible for p$K_a$ shifts undergone by guests upon complexation with CB*n*.[55,71-74] In fact, already in the original study, the Dapoxyl/CB7 reporter pair has been implemented for a protolytic displacement assay, initially postulated for *p*-sulfonatocalix[4]arene (CX4) and 2,3-diazabicyclo[2.2.2]-oct-2-ene (DBO).[61] The presence of an analyte, in addition to causing the "conventional" displacement, also changes the protonation state of the fluorescent dye as a consequence of its relocation into the bulk phase. Indicator displacement assays involving supramolecular complexes consisting of cationic fluorescent dyes and CB*n* have followed, facilitating the sensing and quantification of amino acids,[75] biogenic amines,[76-78] ionic liquids,[79,80] and transition metals.[81] These examples refer to positively charged guests reflecting the cation-receptor properties of CB*n*. The extraordinary affinity and selectivity of CB*n* towards neutral analytes have

been in detail investigated in the present work, also by means of the indicator displacement strategy, as discussed in Chapter 2.

## 1.4 APPLICATION TO TIME-RESOLVED MONITORING OF ANALYTES

The indicator displacement sensing principle using fluorescent dyes/macrocycles as reporter pairs, as seen above, has been implemented for the detection of a wide variety of analytes. However, the applicability of this methodology is not limited to assessing absolute concentrations, but can be expended to directly measure *changes* in analyte concentration, such as during enzymatic transformations. This establishes an important biochemical application, since being able to monitor enzymatic processes is not only of paramount importance for fundamental enzymology, but also for pharmaceutical-industrial screening in the context of drug discovery.

Among the different methodologies for following enzymatic reactions fluorescence-based assays stand out due to their high sensitivity, short detection times, and the possibility for continuous monitoring as well as scale-up to high-throughput-screening (HTS) format.[82,83] Within the area of fluorescence-based assay design, during my MSc studies, I have become familiar with enzyme assays employing singly labeled substrates. The label was a special noninvasive fluorophore, namely an asparagine derivative of the DBO azo-chromophore (Dbo, Scheme 1.4.1).[84,85] The assay strategy, relying on the collision-induced fluorescence quenching of Dbo by natural amino acids such as tryptophan and tyrosine, allowed for a time-resolved continuous monitoring of the activity of several proteases, phosphatases, and kinases in homogeneous solution (Scheme 1.4.1, Appendix 1 and 2).[86,87] Additionally, owing to the exceptionally long fluorescence lifetime of Dbo (300 ns in water)[88] the assays could be alternatively performed using nanosecond time-resolved fluorescence (Nano-TRF) detection,[89] which allows for background emission suppression, and thereby an increased assay performance.

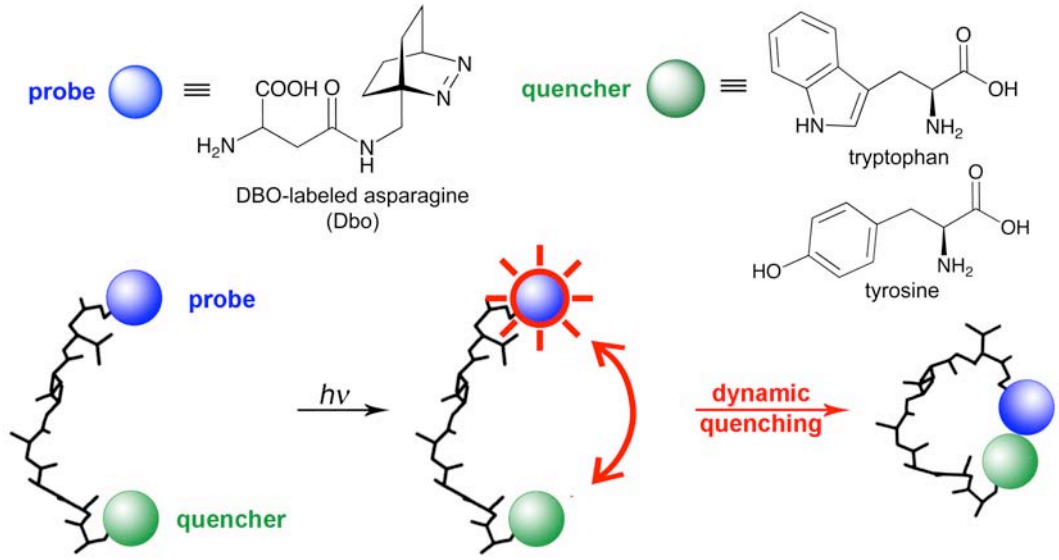


**Scheme 1.4.1.** Fluorescence quenching of Dbo by natural amino acids forms the basis of fluorescence-based enzyme assays using singly labeled substrates (Ref. [86] and [87]).

The breakthrough in assay design took place in our research group in 2007 when a novel methodology was implemented, complementary to established techniques, particularly those involving fluorescently and radioactively labeled substrates or tagged product-specific antibodies.[76] The new line of assays has been coined *supramolecular tandem assays* and it relies on a combination of the indicator displacement strategy involving supramolecular fluorescent dye/macrocycle reporter pairs with enzymatic reactions. The supramolecular tandem enzyme assays allow for a real-time monitoring of changes of analyte concentration as it happens in the course of an enzymatic reaction. The analyte may either be depleted, i.e., the substrate, or formed, i.e., the product. Note that these assays are highly sensitive and they operate in a label-free fashion in homogeneous solution without the need for incubation steps, which have become a burden in antibody and radioactivity-based assays.

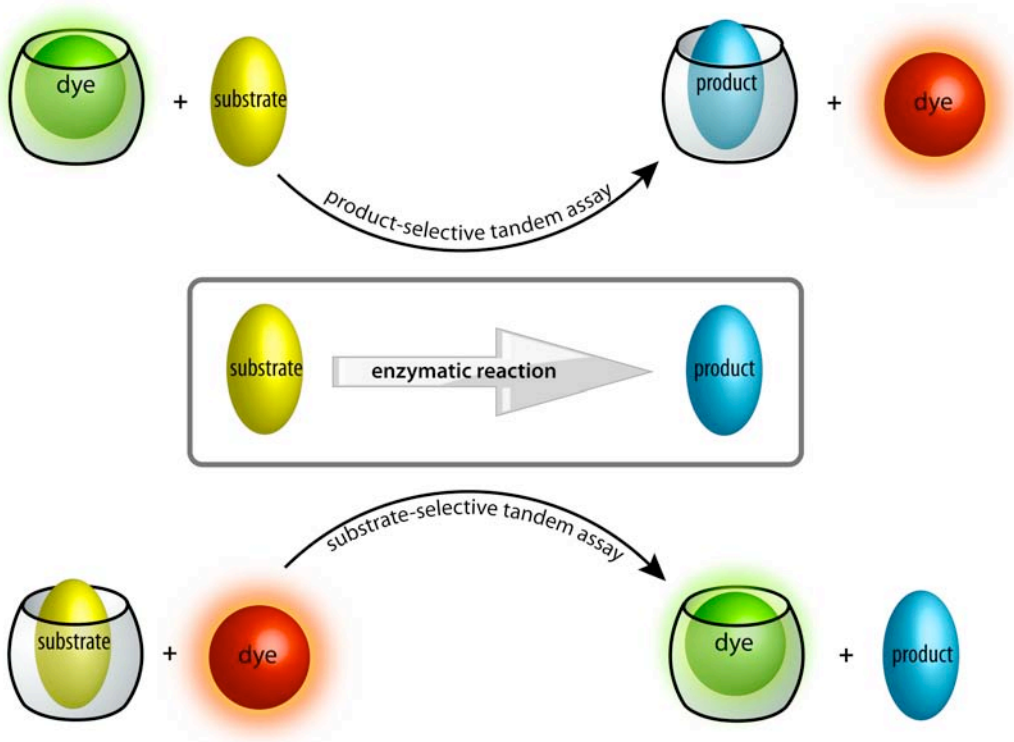


**Scheme 1.4.2.** The concept of supramolecular tandem assays, which allow time-resolved monitoring of changes in analyte concentration during enzymatic transformations.

Whereas in most assays a strong specificity of the receptor for the analyte is required, this is not the case for supramolecular tandem assays. Here, it is only a differential binding between two analytes, i.e., the substrate and the product of the enzymatic reaction, towards a macrocyclic receptor in combination with a fluorescent dye that is necessary. This way, the assay is performed using a reporter pair, which is responsive to the concentration changes caused by the enzymatic reaction (Scheme 1.4.2). Two sensing principles can be differentiated. First, the formation of a strongly binding product can be monitored. In this case, the dye resides in its complexed form before the enzymatic reaction is initiated. The addition of the enzyme triggers a continuous displacement of the dye caused by the higher affinity product (*product-selective assay*). Conventional indicator displacement assays, especially antibody-based ones are conducted in this mode. The second possibility relates to the situation in which the substrate binds more strongly with the macrocyclic receptor as compared to the enzymatic product. In this scenario, the reaction is followed *via* an uptake of the dye into the

macrocyclic cavity as a result of concomitant substrate depletion (*substrate-selective assay*). Depending on the photophysical properties of the fluorescent dye and macrocycle, the concentration changes induced by the enzyme can be monitored either through a fluorescence increase (switch-ON) or a fluorescence decrease (switch-OFF).

The original studies conceptualizing supramolecular tandem assays focused on the study of amino acid decarboxylases (lyases, EC4).[76] The conversion of different amino acids into biogenic amines by 6 different decarboxylases has been monitored using the Dapoxyl/CB7 reporter pair. Specifically, the concentration changes affected by the enzymatic reactions – a weakly competing substrate (an amino acid) being depleted and a strongly competing product (a biogenic amine) being formed – could be correlated and quantified. The supramolecular tandem assay principle has also been extended to other classes of enzymes for time-resolved monitoring of concentration fluctuations as they are inflicted by the enzymatic activity. Such enzymes are hydrolases, (EC3, e.g., arginase,[78] thermolysine,[90] acetylcholinesterase[43]) or oxidoreductases (EC1, e.g., diamine oxidase[78] and choline oxidase[43]). Two additional assays designed for monitoring the depletion of enzymatic substrates by potato apyrase, a phosphohydrolase, and for detecting the formation of an enzymatic product by Dim-5, a histone lysine methyltransferase, are described in detail in Chapter 3, as they are an integral part of the present doctoral work.

The Nau research group, leading in the development of supramolecular tandem assays, has already established a substantial library of reporter pairs built up by combinatorial screening of water-soluble macrocycles with fluorescent dyes. Importantly, the absolute concentrations of macrocycle and fluorescent dye as well as their relative ratio can be adjusted to the preferred analyte concentration range of the particular enzyme of interest and the required sensitivity. In addition to monitoring the changes associated with the enzymatic activity and extracting enzyme-kinetic parameters, supramolecular tandem assays are also suitable for studying the effects of inhibitors and activators, illustrating their potential for both, academic investigations as well as for pharmaceutically relevant screening applications.

# CHAPTER 2

## *– Encapsulation of Volatile Hydrocarbons by Cucurbiturils –*

## 2.1 FEATURES OF THE INNER CUCURBIT[*n*]URIL CAVITY – WHAT DETERMINES HYDROPHOBIC INTERACTIONS

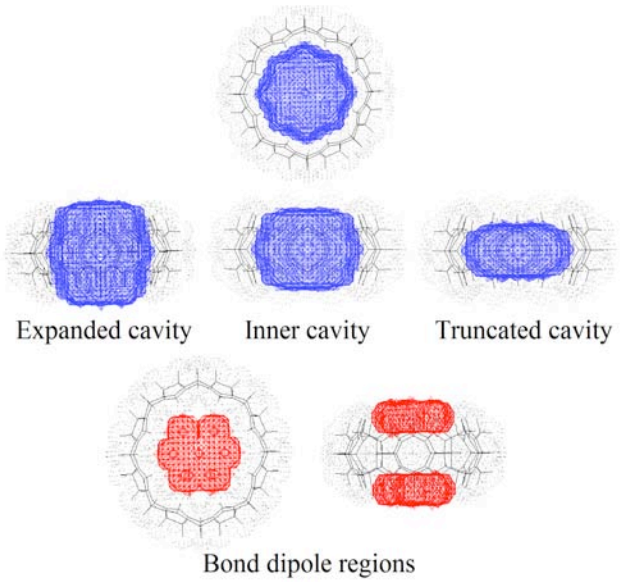


**Figure 2.1.1** Top and side views of the distinct cavities and bond dipole regions of cucurbit[*n*]urils.

A major part of my PhD research work is related to studying the encapsulation of neutral molecules, particularly of volatile hydrocarbons, by cucurbit[*n*]urils, CB*n*. While in supramolecular chemistry this class of macrocycles has been abundantly documented for its cation-receptor properties, we have now focused on investigating their binding propensities towards *neutral* guests. It is already well known that these supramolecular hosts are able to encapsulate hydrophobic residues within their *inner cavity* (Figure 2.1.1), which we have recently defined as the confined space between the carbonyl portals.[34] However, this has always been considered a secondary driving force for complexation, with the major one being generated from ion-dipole interactions between positively charged guests and the electronically rich CB*n* portals. Accordingly, reported studies on the complexation of neutral molecules by CB*n* have remained scarce. Herein, I have undertaken an extensive study on the binding of structurally simple neutral guests with CB*n*, thereby eliminating interferences associated with charge-dipole interactions. This allows for an

isolation of the *hydrophobic driving force* for complexation, which could be explored and related to the peculiar physical properties of the CB cavity, which will also be shortly introduced.

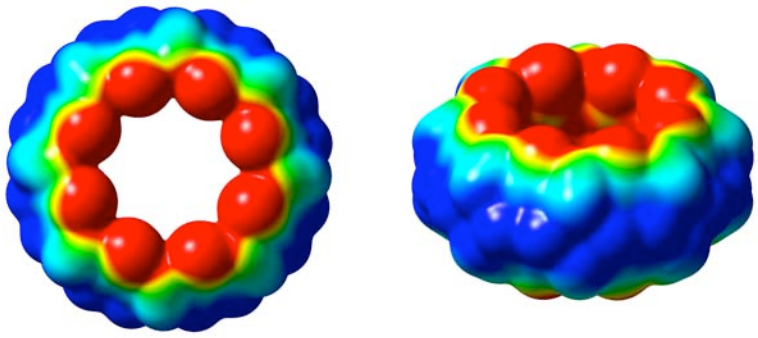

**Figure 2.1.2.** Electrostatic potential map (top and side view) of CB8 revealing the negatively charged carbonyl regions (in red) and the electron-deficient equatorial region (in blue).

CB*n* macrocycles have generally been assigned a hydrophobic interior capable of hosting neutral guests or organic residues, which can be qualitatively estimated from their electrostatic potential map (Figure 2.1.2). The highly electron-deficient equatorial region can be readily visualized, contrasting the electron-rich carbonyl-lined portals. However, this information does not tell us much about the hydrophobicity of CB*n* or what renders their interior hydrophobic. Exploratory investigations inside the cavity of cucurbiturils, particularly for CB7, have already been reported with several solvatochromic probes.[54,91] In all cases, a polarity similar to alcohols or alcohol:water mixtures was reported, which is also the case for other related macrocycles, CDs or CX*n*. Overall, since the polarity detected is lower than that of water, one can generally describe the CB interior as hydrophobic. Furthermore, within the present project, I have investigated whether the interior of these macrocycles allows housing of hydrocarbons, such as small alkanes, which are *par excellence* hydrophobic compounds. Their complexation was not only confirmed, but also led to a further investigation of the factors that contribute to the relocation of these hydrocarbons from the aqueous environment into the inner CB cavity (see next sections).

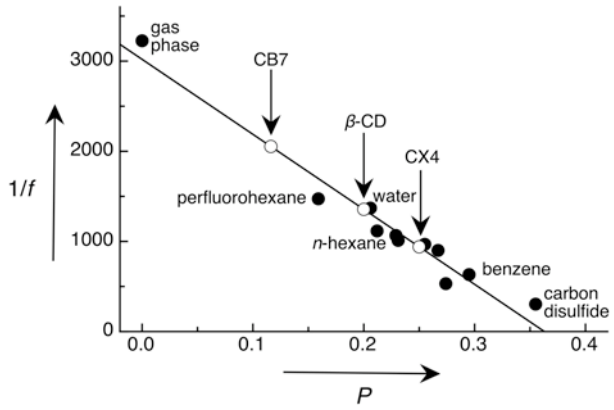


**Figure 2.1.3.** Linear correlation of the inverse oscillator strength, 1/*f*, of DBO and the polarizability, *P*, of the environment. White circles mark interpolated values for macrocyclic cavities.

The most striking feature of the CB inner cavity is its extremely low polarizability/refractive index, which is closer to that of gas phase than to that of any other known solvent. This peculiar property has been exposed using DBO, a neutral azoalkane with an extremely long-lived fluorescence lifetime (up to 1 μs), as solvatochromic probe. Its full immersion, not only in CB7, but also in similar supramolecular microenvironments, such as in CX4 and β-CD, allows for an actual exploration of the inner cavities of these macrocycles. Experimentally, the oscillator strength, *f*, of the near-UV absorption band of DBO was measured in gas phase, as well as in different solvents and supramolecular environments. An empirical linear correlation was established between its inverse, 1/*f*, and the bulk polarizability, *P*.[92] As seen in Figure 2.1.3, when compared to related macrocycles, the polarizabiliy of CB cavity falls below that of CDs, while hosts with an aromatic structural topology such as CX*n*, exhibit much higher values. Cyclodextrins have C–H bonds pointing towards the inside of the cavity, and thus their interior has been characterized as "alkane-like". Calixarenes contain aryl π systems, which naturally render their interior as "aromatic". In contrast, CB*n* have neither bonds, nor lone pair orbitals pointing inwards and the electron density is effectively displaced to the carbonyl oxygens at the upper and lower rims; moreover, their concave structure causes the electron density at the ureido nitrogen to be directed towards the outside of the cavity. The extremely low polarizability inside the CB cavity has also provided the first experimental evidence for Cram's daring postulate, initially formulated for hemicarcerands, that

the inner space of such molecular containers can represent a completely new phase of matter.[93,94]

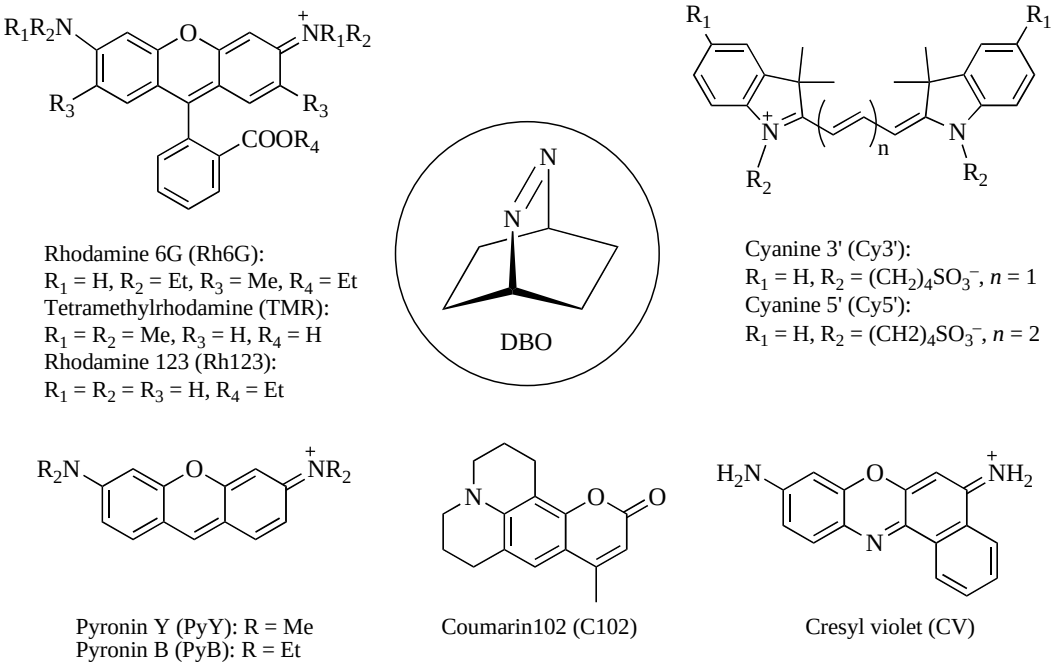


Rhodamine 6G (Rh6G):
$R_1$ = H, $R_2$ = Et, $R_3$ = Me, $R_4$ = Et
Tetramethylrhodamine (TMR):
$R_1$ = $R_2$ = Me, $R_3$ = H, $R_4$ = H
Rhodamine 123 (Rh123):
$R_1$ = $R_2$ = $R_3$ = H, $R_4$ = Et

Cyanine 3' (Cy3'):
$R_1$ = H, $R_2$ = $(CH_2)_4SO_3^-$, $n$ = 1
Cyanine 5' (Cy5'):
$R_1$ = H, $R_2$ = $(CH2)_4SO_3^-$, $n$ = 2

Pyronin Y (PyY): R = Me
Pyronin B (PyB): R = Et

Coumarin102 (C102)

Cresyl violet (CV)

**Scheme 2.1.1.** Structures of fluorescent dyes displaying fluorescence lifetime-enhancing effects upon complexation by CB7.

The first consequence of the low CB*n* polarizability is reflected in the photophysical properties of the encapsulated fluorescent dyes, specifically, with respect to their longer fluorescence lifetimes, $\tau_0$, in low-polarizability environments. This is due to the dependence of the radiative decay rate, $k_r$, on the square of the refractive index, $n^2$ (the Strickler-Berg equation), which in turn is directly related to the polarizability of the environment, $P = (n^2-1) / (n^2+2)$.[95] The radiative decay rates of several fluorophores have been measured in the presence of CB7, and extremely low values were extracted, while exceedingly high fluorescence lifetimes were recorded. These experiments have in fact provided the direct spectroscopic evidence for the earlier empirical correlation between oscillator strength and polarizability. DBO, for instance, holds the world record with respect to its fluorescence lifetime, which is above 1 μs in aqueous solution.[96] Numerous fluorescent dyes, including the commercially relevant rhodamines, coumarins, pyronins, oxazines, and cyanines, display their longest fluorescence lifetimes ever recorded in the inside of the CB cavity, including

those that are too bulky to be completely encapsulated by CB*n* (Scheme 2.1.1).[54,56]

The other implication of such an extremely low polarizability inside a macrocyclic host is reflected on the chemical interactions involving supramolecular assemblies. Polarizability is defined as the ability of a molecule's electron density to change or distort as a response to an external electric field, such as that inflicted by the presence of an ion or a dipole. Its importance in noncovalent interactions is highlighted by the London formula on the contribution of dispersion interactions to the attraction between two molecular species, and its driving force in host-guest complexation involving cyclophanes has been already acknowledged.[97]

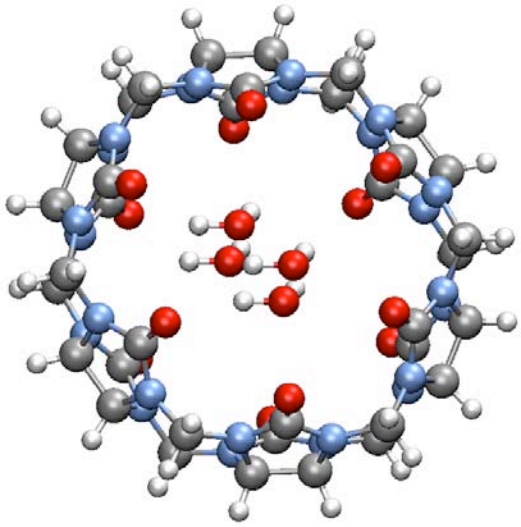

**Figure 2.1.4.** Crystal structure of CB6 with four very-high-energy water molecules inside its inner cavity (from ref.[98]).

The exceedingly low polarizability of the CB cavity and its implications towards the thermodynamics of complexation between organic residues or neutral guests *via* hydrophobic interactions deserves special attention. It has been postulated that in aqueous solution hydrophobic and dispersion interactions do not only reach a maximum, but also that their separation is incredibly difficult, if not impossible.[99] In the case of CB*n*, however, the situation is different since their cavity is less polarizable than water. In this case, hydrophobic guests would in fact rather prefer to interact with the solvent *via* dispersion interactions than with

the inner CB cavity. As a result, dispersion interactions certainly do not afford an enthalpic driving force for guest inclusion and the complexation of neutral guests with CB*n* can be considered as *purely hydrophobic* in nature.

**Table 2.1.1.** Binding affinities and volumes of hydrophobic residues encapsulated by the CB7 cavity.[a]

| Recognition motif, R | Guest | $K$ [$M^{-1}$] | V [$Å^3$][b] |
|---|---|---|---|
| R = 1-adamantyl | 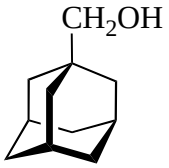 1-hydroxymethyl-adamantane | $2.3 \times 10^{10}$ | 147 |
| R = ferrocenyl |  hydroxymethyl-ferrocene | $3.2 \times 10^{9}$ | 141 |
| R = bicyclo[2.2.2]octane | 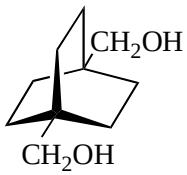 BCO | $6.1 \times 10^{9}$ | 121 |
| R = 2,3-diazabicyclo[2.2.2]-oct-2-ene[c] |  DBO | $5.8 \times 10^{6}$ | 111 |

[a] From ref.[100]. [b] Calculated volume corresponds to that of the immersed residue, R, in the CB7 cavity. Volume calculation was performed with the QSAR module of HyperChem[101] after optimization with the AM1 semiempirical method. [c] From ref.[102]

The first neutral guests detected to form inclusion complexes with CB*n* are water molecules, found in several crystal structures.[34] Their presence is inevitable and we have recently estimated the occupancy of the inner cavities of CB*n* with these very-high-energy guests. As expected, the number of water

molecules found in the absence of other encapsulated guests increases with the size of the macrocyclic cavity: CB5 houses two water molecules, CB6 four (Figure 2.1.4), CB7 eight, and CB8 twelve molecules.[34] The number of expelled water molecules upon encapsulation of a guest can be estimated from the guest volume. The entropic contribution of the hosted water molecules represents, in addition to the "unimportance of dispersion interactions" (*vide supra*), a significant aspect of the driving force that leads to the encapsulation of hydrophobic residues inside the CB macrocycles.

To illustrate how these unusual characteristics of the CB inner cavity are influential for the hydrophobic driving force leading to complexation, let us take the examples of several selected neutral guests or residues previously reported to form inclusion complexes with CB*n*. For instance, the tricyclic 1-hydroxymethyl-adamantyl, and the bicyclics hydroxymethyl-ferrocenyl, the bicyclo[2.2.2]octane-derivative (BCO), and DBO, are known to bind strongly with CB7. In fact, the binding constants of some of these residues (with appended ammonium groups) with CB7 are so high, that they were compared to the biotin-avidin affinity.[51,100] Initially, attractive van der Waals interactions have been held responsible for the high binding between the hydrophobic cores of the guests and the CB cavity. However, upon closer inspection, it can be noted that all these guests are able to completely remove all water molecules, usually residing in the inner CB7 cavity. Thus, in reality, the differences in binding constants (Table 2.1.1) are due to the differential solvation of the hydrophobic residues. Note that this is a significant factor in the complexation thermodynamics of guest molecules with any macrocycle, not only with CB*n*. Since both, adamantyl and ferrocenyl, residues are almost isosteric (approximately same volume), one would expect identical affinities towards CB7. Yet, adamantyl displays slightly higher binding affinity, which can be explained by the differences in polarizability of the two residues: the more polarizable ferrocenyl undergoes a better solvation in water, leading to dispersive interactions to favor a stabilization of the residue in bulk water. A similar situation is encountered for DBO and BCO. The three orders of magnitude lower binding constant of DBO can be ascribed to the dipolar azo group, which renders this neutral compound highly water-soluble and polarizable. Consequently, a higher energy input is necessary for its desolvation. In fact, it has been reassuring to see how these results are highly supportive also towards our

new findings with respect to the encapsulation of hydrocarbons by CB*n*. For instance, as we will see in the next section, the highly electron-rich benzene (89 $Å^3$) was found to have a very low affinity towards CB6 (< $10^3$ $M^{-1}$), in contrast to less polarizable cyclopentane (86 $Å^3$), which reveals an extraordinarily high binding constant (~ $10^6$ $M^{-1}$).

In view of these particular properties of the CB inner cavity, we have decided to explore in detail the complexation of *neutral guests* with this class of macrocycles, whose chemistry is presently unfolding (an example is the special issue on "Cucurbiturils" in the *Israel Journal of Chemistry*, May 2011). Particularly, the binding of *small* neutral molecules is useful, not only because the charge-dipole interactions are being eliminated, which otherwise become dominant, but also since a complete immersion inside the inner cavity is feasible. This allows for an exploration of size, properties, as well as the fundamental intermolecular interactions between the guests and the inner CB cavity leading to the formation of discrete supramolecular assemblies, which I will describe next.

## 2.2 A SUPRAMOLECULAR GAS-SENSING ENSEMBLE WITH CB6

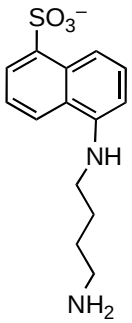


**NAS-P**

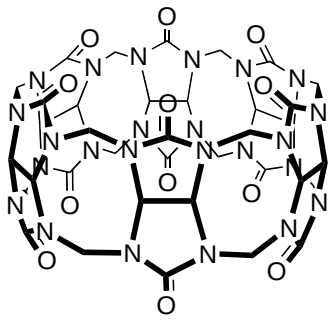

CB6

In order to monitor the binding of several volatile hydrocarbons to cucurbit[6]uril, CB6, in a time-resolved fashion we chose the indicator displacement methodology using our recently developed anchor dye approach.[77] Specifically, the fluorescent dye, **NAS-P** has been synthesized by attaching a putrescine anchor (ensuring strong binding with CB6) to the microenvironmentally sensitive 1-naphtylamine-5-sulfonic acid chromophore (ensuring a significant fluorescence change upon binding). The strong affinity between **NAS-P** and CB6 in combination with the large fluorescence response

upon complexation allowed for experiments to be performed not only in 50 mM NaOAc, but also in salt-free aqueous solution (Figure 2.2.1). This is a particular advantage offered by the extraordinary sensitivity associated with fluorescence-based indicator displacement assays. Specifically, it allows the use of very low concentrations (in our case low μM range, below the solubility limit of CB6), which is not possible with other established techniques, such as NMR, where considerably higher concentrations (typically mM range) are required.

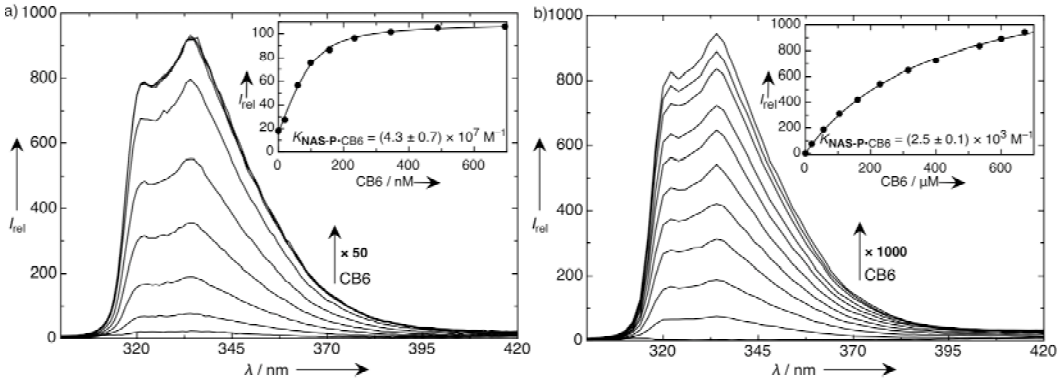


**Figure 2.2.1.** Fluorescence spectra ($\lambda_{exc}$ = 283 nm) of a) 4 μM **NAS-P** with increasing concentrations of CB6 in 1 mM HCl, pH 3.0, and b) 10 μM **NAS-P** with increasing concentrations of CB6 in 50 mM NaOAc, pH 5.5. The nonlinear fittings (insets, $\lambda_{obs}$ = 334 nm) were made according to a 1:1 complexation model, from which the association constants were derived. The very tight binding of the dye with CB6 at pH 3.0 required the use of a lower dye concentration (100 nM, titration curve in inset) to achieve higher accuracy in the determination of the absolute binding constant.

Using a fluorescent dye displacement approach, we were able for the first time to monitor in real-time the encapsulation of various hydrocarbons by CB*n* macrocycles. The working principle is depicted in Figure 2.2.2. The addition of gaseous analyte to the pre-assembled and highly fluorescent **NAS-P**•CB6 reporter pair results in a continuous displacement of the dye. The changes in analyte concentration have an immediate onset, signaling the fast exchange on the time scale of the experiment. The saturation limit is concomitantly reached with the final plateau of the fluorescence intensity, where the concentration of the volatile analyte corresponds to its well-known aqueous solubility.

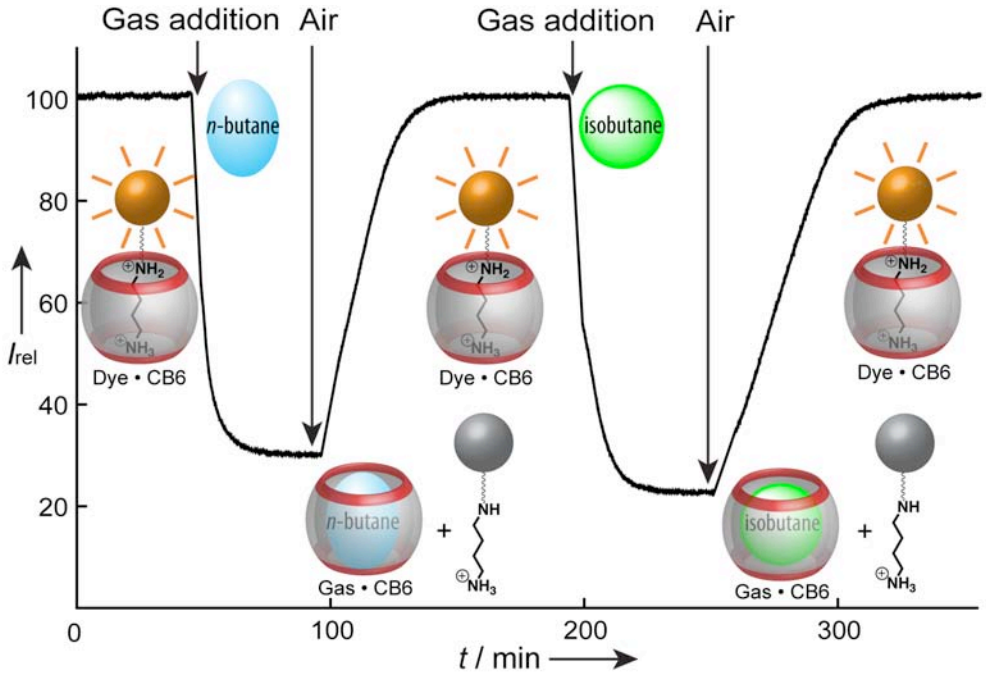


**Figure 2.2.2.** Fluorescence-based approach for time-resolved monitoring of hydrocarbon encapsulation and sensing using CB6 in aqueous solution. The trace refers to actual experiments with sequential uptake and release of *n*-butane and isobutane.

Note in Figure 2.2.3 the markedly different fluorescence responses corresponding to the investigated hydrocarbons upon addition to the **NAS-P•**CB6 complex. To our surprise, the affinities of neutral guests towards CB6 are exceedingly high (in fact, the largest ones ever reported with macrocycles),[103-113]and the high selectivity exhibited by CB6 stands out also when compared to previously investigated containers (Table 2.2.1).

**Table 2.2.1.** Binding constants of hydrocarbons with CB6.

| | Hydrocarbon [Volume / Å$^3$][b] | PC[c] [%] | $K$ [10$^3$ M$^{-1}$][a] | |
|---|---|---|---|---|
| | | | water, pH 3.0[d] | NaOAc, pH 5.5 |
| C1 | methane [29] | 20 | < 2 | < 0.05 |
| C2 | ethane [45] | 32 | 24[e] | 2.6 ± 0.7 |
| | ethene [41] | 29 | 3.9 | 0.25[e] |

| | | | | |
|---|---|---|---|---|
| | acetylene [35] | 25 | 0.11[e] | 0.047[e] |
| C3 | propane [63] | 44 | 180[e] | 10 ± 5 |
| | propene [58] | 41 | 25[e] | 1.4 |
| C4 | *n*-butane [80] | 56 | 280 | 4.4 |
| | 1-butene [75] | 53 | 79 | 1.3 |
| | *cis*-2-butene [74] | 52 | 150 | 2.1 |
| | *trans*-2-butene [74] | 52 | 21 | 0.32 |
| | isobutane [79] | 56 | 850 ± 190 | 28 ± 15 |
| | isobutene [75] | 53 | 84 | 1.9 |
| C5 | *n*-pentane [96] | 68 | 9 ± 4 | 0.14 |
| | isopentane [96] | 68 | 15 ± 5 | 0.30 |
| | neopentane [96] | 68 | < 2 | < 0.05 |
| | cyclopentane [86] | 61 | 1300 ± 300 | 35 ± 24 |
| ≥C6 | higher alkanes[f] [> 102] | > 72 | < 2 | < 0.05 |

[a] Determined by competitive fluorescence titrations with the **NAS-P•**CB6 reporter pair at 298 K; error in data is 20% unless specified differently. [b] Obtained from AM1-optimized geometries. [c] Packing coefficient, obtained by dividing the guest volume by the inner cavity volume of CB6 (142 Å$^3$, from ref.[34]). [d] Adjusted with 1 mM HCl. [e] 10% error. [f] *n*-hexane, isohexane, 2,3-dimethylbutane, cyclohexane, *n*-heptane.

In all cases, the binding constants were calculated by assuming a 1:1 complexation stoichiometry *via* the following methods:

*i*) Repetitive end-point measurements of the fluorescence intensity of gas-saturated solutions. The binding constants were calculated according to eq. 2.1, where $I_{obs}$ stands for the absolute change in fluorescence intensity upon dye displacement.

$$K_c = \frac{\left\{ \begin{array}{l} I_g([G]_0 I_{gh} K_G - [G]_0 I_{obs} K_G - [H]_0 I_{gh} K_G + [H]_0 I_{obs} K_G) + \\ [G]_0 {I_{obs}}^2 K_G + [H]_0 {I_{gh}}^2 K_G - [G]_0 I_{gh} I_{obs} K_G - [H]_0 I_{gh} I_{obs} K_G \end{array} \right\}}{C_s (I_g - I_{gh})(I_g - I_{obs})} - \frac{1}{C_s} \quad (2.1)$$

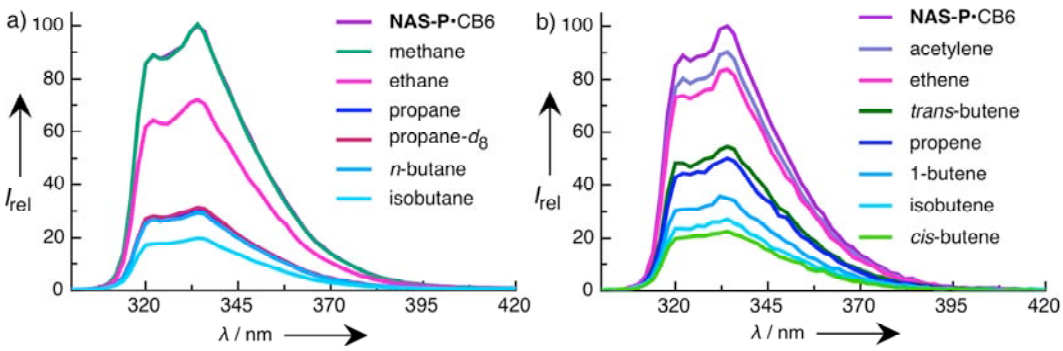


**Figure 2.2.3**. Displacement of **NAS-P** (4 μM) from CB6 (4 μM) monitored by fluorescence after saturation of aqueous solutions with different gaseous a) alkanes and b) alkenes and acetylene. Measurements in water at pH 3.0, $\lambda_{exc}$ = 283 nm. Note that hydrocarbons showing similar displacements may exhibit different binding constants due to varying solubilities.

*ii*) Representative titrations at different gas pressures, and therefore different gas concentrations (by assuming Henry's law) afforded 1:1 isotherms (Figure 2.2.4). A competitive binding model was used and the concentration of gas at 1000 mbar was taken as its known aqueous solubility (eq. 2.2). For the determination of binding constants of analytes by competitive displacement, we fixed the binding constant of the dye, $K_G$, as $4.3 \times 10^7$ $M^{-1}$ in 1 mM HCl (pH 3.0) and $2.5 \times 10^3$ $M^{-1}$ in 50 mM NaOAc (pH 5.5). It is important to note that the choice of a slightly different dye binding constant would affect the absolute values, but not the relative values among the different analytes.

$$FI = I_g + \left(I_{gh} - I_g\right)\frac{K_G[H]}{1 + K_G[H]}$$

$$\text{with } [H] = \frac{K_G[H]_0 - K_C[C]_S - K_G[G]_0 - 1 + S}{2\left(K_G + K_C K_G [C]_S\right)} \qquad (2.2)$$

$$\text{and } S = \sqrt{\left(1 - K_G[H]_0 + K_C[C]_S + K_G[G]_0\right)^2 + 4\left(K_G + K_C K_G [C]_S\right)[H]_0}$$

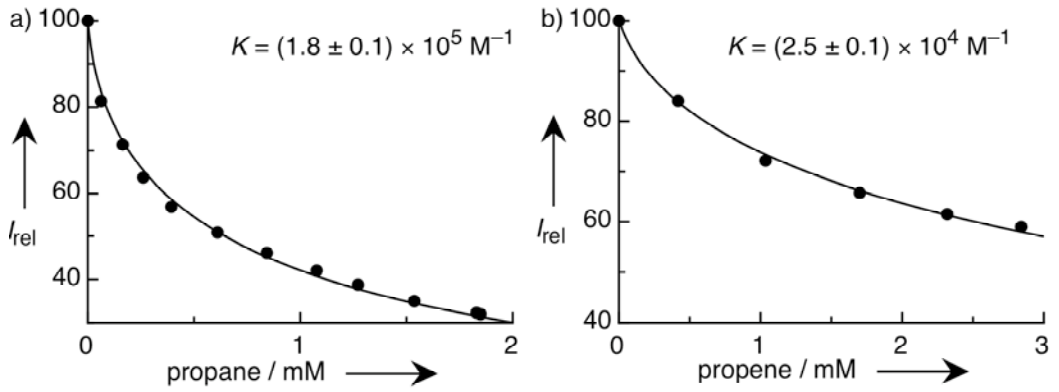


**Figure 2.2.4.** Plot of the fluorescence intensity of competitive displacement of **NAS-P** (4 μM) from CB6 (4 μM) at different concentrations (pressures) of a) propane and b) propylene in 1 mM HCl, pH 3.0 ($\lambda_{exc}$ = 283 nm, $\lambda_{obs}$ = 334 nm). The nonlinear fittings were made according to eq. 2.2.

Structural evidence for the inclusion of the gases was furbished by $^1$H NMR investigations (see example for isobutane in Figure 2.2.5). On one hand, these measurements were limited to salt-containing (50 mM $Na_2SO_4$) $D_2O$ solutions, where the solubility of CB6 reached the mM range. On the other hand, only the lower, most water-soluble alkanes (up to C4) could be examined by this method. In the presence of CB6, a new set of upfield-shifted resonances emerged ($\Delta\delta$ = 0.71–0.92), corresponding to the encapsulated gases being in slow exchange with their free forms. Integration of the proton signals, using maleic acid as a standard, provided independent values for the binding constants (eq. 2.3). These were in satisfactory agreement with those obtained *via* fluorescence measurements, considering the change of $H_2O$ to $D_2O$ and the slightly higher (100 mM) sodium ion content. In the case of methane and neopentane, as expected from the absence of a fluorescence response, no new proton signals could be observed in the presence of CB6.

$$K = \frac{[HG]}{[H]_{free}[G]_{free}} = \frac{[G]_{bound}}{([H]_0 - [G]_{bound})[G]_{free}} \qquad (2.3)$$

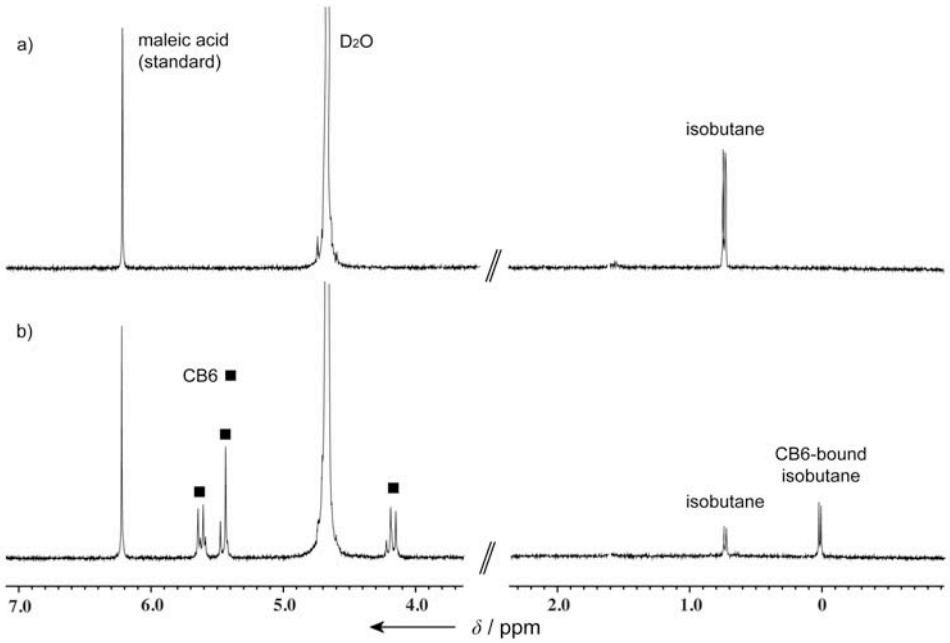


**Figure 2.2.5.** $^{1}$H NMR spectrum of a non-saturated isobutane solution a) before and b) after addition of CB6 in 50 mM $Na_2SO_4$–$D_2O$ solution, using maleic acid as standard (2.5 mM). The slow exchange between the gas and the host is illustrated by the additional upfield-shifted resonance corresponding to encapsulated isobutane. Integration of the signals provided the concentration of host (0.35 mM) and those of free (0.14 mM) and bound (0.25 mM) gas, which afforded a binding constant of $1.7 \times 10^4$ $M^{-1}$ according to eq. 2.3.

In order to visualize the hole-size and cavity-height matching of CB6 towards the different guests, we can take a look at the optimized geometries of the complexes in Figure 2.2.6. A perfect match is not dependent only on the size or length of the guests (*n*-butane *vs.* 1-butene), but also on the shape or geometry of the guests (isobutane *vs.* *n*-butane). These considerations are illustrative of the binding constants obtained in Table 2.2.1.

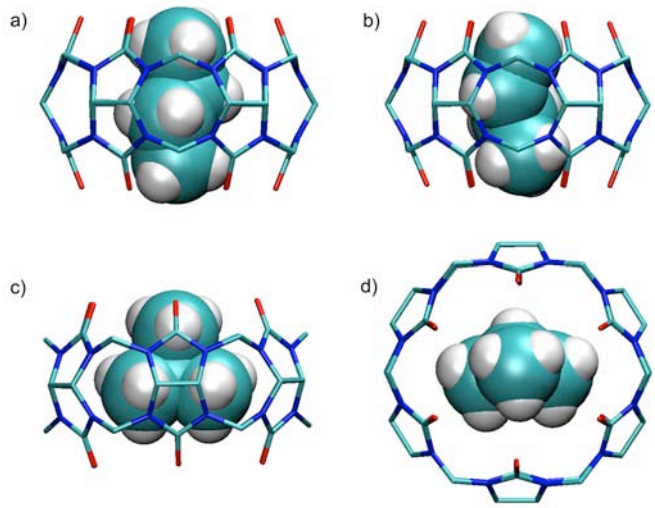


**Figure 2.2.6.** Optimized geometries of the CB6 complexes with a) *n*-butane, b) 1-butene, c) isobutane (side view), and d) isobutane (top view) at the B3LYP/6-31G** level of theory (gas phase) performed by K. I. Assaf.

On the basis of constitutional selectivity displayed by CB6 (branched and cyclic hydrocarbons being preferred over elongated ones), one may at first expect neopentane to also form an inclusion complex. In addition to its essentially perfect spherical geometry, neopentane possesses the same volume (96 $Å^3$) as its other two isomers, isopentane, and 2,3-diazabicyclo[2.2.1]hept-2-ene, which do show a moderate to strong affinity for CB6 Table 2.2.1 and ref.[50], respectively. However, in the case of neopentane neither a fluorescence response, nor an upfield shift in the NMR signal was observed, corroborating this way an earlier observation by Mock, which states that neopentylammonium does not form an inclusion complex with CB6,[48,49] a consequence of the constrictive binding exhibited by the CB6 portals.[108,114] The absence of binding for neopentane combined with the CB6 selectivity has served in our case to illustrate how our study may be practically relevant for real applications.

The fact that the commercial neopentane in highest available purity (99%) contained an unknown impurity at 1.66 ppm was a serendipitous finding. Addition of solid CB6 resulted in a complete removal of the impurity, affording a highly pure neopentane solution (Fig. 2.2.7), as could be anticipated from the selectivity in Table 2.2.1. This example highlights how the differential binding of CB6 to different analytes can be applied to real applications.

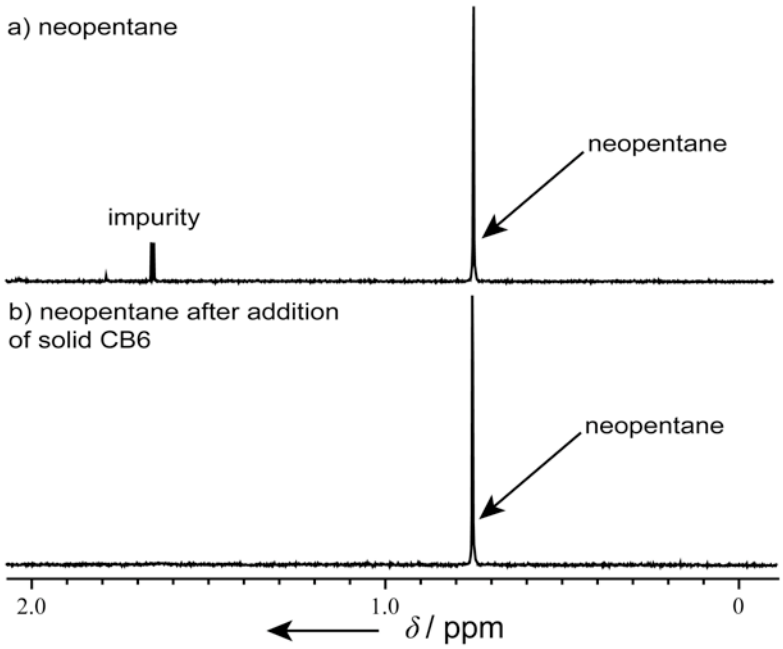


**Figure 2.2.7.** $^{1}$H NMR spectra of neopentane-saturated $D_2O$ before and after addition of CB6.

A general rule, proposed by Rebek, with respect to size selectivity of encapsulated guests is the "55% solution",[115,116] which predicts an optimum packing coefficient (PC, defined as volume of the guest divided by volume of host cavity) associated with the highest affinity. The rule takes into account the *capacity* of a certain cavity rather than its *volume*. The size-selectivity in our case, too, can be rationalized by considering the PCs of the different gases towards CB6 (Table 2.2.1). Note that the maximum affinities are reached for isobutane and cyclopentane where PC values of 56-61% are reported, well in line with the 55% solution. Higher or lower values are tolerated, but they do come at the expense of lower binding constants. For example, the slightly larger pentane isomers (96 Å$^3$), show considerably lower binding constants, as can be noticed in Table 2.2.1.

In addition to size-selectivity and constitutional selectivity (branched and cyclic hydrocarbons being preferred over elongated ones), CB6 can also differentiate between saturated (*alkanes*) and. unsaturated (*alkenes*) hydrocarbons, with a preference for the former by a factor of 4-10 times. Interestingly, this cannot be due to the minimal size difference, but rather to the higher water solubility of alkenes. Therefore, these analytes are better solvated in water than their saturated counterparts, consequently experiencing a weaker solvophobic

driving force for complexation, similar to the DBO/BCO example given in Section 2.1.

A limitation of the CB6 homologue is its very low water solubility (up to 30 μM),[50] such that previous binding constants could only be extracted in either mixed solvents, such as with formic acid,[117] or in the presence of salts (typically 50-200 mM $Na_2SO_4$). Such conditions are, however, known to reduce the affinity considerably, due to the competitive binding effect of the cations at the carbonyl rims.[50,118,119] The set of experiments we have provided in this study is particularly useful also for an insight into the salt effect (a concentration of 50 mM $Na^+$ has been employed), as no such systematic study involving uncharged guests has been previously performed. It is interesting to see that even though the cations neither do they interact with the hydrocarbons, nor do they bind in the inner CB6 cavity, their presence is revealed by one to two orders of magnitude lower binding constants. There appears to be also a size dependence, with the salt effects being more pronounced for the longer hydrocarbons (C4, C5 *vs.* C2) where the steric hindrance manifests itself more strongly (Table 2.2.1).

**Table 2.2.2.** Binding constants of selected neutral guests with CB6: a comparison with the available literature.

| Guest [Volume/Å$^3$][b] | PC[c] [%] | $K$ [$10^3$ M$^{-1}$][a] | | | |
|---|---|---|---|---|---|
| | | water, pH 3.0[d] | | NaOAc, pH 5.5 | |
| | | this work | literature | this work | literature |
| Xe [43] | 30 | 3.8 | 3.4[e] | 0.22 | 0.18[e], 0.21[f] |
| $SF_6$ [52] | 37 | 660 | n.a. | 32 | 31[g] |
| tetrahydrofuran [77] | 54 | 30 | n.a. | 1.7 | 1.7[h] |
| cyclopentanone [87] | 61 | 3.2 | n.a. | 0.8 | 2.2[i] |
| benzene [89] | 63 | < 2 | n.a. | < 0.05 | 0.027[i] |

[a] Determined by competitive fluorescence titrations with the **NAS-P**·CB6 reporter pair at 298 K; error in data is 20%. [b] Obtained from AM1-optimized geometries. [c] Obtained by dividing the guest volume by the inner cavity volume of CB6 (142 Å$^3$, from ref.[34]). [d] Adjusted by addition of 1 mM HCl. [e] Data for an alkylated CB6 derivative, from ref.[120], by isothermal titration calorimetry. [f] From ref.[121,122], by $^{129}$Xe

and $^{1}$H NMR. [g] From ref.[123], by $^{19}$F and $^{1}$H NMR. [h] From ref.[122], by $^{1}$H NMR. [i] From ref.[124], by $^{1}$H NMR.

The fluorescence-based methodology for determining the affinity of neutral analytes that I introduced herein was additionally cross-checked with some of the existing literature values, offering an excellent agreement (Table 2.2.2). Unfortunately, the literature data available so far are limited to saline solutions (with Xe being the only exception binding with an alkylated CB6 derivative). In addition to the Xe•CB6 complex, the group of Kim has also recently characterized, however in the solid state, the inclusion complex between $CO_2$ and CB6, where two molecules of guest were found inside the macrocyclic cavity (due to the very small volume of $CO_2$ (31 Å$^3$).[125] Data regarding the complexation of hydrocarbons or gases by CB7 or larger homologues are unfortunately missing in the literature.

A few other examples, which add to this limited set of investigated neutral guests with CB*n*, are only qualitative in nature, and, therefore, have not been included in Table 2.2.2. Notably, CB5 has been reported to form inclusion complexes with small gases,[126] such as He, Ne, $H_2$, Kr, Xe, $CH_4$, $N_2$, $O_2$, Ar, $N_2O$, NO, CO, $CO_2$, acetylene, as well as with small solvent molecules such as acetonitrile and methanol.[127] The encapsulation of methane by CB5 could also have been anticipated from our study, from which it is evident that while highly significant, this hydrocarbon is simply too small to be effectively encapsulated by CB6. This observation also brings me to another aspect of the presently described work. While obtaining experimental data, e.g., binding constants, is essential, as it stands at the basis of any scientific work, being able to make predictions, or in other words having a certain "scientific common sense" for estimating outcomes or trends is also imperative in any research. For instance, I believe that a thorough understanding of the unique characteristics of the CB inner cavity and the systematic set of results on the complexation between hydrocarbons and CB*n* can be the starting point of future studies. This study does not only allow for predictions on the affinity and selectivity of CB*n* macrocycles, but could also be particularly relevant for computational simulations meant to reproduce hydrophobic effects in supramolecular host-guest systems.

## 2.3 A STEP FURTHER: HYDROCARBON BINDING TO CB7

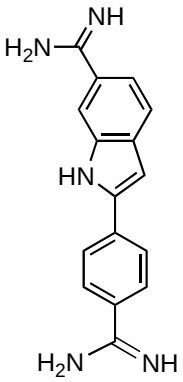


**DAPI**

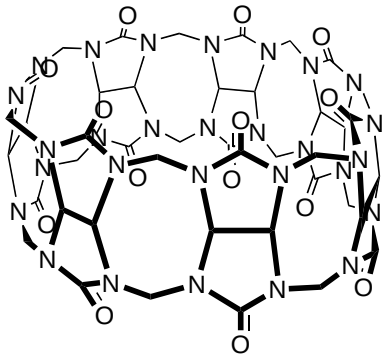

CB7

Encouraged by the unexpectedly high binding constants observed for hydrocarbon binding with CB6, we also proceeded to the next higher homologue, CB7. Herein, I would like to show the preliminary results obtained so far. In contrast to CB6, several reporter dyes are known for CB7.[55] To allow measurement at pH 3.0 and thereby direct comparison with the results for CB6, we selected the rather pH-independent probe 4',6-diamidino-2-phenylindole, **DAPI**, which upon complexation by CB7 undergoes a large fluorescence enhancement in aqueous solution ($\lambda_{exc}$ = 361 nm, $\lambda_{obs}$ = 468 nm).[79] The binding constant (Figure 2.3.1) was determined as (8.8 ± 1.0) × $10^6$ $M^{-1}$ (literature value: 1.1 × $10^7$ $M^{-1}$ from ref.[79]).

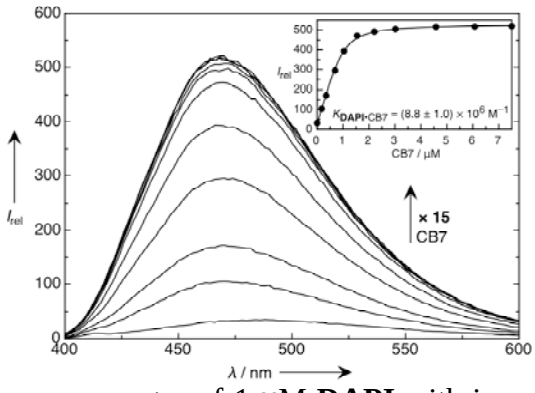


**Figure 2.3.1** Fluorescence spectra of 1 μM **DAPI** with increasing concentrations of CB7 in 1 mM HCl, pH 3.0 ($\lambda_{exc}$ = 361 nm). The nonlinear fitting (inset) based on the fluorescence plots ($\lambda_{obs}$ = 468 nm) assumes a 1:1 complexation model, from which the association constant was derived.

Transfer of hydrocarbons into the aqueous **DAPI**•CB7 (1.0 μM **DAPI** and 2.0 μM CB7) solutions resulted again in a time-resolved, continuous decrease of the fluorescence intensity, and a plateau region was reached from which the binding constants were determined, analogously to the procedure for CB6 (repeated end-point measurements). Alternatively, independent titrations at varying gas concentrations (by either varying the pressure and assuming Henry's law or by determining the gas content by $^1$H NMR in $D_2O$ solutions) were also carried out (Figure 2.3.2).

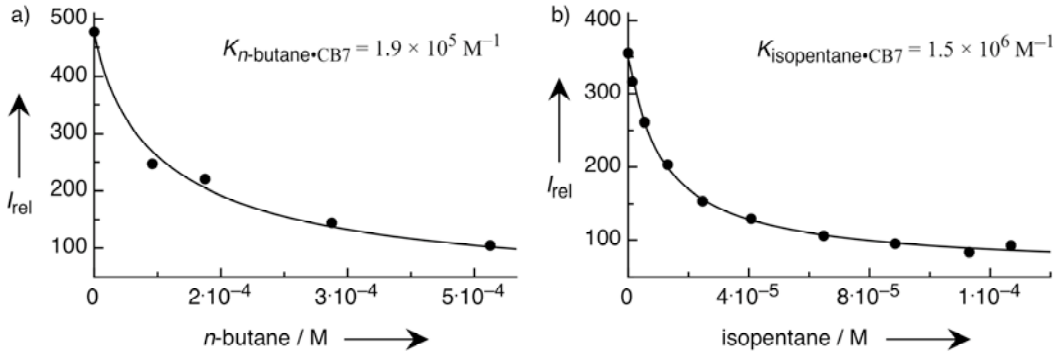


**Figure 2.3.2** Plot of the fluorescence intensity of competitive displacement of **DAPI** (1 μM) from CB7 (2 μM) upon addition of a) different concentrations (pressures) of *n*-butane and b) increasing concentration of isopentane added from a concentrated stock of 0.22 mM isopentane, (determined by $^1$H NMR). Both titrations were carried out in 1 mM HCl, pH 3.0 ($\lambda_{exc}$ = 361 nm, $\lambda_{obs}$ = 468 nm). The nonlinear fittings were made according to eq. 2.2.

Expectedly, the maximum of the binding constants for CB7 (Table 2.3.1), when compared to those for CB6 (Section 2.2), was displaced towards larger alkanes. Among the gaseous analytes the highest affinity was identified for neopentane ($1.7 \times 10^6\ M^{-1}$), which showed no complexation with CB6. A preferential binding of the more spherical branched hydrocarbons over their linear isomers (e.g., neopentane *vs.* *n*-pentane), as well as the lower affinity of the unsaturated analytes compared to the saturated ones (e.g., 1-butene *vs.n*-butane) was also found for CB7.

**Table. 2.3.1.** Binding constants of hydrocarbons and selected neutral guests with CB7 in water, pH 3.0.[a]

| | Guest [Volume/Å$^3$][b] | PC[c] [%] | $K$ [$10^3$ M$^{-1}$] |
|---|---|---|---|
| | *hydrocarbons* | | |
| ≤ C3 | short hydrocarbons [≤ 63] | ≤ 26 | ---[d] |
| C4 | *n*-butane [80] | 33 | 170 ± 40 |
| | 1-butene [75] | 31 | 36 ± 0.7 |
| | isobutane [79] | 33 | 270 ± 80 |
| | isobutene [75] | 31 | 52 ± 15 |
| C5 | *n*-pentane [96] | 40 | 320 ± 80 |
| | isopentane [96] | 40 | 1470 ± 660 |
| | neopentane [96] | 40 | 2100 ± 960 |
| | cyclopentane [86] | 35 | 520 ± 260 |
| C6 | *n*-hexane [113] | 47 | 1800 ± 700 |
| | isohexane [113] | 47 | 1300 ± 300 |
| | 2,3-dimethylbutane [113] | 47 | 8100 ± 5000 |
| | cyclohexane [102] | 42 | 2200 ± 1400 |
| | benzene [89] | 37 | 20 ± 8 |
| C7 | *n*-heptane [130] | 54 | 3300 ± 700 |
| C8 | *n*-octane [147] | 61 | 4500 ± 700 |
| C9 | *n*-nonane [164] | 68 | 13000 ± 2000 |
| | *selected guests* | | |
| | cyclopentanone [87] | 36 | 55 ± 15 |
| | tetrahydrofuran [77] | 32 | 3.5 ± 0.2 |
| | furan [67] | 28 | 0.55 ± 0.06 |
| | *fluorinated guests* | | |
| | perfluorohexane [152] | 63 | 8900 ± 2300 |
| | methylperfluorocyclohexyl [116] | 48 | 8500 ± 1300 |

[a] Determined by competitive fluorescence titrations with the **DAPI**·CB7 reporter pair, at 298 K. [b] Obtained from AM1-optimized geometries. [c] Packing coefficient, obtained by dividing the guest volume by the inner cavity volume of CB6 (242 Å$^3$, from ref.[34]). [d] Weak binding.

As deduced on one side from the larger inner cavity volume of CB7 (242 Å$^3$),[34] and on the other side from the fluorescence responses detected, CB7 encapsulates also higher alkanes with very high, but relatively constant binding constants (> $10^6$ M$^{-1}$), which provides another contrast to CB6. Whether this is

due to a curling or back-folding of the longer alkanes within the inner cavity, or due to the fact that the threading of the longer alkyl chains through the larger CB7 portals does not require a desolvation of the carbonyl groups remains to be scrutinized *via* future computational studies. Of particular interest is the encapsulation of perfluorinated guests by CB*n*. Due to polarizability considerations, of both guest and inner CB cavity, a very strong binding has been anticipated. This is also what has been observed within the preliminary results corresponding to perfluorohexane and methylperfluorocyclohexyl; further investigations will follow.

The CB6 and CB7 studies comprise the most extensive sets of experiments dealing with the binding of neutral guests, such as low-molecular-weight hydrocarbons by this class of macrocycles. For the first time, the fluorescence-based indicator-displacement methodology, as described herein, has been implemented for assessing affinities of volatile compounds towards macrocycles, as well as for a real time-monitoring of their encapsulation in relation to concentration changes. While the experimental results are of fundamental importance towards a better understanding of the hydrophobic forces that trigger host-guest complexation in supramolecular assemblies involving CB*n*, the neopentane purification example described above, shows that immediate practical applications can be readily envisaged, mainly with respect to gas separation, storage, and sensing.

# CHAPTER 3

## *– Analyte Sensing in the Course of Enzymatic Reactions –*

In Chapter 2, I have shown how reporter pairs composed of water-soluble macrocycles and fluorescent dyes can be used for time-resolved monitoring of concentration changes for volatile hydrocarbons and gases in general. Supramolecular tandem assays (see Chapter 1) can be similarly used for following changes in analyte concentration, specifically when the analyte of interest serves as substrate or product of an enzymatic reaction. While the methodology of supramolecular tandem assays has been established for amino acids as substrates and decarboxylases as enzymes, my task in the course of my PhD studies was three-fold:

1. Introduce for the first time *anion-receptors as macrocycles* to broaden the scope of the method. The project resulted in the development of a supramolecular tandem assay for direct continuous monitoring of dephosphorylation of ATP, in particular, and nucleotide triphosphates, in general.

2. Transfer the methodology to *biological transformations of biomacromolecules*, particularly to methylation of lysine residues in extended peptides. Using the tandem strategy we were able for the first time to monitor the formation of trimethylated peptides in homogeneous solution in a label-free, time-resolved, continuous fashion.

3. Establish a convenient methodology for monitoring the enzymatic activity of L-aspartate-α-decarboxylase with the final goal of *validating the potential of drug-like inhibitor molecules* against the enzyme, which were obtained from a structure-based high-throughput *virtual* screening.

## 3.1 IMPLEMENTATION OF ANION-RECEPTOR MACROCYCLES FOR MONITORING TIME-RESOLVED CHANGES OF NUCLEOTIDE CONCENTRATIONS

Since our initial reports on tandem assays were limited to cationic analytes using cation-receptor macrocycles, the focus of my present project was shifted towards investigating enzymatic transformations involving anionic metabolites, such as nucleotides, and particularly adenosine triphosphate (ATP). Numerous supramolecular receptors for nucleotides have already been introduced with the general aim to achieve a high selectivity and ultimate goal to construct biological sensors (see Chapter 1). While some of the reported receptors operate in aqueous solution and partly under physiological conditions, practical applications have nonetheless remained scarce. In order to design a supramolecular tandem assay involving negatively charged metabolites the use of macrocycles with anion-receptor properties is required.[8]

The first step I had to take, which in fact is an essential stage for the design of any supramolecular tandem assay, was to establish an appropriate reporter pair. Our desiderata in this respect were as follows: *i*) a large fluorescence response upon dye complexation; *ii*) a strong macrocycle-dye binding; and *iii*) a large differentiation in binding between nucleotide tri- and monophosphates, which coincide with the substrates and the products of the dephosphorylation reactions. I proceeded by screening a combinatorial library consisting of ten water-soluble anion receptors, which were partly known to complex with nucleotides,[44,68,128-130] in combination with nine water-soluble fluorescent dyes (Charts 3.1.1 and 3.1.2).

Following the combinatorial screening, two reporter pairs were identified and implemented into our supramolecular tandem assay methodology. A novel reporter pair consisting of the amino-γ-cyclodextrin **1** in combination with 2-anilinonaphthalene-6-sulfonate (ANS) was established. Among the systems previously reported in the literature, the one introduced by Ramaiah and co-workers consisting of cyclophane **2** and 8-hydroxy-1,3,6-pyrene trisulfonate (HPTS) as dye,[67] showed particular promise. The main advantage of the **2**/HPTS reporter pair, which was suggested to me by Dr. Andreas Hennig, was the

differential affinity of macrocycle **2** towards ATP, ADP, and AMP as concluded from indicator displacement experiments. Since macrocycle **2** was not available in our laboratory, I synthesized it according to the literature,[128] with minor modifications (Scheme 3.1.1).

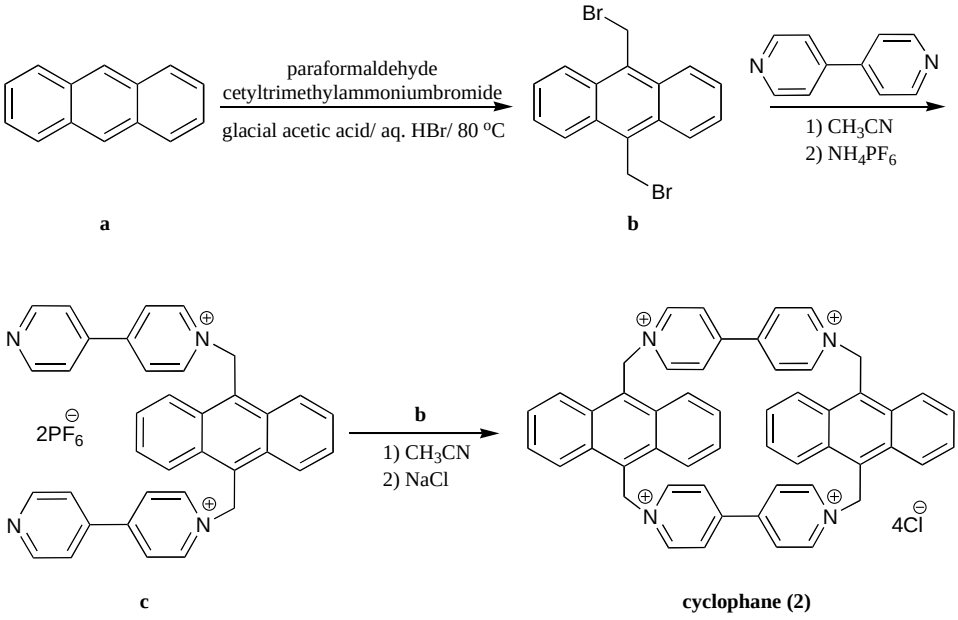


**Scheme 3.1.1.** Cyclophane (**2**) synthesis (*cf.* Chapter 4 for experimental details).

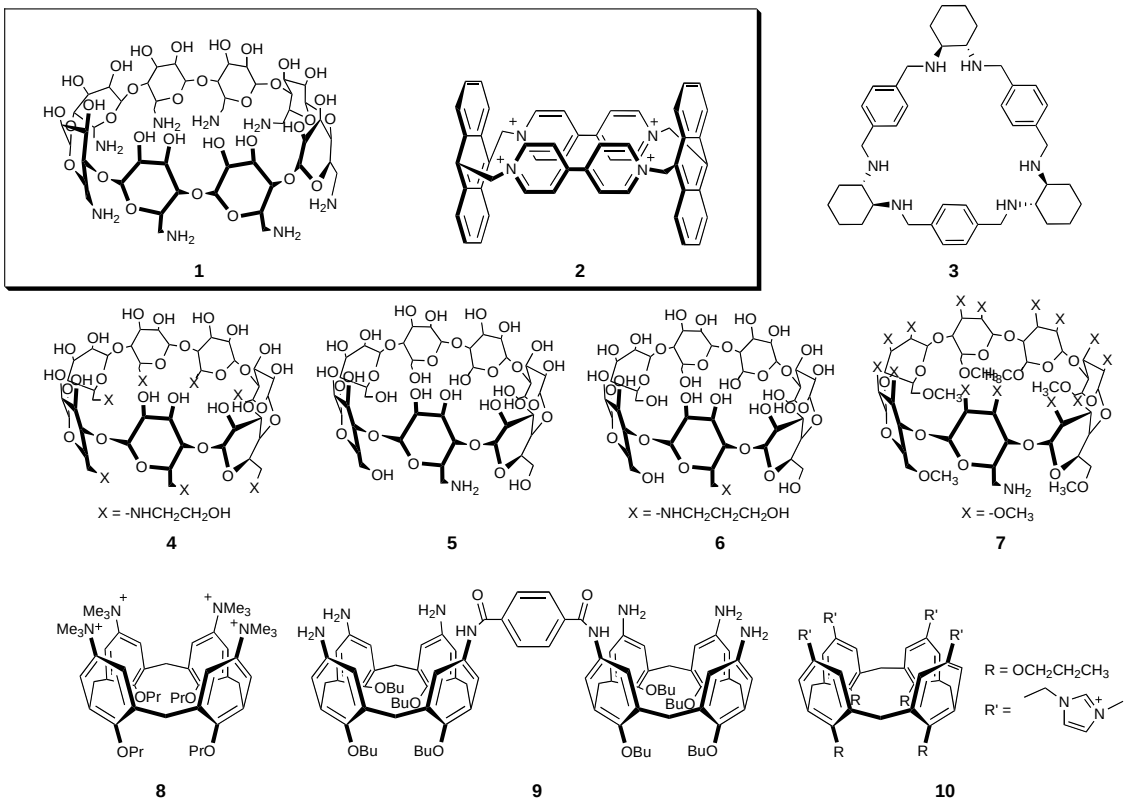


**Chart 3.1.1.** Investigated macrocycles with anion-receptor properties.

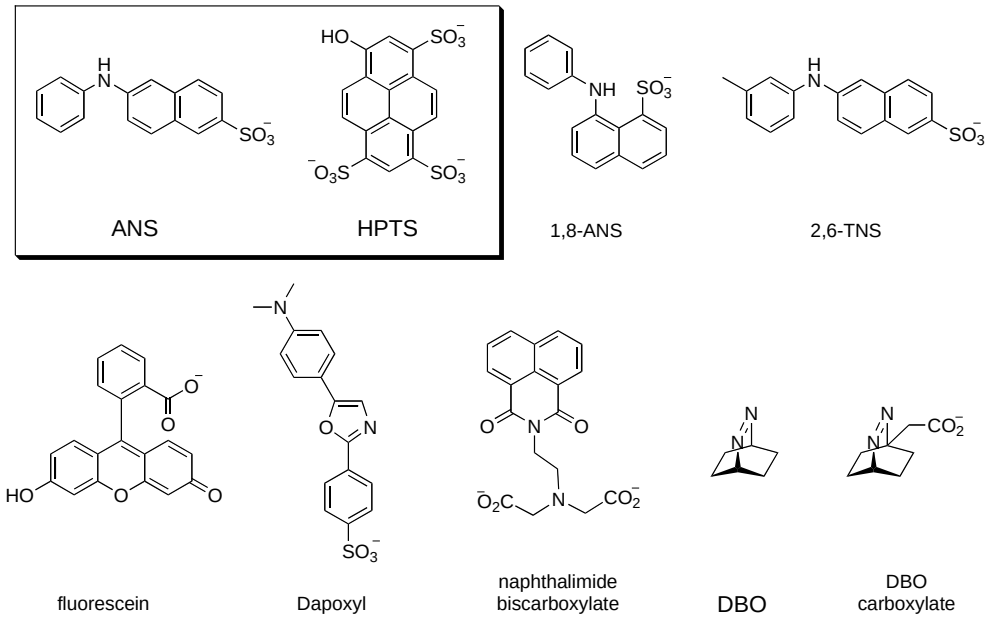


**Chart 3.1.2.** Anionic and neutral fluorescent dyes investigated in combination with the macrocycles in Chart 3.1.1.

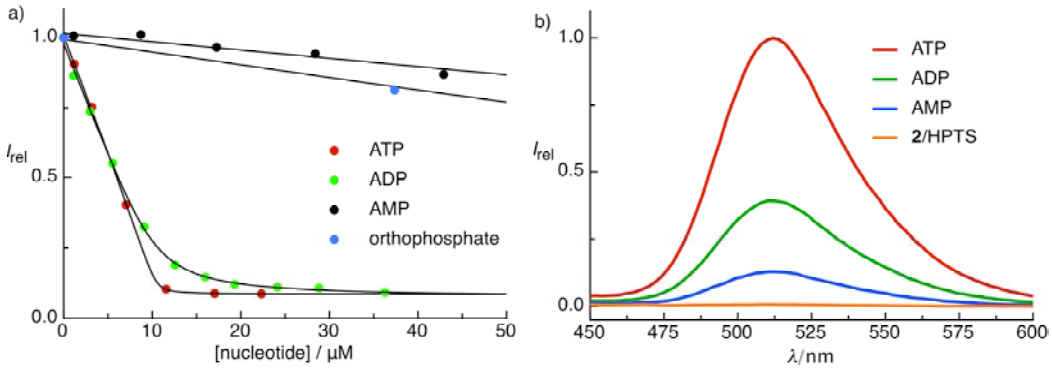


**Figure 3.1.1.** a) Changes in fluorescence intensity of the **1**/ANS reporter pair (10 µM **1** and 25 µM ANS, $\lambda_{exc}$ = 318 nm) upon displacement by varying concentrations of ATP, ADP, AMP, and orthophosphate ($\lambda_{obs}$ = 462 nm) in NaOAc buffer, pH 5.5. b) Changes in fluorescence spectra of the **2**/HPTS reporter pair (both 6.3 µM, $\lambda_{exc}$ = 403 nm) upon addition of ATP, ADP, and AMP (4 mM) in succinate buffer, pH 6.5.

For both ANS and HPTS, the addition of macrocycles **1** and **2**, respectively, resulted in strong fluorescence responses, either enhancement (for ANS, by a factor of 17), or quenching (for HPTS, by a factor larger than 2000). The addition of different nucleotides caused a reversal of these changes due to

their competitive binding as can be seen from Figure 3.1.1, with both reporter pairs exhibiting a charge-dependent differentiation, e.g., between ATP, ADP, and AMP (binding constants in Table 3.1.1). However, the main goal was not to simply detect the analytes of interest, but rather to be able to monitor the real-time concentration changes, as they occur during the dephosphorylation process catalyzed by potato apyrase. The enzyme (an ATP-diphosphohydrolase, E.C. 3.6.1.5) hydrolyzes phosphate bonds of organic and inorganic compounds and its activity has been characterized in both animal and plant tissues.[131-134]

**Table 3.1.1.** Binding constants of **1** and **2** with the substrate as well as with the intermediary and final enzymatic products.

| Guest | $K/(10^6\ M^{-1})$ (**1**)[a] | $K/(10^3\ M^{-1})$ (**2**)[b] |
|---|---|---|
| ATP | 100 ± 60 | 4.5 ± 1.0 |
| ADP | 2.8 ± 0.8 | < 1 |
| AMP | 0.011 ± 0.003 | < 1 |
| Orthophosphate | 0.05 ± 0.01 | < 0.1 |

[a] Determined by competitive fluorescence titrations using **1**/ANS in 50 mM NaOAc buffer, pH 5.5, *cf.* Fig. 3.1.1a. The binding constant of **1**/ANS was $(1.7 \pm 0.1) \times 10^4\ M^{-1}$. [b] Determined by competitive fluorescence titrations using **2**/HPTS in 10 mM phosphate buffer, pH 7.4. The binding constant of **2**/HPTS was determined as $(7 \pm 3) \times 10^6\ M^{-1}$.

The working principle of the assay is illustrated in Scheme 3.1.2 and it relies on the propensity of the positively charged macrocycles **1** and **2** to form self-assembled complexes with the negatively charged guests, such as ANS and HPTS, as well as ATP. Behaving as a strong competitor, ATP displaces the fluorescent dyes, resulting in a low or high initial fluorescence intensity, respectively. Upon enzymatic dephosphorylation, AMP and orthophosphate are being formed as the final products, which, in turn, behave as weak competitors due to their lower net negative charge. Drawing inspiration from the indicator displacement principle, a continuous uptake of the fluorescent dyes with the macrocycles takes place, facilitated by the depletion of the competing substrate, ATP. This results in a switch-ON (for **1**/ANS) or switch-OFF (for **2**/HPTS) fluorescence response, which allows for a highly sensitive monitoring of the *concentration changes* of the analytes during the enzymatic conversion (Figure

3.1.2). The occurrence of the enzymatic reaction on the same time scale was independently monitored by $^{31}$P NMR (Figure 3.1.3).

Conceptually, the resulting tandem assay can be qualified as substrate-selective because the substrate binds more strongly than the product. Since the guest-macrocycle exchange equilibria are faster than the enzymatic reactions, the response of the system to *concentration changes* is immediate and it allows for *real-time continuous kinetic monitoring*.

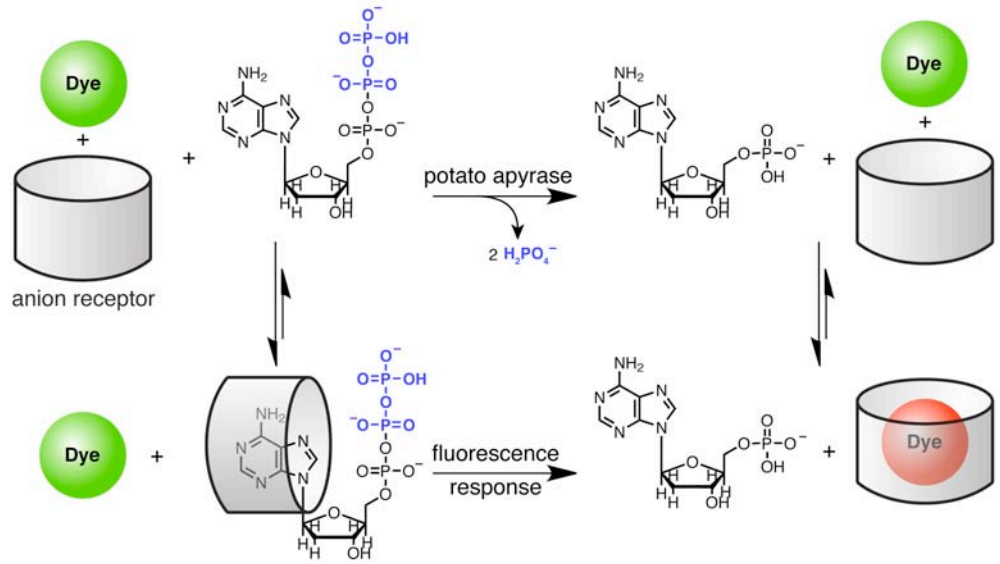


**Scheme 3.1.2.** Working principle of a substrate-selective supramolecular tandem assay for monitoring ATP depletion by dephosphorylation.

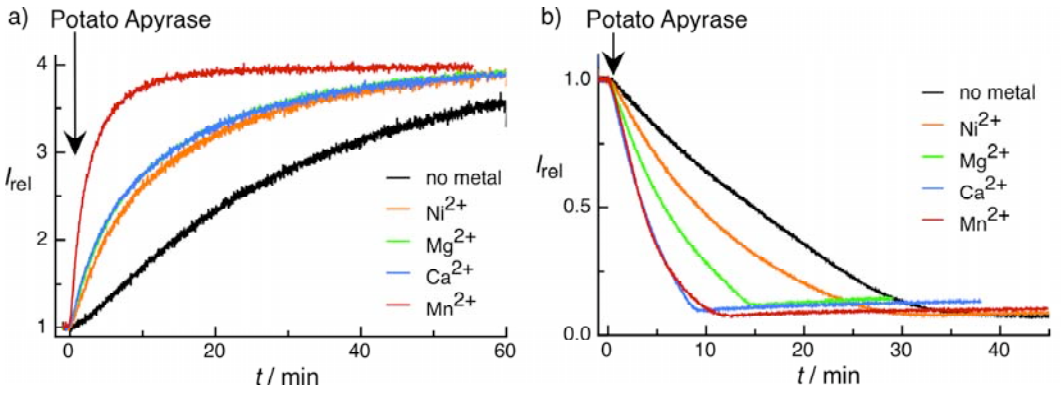


**Figure 3.1.2.** Evolution of normalized fluorescence intensity monitoring potato apyrase activity with and without activating metal ions (1.7 mM). Assays were initiated by addition of a) 25 μg/ml enzyme to ATP (25 μM) with the **1**/ANS reporter pair (25 μM both) and b) 100 μg/ml enzyme to ATP (2.3 mM) with the **2**/HPTS reporter pair (6.3 μM both).

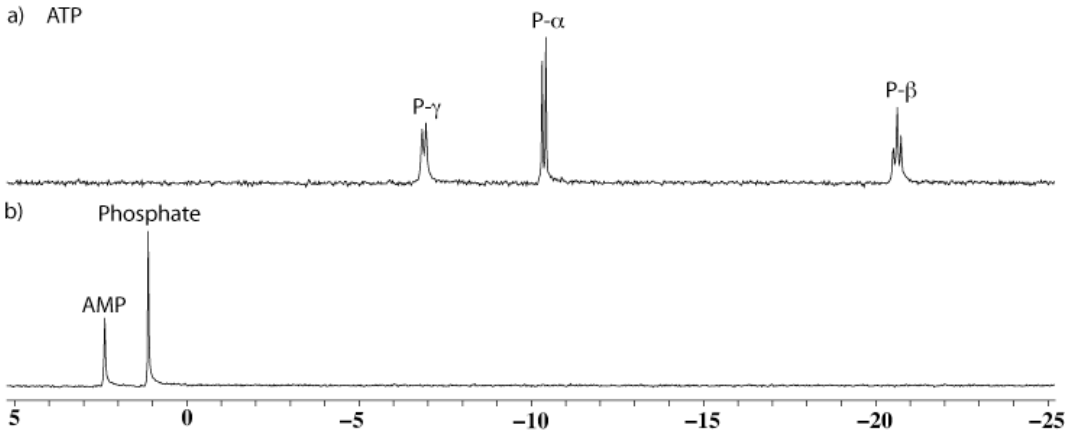


**Figure 3.1.3.** $^{31}$P NMR spectra of 5 mM ATP in $D_2O$ with 1.6 mM $CaCl_2$ a) before and b) after enzymatic conversion to AMP and orthophosphate.

Enzyme assays applicable for screening of inhibitors are highly desirable, especially in the pharmaceutical industry. While the potential of tandem assays to screen for inhibitors has been demonstrated,[43,78,90] the ATP depshosphorylation assay offered for the first time the complementary opportunity for *screening of activators*, namely divalent metal ions ($Ni^{2+}$, $Mg^{2+}$, $Mn^{2+}$, and $Ca^{2+}$). In all cases, rate enhancements by a factor of 1.3 to 17 were observed (Figure 3.1.2), with $Ca^{2+}$ and $Mn^{2+}$ being the most potent activators, consistent with literature findings obtained by more laborious and complex multi-step colorimetric and isotope-based immunoassays.[132-134]

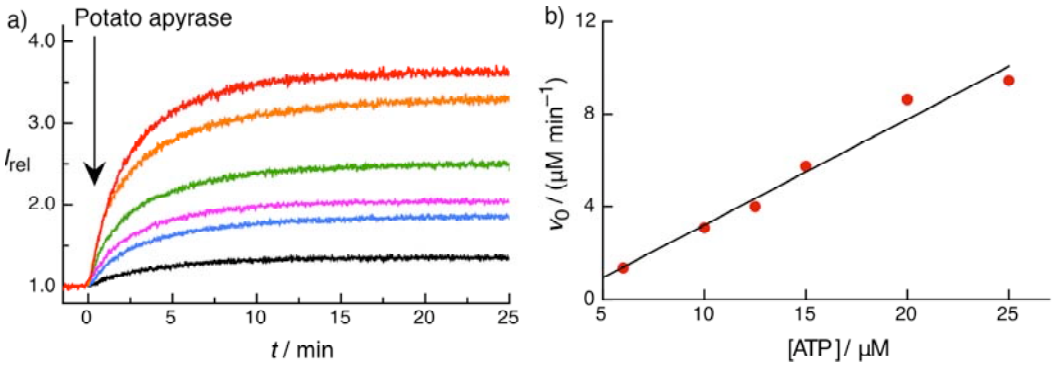


**Figure 3.1.4.** a) Evolution of normalized fluorescence intensity monitoring potato apyrase activity at different substrate (ATP) concentrations with the **1**/ANS reporter pair (both 25 μM, in NaOAc buffer, pH 5.5, with 1.8 mM $Mn^{2+}$, $\lambda_{exc}$ = 318 nm, $\lambda_{obs}$ = 462 nm). ATP concentrations (in μM) are, from bottom to top

trace: 6, 10, 12.5, 15, 20, and 25. b) Plot of the initial rates, $v_0$, *versus* substrate concentration and linear correlation line. The initial rates were obtained by linear fits of the normalized intensities (assuming a conversion linear with the fluorescence intensity and full conversion at the plateau region).

In addition to the opposite fluorescence responses, the two reporter pairs are also complementary with respect to their affinities towards the concentration ranges of the analytes, μM and mM, respectively, which determine the substrate concentration at which the assay is being carried out. The reported $K_M$ values for potato apyrase range from 24 μM to 200 μM,[132,133] which means that the **1**/ANS and **2**/HPTS reporter pairs allow for adjustment at will of the analyte concentration, either below or above the $K_M$ value. Consequently, when using the **1**/ANS reporter pair, the initial rates do increase linearly with the substrate concentration (Figure 3.1.4), in contrast to the situation in which **2**/HPTS is employed. In this scenario, since a large excess of substrate is being used, the enzyme kinetics is expected to be zero-order with respect to the substrate concentration and carried out at a rate, which we assigned to the maximum velocity, $v_{max}$. Experimentally, the $v_{max}$ value obtained was 0.17 μmol/min, in excellent agreement with the reported commercial activity of the enzyme (0.19 μmol/min). As shown for both reporter pairs, the initial rates of ATP dephosphorylation were directly proportional to the enzyme concentration (Figure 3.1.5).

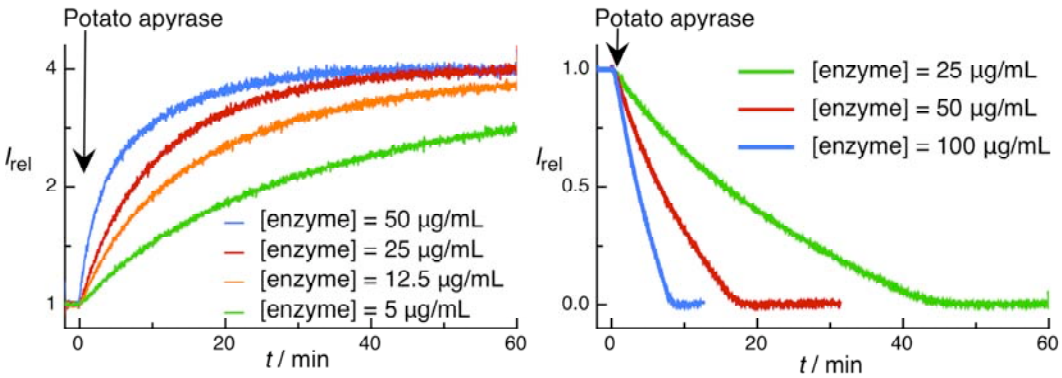


**Figure 3.1.5.** Evolution of normalized fluorescence intensity monitoring potato apyrase activity at different enzyme concentrations a) with the **1**/ANS reporter pair (both 25 μM, in NaOAc buffer, pH 5.5, with 1.8 mM $Ca^{2+}$, $\lambda_{exc}$ = 318 nm,

$\lambda_{obs}$ = 462 nm) and ATP (25 μM) as substrate, and b) with the **2**/HPTS reporter pair (both 6.3 μM, in sodium succinate buffer, pH 6.5, with 1.6 mM $Ca^{2+}$, $\lambda_{exc}$ = 403 nm, $\lambda_{obs}$ = 512 nm) and ATP (2.3 mM) as substrate.

Finally, even though the present assay has been explored in detail for monitoring the depletion of ATP by potato apyrase, or conversely for monitoring the enzymatic activity *via* ATP depletion, the system may be extended to other nucleotides as well. All nucleotide triphosphates caused fluorescence responses *via* competitive displacement (fluorescence decreases for the **1**/ANS reporter pair and fluorescence increases for the **2**/HPTS reporter pair, Figure 3.1.6). The "poor" selectivity of these two anion receptors presents in fact an advantage for tandem assays, allowing dephosphorylation of several nucleotides to be monitored (Figure 3.1.7).

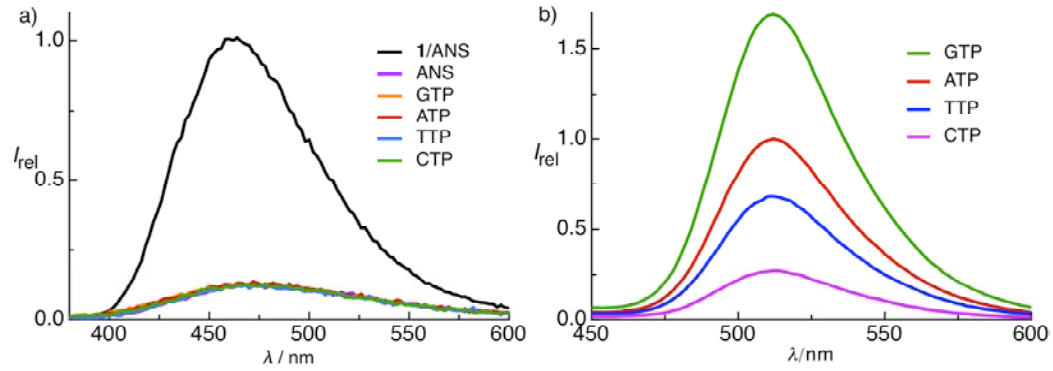


**Figure 3.1.6.** a) Changes in fluorescence intensity of the **1**/ANS reporter pair (10 μM **1** and 25 μM ANS) upon displacement by different nucleotide triphosphates (16 μM). b) Changes in fluorescence spectra of the **2**/HPTS reporter pair (both 6.3 μM) upon addition of different nucleotide triphosphates.

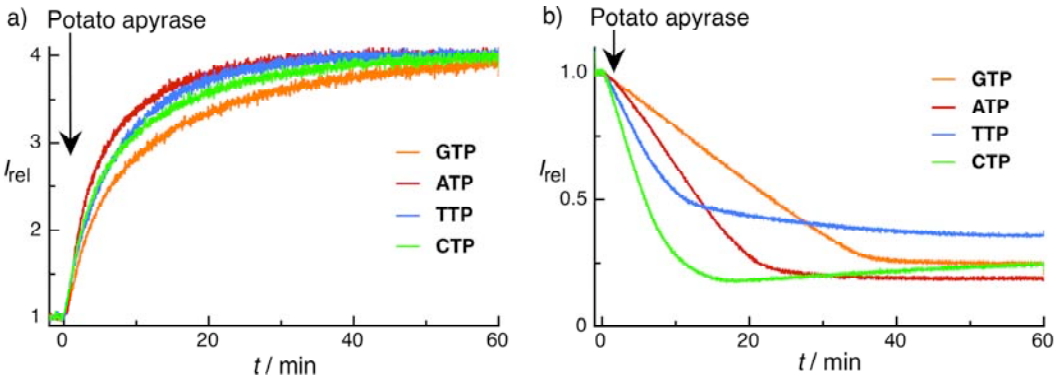


**Figure 3.1.7.** Evolution of normalized fluorescence intensity monitoring

dephosphorylation of various nucleotide triphosphates. Assays were initiated by addition of a) 12.5 μg/ml potato apyrase in the presence of **1**/ANS (25 μM both) to nucleotides (25 μM), and b) 100 μg/ml potato apyrase in the presence of **2**/HPTS (6.3 μM both) to nucleotides (4 mM).

In conclusion, I was able to successfully introduce and exploit the use of macrocycles with anion-receptor properties within the area of supramolecular tandem assays. Specifically, the biocatalytic dephosphorylation of ATP, as well as of other nucleotides by potato apyrase was explored. Additionally, the present assay should also be transferable to the monitoring of other related enzymes. Given that ATP is the most commonly employed cofactor, a general assay for monitoring ATP consumption, could, in fact, lead to a remarkable biochemical application. The results presented herein have resulted in a full-article publication (Appendix 4).

## 3.2 TIME-RESOLVED CONTINUOUS MONITORING OF HISTONE TAIL LYSINE METHYLATION

While they have been applied to a wide variety of enzyme classes (see Chapter 1.4), up to now supramolecular tandem assays have been to a certain degree restricted to – even though highly biologically relevant – structurally simple, low-molecular-weight biomolecules, such as amino acids, biogenic amines, and choline type compounds.[43,75,76,78] The most complex analytes involved nucleotides (Chapter 3.1),[135] and just recently, the tandem assay has also been applied to short peptides (up to 5 amino acids) for monitoring protease activity.[90] My second objective has been to transfer the supramolecular tandem assay methodology for monitoring methylation of lysine residues within extended and complex biomacromolecular peptide substrates. Specifically, the enzymatic activity of *Neurospora crassa* Dim-5, an example of a histone lysine methyltransferase (HKMT), has been investigated. The present project has been part of a collaboration with the biochemical research group of Prof. Albert Jeltsch, Jacobs University Bremen, who has provided us with the Dim-5 enzyme, which needed to be expressed and purified, as it is not commercially available.

Histone lysine methyltransferases (HKMTs) are enzymes responsible for lysine methylation at specific sites of histone tails using *S*-adenosyl-L-methionine (AdoMet) as methyl donor, which, following ATP, is the second most common enzyme cofactor.[136,137] Histone methylation plays a major role in gene regulation,[138] and therefore abnormal modifications have been associated with several disorders and diseases, including cancer.[139,140] Up to now, most assays able to detect methylation rely on radioactive labeling of AdoMet.[141-144] Label-free assays rely on classical chromatographic or mass spectrometric detection,[145,146] the use of specific antibodies,[147-149] and recently, quantum dot fluorescence energy transfer was reported as an alternative technique to signal DNA methylation.[150] All methyltransferases share a common by-product, *S*-adenosyl-L-homocysteine (AdoHcy), and therefore, several assays focused on tracking AdoHcy production by coupling secondary enzymes. For instance, AdoHcy can be converted into *i*) adenine and then hypoxanthine, which can be detected by its characteristic, even if short-wavelength, absorption at 265 nm;[151] *ii*) homocysteine, which can itself react with various reagents to allow fluorometric[152,153] or colorimetric detection;[154] or into *iii*) ATP *via* three sequential enzyme-coupled reactions, which can be ultimately measured using a luciferase kit.[155] Although some of the existing assays certainly stand out due to their high sensitivity, obvious drawbacks, such as the need for multiple immobilization and separation steps, chemical follow-up reactions, additional enzymatic transformations, the use of radiotracers, and the limitation to discontinuous monitoring, still remain. Some of these aspects are severe impediments towards quantitative enzymological kinetic studies and pharmaceutical-industrial high-throughput screening.

Given the potential therapeutic role of inhibitors for HKMTs, the development of more efficient and convenient screening methods for these enzymes, such as sensitive, fluorescence-based assays, is emerging as a key challenge.[156-161] In order to do so, we have applied the supramolecular tandem assay strategy. Dim-5 is known to processively introduce three methyl groups to the target lysine residue belonging to the histone tail.[162] The target primary amine residue of lysine ($pK_a$ = 10.5), which is in fact partly deprotonated at the working pH, is the one which is enzymatically converted into a quaternary ammonium group with a permanent positive charge. Therefore, the enzymatic

reaction does not only trigger the addition of three methyl groups, which alter the overall size and geometry of the final peptide product, but also changes the charge status of the peptide.

Recall that the key requirement for a suitable reporter pair in any tandem assay is the differential binding between the substrate and the product of the enzymatic reaction with the macrocyclic host. Complementary to the tandem assay for nucleotides (Chapter 3.1), the methylation assay was performed in the *product-selective mode*, exploiting the preferential binding of the product towards the macrocycle. To this end, we have chosen *p*-sulfonatocalix[4]arene (CX4), a cation-receptor macrocycle, which is well known to bind ions (and presumably also trimethylated histone tails peptides) with *high* affinity, and regular amino acid residues (and presumably also unmodified histone tail peptides) with *low* affinity.[43,61,163] In fact, macrocycles of the calixarene and resorcinarene type have been extensively investigated for sensing of cationic bioanalytes, particularly neurotransmitters such as choline, carbamoylcholine, acetylcholine, and L-carnitine (see Chapter 1).[9,10,43,61,64,164,165] As fluorescent dye, lucigenin (LCG, *N*, *N*'-dimethyl-9,9'-biacridinium dinitrate) was selected, whose photophysical behavior in the presence of CX4 has been recently reported by Guo *et al.*[43]

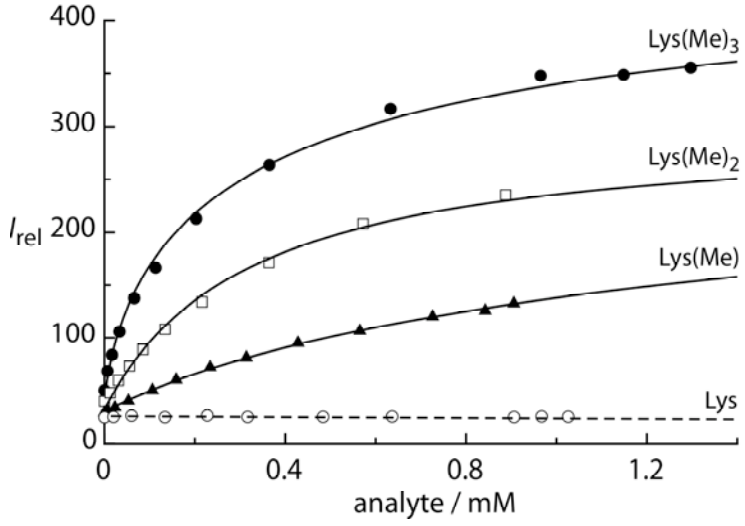


**Figure 3.2.1.** Competitive fluorescence displacement titrations with model compounds using the CX4/LCG reporter pair (1.5 μM/1 μM), $\lambda_{exc}$ = 369 nm, $\lambda_{obs}$ = 510 nm, glycine buffer, pH 10, 25 ºC. The solid lines are fitted to the data. The dashed line shows the baseline (with no response) on which the data points for lysine fall.

LCG is a highly fluorescent dye in its free form, but upon complexation with CX4 (in the present buffer: $K = 2.2 \times 10^7$ $M^{-1}$, essentially identical with the value obtained in ref.[43]) it experiences a full electron transfer, which results in a strong fluorescence quenching. After selecting the reporter pair, the immediate steps towards designing the assay involved competitive fluorescence displacement titrations with model compounds for the substrate and the product of the enzymatic reaction (i.e., lysine and trimethylated lysine, respectively), as well as for the intermediary products (mono- and dimethylated lysine) (Figure 3.2.1). The use of such simple model compounds allows predictions on the differential affinity of the substrate and product of the methylation reaction towards the macrocyclic host. This is extremely useful, when the more complex biomacromolecular analytes are not readily available, such as in our situation. The natural amino acid lysine showed no binding upon addition to the solution containing the CX4/LCG reporter pair, at least not in the investigated concentration range (up to 1 mM). As expected, among the methylated derivatives, the permanently positively charged trimethylated lysine proved to be a strong competitor against the LCG dye for binding to CX4, revealing the highest fluorescence enhancement among the model compounds. Fitting according to a competitive displacement model afforded a binding affinity of $1.3 \times 10^5$ $M^{-1}$ towards CX4, in good agreement to the one obtained for the binding of tetramethylammonium ($1.2 \times 10^5$ $M^{-1}$), acetylcholine ($1.0 \times 10^5$ $M^{-1}$), and carbamoylcholine ($1.1 \times 10^5$ $M^{-1}$),[61] suggesting that the quaternary ammonium group is responsible for the high-affinity binding of CX4.

One has to keep in mind that for tandem assays, a strong affinity or selectivity towards the macrocycle is not a requirement, but rather a difference in binding constants by a factor of 10 or more between the product and the substrate of the enzymatic reaction towards the macrocycle.[78] As can be seen from the titration plots (Figure 3.2.1), even when working in low μM concentrations of substrate, a clear fluorescence response should result when the substrate is enzymatically converted to the trimethylated product. It should be noted in advance that the differentiation expected from the titration experiments with the simple amino acids could not be experimentally realized for the histone tail

peptide methylation. This was due to a smaller differentiation of the actual peptides with CX4; nonetheless, it remained sufficiently large to allow robust assays to be conducted.

**Table 3.2.1**. Peptide substrates assayed in this study

| Entry | Peptide sequence | Assay type employed | |
|---|---|---|---|
| | | Immobilized[a] | Homogeneous[b] |
| **S1** | ARTKQTA**RKSTG**GKA | × | |
| **S2** | RTKQTA**RKSTG**GKAP | ×[c] | × |
| **S3** | TKQTA**RKSTG**GKA | × | |
| **S4** | KQTA**RKSTG**GKA | × | |
| **S5** | QTA**RKSTG**GK | × | |
| **S6** | QTA**RKSTG**GS | × | × |
| **S7** | KQTA**RKSTG**GKAPRK | × | |
| **S8** | KQTA**RKSTG**GKAPR | × | |
| **S9** | KQTA**RKSTG**GKAP | × | |
| **S10** | KQTA**RKSTG**GKA | × | |
| **S11** | KQTA**RKSTG**GK | × | |

[a] Methylation was detected by following the transfer of radioactively labeled methyl groups from AdoMet to the membrane-immobilized peptides (SPOT synthesis), *cf.* ref.[166] [b] Methylation was followed by using the supramolecular tandem methodology in homogeneous solution. [c] Note that the SPOT-synthesized peptide lacked the *C*-terminal proline residue.

Certainly, the "real" peptides corresponding to the unmethylated and trimethylated histone tail required in the assay are structurally very different from the isolated amino acids (lysine and trimethylated lysine) that we have taken as models. For example, while lysine showed negligible binding to CX4, the substrate did show significant binding (*vide infra*), presumably because electrostatic repulsion is most pronounced for the amino acid, whose carboxylate group is juxtaposed to the sulfonato groups of the macrocycle when in complex. However, the only changes triggered by the methylation reaction take place at the lysine amino group, and, therefore, assuming everything else remains constant, the increase in the affinity of product *versus* that of substrate would be relatively the same as the affinity of trimethylated lysine *versus* that of lysine. Among the

peptide sequences of interest (Table 3.2.1), we have selected two substrates, **S2** (RTKQTA**RKSTG**GKAP) and **S6** (QTA**RKSTG**GS) as model compounds to establish a novel supramolecular tandem assay for HKMTs.

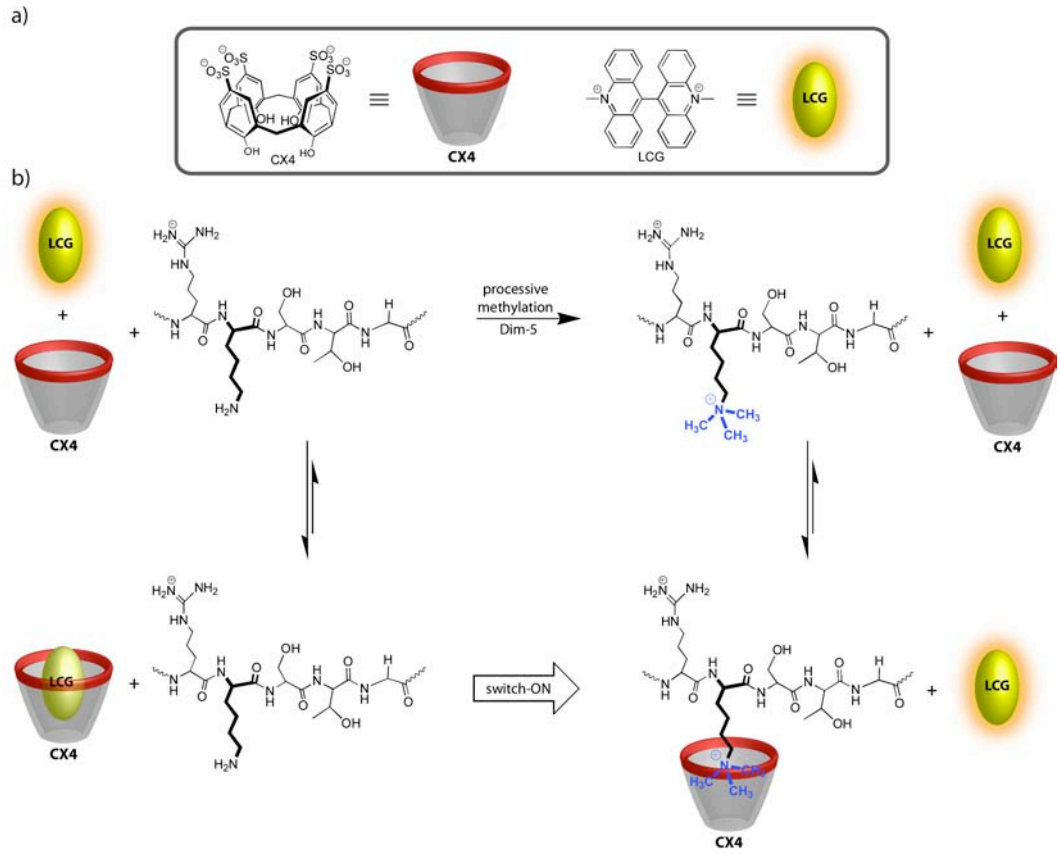


**Scheme 3.2.1.** a) Chemical structures of the reporter pair employed for monitoring the Dim-5 activity, comprised of the macrocycle *p*-sulfonatocalix[4]arene (CX4) and the fluorescent dye lucigenin (LCG). b) Working principle for monitoring the processive methylation of the H3 tail by Dim-5 using the supramolecular tandem assay approach. The target lysine of the enzyme is shown in boldface.

The working principle of our assay for monitoring Dim-5 activity is illustrated in Scheme 3.2.1. The substrate is schematically shown as a short peptide containing the recognition motif for the Dim-5 enzyme (R**K**STG), with K being the methylation site.[143] The substrate of the enzymatic reaction contains only an unmethylated lysine residue, and, based on the low affinity determined for the amino acid lysine (Figure 3.2.1) with the macrocycle CX4, was expected to behave as a weak competitor, unable to effectively displace the dye. Therefore, a

large fraction of LCG remains bound to (and quenched by) CX4, which consequently results in a low fluorescence signal being detected. The addition of the enzyme results in the formation of trimethylated lysine at the target K9 residue, which, in contrast to the unmethylated substrate, again based on the model studies with the trimethyl lysine (Figure 3.2.1), exhibits a much higher affinity towards the host. As the enzymatic reaction proceeds in the presence of the CX4/LCG reporter pair, the fluorescent dye is being continuously displaced from the cavity of the host by the higher affinity trimethylated product. Complying with the product-selective supramolecular tandem assay concept, methylation is accompanied by a fluorescence intensity increase (switch-ON response), which allows for time-resolved online monitoring of the Dim-5 activity in homogeneous solution.

We investigated the enzymatic methylation of free, non-immobilized substrates. We first selected substrate, **S2** (Table 3.2.1), which contains 15 amino acids and corresponds in sequence to the *N*-terminal H3 tail (but lacking the first alanine residue as in **S1**).

A characteristic steady-state fluorescence trace of the methylation assay is shown in Figure 3.2.2, where the effects of all individual assay ingredients on the fluorescence signal can be monitored step-by-step as they are being successively added. CX4 significantly quenches the fluorescence of LCG, which is partially recovered upon adding substrate **S2**, owing to its moderate binding. The subsequent addition of the cofactor, AdoMet has comparably a small effect on the fluorescence intensity. Finally, the methylation reaction is initiated by the addition of the enzyme, Dim-5, which causes a continuous increase in fluorescence intensity. By generating the trimethylated peptide, Dim-5 produces a strong competitor, which is capable of quantitatively displacing LCG from the CX4 cavity, thereby largely recovering the initial fluorescence of the uncomplexed dye. As the fluorescence reaches a plateau region, the full conversion of the substrate is signaled.

Even though all analytes have a certain effect on the fluorescence intensity (Figure 3.2.2), only Dim-5 brings about the time-resolved change, which is the fingerprint of the enzymatic activity itself. That the time course corresponded indeed to the methylation reaction, was independently verified by drawing aliquots from a reaction mixture at different time points and performing

conventional MALDI-TOF MS analysis of the reaction mixture. Expectedly, experiments in the absence of Dim-5 or in the absence of AdoMet, did not show any significant fluorescence change, as no methylation reaction could take place (negative control experiments).

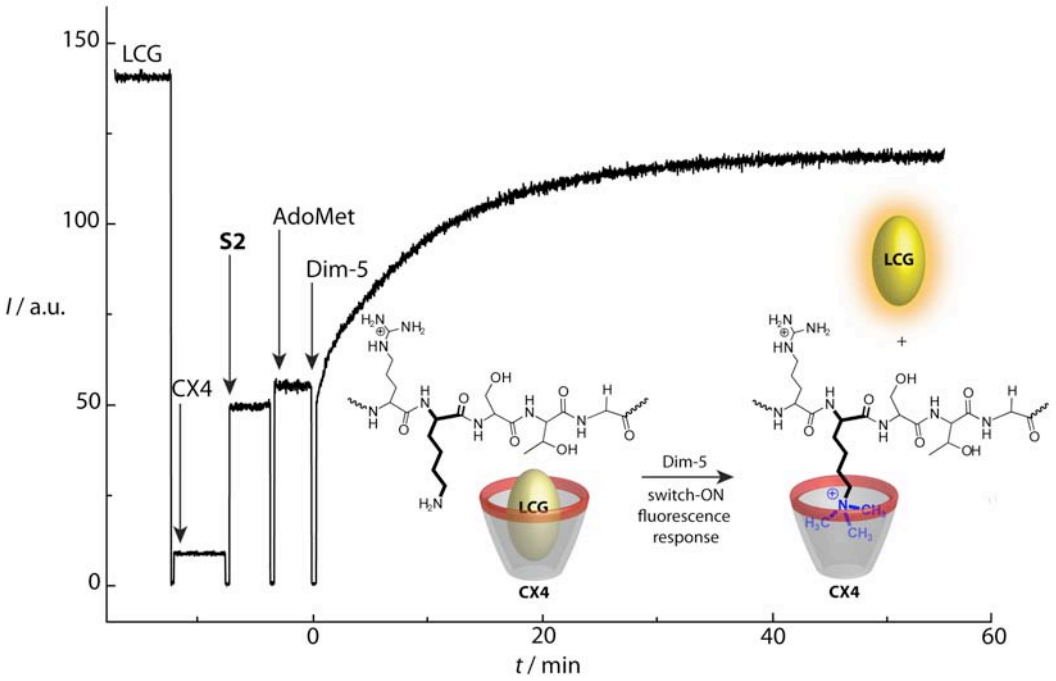


**Figure 3.2.2.** Development of the fluorescence intensity ($\lambda_{exc}$ = 369 nm, $\lambda_{obs}$ = 510 nm) by using the CX4/LCG reporter pair (500 nM/100 nM) for monitoring the methylation of peptide **S2** (5 μM) in the presence of AdoMet (15 μM, the cofactor). The enzymatic reaction was initiated by addition of Dim-5 (100 nM) at $t$ = 0 min, in 5 mM glycine buffer, pH 10, at 25 °C.

Although Dim-5 has been well characterized,[143,144,166-169] only *via* the supramolecular tandem assay strategy a continuous monitoring of the enzyme kinetics is now feasible. The sensitivity of the assay has been limited to ca. 2 μM (below this value insufficient displacement of the product applied) and to the upper end near 10 μM (above this value the substrate caused a too large displacement). The $K_M$ of Dim-5 (7.4 μM)[143] fell exactly within the accessible substrate concentration range, such that substrate **S2** did only show an approximately linear concentration dependence of the initial rates below ca. 5 μM (Figure 3.2.3). Assays were consequently performed under conditions at which the enzyme concentration is rate limiting (typically 5-10 μM substrate **S2** and 3-

fold excess of AdoMet). This was confirmed by running the assays at different enzyme concentrations (Figure 3.2.4), which revealed the expected linear dependence of the initial reaction rates, $v_0$, on enzyme concentration.

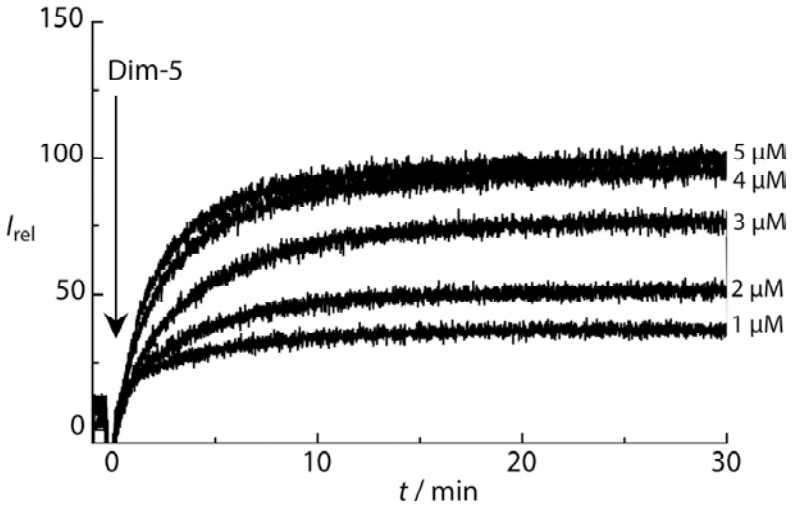


**Figure 3.2.3.** a) Development of fluorescence intensity ($\lambda_{exc}$ = 369 nm, $\lambda_{obs}$ = 510 nm) using the CX4/LCG reporter pair (1.5 µM/1 µM) for monitoring methylation of H3K9 at different substrate concentrations (1-5 µM). The enzymatic reactions were initiated by addition of Dim-5 (150 nM) at *t* = 0 min, in 5 mM glycine buffer, pH 10, at 25 °C.

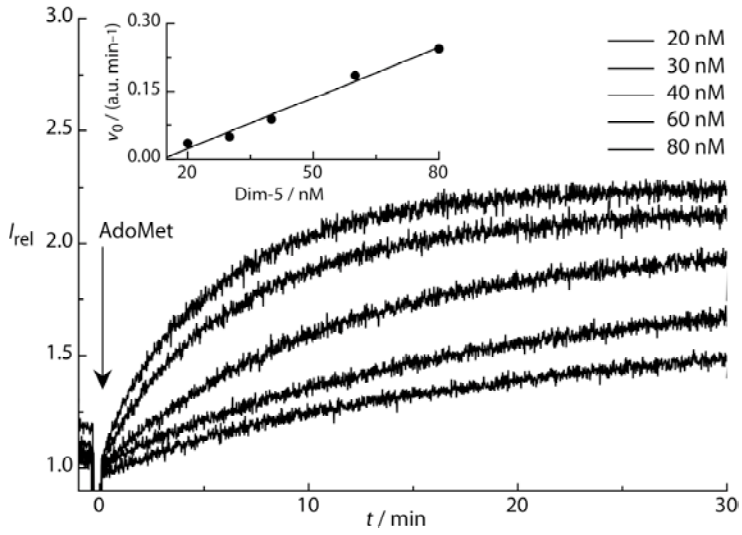


**Figure 3.2.4.** Development of normalized fluorescence intensity ($\lambda_{exc}$ = 369 nm, $\lambda_{obs}$ = 510 nm) monitoring methylation of 5 µM **S2** at different Dim-5 concentrations (20–80 nM) using the CX4/LCG reporter pair (1 µM/0.5 µM). The enzymatic reactions were initiated by addition of 15 µM AdoMet at *t* = 0 min in

glycine buffer, pH 10, at 25 °C. The inset shows the linear correlation between the initial methylation rates, $v_0$, and the different Dim-5 concentrations.

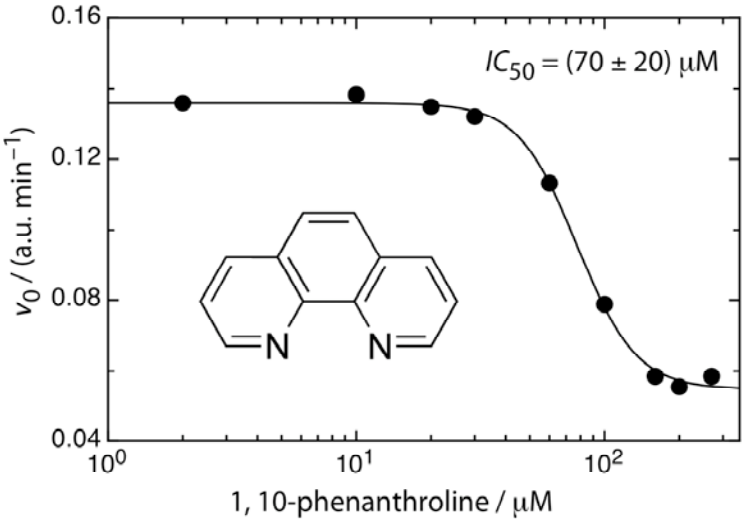


**Figure 3.2.5.** Dose-response curve for inhibition of Dim-5 (150 nM) by 1,10-phenanthroline (0–270 μM) in the presence of 5 μM **S2** by using the CX4/LCG reporter pair (500 nM/100 nM) in 5 mM glycine buffer, pH 10, at 25 °C. The non-vanishing reaction rate at high inhibitor concentration may be due to a residual amount of monomethylation of the substrate (see text).

A unique feature of Dim-5 is the presence of a Zn3Cys9 metal cluster in its pre-SET domain (*S*u(var)3-9, *E*n(zeste) and *T*rithorax)[170], where nine cysteine residues coordinate three zinc ions in an equilateral triangular fashion. However, the zinc content determined for Dim-5 suggests that a fourth zinc ion is present in its structure, coordinated by three cysteines belonging to the post-SET domain and a fourth cysteine found near the active site.[167] Whereas the triangular zinc cluster is a stable motif, the fourth zinc is much more labile, and its capture by chelating compounds such as 1,10-phenanthroline or EDTA results in a reduction, and eventually complete noncompetitive inhibition, of its enzymatic activity.[167] To demonstrate the applicability and potential of the described tandem assay for the screening of methyltransferase inhibitors, we carried out inhibition experiments with 1,10-phenanthroline as transition metal chelator. We first confirmed the absence of trimethylation of peptide **S2** by MALDI-TOF at high concentration of 1,10-phenanthroline (200 μM); only a residual peak of

monomethylated product was observed. We then conducted the assay at increasing concentrations of inhibitor and extracted an $IC_{50}$ value of 70 ± 20 μM from the dose-response curve (Figure 3.2.5), which under the selected concentration conditions corresponds directly to the inhibition constant, $K_i$.[171] Alternatively, the $IC_{50}$ value can also be determined from the fluorescence intensity responses (plateau regions), which present an independent measure of the enzymatic activity. The $K_i$ value determined for 1,10-phenanthroline by tandem assay is well in line with a previous single-point estimate (reduction of Dim-5 activity by approximately 65% in the presence of 100 μM of the same chelator).[167]

The crystal structures of Dim-5 with and without bound peptide substrate are known,[162,167] allowing for insights into the methylation mechanism. The substrate specificity was analyzed using peptide array SPOT synthesis on cellulose membranes, which allows for large libraries of different peptides to be conveniently synthesized and assayed.[166] The methylation activity of Dim-5 towards the different surface-immobilized peptide sequences was followed by the enzymatic transfer of radioactive AdoMet onto the membrane-immobilized peptide substrates.

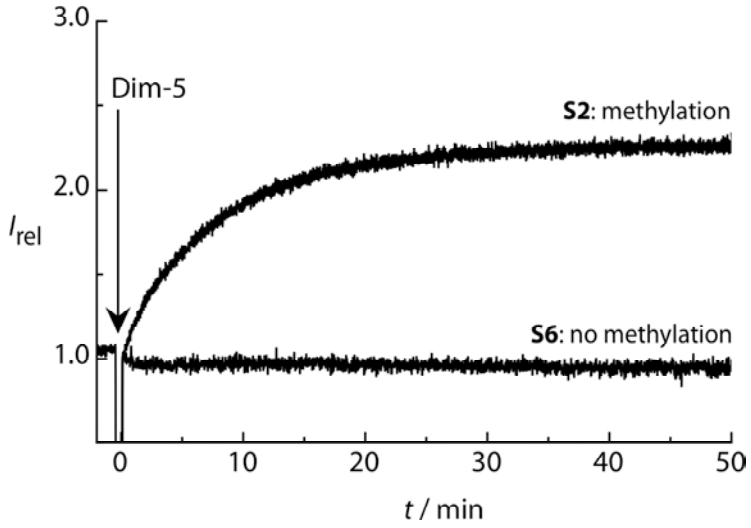


**Figure 3.2.6.** Fluorescence response of substrates **S2** and **S6** (both 7 μM) in tandem assays using the CX4/LCG reporter pair (500 nM/100 nM) in 5 mM glycine buffer, pH 10, at 25 °C, in homogeneous solution. Methylation (or the absence thereof) was verified by MALDI-TOF.

Apart from the main peptidic substrate **S2**, additional substrate sequences (Table 3.2.1) were tested by Dr. Srikanth Kudithipudi (Prof. Albert Jeltsch's research group) using the established SPOT technique. All peptides contained the recognition motif of Dim-5, i.e., residues 8–12 of the H3 *N*-terminus, which is considered to be crucial for the enzyme activity.[166] Our idea was to monitor the implications on methylation of additional substrates, whose length became shorter, both from the *N*- as well as the *C*-terminus. Preliminary SPOT results showed that all immobilized peptides underwent methylation, however, additional experiments are in progress.

The tandem assays described herein have the advantage that they operate in homogeneous solution, however, at the expense of requiring preparative amounts of substrates, as they become accessible by solid-phase peptide synthesis. We therefore limited these assays to substrate **S2** and to a shorter derivative, substrate **S6**. Surprisingly, the tandem assay produced no fluorescence response for substrate **S6** (Figure 3.2.6), suggesting that no methylation occurs in homogeneous solution. These results were corroborated by MALDI-TOF analysis, which also signaled the absence of significant enzymatic activity towards this peptide. Experimentally definitive, when the methylation was carried out under competitive conditions, i.e., in the presence of equimolar amounts of peptides **S2** and **S6**, only the former was enzymatically converted.

It transpires that in addition to the essential presence of the recognition motif, additional considerations, such as the length of the substrate and the phase (homogeneous solution *versus* surface-immobilized substrates), require attention to achieve a more detailed understanding of Dim-5 enzyme specificity. The availability of complementary assays operational under diverse conditions is consequently highly desirable.

We have successfully implemented the supramolecular tandem assay approach for continuous and label-free monitoring of Dim-5 lysine methyltransferase activity, which involved for the first time the use of complex biomacromolecular substrates. The assay bypasses biotinylation as well as radiolabeling and should be transferable to other protein lysine methyltransferases (EC 2.1) to the degree that *trimethylated* lysine residues are generated. It complements existing assay approaches in that it allows monitoring of the enzymatic activity in homogeneous solution and is inherently suitable, owing to

the use of fluorescence for detection, for inhibitor and activator screening. The manuscript corresponding to the project herein has been accepted for publication and is currently in press.[172]

## 3.3 VALIDATION OF DRUG-LIKE INHIBITORS USING NUCLEAR MAGNETIC RESONANCE ($^1$H NMR)

L-aspartate-α-decarboxylase (ADC, E.C. 4.1.1.15), encoded by the *E. coli panD* gene, is an enzyme responsible for the conversion of L-aspartate to β-alanine and its activity has been shown to be crucial for the growth of several microorganisms, particularly *Mycobacterium tuberculosis* (Mtb).[173,174] This is due to the fact that β-alanine contributes to the synthesis of panthotenate (vitamin $B_5$), the precursor of Coenzyme A (CoA). It has been shown that impairing the ability of CoA formation leads to a significant reduction in Mtb virulence,[175] which motivated us to consider ADC as a potential target for therapeutic intervention against tuberculosis. The project has been conducted within a collaboration with Prof. Kunchithapadam Swaminathan, National University of Singapore, who provided us with the enzyme and the potential drug-like inhibitor molecules for experimental testing.

The existing assays for ADC involve laborious derivatization and separation steps,[173,176] or radiometric[177] and manometric techniques,[178] which render them unsuitable for inhibitor screening applications. Even though within our own research group we have developed supramolecular tandem assays for decarboxylases, those for ADC would be highly different due to two reasons: *i*) they would require the use of anion-receptor macrocycles (all previous tandem assays for decarboxylases employed macrocycles with cation-receptor properties),[75,76] and *ii*) the differentiation between such simple analytes as aspartate and β-alanine remains a great supramolecular challenge.[69] While a fluorescence-based supramolecular tandem assay for ADC remains to be developed, we have initially adopted a different approach, namely the use of $^1$H NMR. The experimental results, described herein, were obtained in our laboratory during a short research visit of our collaborators.

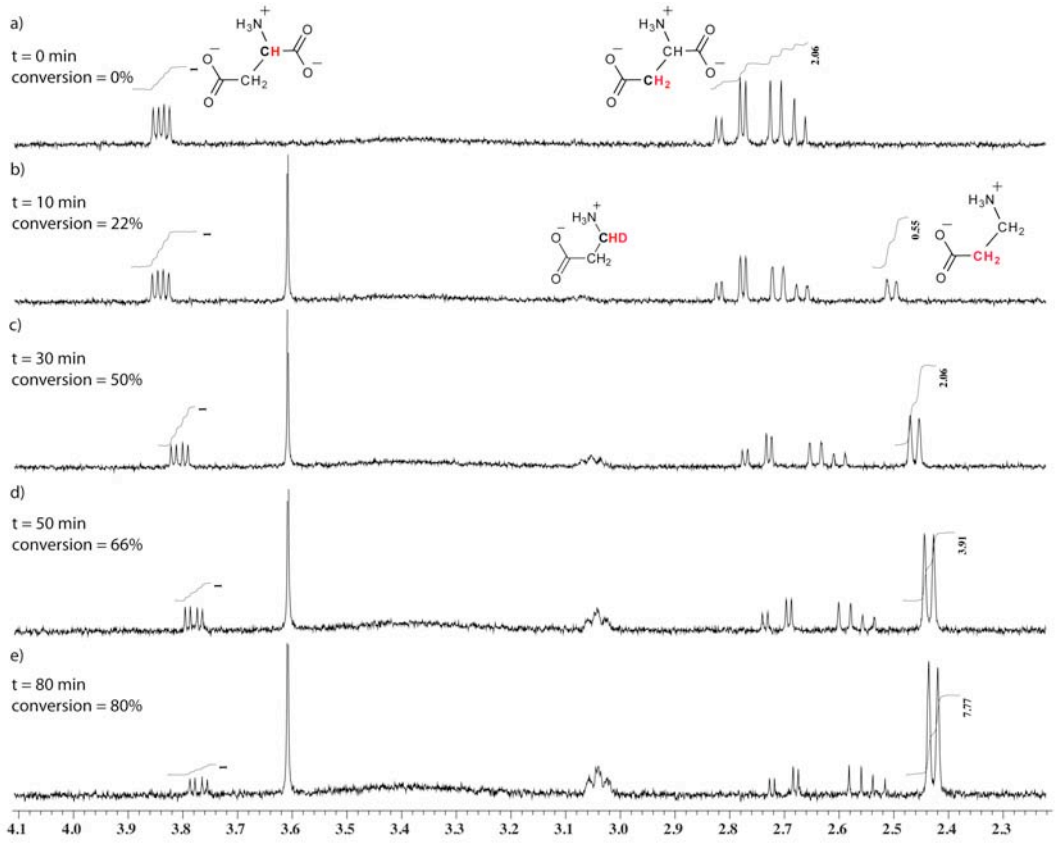


**Figure 3.3.1.** Selected $^{1}$H NMR spectra of 1 mM L-aspartate a) before and b) to e) (10-80 min) after addition of 3 μM ADC in $D_2O$ at 25 $^{o}$C. The diminishing signals of L-aspartate and the emerging of those corresponding to β-alanine have permitted a direct monitoring of the enzymatic transformation and integration of the proton signals have allowed for a kinetic profiling of the reaction (*cf.* Figure 3.3.2).

Before proceeding to inhibitor screening, the enzymatic assay has been optimized with respect to substrate and enzyme concentration. The conversion rates were found to be directly proportional to the enzyme concentration, which we adjusted such that the catalytic reaction could be conveniently monitored. On the other hand, the use of $^{1}$H NMR implies a discontinuous monitoring and a restriction to mM concentration range, as imposed by the instrument sensitivity. However, these considerations did not impede us from monitoring the reaction of interest in a convenient fashion. To this end, the conversion of 1 mM L-aspartate in the presence of 3 μM ADC could be conveniently followed (Figure 3.3.1). L-aspartate shows two resonances, in a 1:2 ratio (Figure 3.3.1a). Upon addition of ADC, the signals corresponding to the product start to emerge in time while those

of the substrate L-aspartate diminish, and eventually completly disappear (Figure 3.3.1 b to e). Note that, based on its structure, one would also expect two different peaks for β-alanine (these were confirmed by simply taking a $^1$H NMR of the commercial analyte). However, only the signals corresponding to the protons adjacent to the carboxylate group could be quantified in the course of the enzymatic reaction (at approximately $\delta$ = 2.44 ppm). This is a consequence of the fact that the reaction is carried out in $D_2O$, and, therefore, the newly acquired β-alanine hydrogen is, in fact, a deuterium atom. This is also in line with both the broadness of the signal identified at approximately $\delta$ = 3.04 ppm and the splitting pattern (a doublet) of the upfield-shifted protons.

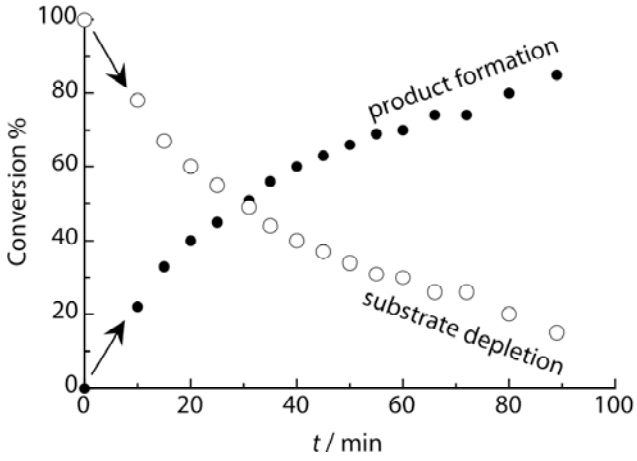


**Figure 3.3.2.** Kinetic monitoring of ADC activity carried out using 1 mM L-aspartate and 3 μM enzyme. The different points correspond to the individual $^1$H NMR spectra taken at various times upon initiating the reaction in $D_2O$ at 25 $^o$C.

Accordingly, the depletion of the L-aspartate substrate and the concomitant formation of β-alanine can be clearly detected and, upon integration, also quantified. This has finally allowed us to extract a kinetic profile of the enzyme (Figure 3.3.2), which does not only depict a time-resolved monitoring of β-alanine formation as a result of the enzymatic activity, but also serves as a basis for subsequent inhibition studies. We have carried out the inhibition experiments in a similar manner, and the enzymatic conversion at specific reaction times in the presence of inhibitor was compared to that in its absence, as defined by a relative inhibitory effect, $k_{rel}$ (*vide infra*). Please note that since it is desirable to work in

the linear region of the enzyme kinetic trace, we have focused on the conversion percentages at $t < 40$ min.

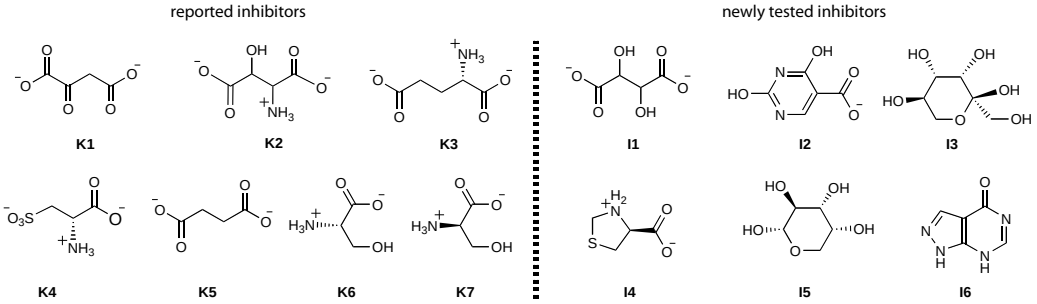


**Scheme 3.3.1.** Chemical structures of known and computationally identified potential inhibitors against ADC, obtained *via* virtual screening.

**Table 3.3.1.** Relative inhibitory effects of selected reported and newly tested compounds against ADC.[a]

| | Compound | Conversion %[b] | $k_{rel}$[c] | Classification |
|---|---|---|---|---|
| | *Reported compounds*[177] | | | |
| **K1** | oxaloacetate | 0 | 0 | very strong |
| **K2** | β-hydroxy-aspartate | 18 | 0.36 | strong |
| **K3** | L-glutamate[d] | 16 | 0.39 | strong |
| **K4** | L-cysteate | 20 | 0.40 | strong |
| **K5** | succinate | 32 | 0.64 | moderate |
| **K6** | L-serine | 45 | 0.80 | weak |
| **K7** | D-serine | 48 | 0.96 | insignificant |
| | *Newly tested compounds* | | | |
| **I1** | L-tartrate[e] | 12 | 0.24 | strong |
| **I2** | 2,4-dihydroxypyrimidine-5-carboxylate | 27 | 0.54 | moderate |
| **I3** | D-tagatose[f] | 45 | 0.80 | weak |
| **I4** | (S)-thiazolidin-3-ium-4 carboxylate | 48 | 0.96 | insignificant |
| **I5** | (2S,3S,4R,5R)-tetrahydro-2H-pyrano-2,3,4,5-tetraol | 48 | 0.96 | insignificant |
| **I6** | 1H-pyrazolo[3,4-d]pyrimidin-4(7H)-one | 48 | 0.96 | insignificant |

[a] The measurements were performed using 1 mM L-aspartate, 3 μM ADC, and 1 mM potential inhibitor in $D_2O$, at 25 $^oC$. [b] The conversion percentage corresponds to the

product formed by integration of the NMR signals corresponding to substrate and product of the enzymatic reaction after 30 min upon addition of the enzyme. In the absence of inhibitor the conversion corresponds to 50% under the present conditions. The absolute values were averaged from at least two measurements. [c] The relative inhibitory effect, $k_{rel}$ is defined as (conversion % in the absence of a potential inhibitor) / (conversion % in the presence of a potential inhibitor). The measurement time is not a limitation, as the conversion % can be compared to the reference kinetic profile in Figure 3.3.2). [d] The experiment was carried out under conditions corresponding to 33% conversion in the absence of inhibitor. [e] D-tartrate has been also tested, and a $k_{rel} = 0.35$ was extracted. [f] A $k_{rel} = 0.74$ was observed upon preincubation with ADC for 1 hour at room temperature.

The newly identified compounds were obtained *via* bioinformatics using the crystal structure of ADC, which has been recently reported.[174] The virtual identification of the potential inhibitors, **I1** – **I6** for the enzyme (Scheme 3.1.1) relied on a structure-based screening, aiming for a tight binding of these molecules to the active (and well-conserved) residues of ADC responsible for catalysis. These studies have been conducted by Ms. Reetu Sharma (PhD student in the research group of Prof. Swaminathan). Among the already reported compounds exhibiting an inhibitory effect towards ADC are **K1** – **K7** (Scheme 3.1.1), which we have also tested experimentally. Their effect on the enzymatic conversion has been reported *via* a radioactivity-based methodology.[177]

The final inhibition results are compiled and presented in Table 3.3.1. The screening experiments were performed in the presence of 1 mM inhibitor, which may be regarded as a relatively high inhibitor concentration. The mM range of concentration was necessary in order to see an effect for most compounds, as well as a measure for comparison of their inhibitory potential. Additionally, the literature data revealed inhibition constants of the previously investigated compounds in the mM range as well, suggesting that no effective inhibitors for ADC have been yet identified. Among all the tested compounds, oxaloacetate seems to be the most effective one showing a complete inhibition of the ADC activity ($k_{rel} = 0$) followed by the newly identified L-tartaric acid ($k_{rel} = 0.24$). Note that all previously identified compounds are dicarboxylic acids, since they presumably act as competitive inhibitors for the enzyme. The only two exceptions are L- and D-serine, which have been reported to inhibit the reaction. Particularly

D-serine was found to be 45% more potent as its L- isomer ($K_i$ = 0.16 mM *vs.* $K_i$ = 0.73 mM, repectively). According to our experiments, neither D- nor L-serine showed a considerable inhibitory effect towards ADC. Among the compounds obtained from the virtual screening, those possessing inhibitory potential were, as those found in the literature, limited to negatively charged ones. L-tartrate, **I1** was found to be the most potent inhibitor. Compound **I2**, even though weaker by a factor of two, showed also an inhibitory effect ($k_{rel}$ = 0.24). Most certainly, this is due to its lower affinity towards the enzyme active site, as compared to the dicarboxylate compunds. Surprisingly, **I3**, which is a neutral compound, has exhibited an inhibitory effect ($k_{rel}$ = 0.74), but only upon preincubation with the enzyme. In this context, please note that all compounds have been additionally checked upon preincubation with ADC; however, no changes with respect to the inhibition potential have been identified, except for **I3**. The fact that **I4** showed no detectable inhibitory effect, not even after preincubation for 1 hour is still not accounted for. Our data reveal that the interaction between the potential inhibitors and the active site of ADC is mainly governed by electrostatic interactions, with the carboxylate groups being essential for inhibition. In addition to the L- and D-serine example, we have also included D-tartrate in our experiments, even though its structure had not yet been identified by bioinformatics. A similar inhibitory effect as for its counterpart L- isomer has been observed.

In conclusion, we were able to monitor β-alanine formation from L-aspartate during enzymatic conversion *via* $^1$H NMR. This is the first label-free assay study reported for ADC, and it clearly stands out due to its simplicity. Additionally, its functionality has been reflected by its successful screening for ADC inhibitors, which could unfold promising drug targets against tuberculosis. We have tested several compounds for their inhibitory potential against ADC, particularly those identified through bioinformatics approaches by our collaborators. Even though the presented technique is satisfactory for an initial screening, the ultimate goal is to construct a supramolecular tandem assay, which is sufficiently robust to be implemented into a pharmaceutical-industrial screening of inhibitors for this enzyme.

# CHAPTER 4

## *– Experimental Section –*

## 4.1 BINDING OF HYDROCARBONS TO CUCURBITURILS

### 4.1.1. MATERIALS

Gases of highest commercial purity (≥ 99%) were purchased from Air Liquide, Germany, except for the 2-butenes (Sigma-Aldrich, Germany), neopentane (ChemSampCo, USA), propane-$d_8$ (ISOTEC™, USA), and 2-methylpropane-$d_{10}$ (CDN Isotopes, Canada). Liquid hydrocarbons were from Sigma-Aldrich, Germany. Fluorescent dye **DAPI** was obtained from Molecular Probes, and the **NAS-P** fluorophore has been synthesized according to our anchor dye approach,[77] by my colleague, Ms. Alexandra I. Lazar.[179] CB6 was synthesized as reported[28,29] and an independently prepared sample (which afforded the same results) was kindly provided by Dr. H.-J. Buschmann. CB7 was synthesized according to the literature within our group.[30,31,33]

### 4.1.2. METHODS

Fluorescence measurements were done with a Varian Eclipse fluorometer at 25.0 ± 0.1 °C (using an external Peltier thermostat). Experiments for the sensing of gaseous hydrocarbons and noble gases were performed in a rubber-sealed long-neck quartz cuvette. The different gases were administered to the aqueous mixture containing the dye•CB*n* complex by slowly purging (*ca*. 1 bubble per second) with a needle (Figure 4.1.1).

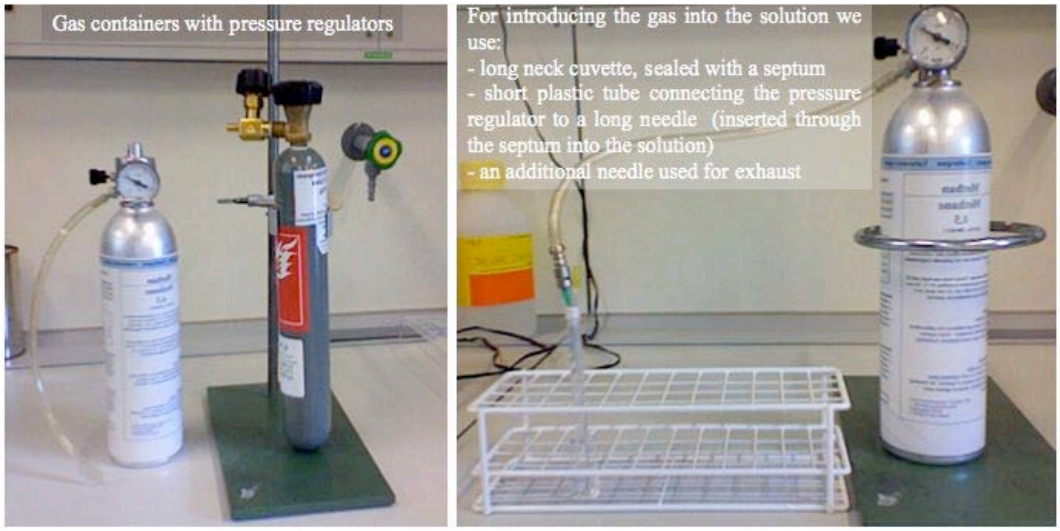


**Figure 4.1.1.** Gas sensing bubbling set-up.

For the on-line monitoring of the uptake of volatile liquid analytes, we employed $N_2$ as carrier gas for transferring the hydrocarbon of interest through the gas phase into the aqueous solution containing the reporter pair until the solubility limit was reached. Experiments at varying gas pressures were performed by deaerating a home-built cuvette (Figure 4.1.2) by three freeze-pump-thaw cycles and subsequently dosing different gas pressures (0-1000 mbar) on a vacuum manifold, as detailed in our previous gas-phase work.[180] The water vapor pressure at 298 K was considered to be 32 mbar. Acetylene was also dosed in this manner (instead of bubbling) to avoid the accumulation of acetone, an ubiquitous stabilizer in acetylene samples. For those hydrocarbons, which showed no immediate effect on the fluorescence signal, the solutions were exposed for a prolonged time (several hours) to exclude the possibility of a slower guest exchange kinetics being responsible for the absence of binding.

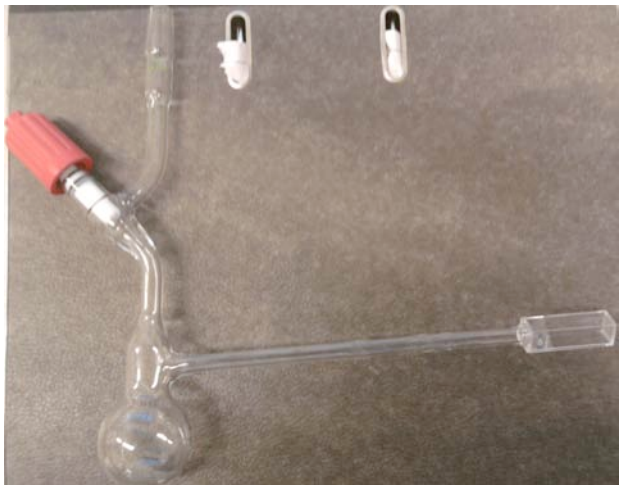

**Figure 4.1.2.** Home-built cuvette employed for applying different gas pressures.

### 4.1.3. COMPUTATIONAL DETAILS

Calculated molecular volumes of the investigated analytes are compiled in Table 2.2.1. They have been obtained using the Hyperchem[101] package after conducting a semi-empirical AM1 geometry optimization in search for energy minima of the potential energy surfaces. Each minimum was conjugate-gradient minimized to $\leq 0.01$ kcal $Å^{-1}mol^{-1}$. Volume calculations of the energy-minimized structures were performed within the Quantitative Structure-Activity Relationship (QSAR) module. The obtained values are in agreement with reported values.[105]

Density functional theory calculations (Chapter 2, Figure 2.2.6) were performed by my colleague Khaleel I. Assaf with Gaussian 03W.[181]

## 4.2 ENZYME ASSAYS

### 4.2.1. MATERIALS

The macrocycles and dyes shown in Charts 3.1.1 and 3.1.2 were obtained from the following sources: 2-Anilinonaphtalene-6-sulfonic acid (ANS), and Dapoxyl were obtained from Molecular Probes; 8-Anilinonaphtalene-1-sulfonic acid (1,8-ANS), 8-hydroxy-1,3,6-pyrene trisulfonic acid (HPTS), 6-(*p*-toluidino)-2-naphtalene-sulfonic acid (2,6-TNS), fluorescein sodium, GTP, and ADP were purchased from Fluka; naphthalimide biscarboxylate, 2,3-diazabicyclo[2.2.2]oct-2-ene (DBO), and DBO carboxylate were synthesized according to the literature within our research group.[182-184] ATP, AMP, CTP, TTP, and apyrase (grade I, from potato, 7.7 U/mg) were from Sigma-Aldrich. The cyclodextrin samples octakis(6-amino-6-deoxy)-γ-cyclodextrin (**1**), heptakis(6-deoxy-6-*N*-(2-hydroxy)ethylamino)-β-cyclodextrin (**4**), 6-monoamino-6-monodeoxy-β-cyclodextrin (**5**), 6-monodeoxy-6-mono(3-hydroxy)propylamino-β-cyclodextrin (**6**), heptakis(2,3-di-*O*-methyl)-hexakis(6-*O*-methyl)-6-monodeoxy-6-monoamino-β-cyclodextrin (**7**) were obtained as hydrochloride salts from CycloLab, Hungary. The synthesis of the cyclophane (**2**) was performed according to the literature with minor modifications (see below).[67] Trianglamine (**3**) was kindly supplied by Prof. N. Kuhnert, Jacobs University Bremen, Germany. The bis-calixarene (**9**) was synthesized according to the literature,[68] whereas calixarenes (**8**) and (**10**) were kindly supplied by Prof. J. Schatz, Universität Erlangen-Nürnberg, Germany.

Peptides **S2** and **S6** (Table 3.2.1) were obtained from Biosyntan GmbH, Germany, in >99% HPLC purity. Immobilized peptide substrates were prepared by Dr. Srikanth Kudithipudi (Jeltsch research group, Jacobs University Bremen) using SPOT synthesis according to the reported procedure.[166,185,186] *N*,*N*'-dimethyl-9,9'-biacridinium dinitrate (LCG), *p*-sulfonatocalix[4]arene (CX4), 1,10-phenanthroline, and *S*-adenosyl-L-methionine (AdoMet) were purchased from Sigma-Aldrich. Dim-5 was kindly provided by the Jeltsch research group.

### 4.2.2. CYCLOPHANE (2) SYNTHESIS

All materials were purchased in highest commercially available purity and used without further purification. A very old, but still very pure anthracene sample was used (originally purchased from Bayer), kindly provided by Thomas Schwarzlose from his extensive chemical reserves. Paraformaldehyde, aqueous HBr (48%), and toluene were obtained from AppliChem. 4,4'-Bipyridyl, $NH_4PF_6$, and $CH_3CN$ were purchased from Fluka. Glacial acetic acid, $CH_2Cl_2$, and NaCl were from Sigma-Aldrich. The synthesis of the cyclophane (**2**) was performed in three steps with minor modifications of the published literature (see Chapter 3, Scheme 3.1.1).[128]

**Synthesis of 9,10-Bis(bromomethyl)anthracene (b).**[187] A mixture of anthracene, **a** (10 g, 0.056 mol), paraformaldehyde (10 g, 0.33 mol), cetyltrimethylammoniumbromide (0.224 g), and glacial acetic acid (14 mL) were stirred at room temperature. Subsequently, 35 mL aqueous HBr (48%) were added dropwise to the mixture over 1 h, which caused a change in color from white to yellow. The reaction mixture was stirred and heated to 80 $^oC$ for 5 h. After cooling, the reaction mixture was filtered, washed with water, and dried under vacuum. The yellow solid was then recrystallized from toluene at 130 $^oC$ (1 g of crude product required approximately 300-400 mL of solvent). Decomposition of the compound by light was prevented by covering the flask with aluminum foil. Yield obtained: 10 g (49%), (lit. 90%).[187]

$^1H$ NMR (400 MHz, $CDCl_3$): δ 8.38-8.36 (m, 4H), 7.69-7.66 (m, 4H), 5.51 (s, 4H).

**Synthesis of 1,1'-[9,10-Anthrylbis(methylene)]bis-4,4'bipyridinium bis(hexafluorophosphate) (c).**[128] 9,10-Bis(bromomethyl)anthracene, **b** (0.69 g, 1.89 mmol) was added over a period of 30 min to a solution of 4,4'-bipyridyl (1.48 g, 9.48 mmol) in dry $CH_3CN$ (17.5 mL) at room temperature, under nitrogen. The reaction mixture was refluxed for 4 h at 80 $^oC$ and then cooled to room temperature. The viscous, yellow reaction mixture was filtered, washed with dry $CH_3CN$ (10 mL), and dissolved in $H_2O$ (120 mL). The aqueous solution was washed with $CH_2Cl_2$ three times, 10 mL each time, and water was then removed under vacuum to give a solid orange residue. The orange solid was dissolved in hot $H_2O$, and a saturated solution of $NH_4PF_6$ was added to yield a light-yellow precipitate, which was then filtered. Yield obtained: 1.71 g (77%), (lit. 88%).

Please note that none of the two recrystallizations reported in the literature (from $H_2O$ and $CH_3CN$) were feasible for our sample,[128] which was $^1H$ NMR pure ( > 95%).

$^1H$ NMR (400 MHz, $CD_3COCD_3$): 9.21-9.19 (d, 4H), 8.82-8.80 (m, 4H), 8.71-8.69 (m, 4H), 8.59-8.58 (d, 4H), 7.89-7.88 (m, 4H), 7.82-7.80 (m, 4H), 7.39 (s, 4H).

**Synthesis of the cyclic derivative (2).**[128] A solution of **b** (0.282 mg, 0.77 mmol) and **c** (940 mg, 1.16 mmol) in dry $CH_3CN$ (94 mL) was heated under reflux at 80 $^oC$ for 24 h under nitrogen. The reaction mixture was then cooled to room temperature, filtered, and washed with dry $CH_3CN$ (10 mL). The red-orange precipitate was dissolved in $H_2O$ (100 mg of solid required approximately 3 L $H_2O$!), and washed three times with $CH_2Cl_2$, 4 mL each time. Precipitation was induced by adding solid NaCl (approximately 100 g NaCl was required for precipitate formation from 1 L of dissolved crude product), which ultimately yielded the product in the form of an orange powder floating at the surface of the aqueous solution. Upon drying under vacuum, the final product was obtained in 11% yield (110 mg), (lit. 26%). The reported recrystallization from a mixture of (1:3) water and methanol was again not feasible.[128]

$^1H$ NMR (400 MHz, $D_2O$): 8.88-8.86 (d, 8H), 8.38-8.22 (m, 16H), 7.67-7.65 (m, 8H), 6.99 (s, 8H).

### 4.2.3. INSTRUMENTATION

Fluorescence spectra, intensities, and time courses were recorded on a Varian Eclipse fluorometer at ambient temperature or at 25.0 ± 0.1 $^oC$ (using an external Peltier thermostat, only for the enzyme assays). UV measurements were performed with a Varian Cary 4000 UV-Vis spectrophotometer. $^1H$ and $^{31}P$ NMR were carried out using a Jeol JNM-ECX 400 spectrometer. MALDI-TOF mass spectra were collected using an Autoflex II instrument (Bruker Daltonics, Bremen, Germnay).

### 4.2.4. ENZYME ASSAYS

For the potato apyarase assays, stock solutions of substrate (nucleotides), host (**1** or **2**), fluorescent dye (ANS or HPTS), and enzyme were prepared in 50 mM sodium acetate buffer, pH 5.5, with 1.6–1.8 mM $MnCl_2$ (when using **1**/ANS

reporter pair) and in 10 mM sodium succinate buffer, pH 6.5, with 1.6–1.8 mM $CaCl_2$ (when **2**/HPTS was employed). Careful control of the pH was required to obtain reproducible fluorescence intensities. The required volumes of all stock solutions were calculated to afford the final concentrations in 1 mL total assay volume. All assays were conducted using equimolar mixtures of host and fluorescent dye (25 μM for **1**/ANS and 6.3 μM for **2**/HPTS). The volumes of nucleotide stock solutions were calculated to obtain the respective concentrations. The enzymatic reactions were initiated by adding an aliquot from a stock solution of 1 mg $mL^{-1}$ enzyme.

The methylation assays were performed in 5 mM glycine buffer, pH 10.0 ± 0.1, in a 700 μL quartz cuvette (final reaction mixture volume 500 μL) at 25.0±0.1 $^{o}$C (using an external Peltier thermostat). The reactions were initiated by addition of enzyme. For the inhibition studies, solutions of Dim-5 and 1,10-phenanthroline (2-270 μM) were pre-incubated for 15 min at 4 $^{o}$C.

The L-aspartate-α-decarboxylase assays were carried out using 1 mM L-aspartate in $D_2O$ at 25 $^{o}$C. The enzymatic reactions were initiated by addition of 3 μM enzyme.

# CHAPTER 5

## *Preliminary Results Towards Future Projects*

## *– What's Next? –*

In the earlier two chapters I have tried to cover the main projects I have been involved with for the past three years. These studies are illustrative of my areas of interest, which encompass the development of fluorescence-based sensors for monitoring of changes in concentrations of biologically and environmentally relevant analytes, either while undergoing enzymatic transformations, or within their time-resolved encapsulation by macrocyclic containers. As it can be noticed, the projects described so far have mostly been taken to an end. In contrast to a project, which may be considered to have been fully explored and concluded, follow-up ideas and inspiration towards future studies will always be there. In Chapter 5, I would like to include a few preliminary results and thoughts, which I hope, can contribute towards the myriad of opportunities for related future projects.

## 5.1 HYDROCARBON BIOSYNTHESIS AND DEGRADATION BY MARINE BACTERIA

A promising follow-up study could arise by implementing the sensing methodology used in Chapter 2 into the catalytic activity of microorganisms responsible for hydrocarbon biosynthesis and degradation. As a matter of fact, selective oxyfunctionalization of hydrocarbons remains one of the greatest challenges of contemporary chemistry, as synthetic methods for introducing hydroxyl groups and causing C–H bond cleavage are scarce.[188,189] However, several marine bacteria able to catalyze selective oxidations of hydrocarbons have been recently identified. These alkane-assimilating organisms encode specific hydroxylases, which are enzymes responsible for oxidative biotransformations of hydrocarbons.[189]

Among the biocatalysts that come to mind is butane monooxygenase from *Pseudomonas butanovora*, which is known to specifically degrade butane as well as C2-C9 alkanes.[190] Another enzyme of interest is the more specific *Gordonia* sp. TY-5 propane monooxygenase,[191] which oxidizes propane at the 2-position.[191] Besides an understanding of these alkane-assimilating organisms at the genome level, site-directed mutagenesis has been used to increase the catalytic turnover and selectivity of these enzymes. Sensitive screening methodologies for

efficient monitoring of the enzymatic conversions are consequently highly desirable, as these cannot be achieved by conventional gas-chromatographic approaches. Existing assays, on the other hand, require substrate analogues, or (indirectly) monitor the depletion of NADPH (a required cofactor for alkane hydroxylases), which suffer from various disadvantages.[188]

The results presented in Chapter 2 have shown that reporter pairs such as **NAS-P**•CB6 or **DAPI**•CB7 can be used to follow changes in concentration of hydrocarbons in aqueous solution, which paves the way to a novel tandem assay for monitoring the enzymatic biosynthesis or degradation of alkanes or alkenes. Figure 5.1.1 is a graphic depiction of the *expected* fluorescence response induced by such enzymatic transformations. For instance, intermediates of fatty acids, such as aldehydes (weak binders to CB) are being converted to alkanes (strong binders to CB) by aldehyde decarbonylases,[192] which in turn, are biodegraded to oxidated products, such as alcohols (again, weak binders) by alkane hydoxylases.[189]

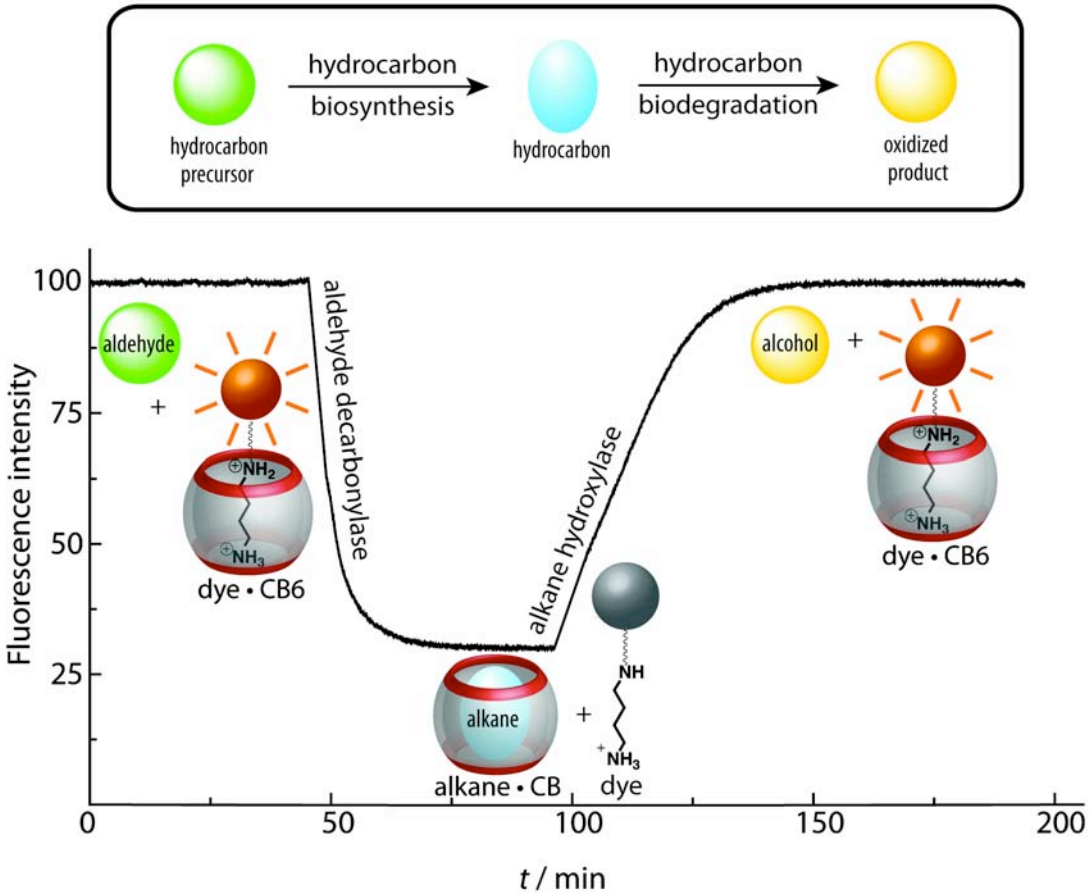

**Figure 5.1.1** Anticipated fluorescence responses corresponding to hydrocarbon formation and degradation, respectively, induced by enzymatic transformations.

In fact, any process *depleting or forming hydrocarbons in water*, even if originating from whole cells, bacteria, or complex protein extracts, could be followed by this fluorescence-based indicator displacement methodology. The robustness of tandem assays for potential biotechnological applications has already been demonstrated, since these assays are also suitable for crude enzyme extracts, or whole cells expressing the enzyme of interest.[76] That the method actually allows the time-resolved monitoring of hydrocarbons, e.g., butane, isobutane, or propane, can be anticipated from the initial results (Chapter 2 and Appendix 6). Accordingly, in the enzymatic degradation of small hydrocarbons, the nonpolar substrates are known to bind tightly to CB6 or CB7 (in fact, stronger than to other macrocycles), causing a displacement of the fluorescent dye from the macrocycle, while the (polar) oxidized products are known to exhibit little affinity towards CB6.[34] This way, the reaction can be monitored by a fluorescence increase caused by an uptake of the fluorescent dye by the host, facilitated by the depletion of the competing substrate (Figure 5.1.1).

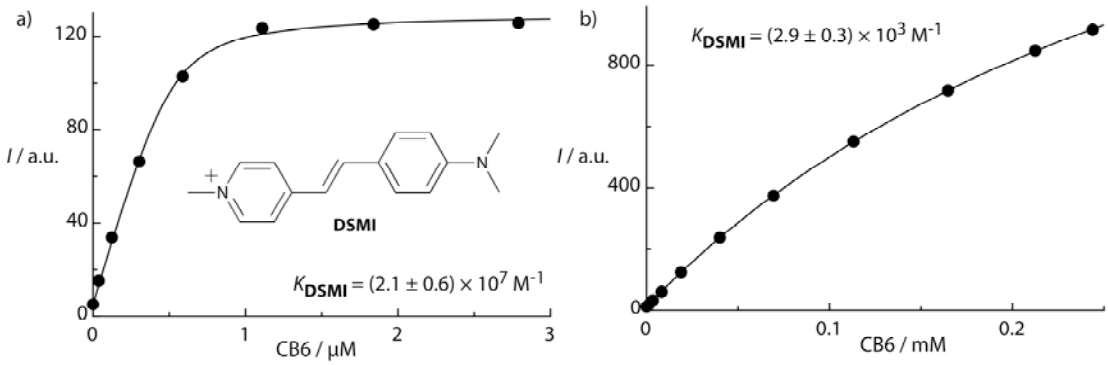


**Figure 5.1.2.** Fluorescence spectra ($\lambda_{exc}$ = 458 nm, $\lambda_{obs}$ = 610 nm) of a) 0.5 μM **DSMI** with increasing concentrations of CB6 in 1 mM HCl, pH 3.0, and b) 10 μM **DSMI** with increasing concentrations of CB6 in 50 mM NaOAc, pH 5.5. The nonlinear fittings were made according to a 1:1 complexation model, from which the association constants were derived.

An alternative to the **NAS-P** fluorophore is trans-4-[4-(dimethylamino)styryl]-1-methylpyridinium iodide, **DSMI**, recently reported for

its very high fluorescence enhancement upon encapsulation by CB6.[193] To allow direct comparison, I have already tested the **DSMI•**CB6 reporter pair (Figure 5.1.2) for its suitability to detect volatile hydrocarbons, which afforded essentially the same results as when using **NAS-P** as indicator. **DSMI** is a commercially available fluorescent dye and its long-wavelength absorption ($\lambda_{max}$ = 458 nm) renders it the indicator of choice when applications involving biomolecules, i.e., enzyme assays, are being envisaged. It is well known that bioanalytes, such as peptides or enzymes very often absorb strongly at lower wavelengths (around 280 nm), which coincide with the absorption of the **NAS-P** fluorophore ($\lambda_{exc}$ = 283 nm).

This project could be embedded in a local collaboration with a marine microbiology research group (Prof. Matthias Ullrich) who could provide the cell-free, dialyzed secreted protein extracts produced by the marine microorganisms of interest. Specifically, the biocatalytic activity of proteins secreted by *Marinobacter adhaerens* HP15 as well as by *Marinobacter hydrocarbonoclasticus* could be investigated. Note that the ecological and cellular roles of the former have been already well-characterized by the Ullrich group,[194] while the latter is firmly established as an aerobic bacteria capable of saturated hydrocarbon degradation.[195] A comparative analysis of secreted proteins obtained from both organisms, which are genetically highly similar but biochemically diverse, using the methods described herein, will allow important new insights to the ecological and molecular functions of marine bacteria.

## 5.2 ADVANCEMENTS TOWARDS CONVENIENT ENZYME ASSAYS

### PHSOPHATASES AND KINASES

Phsphorylation and dephosphorylation of tyrosine residues in proteins are important regulatory mechanisms for biological signal transduction and their malfunction has been associated with numerous diseases.[196-199] Consequently, convenient and robust assays able to monitor such processes, initiated by enzymes known as kinases and phosphatases, are urgently required in pharmaceutical drug discovery, as well as in fundamental research. In 2007, we have introduced a fluorescence-based single-label assay for monitoring tyrosine phosphorylation and dephosphorylation (Chapter 1.4, Appendix 2).[87] Herein, I would like to propose

the development of an alternative, label-free assay for following phosphorylation and dephosphorylation of tyrosine by applying the principles of supramolecular tandem assays. Up to now, preliminary experiments have been carried out towards this goal, both by Ms. Lora Angelova (during a laboratory rotation) and myself, which I would like to present below. These results have been obtained by designing an assay for acid phosphatase, which, nonetheless, should be transferable to other phosphatase, and alternatively to kinases.

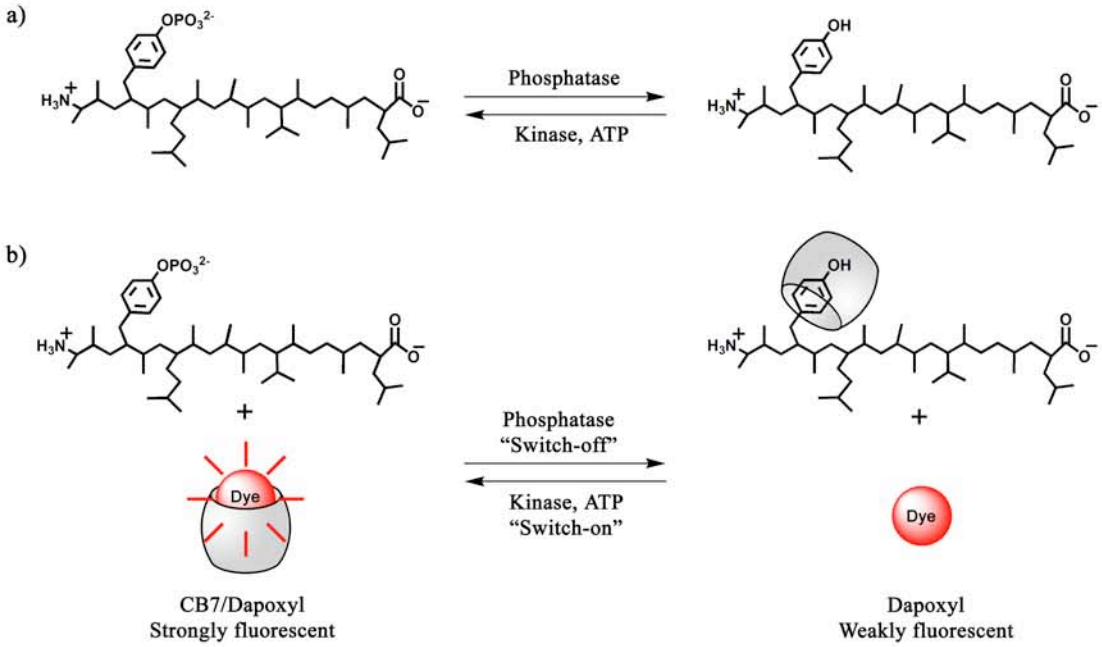


**Scheme 5.2.1.** (a) Illustration of the enzymatic activity of phosphatases and kinases. (b) Supramolecular tandem assay for monitoring the activity of phosphatases and kinases.

During a lab rotation, Ms. Angelova implemented the CB7/Dapoxyl reporter pair for monitoring the dephosphorylation of both phosphotyrosine (pTyr, employed as a model compound, Figure 5.2.1a) and a pTyr-containing model peptide (EEEE-pY-GE-$NH_2$, Figure 5.2.1b). The working principle relies on the differential binding of the negatively charged substrate, pTyr and the dephsophorylated natural amino acid tyrosine (Tyr) (Scheme 5.2.1). While pTyr shows no affinity towards CB7, a binding constant of $K = (2.7 \pm 0.4) \times 10^4$ $M^{-1}$ for Tyr was extracted. The value is, in fact, almost identical to the affinity of

Dapoxyl towards the host ($K$ = (2.0 ± 0.2) × $10^4$ $M^{-1}$).[55] Consequently, the dephosphorylation process initiated by acid phosphatase could be monitored *via* a decay in fluorescence intensity as a result of the continuous dye displacement from the CB7 cavity by the product being formed, which complies with the *product-selective* tandem assay principle.

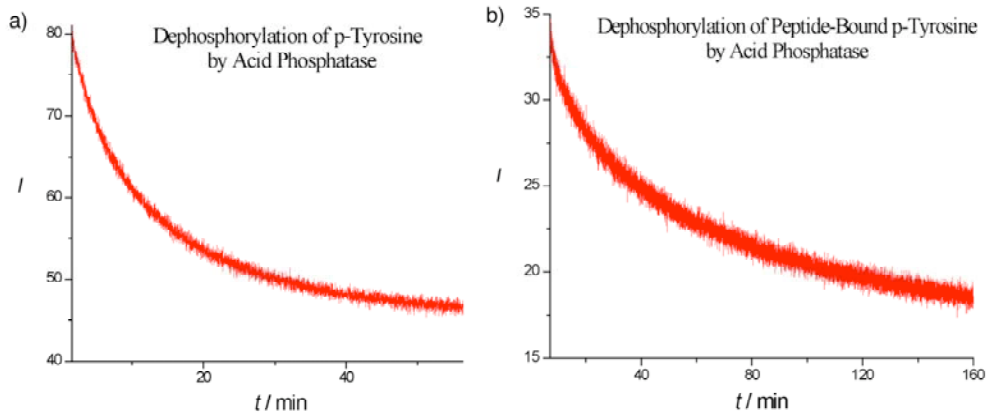


**Figure 5.2.1.** Evolution of steady-state fluorescence intensity monitoring the activity of acid phosphatase using CB7 and Dapoxyl as reporter pair. a) Dephosphorylation of pTyr, initiated by addition of acid phosphatase (0.16 mg/mL) to a mixture of CB7 (10 μM), Dapoxyl (2.5 μM), and pTyr (60 μM) in 10 mM $NH_4OAc$, pH 6.0. b) The assay was initiated by addition of acid phosphatase 0.32 mg/mL to CB7 (5 μM), Dapoxyl (1.25 μM), and peptide (50 μM) in 10 mM $NH_4OAc$, pH 6.0.

Since a reporter pair allowing monitoring of the enzymatic activity *via* a switch-OFF fluorescence response was already available, my intention was to identify a second pair that would allow the enzymatic course to be signaled by a switch-ON fluorescence response, which is frequently preferred. To this end, I have identified the amino-β-CD (Scheme 5.2.2) in combination with the polarity-sensitive fluorescent dyes 2-anilinonaphthalene-6-sulfonate (2,6-ANS) and 1-anilinonaphthalene-8-sulfonate (1,8-ANS). Both fluorescent dyes undergo a fluorescence increase upon encapsulation; the enhancement factors, as well as the binding constants obtained, are highly pH sensitive (documented for 1,8-ANS in Table 5.2.1). In order to reach a higher assay sensitivity, a preference for 2,6-ANS was imposed by its higher binding constant towards the macrocycles as compared

to that of 1,8-ANS ($K_{2,6\text{-ANS}}$ = (2.78 ± 0.13) × $10^4$ $M^{-1}$ *vs.* $K_{1,8\text{-ANS}}$ = (2.38 ± 0.10) × $10^3$ $M^{-1}$).

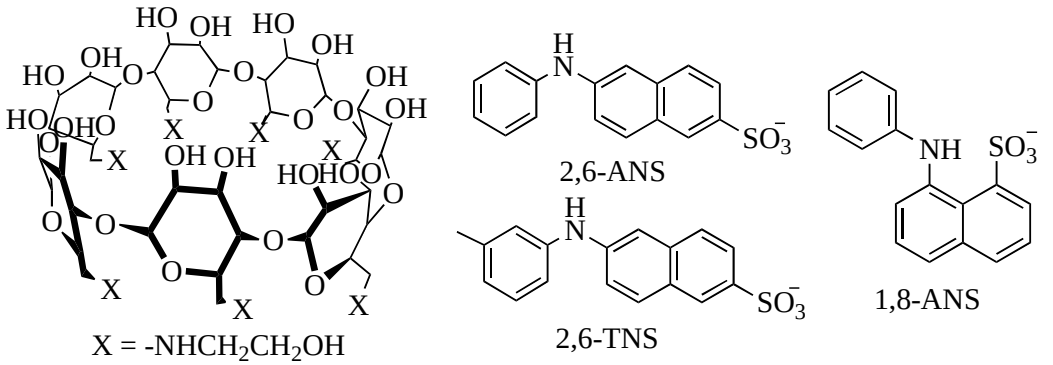


**Scheme 5.2.2.** Chemical structures corresponding to an amino-β-CD studied in combination with anionic fluorescent dyes.

**Table 5.2.1.** Fluorescence enhancements and binding constants of 1,8-ANS with amino-β-CD at different pH values.

| pH[a] | $I_{gh}/I_g$ | $K$ [$10^3$ $M^{-1}$][b] |
|---|---|---|
| 5.0 | 30 | 2.70 ± 0.09 |
| 5.5 | 40 | 2.38 ± 0.10 |
| 6.0 | 50 | 2.16 ± 0.08 |
| 7.0 | 41 | 0.73 ± 0.02 |

[a] 50 mM sodium acetate was used, except for pH 7.0 (Tris buffer). [b] Obtained from direct fluorescence titrations ($\lambda_{exc}$ = 350 nm, $\lambda_{obs}$ = 495 nm) by assuming a 1:1 complexation model.

In contrast to CB7, the amino-β-CD possesses anion-receptor properties, illustrated by its very high affinity towards pTyr ($K_{pTyr}$ = (1.8 ± 0.6) × $10^6$ $M^{-1}$), which could be quantified both through a direct titration, where the fluorescence of pTyr itself was monitored ($\lambda_{exc}$ = 228 nm; $\lambda_{obs}$ = 296 nm), as well as through a competitive displacement titration of 2,6-ANS. Since Tyr showed a negligible affinity for the host, a *substrate-selective* tandem assay for acid phosphatase could be established (Figure 5.2.2). The enzymatic conversion was expected to proceed *via* a fluorescence enhancement, which was indeed observed (Figure 5.2.3). Even though the assay has not been yet fully optimized, the robustness of supramolecular tandem assays has once again been illustrated. Moreover, the fluorescence enhancement obtained upon dephosphorylation (by a factor of two)

is in excellent agreement with the displacement exhibited by pTyr during the competitive displacement titration (Figure 5.2.2). Additionally, a thorough enzymatic analysis, inhibition studies, as well as an investigation of the reverse reaction by kinases would be the next goals, which, based on the initial results shown here, are not far-fetched.

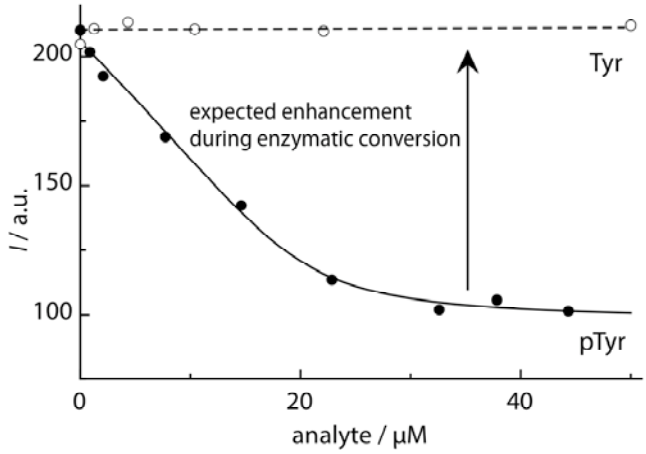


**Figure 5.2.2.** Differential binding of the model copmpounds pTyr and Tyr towards amino-β-CD. The two competitive fluorescence displacement titrations were carried out by using the amino-β-CD/2,6-ANS reporter pair (both 25 µM, $\lambda_{exc}$ = 318 nm; $\lambda_{obs}$ = 470 nm) in 50 mM acetate buffer, pH 5.5.

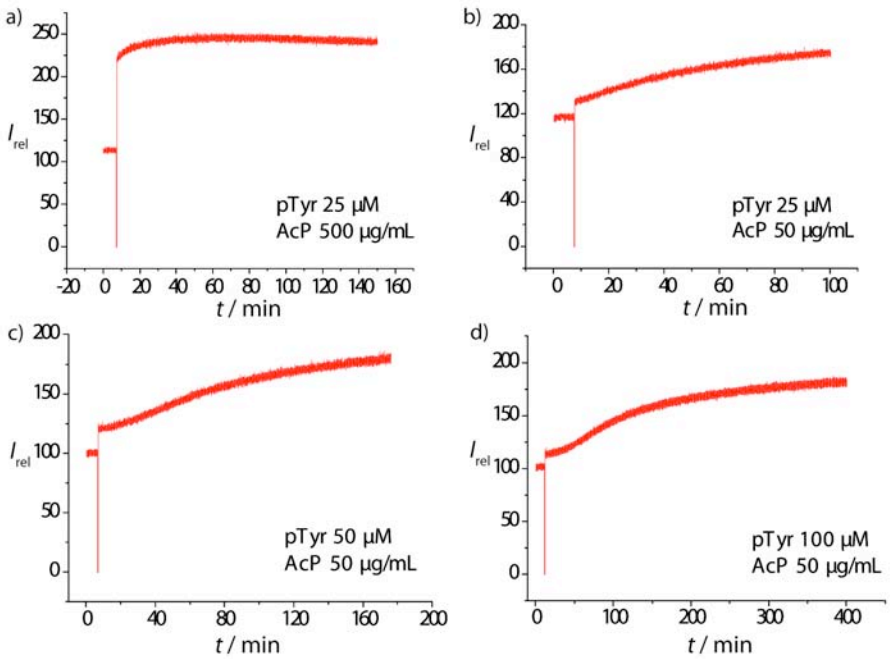

**Figure 5.2.3.** Preliminary results of the evolution of steady-state fluorescence intensity monitoring the activity of acid phosphatase using the amino-β-CD/2,6-ANS reporter pair (both 25 μM, $\lambda_{exc}$ = 318 nm; $\lambda_{obs}$ = 470 nm) in 50 mM acetate buffer, pH 5.5.

### INORGANIC PYROPHOSPHATASES AND PHOSPHODIESTERASES

During the extensive investigations towards finding a suitable reporter pair for ATP-dependent enzymes (see Chapter 3.1), I have come across a rather peculiar selectivity of the amino-β-CD towards the different phosphate-based anions. As can be seen in Figure 5.2.4a, a very high, and approximately identical affinity towards polyphosphates (diphosphate, metaphosphate, and triphosphate) was obersved ($K > 10^6$ $M^{-1}$). Monophosphate, was, of course, expected to have a lower affinity, which is reflected in its 3 orders of magnitude lower association constant. One might immediately attribute the differences in binding to the net negative charges that each of these phosphate compound possesses. Interestingly, however, when comparing monophosphate with metaphosphate (both containing the same number of negative charges, i.e., three), a size selectivity of the macrocycle became apparent because of the much higher binding constant of the more voluminous guest, i.e., metaphosphate.

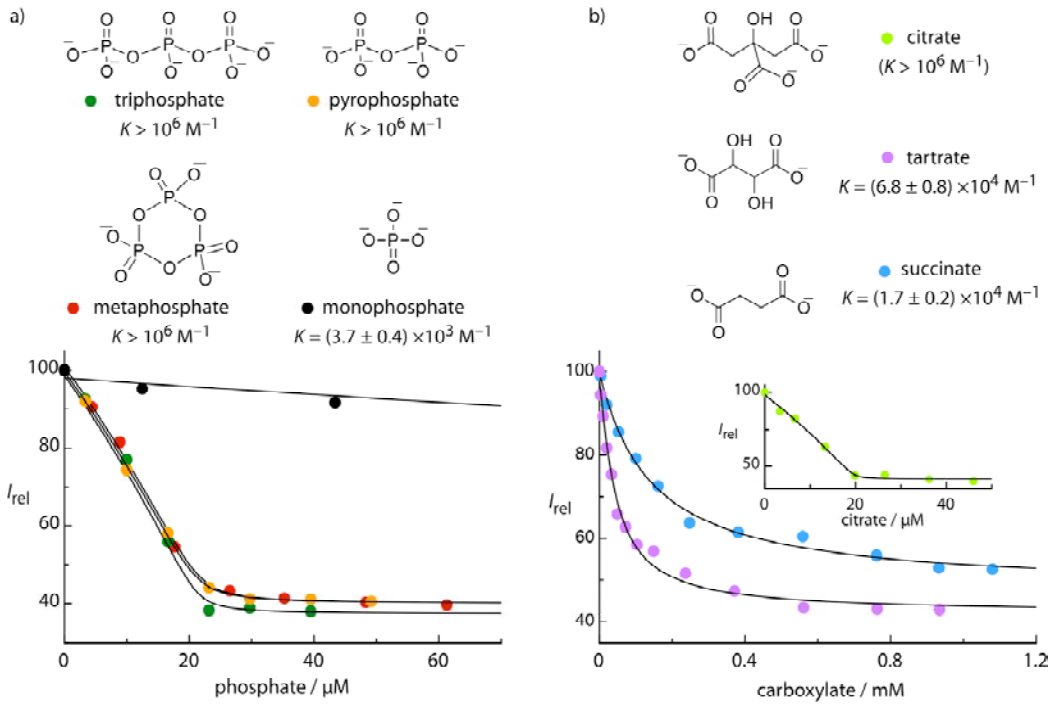

**Figure 5.2.4.** Changes in fluorescence intensity ($\lambda_{exc}$ = 317 nm; $\lambda_{obs}$ = 500 nm) of the amino-β-CD/2,6-TNS ($K_{2,6\text{-TNS}}$ = (3.0 ± 0.2) × $10^4$ $M^{-1}$) upon displacement by varying concentrations of a) triphosphate, diphosphate, metaphosphate, and monophosphate, and b) citrate, tartrate, and succinate in 50 mM NaOAc buffer, pH 5.5.

Despite its poor selectivity, the moderate preference that amino-β-CD showed towards the monophosphate could be exploited for real-time monitoring of the depletion or breakdown of the larger phosphates into smaller inorganic phosphate molecules. Such a transformation can be attributed, for instance, to inorganic phosphatases. These enzymes play an important role in lipid degradation by hydrolyzing pyrophosphate, which, as we can see in Figure 5.2.4a, has a very high affinity for the amino-β-CD cavity. The enzymatic products, i.e., the monophosphate ions, conveniently display a much lower affinity. Accordingly, the differential binding between the substrate and the product of the enzymatic reaction, in combination with amino-β-CD/2,6-TNS as a reporter pair, could in the near future allow for the development of a convenient fluorescence-based assay for pyrophosphatases.

In addition to sensing phosphate anions, the amino-β-CD/2,6-TNS reporter pair can also be implemented for the detection of carboxylate anions (Figure 5.2.4b). For instance, citrate displays a very strong binding towards the host ($K$ > $10^6$ $M^{-1}$), whereas the dicarboxylates succinate and tartrate show moderate to high affinities ($K$ ~ $10^4$ $M^{-1}$). Unfortunately, no displacement of the dye could be observed when employing aspartate as analyte, which rendered this reporter pair unsuitable for implementation into the design of a supramolecular tandem assay for L-aspartate-α-decarboxylase (Chapter 3.3).

As could be seen in Chapter 3, the use of aminated cyclodextrins is not limited to the encapsulation of small anionic compounds, but can also be extended to more complex guests, such as ATP. In addition to the investigated nucleotides in Chapter 3, I have also studied the effect that cAMP has on the fluorescence of the reporter pair composed of γ-CD, **1** and 2,6-ANS. The negligible binding of cAMP highly contrasts the action of ATP as a highly effective competitor against 2,6-ANS for the macrocyclic cavity. In fact, cAMP, an important second

messenger in signal transduction, is synthesized from ATP by adenylyl cyclase (e.g., adenylyl cyclase toxin from *Bordetella pertussis*, is commercially available from Sigma-Aldrich).[200]

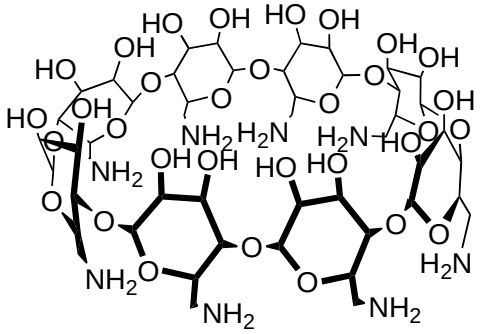

**1**

As mentioned before, the differential binding of a substrate and product of an enzymatic reaction stands at the basis of a supramolecular tandem assay. cAMP, corresponding to the product being formed, has essentially no affinity towards the macrocycle, whereas ATP is capable of quantitative dye displacement (Figure 5.2.5a). This seems a perfect scenario for the design of a tandem assay. However, when setting up an assay one does need to take into account all the possible by-products or intermediates that might occur as a result of the enzymatic conversion. For instance, in our present situation, pyrophosphate (PPi) is the by-product being formed. As seen earlier (see above and Chapter 3.1), amino-modified CDs do have a strong tendency to bind such highly negatively charged analytes, and a differentiation between di- and triphsophates may be missing. At first, this may seem a real impediment for setting up the assay. However, a way to tackle such a problem is to establish an enzyme-coupled tandem assay, a concept recently reported for monitoring the conversion of neurotransmitters, such as acetylcholine and choline.[43] Specifically, upon conversion of ATP to cAMP and PPi, addition of inorganic pyrophosphatase, as a second enzyme, would result in a final reaction mixture with monophosphate and cAMP being the major products, which display a very small or negligible effect on the fluorescence of the reporter pair. This way, the resulting enzyme-coupled tandem assay for monitoring cAMP formation should proceed *via* a switch-ON fluorescence response (Figure 5.2.5a).

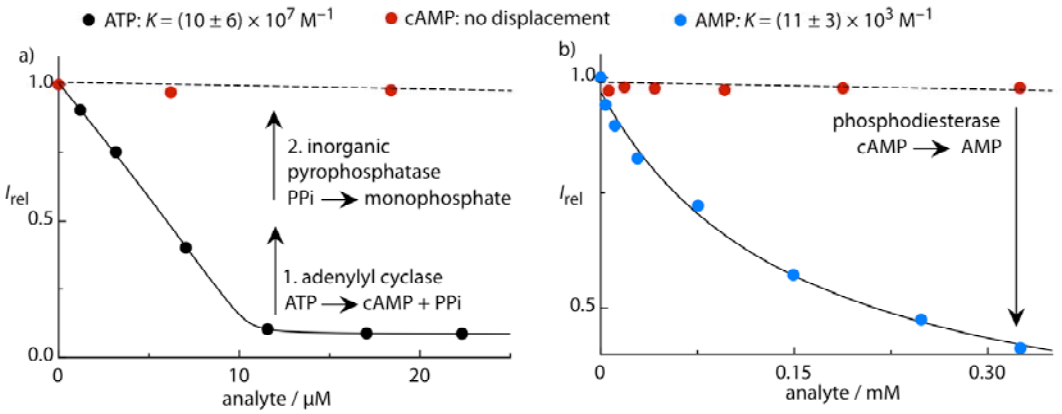


**Figure 5.2.5.** Changes in fluorescence intensity ($\lambda_{exc}$ = 318 nm, $\lambda_{obs}$ = 462 nm) of the **1**/ANS reporter pair (10 µM/25 µM) upon displacement by varying concentrations of a) ATP and cAMP, and b) AMP and cAMP in 50 mM NaOAc buffer, pH 5.5. The arrows show the presumed fluorescence responses as a result of enzymatic coversion.

Finally, the depletion of cAMP to AMP by a phosphodiesterase could potentially be similarly followed in a direct manner through a fluorescence switch-OFF response (Figure 5.2.5b). Please recall that when designing the ATP dephosphorylation assay in Chapter 3.1, the low affinity of macrocycle **1** towards AMP ("weak" competitor, in strong contrast to ATP) was exploited. Herein, AMP can be seen as a "strong" competitor, since its effect on the fluorescence response should be sufficient, when compared to the unnoticeable displacement induced by cAMP.

As illustrated herein, the flexible interplay between the relative affinities of macrocycles, fluorescent dyes, and the analytes of interest has an enormous potential for manifold applications. Certainly, supramolecular tandem assays offer both an insight into the working mode of enzymes, whose activity govern all living organisms, as well as an opportunity for relevant applications in the pharmaceutical industry, e.g., for drug discovery.

# REFERENCES

[1] C. J. Pederson, *Angew. Chem. Int. Ed.* **1988**, *27*, 1021-1027.
[2] D. J. Cram, *Angew. Chem. Int. Ed.* **1988**, *27*, 1009-1020.
[3] J.-M. Lehn, *Angew. Chem. Int. Ed.* **1988**, *27*, 89-112.
[4] F. Diederich, *Angew. Chem. Int. Ed.* **2011**, *50*, 8-12.
[5] J.-M. Lehn, *Supramolecular Chemistry*, VCH Weinheim, **1995**.
[6] A. P. de Silva, H. Q. N. Gunaratne, T. Gunnlaugsson, A. J. M. Huxley, C. P. McCoy, J. T. Rademacher, T. E. Rice, *Chem. Rev.* **1997**, *97*, 1515-1566.
[7] S. L. Wiskur, H. Ait-Haddou, J. J. Lavigne, E. V. Anslyn, *Acc. Chem. Res.* **2001**, *34*, 963-972.
[8] R. MartÍnez-Máñez, F. Sancenón, *Chem. Rev.* **2003**, *103*, 4419-4476.
[9] M. Inouye, K. Hashimoto, K. Isagawa, *J. Am. Chem. Soc.* **1994**, *116*, 5517-5518.
[10] K. N. Koh, K. Araki, A. Ikeda, H. Otsuka, S. Shinkai, *J. Am. Chem. Soc.* **1996**, *118*, 755-758.
[11] B. T. Nguyen, E. V. Anslyn, *Coord. Chem. Rev.* **2006**, *250*, 3118-3127.
[12] D. Leung, J. F. Folmer-Anderson, V. Lynch, E. V. Anslyn, *J. Am. Chem. Soc.* **2008**, *130*, 12318-12327.
[13] A. T. Wright, N. Y. Edwards, E. V. Anslyn, J. T. McDevitt, *Angew. Chem. Int. Ed.* **2007**, *46*, 8212-8215.
[14] T. Zhang, N. Y. Edwards, M. Bonizzoni, E. V. Anslyn, *J. Am. Chem. Soc.* **2009**, *131*, 11976-11984.
[15] A. D. Hughes, I. C. Glenn, A. D. Patrick, A. Ellington, E. V. Anslyn, *Chem. Eur. J.* **2008**, *14*, 1822-1827.
[16] A. Metzger, V. M. Lynch, E. V. Anslyn, *Angew. Chem. Int. Ed.* **1997**, *36*, 862-865.
[17] J. J. Lavigne, E. V. Anslyn, *Angew. Chem. Int. Ed.* **1999**, *38*, 3666-3669.
[18] T. Zhang, E. V. Anslyn, *Org. Lett.* **2007**, *9*, 1627-1629.
[19] I. Hemilä, S. Dakubu, V.-M. Mukkala, H. Siitari, T. Lövgren, *Anal. Biochem.* **1984**, *137*, 335-343.
[20] M. J. Perry, in *Monoclonal antibodies: Principles and Applications* (Eds.: J. R. Birch, E. S. Lennox), Wiley-Liss, New York, **1995**, pp. 107-120.
[21] D. M. Goldenberg, *Cancer Immunol. Immunother.* **2003**, *52*, 281-296.
[22] R. S. Yalow, S. A. Berson, *J. Clin. Invest.* **1960**, *39*, 1157-1175.
[23] C. S. Lim, J. N. Miller, J. W. Bridges, *Anal. Biochem.* **1980**, *108*, 176-184.
[24] M. Bonizzoni, L. Fabrizzi, G. Piovani, A. Taglietti, *Tetrahedron* **2004**, *60*, 11159-11162.
[25] H. Ait-Haddou, S. L. Wiskur, V. Lynch, E. V. Anslyn, *J. Am. Chem. Soc.* **2001**, *123*, 11296-11297.
[26] L. Fabrizzi, A. Leone, A. Taglietti, *Angew. Chem. Int. Ed.* **2001**, *40*, 3066-3069.
[27] W. M. Nau, A. Hennig, A. L. Koner, in *Springer Ser Fluorescence, Vol. 4* (Ed.: M. N. Berberan-Santos), Springer, **2008**, pp. 185-211.
[28] R. Behrend, E. Meyer, F. Rusche, *Justus Liebigs Ann. Chem.* **1905**, *339*, 1-37.
[29] W. A. Freeman, W. L. Mock, N. Y. Shih, *J. Am. Chem. Soc.* **1981**, *103*, 7367-7368.
[30] A. Day, A. P. Arnold, R. J. Blanch, B. Snushall, *J. Org. Chem.* **2001**, *66*, 8094-8100.
[31] J. Kim, I. S. Jung, S. Y. Kim, E. Lee, J. K. Kang, S. Sakamoto, K. Yamaguchi, K. Kim, *J. Am. Chem. Soc.* **2000**, *122*, 540-541.

[32] S. M. Liu, P. Y. Zavalij, L. Isaacs, *J. Am. Chem. Soc.* **2005**, *127*, 16798-16799.
[33] C. Márquez, F. Huang, W. M. Nau, *IEEE Trans. Nanobiosci.* **2004**, *3*, 39-45.
[34] W. M. Nau, M. Florea, K. I. Assaf, *Isr. J. Chem.* **2011**, *51*, 559-577.
[35] J. Lagona, P. Mukhopadhyay, S. Chakrabarti, L. Isaacs, *Angew. Chem. Int. Ed.* **2005**, *44*, 4844-4870.
[36] C. D. Gutsche, *Calixarenes: An Introduction*, Royal Society of Chemistry, Cambridge, **2008**.
[37] S. Shinkai, T. Mori, H. Koreishi, T. Tsubaki, O. Manabe, *J. Am. Chem. Soc.* **1986**, *108*, 2409-2416.
[38] A. R. Khan, P. Forgo, K. J. Stine, V. T. D'Souza, *Chem. Rev.* **1988**, *98*, 1977-1996.
[39] T. Ogoshi, A. Harada, *Sensors* **2008**, *8*, 4961-4982.
[40] K. A. Connors, *Chem. Rev.* **1997**, *97*, 1325-1357.
[41] M. V. Rekharsky, Y. Inoue, *Chem. Rev.* **1998**, *98*, 1875-1918.
[42] J. Szejtli, *Starch/Stärke* **2003**, *55*, 191-196.
[43] D.-S. Guo, V. D. Uzunova, X. Su, Y. Liu, W. M. Nau, *Chem. Sci.* **2011**, *2*, 1722-1734.
[44] Y. H. Shi, H.-J. Schneider, *J. Chem. Soc., Perkin Trans. 2* **1999**, 1797-1803.
[45] J. Zhao, H. J. Kim, J. Oh, S. Y. Kim, J. W. Lee, S. Sakamoto, K. Yamaguchi, K. Kim, *Angew. Chem. Int. Ed.* **2001**, *40*, 4233-4235.
[46] Y. Feng, X. Xiao, S. F. Xue, Y. Q. Zhang, Q. J. Zhu, Z. Tao, G. A. Lawrance, G. Wei, *Supramol. Chem.* **2008**, *20*, 517-525.
[47] S. Y. Jon, N. Selvapalam, D. H. Oh, J. K. Kang, S. Y. Kim, Y. J. Jeon, J. W. Lee, K. Kim, *J. Am. Chem. Soc.* **2009**, *125*, 10186-10187.
[48] W. L. Mock, N. Y. Shih, *J. Org. Chem.* **1983**, *48*, 3618-3619.
[49] W. L. Mock, N. Y. Shih, *J. Org. Chem.* **1986**, *51*, 4440-4446.
[50] C. Márquez, R. R. Hudgins, W. M. Nau, *J. Am. Chem. Soc.* **2004**, *126*, 5806-5816.
[51] M. V. Rekharsky, T. Mori, C. Yang, Y. H. Ko, N. Selvapalam, H. Kim, D. Sobransingh, A. E. Kaifer, S. Liu, L. Isaacs, W. Chen, S. Moghaddam, M. K. Gilson, K. M. Kim, Y. Inoue, *Proc. Natl. Acad. Sci. U.S.A.* **2007**, *104*, 20737-20742.
[52] B. D. Wagner, P. J. MacDonald, *J. Photochem. Photobiol. A* **1998**, *114*, 151-157.
[53] B. D. Wagner, P. J. MacDonald, M. Wagner, *J. Chem. Educ.* **2000**, *77*, 178-181.
[54] W. M. Nau, J. Mohanty, *Int. J. Photoenergy* **2005**, *7*, 133-141.
[55] A. L. Koner, W. M. Nau, *Supramol. Chem.* **2007**, *19*, 55-66.
[56] J. Mohanty, W. M. Nau, *Angew. Chem. Int. Ed.* **2005**, *44*, 3750-3754.
[57] R. Dsouza, U. Pischel, W. M. Nau, *Chem. Rev.* **2011**, *111*, 7941-7980.
[58] A. Ueno, T. Kuwabara, A. Nakamura, F. Toda, *Nature* **1992**, *356*, 136-137.
[59] H. Ikeda, in *Artificial Receptors for Chemical Sensors* (Eds.: V. M. Mirsky, A. K. Yatsimirsky), Wiley-VCH, Weinheim, **2011**.
[60] S. Tan, W. Chen, A. Satake, B. Wang, Z. Xu, Y. Kobuke, *Org. Biomol. Chem.* **2004**, *2*, 2719-2721.
[61] H. Bakirci, W. M. Nau, *Adv. Funct. Mater.* **2006**, *16*, 237-242.

[62] H. Bakirci, A. L. Koner, M. H. Dickman, U. Kortz, W. M. Nau, *Angew. Chem. Int. Ed.* **2006**, *45*, 7400-7404.
[63] N. Norbakov, P. Timmerman, N. Lidich, B. Urbach, A. Sa'ar, S. Yitzchaik, *Langmuir* **2008**, *24*, 2580-2587.
[64] T. Jin, F. Fujii, Y. Ooi, *Sensors* **2008**, *8*, 6777-6790.
[65] N. Marcotte, A. Taglietti, *Supramol. Chem.* **2003**, *15*, 617-625.
[66] S. Atilgan, E. U. Akkaya, *Tetrahedron Lett.* **2004**, *45*, 9269-9271.
[67] P. P. Neelakandan, M. Hariharan, D. Ramaiah, *J. Am. Chem. Soc.* **2006**, *128*, 11334-11335.
[68] R. Zadmard, T. Schrader, *Angew. Chem. Int. Ed.* **2006**, *45*, 2703-2706.
[69] P. D. Beer, P. A. Gale, *Angew. Chem. Int. Ed.* **2001**, *40*, 486-516.
[70] P. A. Gale, L. J. Twyman, C. I. Handlin, J. L. Sessler, *Chem. Commun.* **1999**, 1851-1852.
[71] J. Mohanty, A. C. Bhasikuttan, W. M. Nau, H. Pal, *J. Phys. Chem. B* **2006**, *110*, 5132-5138.
[72] M. Shaikh, J. Mohanty, P. K. Singh, W. M. Nau, H. Pal, *Photochem. Photobiol. Sci.* **2008**, *7*, 408-414.
[73] N. Saleh, A. L. Koner, W. M. Nau, *Angew. Chem. Int. Ed.* **2008**, *47*, 5398-5401.
[74] A. L. Koner, I. Ghosh, N. Saleh, W. M. Nau, *Can. J. Chem.* **2011**, *89*, 139-147.
[75] D. M. Bailey, A. Hennig, V. D. Uzunova, W. M. Nau, *Chem. Eur. J.* **2008**, *14*, 6069-6077.
[76] A. Hennig, H. Bakirci, W. M. Nau, *Nat. Methods* **2007**, *4*, 629-632.
[77] A. Praetorius, D. M. Bailey, T. Schwarzlose, W. M. Nau, *Org. Lett.* **2008**, *10*, 4089-4092.
[78] W. M. Nau, G. Ghale, A. Hennig, D. M. Bailey, *J. Am. Chem. Soc.* **2009**, *131*, 11558-11570.
[79] M. Megyesi, L. Biczók, I. Jablonkai, *J. Phys. Chem. B* **2008**, *112*, 3410-3416.
[80] L. Biczók, V. Wintgens, Z. Miskolczy, M. Megyesi, *Isr. J. Chem.* **2011**, *51*, 625-633.
[81] M. K. Sinha, O. Reany, G. Parvari, A. Karmakar, E. Keinan, *Chem. Eur. J.* **2010**, *16*, 9056-9067.
[82] P. Gribbon, A. Sewing, *Drug Discov. Today* **2003**, *8*, 1035-1043.
[83] J. Neefjes, N. P. Dantuma, *Nat. Rev. Drug. Discovery* **2004**, *3*, 58-69.
[84] R. R. Hudgins, F. Huang, G. Gramlich, W. M. Nau, *J. Am. Chem. Soc.* **2002**, *124*, 556-564.
[85] F. Huang, R. R. Hudgins, W. M. Nau, *J. Am. Chem. Soc.* **2004**, *126*, 16665-16675.
[86] A. Hennig, M. Florea, D. Roth, T. Enderle, W. M. Nau, *Anal. Biochem.* **2007**, *360*, 255-265.
[87] H. Sahoo, A. Hennig, M. Florea, D. Roth, T. Enderle, W. M. Nau, *J. Am. Chem. Soc.* **2007**, *129*, 15927-15934.
[88] W. M. Nau, X. J. Wang, *ChemPhysChem* **2002**, *3*, 393-398.
[89] A. Hennig, D. Roth, T. Enderle, W. M. Nau, *ChemBioChem* **2006**, *7*, 733-737.
[90] G. Ghale, V. Ramalingam, A. R. Urbach, W. M. Nau, *J. Am. Chem. Soc.* **2011**, *133*, 7528-7535.
[91] M. A. Rankin, B. D. Wagner, *Supramol. Chem.* **2004**, *16*, 513-519.

[92] C. Márquez, W. M. Nau, *Angew. Chem. Int. Ed.* **2001**, *40*, 4387-4390.
[93] D. J. Cram, M. E. Tanner, R. Thomas, *Angew. Chem. Int. Ed.* **1991**, *30*, 1024-1027.
[94] D. J. Cram, *Nature* **1992**, *356*, 29-36.
[95] S. J. Strickler, R. A. Berg, *J. Chem. Phys.* **1962**, *37*, 814-822.
[96] J. Mohanty, W. M. Nau, *Photochem. Photobiol. Sci.* **2004**, *3*, 1026-1031.
[97] R. Castro, M. J. Berardi, E. Cordova, M. Ochoa de Olza, A. E. Kaifer, J. D. Evanseck, *J. Am. Chem. Soc.* **1996**, *118*, 10257-10268.
[98] S. Lim, H. Kim, N. Selvapalam, K. J. Kim, S. J. Cho, G. Seo, K. Kim, *Angew. Chem. Int. Ed.* **2008**, *47*, 3352-3355.
[99] H.-J. Schneider, *Angew. Chem. Int. Ed.* **2009**, *48*, 3924-3977.
[100] S. Moghaddam, C. Yang, M. V. Rekharsky, Y. H. Ko, K. Kim, Y. Inoue, M. K. Gilson, *J. Am. Chem. Soc.* **2011**, *133*, 3570-3581.
[101] HyperChem, Ver. 7.01, Hypercube, Inc., Gainesville, FL.
[102] A. L. Koner, C. Márquez, M. H. Dickman, W. M. Nau, *Angew. Chem. Int. Ed.* **2011**, *50*, 545-548.
[103] L. Garel, J.-P. Dutasta, A. Collet, *Angew. Chem. Int. Ed.* **1993**, *32*, 1169-1171.
[104] N. Branda, R. Wyler, J. Rebek, Jr., *Science* **1994**, *263*, 1267-1268.
[105] A. Shivanyuk, A. Scarso, J. Rebek, *Chem. Commun.* **2003**, 1230-1231.
[106] C. L. D. Gibb, B. C. Gibb, *J. Am. Chem. Soc.* **2006**, *128*, 16498-16499.
[107] D. Ajami, J. Rebek, Jr., *Angew. Chem. Int. Ed.* **2008**, *47*, 6059-6061.
[108] D. J. Cram, M. E. Tanner, C. B. Knobler, *J. Am. Chem. Soc.* **1991**, *113*, 7717-7727.
[109] A. V. Leontiev, A. W. Saleh, D. M. Rudkevich, *Org. Lett.* **2007**, *9*, 1753-1755.
[110] D. M. Rudkevich, *Angew. Chem. Int. Ed.* **2004**, *43*, 558-571.
[111] D. M. Rudkevich, *Eur. J. Org. Chem.* **2007**, 3255-3270.
[112] S. Tartaggia, A. Scarso, P. Padovan, O. De Lucchi, F. Fabris, *Org. Lett.* **2009**, *11*, 3926-3929.
[113] J. Nakazawa, J. Hagiwara, M. Mizuki, Y. Shimazaki, F. Tani, Y. Naruta, *Angew. Chem. Int. Ed.* **2005**, *44*, 3744-3746.
[114] D. J. Cram, M. T. Blanda, K. Paek, C. B. Knobler, *J. Am. Chem. Soc.* **1992**, *114*, 7765-7773.
[115] S. Mecozzi, J. Rebek, Jr., *Chem. Eur. J.* **1998**, *4*, 1016-1022.
[116] B. W. Purse, J. Rebek, Jr., *Proc. Natl. Acad. Sci. U.S.A.* **2006**, *103*, 2530-2534.
[117] H.-J. Buschmann, K. Jansen, E. Schollmeyer, *Thermochim. Acta* **2000**, *346*, 33-36.
[118] M. V. Rekharsky, Y. H. Ko, N. Selvapalam, K. Kim, Y. Inoue, *Supramol. Chem.* **2007**, *19*, 39-46.
[119] Y. Kim, H. Kim, Y. H. Ko, N. Selvapalam, M. V. Rekharsky, Y. Inoue, K. Kim, *Chem. Eur. J.* **2009**, *15*, 6143-6151.
[120] B. S. Kim, Y. H. Ko, Y. Kim, H. J. Lee, N. Selvapalam, H. C. Lee, K. Kim, *Chem. Commun.* **2008**, 2756-2758.
[121] M. El Haouaj, M. Luhmer, Y. H. Ko, K. Kim, K. Bartik, *J. Chem. Soc., Perkin Trans. 2* **2001**, 804-807.
[122] M. El Haouaj, Y. H. Ko, M. Luhmer, K. Kim, K. Bartik, *J. Chem. Soc., Perkin Trans. 2* **2001**, 2104-2107.

[123] L. Fusaro, E. Locci, A. Lai, M. Luhmer, *J. Phys. Chem. B* **2008**, *112*, 15014-15020.
[124] Y. M. Jeon, H. Kim, D. Whang, K. Kim, *J. Am. Chem. Soc.* **1996**, *118*, 9790-9791.
[125] H. Kim, Y. Kim, M. Yoon, S. Lim, S. M. Park, G. Seo, K. Kim, *J. Am. Chem. Soc.* **2010**, *132*, 12200-12202.
[126] Y. Miyahara, K. Abe, T. Inazu, *Angew. Chem. Int. Ed.* **2002**, *41*, 3020-3023.
[127] K. A. Kellersberger, J. D. Anderson, S. M. Ward, K. E. Krakowiak, D. V. Dearden, *J. Am. Chem. Soc.* **2001**, *123*, 11316-11317.
[128] P. P. Neelakandan, M. Hariharan, D. Ramaiah, *Org. Lett.* **2005**, *7*, 5765-5768.
[129] A. V. Eliseev, H.-J. Schneider, *J. Am. Chem. Soc.* **1994**, *116*, 6081-6088.
[130] P. Schwinté, R. Darcy, F. O'Keeffe, *J. Chem. Soc., Perkin Trans. 2* **1998**, 805-808.
[131] J. Molnar, L. Lorand, *Arch. Biochem. Biophys.* **1961**, *93*, 353-363.
[132] M. A. Valenzuela, A. M. Kettlun, M. Mancilla, V. Calvo, N. Fanta, A. Traverso-Cori, *Phytochemistry* **1988**, *27*, 1981-1985.
[133] A. Traverso-Cori, H. Chaimovich, O. Cori, *Arch. Biochem. Biophys.* **1965**, *109*, 173-184.
[134] P. A. Lanzetta, L. J. Alvarez, P. S. Reinach, O. A. Candia, *Anal. Biochem.* **1979**, *100*, 95-97.
[135] M. Florea, W. M. Nau, *Org. Biomol. Chem.* **2010**, *8*, 1033-1039.
[136] G. L. Cantoni, *Annu. Rev. Biochem.* **1975**, *44*, 435-451.
[137] H. L. Schubert, R. M. Blumethal, X. Cheng, *TRENDS Biochem. Sci.* **2003**, *28*, 329-335.
[138] T. Kouzarides, *Cell* **2007**, *128*, 693-705.
[139] S. R. Bhaumik, E. Smith, A. Shilatifard, *Nat. Struct. Mol. Biol.* **2007**, *14*, 1008-1016.
[140] R. A. Varier, H. T. M. Timmers, *Biochim. Biophys. Acta, Rev. Cancer* **2011**, *1815*, 75-89.
[141] B. D. Strahl, R. Ohba, R. G. Cook, C. D. Allis, *Proc. Natl. Acad. Sci.* **1999**, *96*, 14967-14972.
[142] A. Frankel, N. Yadav, J. Lee, T. L. Branscombe, S. Clarke, M. T. Bedford, *J. Biol. Chem.* **2002**, *277*, 3537-3543.
[143] H. Gowher, X. Zhang, X. Cheng, A. Jeltsch, *Anal. Biochem.* **2005**, *342*, 287-291.
[144] P. Rathert, X. Cheng, A. Jeltsch, *Biotechniques* **2007**, *43*, 602-608.
[145] T. Bonaldi, J. T. Regula, A. Imhof, *Methods Enzymol.* **2004**, *377*, 111-130.
[146] Y. Q. Chang, T. Ganesh, J. R. Horton, A. Spannhoff, J. Liu, A. M. Sun, X. Zhang, M. T. Bedford, Y. C. Shinkai, J. P. Snyder, X. D. Cheng, *J. Mol. Biol.* **2010**, *400*, 1-7.
[147] A. H. Peters, S. Kubicek, K. Mechtler, R. J. O'Sullivan, A. A. Derijck, L. Perez-Burgos, A. Kohlmaier, S. Opravil, M. Tachibana, Y. Shinkai, J. H. Martens, T. Jenuwein, *Mol. Cell.* **2003**, *12*, 1577-1589.
[148] K. Sarma, K. Nishioka, D. Reinberg, *Methods Enzymol.* **2004**, *376*, 255-269.
[149] T. L. Graves, Y. Zhang, J. E. Scott, *Anal. Biochem.* **2008**, *373*, 296-306.
[150] V. J. Bailey, B. P. Keeley, C. R. Razavi, E. Griffiths, H. E. Carraway, T. H. Wang, *Methods* **2010**, *52*, 237-241.

[151] K. M. Dorgan, W. L. Wooderchak, D. P. Wynn, E. L. Karschner, J. F. Alfaro, Y. Q. Cui, Z. S. Zhou, J. M. Hevel, *Anal. Biochem.* **2006**, *350*, 249-255.
[152] E. Collazo, J. F. Couture, S. Bulfer, R. C. Trievel, *Anal. Biochem.* **2005**, *342*, 86-92.
[153] C. H. Wang, S. Leffler, D. H. Thompson, C. A. Hrycyna, *Biochem. Biophys. Res. Commun.* **2005**, *331*, 351-356.
[154] C. L. Hendricks, J. R. Ross, E. Pichersky, J. P. Noel, Z. S. Zhou, *Anal. Biochem.* **2004**, *326*, 100-105.
[155] G. Ibáñez, J. L. McBean, Y. M. Astudillo, M. Luo, *Anal. Biochem.* **2010**, *401*, 203-210.
[156] A. Spannhoff, W. Sippl, M. Jung, *Int. J. Biochem. Cell Biol.* **2009**, *41*, 4-11.
[157] A. Spannhoff, A. T. Hauser, R. Heinke, W. Sippl, M. Jung, *ChemMedChem* **2009**, *4*, 1568-1582.
[158] A. Ganesan, L. Nolan, S. J. Crabb, G. Packham, *Curr. Cancer Drug Targets* **2009**, *9*, 963-981.
[159] W. Sippl, M. Jung, in *Methods and Principles in Medicinal Chemistry, Vol. 42*, Wiley-VCH, Weinheim, **2010**.
[160] R. A. Copeland, E. J. Olhava, M. P. Scott, *Curr. Opin. Chem. Biol.* **2010**, *14*, 505-510.
[161] B. Lohse, A. L. Nielsen, J. B. L. Kristensen, C. Helgstrand, P. A. C. Cloos, L. Olsen, M. Gajhede, R. P. Clausen, J. L. Kristensen, *Angew. Chem. Int. Ed.* **2011**, *50*, 9100-9103.
[162] X. Zhang, Z. Yang, S. I. Khan, J. R. Horton, H. Tamaru, E. U. Selker, X. D. Cheng, *Mol. Cell.* **2003**, *12*, 177-185.
[163] J. M. Lehn, R. Meric, J. P. Vigneron, M. Cesario, J. Guilhem, C. Pascard, Z. Asfari, J. Vicens, *Supramol. Chem.* **1995**, *5*, 97-103.
[164] T. Jin, *J. Incl. Phenom. Macrocycl. Chem.* **2003**, *45*, 195-201.
[165] T. Jin, *Sensors* **2010**, *10*, 2438-2449.
[166] P. Rathert, X. Zhang, C. Freund, X. Cheng, A. Jeltsch, *Chem. Biol.* **2008**, *15*, 5-11.
[167] X. Zhang, H. Tamaru, S. I. Khan, J. R. Horton, L. J. Keefe, E. U. Selker, X. D. Cheng, *Cell* **2002**, *111*, 117-127.
[168] H. Tamaru, X. Zhang, D. McMillen, P. B. Singh, J. Nakayama, S. I. Grewal, C. D. Allis, X. D. Cheng, E. U. Selker, *Nature Genetics* **2003**, *34*, 75-79.
[169] R. E. Collins, M. Tachibana, H. Tamaru, K. M. Smith, D. Jia, X. Zhang, E. U. Selker, Y. Shinkai, X. D. Cheng, *J. Biol. Chem.* **2005**, *280*, 5563-5570.
[170] T. Jenuwein, G. Laible, R. Dorn, G. Reuter, *Cell. Mol. Life Sci.* **1998**, *54*, 80-93.
[171] R. B. Brandt, J. E. Laux, S. W. Yates, *Biochem. Med. Metab. Biol.* **1987**, *37*, 344-349.
[172] M. Florea, S. Kudithipudi, A. Rei, M. José Gonzáles-Álvarez, A. Jeltsch, W. M. Nau, *Chem. Eur. J.* **2012**, *18*, in press.
[173] M. K. Ramjee, U. Genschel, C. Abell, A. G. Smith, *Biochem. J.* **1997**, *323*, 661-669.
[174] G. Gopalan, S. Chopra, A. Ranganathan, K. Swaminathan, *Proteins* **2006**, *65*, 796-802.
[175] M. E. Webb, A. G. Smith, C. Abell, *Nat. Prod. Rep.* **2004**, *21*, 695-721.

[176] J. de Villiers, L. Koekemoer, E. Strauss, *Chem. Eur. J.* **2010**, *16*, 10030-10041.
[177] J. M. Williamson, G. M. Brown, *J. Biol. Chem.* **1979**, *254*, 8074-8082.
[178] L. M. Abell, M. H. O'Leary, *Biochemistry* **1988**, *27*, 5933-5939.
[179] J. Rohacova, A. I. Lazar, W. M. Nau, unpublished results.
[180] D. Klapstein, U. Pischel, W. M. Nau, *J. Am. Chem. Soc.* **2002**, *124*, 11349-11357.
[181] M. J. Frisch, G. W. Trucks, H. B. Schlegel, G. E. Scuseria, M. A. Robb, J. R. Cheeseman, J. A. Montgomery, Jr., T. Vreven, K. N. Kudin , J. C. Burant, J. M. Millam, S. S. Iyengar, J. Tomasi, V. Barone, B. Mennucci, M. Cossi, G. Scalmani, N. Rega, G. A. Petersson, H. Nakatsuji, M. Hada, M. Ehara, K. Toyota, R. Fukuda, J. Hasegawa, M. Ishida, T. Nakajima, Y. Honda, O. Kitao, H. Nakai, M. Klene, X. Li, J. E. Knox, H. P. Hratchian, J. B. Cross, V. Bakken, C. Adamo, J. Jaramillo, R. Gomperts, R. E. Stratmann, O. Yazyev, A. J. Austin, R. Cammi, C. Pomelli, J. W. Ochterski, P. Y. Ayala, K. Morokuma, G. A. Voth, P. Salvador, J. J. Dannenberg, V. G. Zakrzewski, S. Dapprich, A. D. Daniels, M. C. Strain, O. Farkas, D. K. Malick, A. D. Rabuck , K. Raghavachari, J. B. Foresman, J. V. Ortiz, Q. Cui, A. G. Baboul, S. Clifford, J. Cioslowski, B. B. Stefanov, G. Liu, A. Liashenko, P. Piskorz, I. Komaromi, R. L. Martin, D. J. Fox, T. Keith, M. A. Al-Laham, C. Y. Peng, A. Nanayakkara, M. Challacombe, P. M. W. Gill, B. Johnson, W. Chen, M. W. Wong, C. Gonzalez, J. A. Pople, *Gaussian 03* Revision E.01; Gaussian, Inc.: Wallingford, CT, 2004.
[182] A. L. Koner, J. Schatz, W. M. Nau, U. Pischel, *J. Org. Chem.* **2007**, *72*, 3889-3895.
[183] R. Askani, *Chem. Ber.* **1965**, *98*, 2551-2555.
[184] A. Hennig, T. Schwarzlose, W. M. Nau, *Arkivoc* **2007**, 341-357.
[185] H. Wenschuh, R. Volkmer-Engert, M. Schmidt, M. Schulz, J. Schneider-Mergener, U. Reineke, *Biopolymers* **2000**, *55*, 188-206.
[186] R. Frank, *J. Immunol. Methods* **2002**, *267*, 13-26.
[187] S. V. Aathimanikandan, B. S. Sandanaraj, C. A. Arges, C. J. Bardeen, S. Thayumanavan, *Org. Lett.* **2005**, *7*, 2809-2812.
[188] A. Glieder, E. T. Farinas, F. H. Arnold, *Nat. Biotech.* **2002**, *20*, 1135-1139.
[189] J. B. van Beilen, E. G. Funhoff, *Appl. Microbiol. Biotechnol.* **2007**, *74*, 13-21.
[190] B. L. Dubbels, L. A. Sayavedra-Soto, D. J. Arp, *Microbiology* **2007**, *153*, 1808-1816.
[191] T. Kotani, T. Yamamoto, H. Yurimoto, Y. Sakai, N. Kato, *J. Bacteriol.* **2003**, *69*, 2421-2430.
[192] A. Schirmer, M. A. Rude, E. Popova, S. B. del Cardayre, *Science* **2010**, *329*, 559-562.
[193] S. Sun, Z. Li, Supramolecular interaction of a hemicyanine with CB[6] and its application as a resettable logic gate in *Second International Conference on Cucurbiturils*, Cambrige, UK, **2011**.
[194] A. Gärdes, E. Kaeppel, A. Shehzad, S. Seebah, H. Teeling, P. Yarza, F. O. Glöckner, H.-P. Grossart, M. S. Ullrich, *Standards in Genomic Sciences* **2010**, *3*, 97-107.
[195] I. M. Head, D. M. Jones, W. F. M. Rölling, *Nat. Rev.* **2006**, *4*, 173-182.

[196] J. A. Adams, *Chem. Rev.* **2001**, *101*, 2271-2290.
[197] S. R. Hubbard, J. H. Till, *Annu. Rev. Biochem.* **2000**, *69*, 373-398.
[198] L. N. Johnson, R. J. Lewis, *Chem. Rev.* **2001**, *101*, 2209-2242.
[199] M. Manger, M. Scheck, H. Prinz, J. P. von Kries, T. Langer, K. Saxena, H. Schwalbe, A. Fürstner, J. Rademann, H. Waldmann, *ChemBioChem* **2005**, *6*, 1749-1753.
[200] C. M. Spangler, C. Spangler, M. Göttle, Y. Shen, W.-J. Tang, R. Seifert, M. Schäferling, *Anal. Biochem.* **2008**, *381*, 86-93.

# APPENDICES

# APPENDIX 1

A. Hennig, M. Florea, D. Roth, T. Enderle, W. M. Nau, “Design of Peptide Substrates for Nanosecond Time-Resolved Fluorescence Assays of Proteases: 2,3-Diazabicyclo[2.2.2]oct-2-ene as a Noninvasive Fluorophore”, *Analytical Biochemistry*, **2007**, *360*, 255-265. Reprinted with permission from Elsevier. Publisher’s version may be found at:
http://www.sciencedirect.com/science/article/pii/S0003269706006816

# Design of Peptide Substrates for Nanosecond Time-Resolved Fluorescence Assays of Proteases: 2,3-Diazabicyclo[2.2.2]oct-2-ene as a Noninvasive Fluorophore

Andreas Hennig[a], Mara Florea[a], Doris Roth[b], Thilo Enderle[b], and Werner M. Nau[a,*]

[a] *School of Engineering and Science, International University Bremen, Campus Ring 1, D-28759 Bremen, Germany*

[b] *F. Hoffmann-La Roche AG, Grenzacherstrasse 124, CH-4070 Basel, Switzerland*

* Corresponding author. Fax: +49 421 2003229, Tel.: +49 421 2003233, *E-mail address:* w.nau@iu-bremen.de

**Running Title**: Nanosecond Time-Resolved Fluorescence Assays

**Subject category**: enzymatic assays and analysis

**Keywords**: enzymes, exopeptidases, fluorescence, proteases, time-resolved assays

***Abstract***. Fluorescence protease assays were investigated with peptide substrates containing 2,3-diazabicyclo[2.2.2]oct-2-ene as a fluorescent amino acid (Dbo). The special characteristic of the fluorophore Dbo is its exceedingly long fluorescence lifetime (ca. 300 ns in water under air), which allows the use of nanosecond time-resolved fluorescence (Nano-TRF) detection to efficiently suppress shorter-lived background emission. In addition, the natural amino acids tryptophan and tyrosine can be employed as intramolecular fluorescence quenchers, which facilitates substrate design. 14 synthetic peptide substrates (composed of 2-19 amino acids) and 5 enzymes (trypsin, pepsin, carboxypeptidase A, leucine aminopeptidase, and chymotrypsin) were investigated and in all 28 examined combinations enzymatic activity was detected by monitoring the increase in steady-state fluorescence with time and determining the reaction rates in terms of the $k_{cat}/K_M$ values, which ranged from 0.2 to 80 × $10^6$ $M^{-1}min^{-1}$. The results suggest an excellent compatibility of the very small and hydrophilic fluorescent probe Dbo with solid-phase peptide synthesis and the investigated proteases. For all 14 peptides the fluorescence lifetimes before and after enzymatic cleavage were measured and Nano-TRF measurements were performed in 384-well microplates. The fluorescence lifetimes of the different peptides provide the basis for the rational design of Dbo-based fluorescent substrates for protease assays. Measurements in Nano-TRF mode revealed, besides efficient suppression of background fluorescence, an increased differentiation between cleaved and uncleaved substrate. The Dbo-based assays can be adapted for high-throughput screening (HTS).

## Introduction

Proteases constitute arguably the most intensively studied class of enzymes and have been subject of extensive research in diverse fields, whether as prototypes for investigating enzyme mechanisms[1] or as sustainable reagents in organic synthesis.[2] A key aspect is their role in numerous physiological processes like digestion, blood coagulation, fertilization, and cell growth, death, and differentiation. Defects in proteolytic digestion are the cause of major diseases like parasitic infections, arthritis, Alzheimer's disease, inflammation, osteoporosis, arteriosclerosis, and cancer. Inhibitors and in some cases activators of proteases do therefore remain prime targets in drug discovery,[3-5] which calls for more convenient and refined methods to detect proteolytic activity, both in laboratory scale as well as in high-throughput screening (HTS)[1] format.[6, 7]

A large variety of protease assays have been developed, among which fluorescence-based assays stand out due to their convenient access, high sensitivity, short detection times, and possibility for continuous monitoring.[6, 7] Early approaches utilized fluorogenic substrates, in which the protease cleaves off the fluorophore itself, accompanied by a functional group interconversion at the fluorophore and a concomitant increase in fluorescence.[8] The disadvantages of this method are well-defined: A synthetic organic residue occupies the *C*-terminal or *N*-terminal region of the cleavage site, the hydrolyzed bond is different from a usual peptide bond, and only one side of the substrate can be altered in mutation studies.[8] To avoid the complications of fluorogenic substrates,[7, 9, 10] fluorescence resonance energy transfer (FRET) has been exploited in combination with doubly labeled substrates, bearing an energy donor on one side of the hydrolyzed bond and an acceptor on the other side (hetero-double labeling, Scheme 1a); since FRET operates over larger distances (typically 20-50 Å), the labels do not need to be placed in immediate proximity of the susceptible bond. Upon proteolytic cleavage, donor and acceptor diffuse apart to become spatially separated, efficient FRET no longer applies, and the intrinsic fluorescence of the probe or the donor is revived (Scheme 1a).[9]

[1] Abbreviations used: CPA, carboxypeptidase A; DBO, 2,3-diazabicyclo[2.2.2]oct-2-ene; Dbo, 2,3-diazabicyclo[2.2.2]oct-2-ene-labeled asparagine; FRET, fluorescence resonance energy transfer; HTS, high-throughput screening; TRF, time-resolved fluorescence; LAP, leucine aminopeptidase; CT, chymotrypsin.

**Scheme 1**: Principles of fluorescent protease assays based on a) FRET (hetero-double-labeling), b) static probe/quencher contact (either with two identical fluorophores, i.e. homo-double-labeling, or single-labeling with Trp as quencher), and c) collision-induced quenching of a probe (Dbo) by a contact quencher (Trp or Tyr).

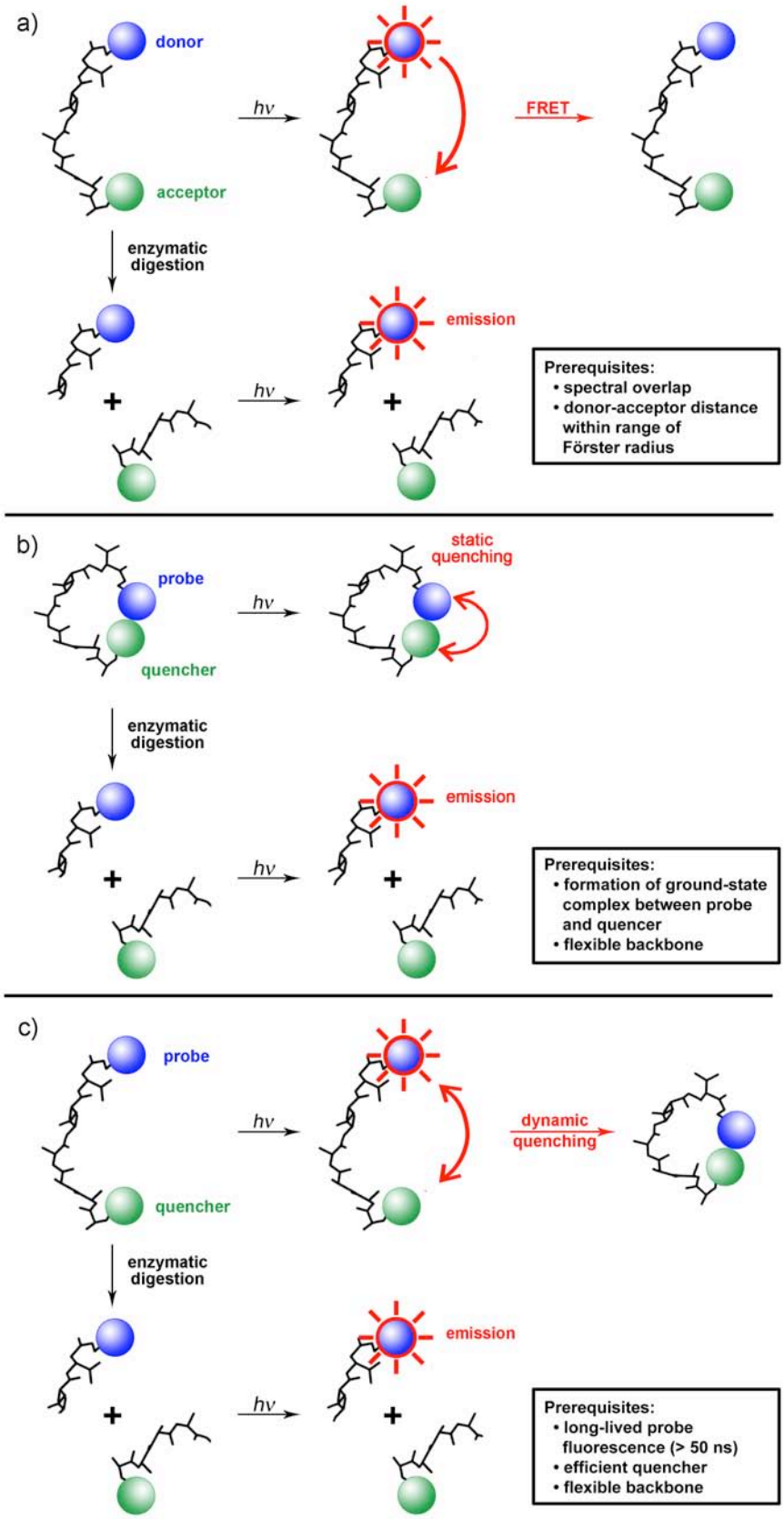

However, the introduction of two different large aromatic dyes (donor and acceptor) into FRET substrates presents still a major obstacle in the design of fluorescent protease assays.[11] The corresponding hetero-double-labeled substrates are prone to undergo specific or unspecific binding as well as steric repulsion with the enzymatic pockets, which has a significant effect on the enzyme kinetics[12] or might even lead to a loss of activity.[13, 14] To remedy, large aromatic dyes are routinely introduced by long tethers, frequently by post-column labeling strategies, which creates additional challenges to synthesis and purification.[10, 15] Additional practical complications arise from the competition of intermolecular with intramolecular FRET and from imperfect excitation of the donor due to unavoidable concomitant absorption of the acceptor. Finally, FRET substrates are generally unsuitable for the investigation of exopeptidases.

The synthetic problems related to FRET substrates have been addressed either by double labeling with the same fluorescent probe (homo-double-labeling),[16, 17] or by a single-labeling approach, in which a natural amino acid, most prominently Trp, could act as quencher.[12, 18] The latter two approaches have recently become popular, but both take the toll that FRET can no longer serve as the quenching mechanism. In the former case (homo-double-labeling), FRET donor and acceptor are identical, and in the latter case the absorption of natural amino acids lies too far in the UV to fulfill the acceptor requirement for spectral overlap, while direct excitation of amino acids as FRET donors requires an undesirable far-UV excitation.[19] Reported homo-double-labeling strategies with rhodamine ground state dimers[16] or single-labeling approaches, e.g., of an oxazine dye with Trp as quencher,[18] require static probe/quencher contact (Scheme 1b), i.e., a substantial fraction of the peptide substrate has to adapt a conformation in which probe and quencher are in contact to allow the native emission to be quenched.[2] The necessity to observe such static contact quenching imposes a different line of requirements for substrate design, e.g., probe/quencher contact becomes difficult when either the separation between probe and quencher needs to be large[20] (the preferred substrate for Botulinum toxin B contains for example 35 amino acids)[13] or when the peptide backbone becomes rigid.[21] Finally, the aggregation of the chromophores required for static quenching alters the native conformation of the substrate.

[2] A static quenching mechanism was also postulated in an early hetero-double-labeling approach with an *o*-aminobenzoyl group as a probe and a *p*-nitrobenzyloxy group as quencher, *cf.* ref. [8],[9] and A. Yaron, A. Carmel, E. Katchalski-Katzir, Intramolecularly quenched fluorogenic substrates for hydrolytic enzymes, Anal. Biochem. 95 (1979) 228-235. The further development of this assay type was not recommended.[8]

We have recently communicated a complementary protease assay based on collision-induced intramolecular fluorescence quenching (Scheme 1c), which was applied to carboxypeptidase A (CPA). [12] Our assay, which is based on 2,3-diazabicyclo[2.2.2]oct-2-ene (DBO)[22] as fluorescent label and Trp (or Tyr) as fluorescence quencher, by-passes several disadvantages of the established assays and can be readily incorporated into the desired substrates through a labeled asparagine (Dbo). In addition, the extremely long fluorescence lifetime of DBO (300 ns in water under air) allows a novel nanosecond time-resolved fluorescence (Nano-TRF) detection in order to suppress background emission and thereby increase the assay performance. Herein, we demonstrate that Nano-TRF assays can in fact be applied to a wide variety of proteases. We have screened 14 peptides for their activity against pepsin, trypsin, CPA, leucine aminopeptidase (LAP), and chymotrypsin (CT) and derived several important aspects of the new method. In particular, we could demonstrate that the differentiation of cleaved and uncleaved peptide can be dramatically improved in Nano-TRF mode. A successful example on pharmaceutical/industrial format demonstrated further, that the Dbo-based assays are suitable for HTS.

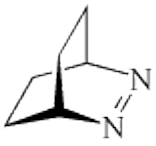


2,3-diazabicyclo[2.2.2]oct-2-ene
(DBO)

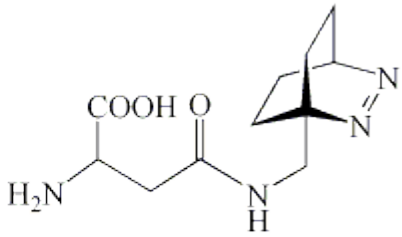


DBO-labeled asparagine
(Dbo)

## Materials and Methods

*Peptide Substrates and Enzymes*

DBO-labeled asparagine was synthesized according to a literature procedure,[20] and may be purchased from Assaymetrics (Cardiff, UK). The polypeptides **1**-**4**,**8**,**9**, and **12** were synthesized by Affina Immuntechnik GmbH (Berlin, Germany) in >95 % purity, except peptide **2** which had a purity of 81 %. The other peptides (**5**-**7**, **10**, **11**, **13**, and **14**) were prepared by Biosyntan GmbH (Berlin, Germany) and obtained in >95 % purity. Trypsin (from bovine pancreas, 2500 U/mg) and chymotrypsin (CT, from bovine pancreas, 1500 U/mg) were from AppliChem (Darmstadt, Germany). Leucine aminopeptidase (LAP, type IV-S, from porcine kidney microsomes, 24 U/mg) was from Sigma. Carboxypeptidase A (CPA, PMSF treated, from bovine pancreas, 64 U/mg) and pepsin (from hog stomach, 3834 U/mg) were from Fluka.

We used a 67 mM phosphate buffer for pH 7 (for CT), a 112 mM borate buffer for pH 8 (for trypsin) and a 30 mM citrate buffer for pH 2 (for pepsin), which were all commercial (AppliChem, Darmstadt, Germany). LAP was activated for 2 hours at 37 °C in 2 mM $MnCl_2$ and 0.05 M Tris (adjusted with HCl to pH 8.5) before use and the assay was performed in 0.05 M Tris (adjusted with HCl to pH 7.8). CPA was assayed as reported.[12]

*Fluorescence Spectroscopy*

Absorption measurements of enzyme and peptide stock solutions were performed with a Varian Cary 4000 spectrophotometer. The following extinction coefficients were used to derive the concentrations: $\varepsilon_{278}$ = 64200 $M^{-1}cm^{-1}$ for CPA,[23] $\varepsilon_{280}$ = 33600 for trypsin,[24] $\varepsilon_{280}$ = 50000 for CT,[25] $\varepsilon_{280}$ = 50700 for pepsin,[26] and $\varepsilon_{282}$ = 320000 for LAP.[27] The concentrations of the peptides were determined by assuming the same extinction coefficients as for the free amino acids Trp[20] and Tyr.[28]

Fluorescence lifetimes were measured by time-correlated single photon counting (FLS920, Edinburgh Instruments) with a Picoquant picosecond pulsed diode laser ($\lambda_{exc}$ = 373 nm, $\lambda_{em}$ = 450 nm, ca. 50 ps pulsewidth) for excitation. The lifetimes recovered by tail-fitting with the instrument-specific software, were monoexponential as judged by a reduced $\chi^2$ of 1.00 ± 0.05 and a random distribution of the weighted residuals around zero; fitting with multiexponential decay functions was therefore not indicated. Kinetic traces were collected with a Varian Eclipse spectrofluorometer, equipped with a thermostated cell holder ($\lambda_{exc}$ = 365 nm, $\lambda_{em}$ = 450 nm).

*Kinetic assays*

1 mM stock solutions of peptides were prepared in water and stored at +4 °C. For measurement an appropriate amount was diluted with the respective buffer solution and the sample was allowed to equilibrate for at least 10 min in a thermostated cell holder at 25.0 ± 0.1 °C. Enzyme stock solutions were freshly prepared on a daily basis in 1 mM HCl (CT and trypsin), 10 % LiCl (CPA), pH 2 buffer (pepsin), or, for LAP, in its activation buffer.

Nano-TRF assays were carried out in black 384-well microplates (Corning NBS) using 50 µl final sample volume with an LF 402 NanoScan FI microplate reader (IOM, Berlin, Germany). An external nitrogen laser (MNL 200, Laser Technik Berlin, Germany) was coupled by glass fibers to a dye laser module, which had a maximum dye emission at 365 nm. The emission was detected at 450 nm with a gate time of 2 µs. Unless stated differently, we used the minimum delay time of 150 ns, which was sufficient to efficiently suppress all short-lived emission.[12]

**Results and Discussion**

The peculiarities of DBO as a non-invasive, hydrophilic, and extremely small organic fluorescent probe have been studied in great detail[29-31] and also applied in the areas of biomolecular and supramolecular chemistry.[20, 21, 32-37] The most useful photophysical property of DBO is its exceedingly long fluorescence lifetime (up to 1 μs, depending on solvent and environment).[38] When introduced into peptides by means of a labeled asparagine (Dbo), peptides with long fluorescence lifetimes (ca. 300 ns) result unless an intramolecular quencher is present. In addition, it was observed that Dbo is also efficiently quenched by four natural amino acids (Trp, Tyr, Met, and Cys).[20] A collision-induced quenching mechanism applies, either exciplex-induced quenching (e.g., for Trp) or hydrogen atom abstraction (e.g., for Tyr), and both quenching pathways require an intimate probe/quencher contact.[20] The intramolecular collision-induced quenching in Dbo-labeled peptides can be exploited in the design of protease assays according to Scheme 1c. Such assays are conceptually interesting because (*i*) they are based on a collision-induced quenching mechanism and (*ii*) they afford cleaved products with a sufficiently long fluorescence lifetime to allow time-resolved detection.

The collision-induced quenching is made possible by the exceedingly long fluorescence lifetime of Dbo (ca. 300 ns in the absence of quenchers), which allows mutual intrachain diffusion and therefore probe/quencher collision with the associated fluorescence quenching to occur within the excited-state fluorescence lifetime of the probe. For comparison, intrachain diffusion, which occurs on a time-scale of ca. 10 ns to 1 μs in short peptides,[20, 21, 33-35] is too slow to cause a sizable fluorescence quenching of conventional fluorescent dyes which have much shorter fluorescence lifetimes (< 5 ns). The collision-induced quenching mechanism (Scheme 1c) allows a very versatile design of peptide substrates for proteases because dynamic fluorescence quenching is feasible for practically all amino acid sequences[21, 33] (except polyprolines)[34] and its efficiency decreases only weakly with increasing probe-quencher separation and has been observed for up to 20 intervening amino acids.[20, 35] In addition, even in cases where collision-induced quenching is less efficient, the detection can be improved by means of the Nano-TRF detection (see below).

The ability to employ natural amino acids as intrinsic fluorescence quenchers presents another asset, because it remedies the necessity to introduce two distinct extrinsic dyes, as is the case in protease assays with FRET substrates (Scheme 1a); this facilitates the design of protease substrates. 14 peptides (**1**-**14**, Table 1) were presently investigated. These were

designed according to known recognition motifs for the different enzymes employed in this study,[39, 40] or were available from independent mechanistic studies.[12, 21, 33, 34] Trypsin and CT were employed as well-investigated model enzymes. Pepsin was selected to demonstrate the pH insensitivity of Dbo, because this enzyme requires pH 2. In addition, we have included exopeptidases (LAP and CPA), which remain challenging targets in enzyme assays, especially for mutation studies when remote residues in the substrate need to be altered.[41]

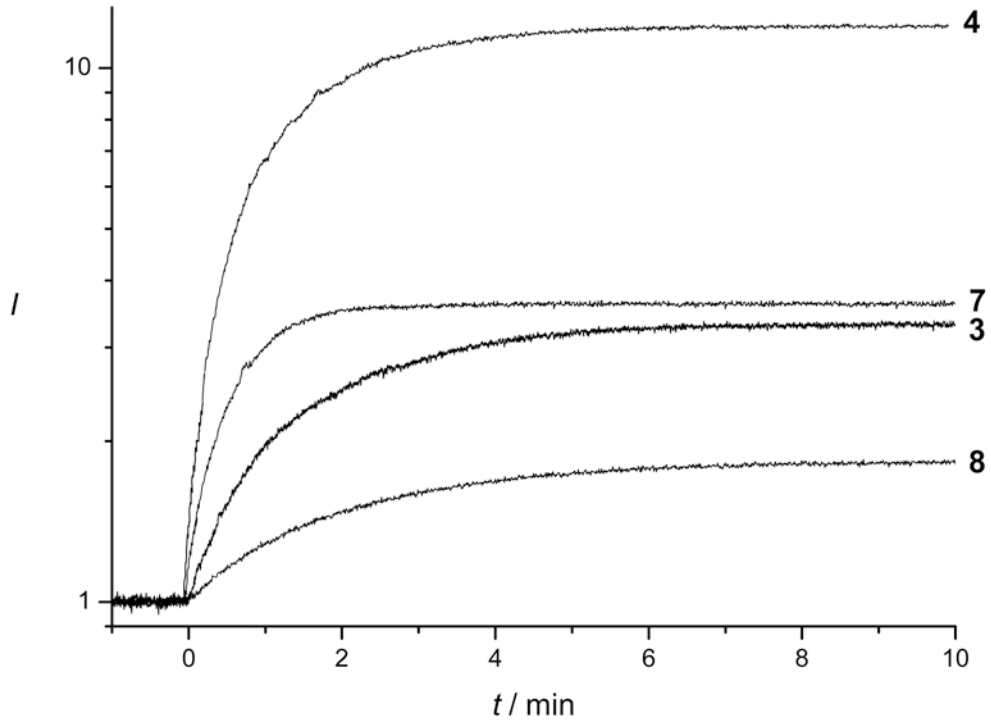


**Fig. 1**: Representative traces (note the logarithmic intensity scale) showing the increase in relative fluorescence intensity (*I*) of the peptides H-WTLTGKX-$NH_2$ (**4**), H-XLSLSRFSWGA-OH (**7**), H-WQIFVKX-$NH_2$ (**3**) and H-YQIFVKX-$NH_2$ (**8**) (all 50 μM) during enzymatic cleavage by trypsin (300 nM), LAP (63 nM), CT (200 nM), and CT (300 nM), respectively.

All peptides were prepared by standard solid phase synthesis by using Fmoc-protected Dbo,[20] thereby eliminating the additional post-column labeling and purification steps required for alternative fluorescence labels.[10, 42, 43] Noteworthy, no complications during synthesis and purification were encountered in any case. Trp was used as fluorescence quencher in analogy to the preliminary report;[12] in addition, we have tested the use of Tyr as an alternative fluorescence quencher (peptides **8**-**10**). The utilization of these two amino

acids not only by-passes the introduction of a second synthetic label, but, as an added advantage, they are intrinsically present in many recognition motifs of proteases.[8-10, 13, 14, 39, 40] All investigated peptides were efficiently cleaved by the corresponding enzymes as could be conveniently monitored with a standard steady-state fluorometer (Figure 1). In all cases, the fluorescence intensity increased continuously upon addition of the enzyme until the characteristic plateau region was reached, signaling quantitative substrate hydrolysis.[3]

The traces were used to derive pseudo-first order rate constants ($k$) by non-linear regression using the known relationship between the fluorescence intensity $I$ *versus* time $t$: $I = I_{max}(1-\exp(-(k)[E]t))$, where [E] is the concentration of protease as determined by UV spectrophotometry.[44] The pseudo-first-order rate constants $k$ equal $k_{cat}/K_M$ under the condition[44] that the initial concentration of substrate is much less than $K_M$, which is met whenever the $k$ values are found to be independent of substrate concentration within the assayed concentration range. Determinations at a minimum of three initial substrate concentrations in the range of 5-100 μM confirmed that this applied in all cases.

The $k_{cat}/K_M$ values in Table 1 allow a comparison of the relative susceptibility of the substrates towards enzymatic cleavage. Generally speaking, the Dbo-labeled peptides were efficiently cleaved with the rates being comparable to those observed for substrates carrying different labels.[17, 19, 45] Importantly, the position of the Dbo chromophore does not affect the enzyme kinetics in a systematic manner, and even if Dbo is placed directly adjacent to the hydrolyzed bond (peptides **1**,**3**,**4**,**8**,**9**, and **14**), the enzymatic activity is not adversely affected. The relative rate constants are also consistent with the known preferences for each enzyme.[39, 40] For example, peptides with a positively charged amino acid residue in their sequence are more efficiently cleaved by trypsin than those lacking such an amino acid.

The observed increase in fluorescence intensity, which ultimately limits the sensitivity of fluorescence protease assays based on the respective substrates, varies for the different peptide/enzyme combinations ($I_{rel}$ in Table 1 and Figure 1). The fluorescence increase depends mainly on the efficiency of fluorescence quenching in the probe/quencher-labeled

[3] We also determined for each enzyme kinetics the fluorescence lifetime once no change in the fluorescence intensities was noted (plateau region in Figure 1); the observation of a monoexponential fluorescence decay confirmed in all cases that the hydrolysis of the substrate was complete. An incomplete substrate conversion could occur, for example, if the protease became inactive during the kinetic run, which would similarly result in the observation of an apparent plateau. In the latter case, a biexponential fluorescence decay would be expected with the fluorescence lifetimes of the uncleaved and partially cleaved forms as components (Table 2). This was in fact observed when lifetime measurements were performed in the rise phase before the plateau was reached, e.g., when a CT assay was intentionally stopped by addition of 1 M HCl.

peptide, because the fluorescence intensity of the cleaved peptide should always resemble that of unquenched Dbo (unless an additional quencher remains present after cleavage).[35] This interpretation is nicely confirmed by the fluorescence lifetimes of the peptides, which were found to be monoexponential both before ($\tau_{Dbo/Q}$) and after ($\tau_{Dbo}$) cleavage (Table 2, see also footnote 3). The relative increase in fluorescence intensity ($I_{rel}$) was found to be in good agreement with the relative increase in fluorescence lifetime ($\tau_{rel}$), although the latter one tended to be higher.[4] As expected, the fluorescence lifetime after cleavage ($\tau_{Dbo}$) was found to be relatively constant (ca. 300 ns) and comparable to the fluorescence lifetime of the unquenched parent chromophore DBO in water under air (325 ns). The fluorescence lifetimes of the uncleaved peptides ($\tau_{Dbo/Q}$) were significantly shorter as a consequence of intramolecular fluorescence quenching; they showed also large variations, which is also the underlying reason for the differential increase in steady-state fluorescence intensity upon cleavage of different substrates (Figure 1). Although not analyzed in detail, the quenching efficiencies depend strongly on the length of the backbone separating probe (Dbo) from quencher (Trp or Tyr)[20, 35] and the flexibility of the backbone as imposed by the types and sequence of amino acids.[21, 33, 34] For example, the length dependence is the reason for the slightly longer fluorescence lifetime of H-XGGW-OH (7.6 ns) compared to H-XGW-OH (5.9 ns) and the dependence on the flexibility manifests itself in the fluorescence lifetimes of the substrates H-WTLTGKX-$NH_2$ (27 ns) and H-WQIFVKX-$NH_2$ (90 ns); the former is rich in flexible amino acids (G,L,T, according to the known flexibility scale),[21] while the latter contains mostly rigid ones (I,V,F,K). Noteworthy, in the case of flexible substrates like H-GSWR$(GS)_7$X-$NH_2$ (50 ns), very efficient quenching was observed even with 15 intervening amino acids.

Peptides bearing Trp as quencher were more efficiently quenched than those with Tyr, which is known to be a weaker quencher.[20, 33] The most direct comparison can be drawn between H-WQIFVKX-$NH_2$ and H-YQIFVKX-$NH_2$, in which the latter substrate had a 2-fold longer fluorescence lifetime than the former one. In principle, by adjusting the pH to higher values (> 12), e.g. by adding NaOH in the course of a stopped assay, it is possible to increase

[4] The smaller increase in steady-state fluorescence intensity compared to the increase in fluorescence lifetimes is presumably due to background emission and fluorescence from unknown short-lived impurities inside the sample (purity > 95 %); the contribution of the background emission may lead to a sizable increase in steady-state fluorescence of the quenched peptide, which decreases the relative increase in fluorescence intensity ($I_{rel}$), but leaves the experimental fluorescence lifetimes of Dbo unaffected, because background emission is much shorter lived and was not considered in the tail fitting of the decay traces.

the efficiency of quenching by Tyr and therefore the differentiation between substrate and product fluorescence. This is because Tyr is deprotonated in strongly alkaline media and the corresponding phenolate anion becomes a stronger quencher of Dbo fluorescence (comparable to Trp).[33]

We have also studied two peptide recognition sequences with natural occurrence of Trp or Tyr, namely H-AEY$^{\downarrow}$AAR$^{\downarrow}$G-OH[46] and H-LSLSR$^{\downarrow}$F$^{\downarrow}$SWGA-OH (arrows indicating the cleavage sites for CT next to the aromatic residues and for trypsin next to arginine).[47] These sequences can be readily used for fluorescence-based protease assays simply by attaching Dbo (X) to the *C* terminus (H-AEYAARGX-OH) or *N* terminus (H-XLSLSRFSWGA-OH). For comparison, a hetero-double-labeling approach would require the synthesis of FRET substrates with two extrinsic residues (X,Z: H-ZAEYAARGX-OH and H-XLSLSRFSWGAZ-OH). In addition, donor and acceptor would be further separated in the FRET (7 and 10 amino acids) than in the Dbo cases (4 and 7 amino acids), which may adversely affect the FRET efficiency and therefore the assay sensitivity.

Finally, we have studied by the single-labeling approach the exopeptidases CPA and LPA, which are enzymes that cleave *C*-terminal and *N*-terminal amino acids, respectively. Recall that a double-labeling approach (FRET) would place an unnatural organic chromophore directly at the recognition site, which does not allow its routine application to exopeptidases. The use of Trp in the recognition site of CPA has already been communicated;[12] as demonstrated herein, Trp can also be used to assay LAP (see Table 1, peptide **6**). As another interesting observation on the side, we found that H-XLSLSRFSWGA-OH, with direct attachment of Dbo, is an excellent substrate for LAP, even better than H-WKRTLRRX-$NH_2$ (Tables 1 and 2). This means that LAP "recognizes" Dbo as an amino acid to be cleaved *N*-terminally, which constitutes an attractive assay principle for HTS. Note, in the context of drug discovery, that LAP has been invoked in various diseases[48] and was recently identified as a prime target for inhibitor design.[49]

*Nanosecond time-resolved fluorescence (Nano-TRF)*

The fluorescence lifetimes of the cleaved peptides (ca. 300 ns) are much longer than typical fluorescence lifetimes of organic fluorophores as well as luminescence due to impurities, sample materials, and scattered light. The formation of this long-lived Dbo emission can be very selectively probed by employing a nanosecond time-resolved fluorescence (Nano-TRF) detection, in which any uninformative short-lived emission (background) can be suppressed by application of a time gate (Figure 2).[12] TRF has

originally become popular in the millisecond time domain for lanthanide chelates,[37, 42, 50-52] but exactly these suffer from the problems, which have been discussed above. First, lanthanide chelates are large ionic molecular entities,[42, 52] which can strongly influence enzyme kinetics.[11] Second, their emission is more accurately referred to as luminescence, because of the nature of the electronic transitions involved, and quenching by natural amino acids does not apply, which leaves only a double-labeling approach and quenching via resonance energy transfer.[53, 54] And third, their labeling proceeds often through long tethers like 1,6-diaminohexyl chains, which complicates routine synthesis.[55]

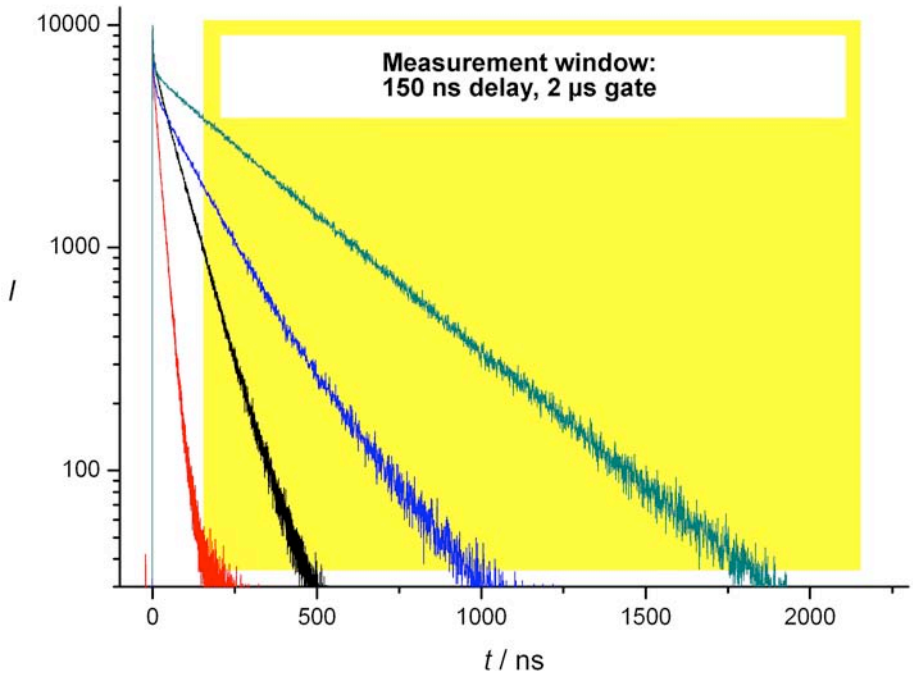


**Fig. 2**: Comparison of the fluorescence lifetimes for different peptides: H-WTLTGKX-$NH_2$ (**4**, 27 ns, red), H-WQIFVKX-$NH_2$ (**3**, 90 ns, black), H-YQIFVKX-$NH_2$ (**8**, 172 ns, blue) and H-X-$NH_2$ (355 ns, green), the last one being the common cleavage product by trypsin. Note the yellow time window which reflects the standard integration window employed for Nano-TRF detection to gate out background emission (sharp peak near $t$ = 0) and to increase the discrimination between uncleaved and cleaved peptide (e.g., red and green trace).

In addition to the suppression of background fluorescence, Nano-TRF can be exploited to increase the differentiation between the cleaved and uncleaved substrate and thereby increase the sensitivity of a potential fluorescence protease assay relative to steady-state measurements.[12, 52] Indeed, an improvement was observed for all substrates investigated in this study (compare $I_{rel,TRF}$ with $I_{rel}$ values in Table 2). In general, the improvement is largest for those substrates, which display the largest differences in fluorescence lifetimes before and

after cleavage (or which display the shortest lifetimes in the uncleaved form). The theoretical increase in fluorescence intensity in Nano-TRF mode, i.e., the integrated fluorescence intensity within the time gate ($I^{theo}_{rel,TRF}$) is calculated in Table 2 and can be compared with the theoretical increase in fluorescence intensity in steady-state mode; the latter corresponds to the ratio of fluorescence lifetimes. As can be seen, the theoretically expected increase is quite dramatic and amounts up to 16 orders of magnitude; these astronomic numbers cannot be experimentally realized, however, as can be deduced from the differentiation factors measured with a commercial Nano-TRF microplate reader ($I_{rel,TRF}$ in Table 2). This limitation is mostly due to instrumental restrictions and can be greatly improved upon by technical modifications; for example, when we changed in an exploratory assay from a setup using a nitrogen dye laser for excitation and a regular photomultiplier tube for detection (this work) to a set-up with a more intense Nd-YAG laser for excitation and an ICCD camera for detection, the differentiation could be further increased by an additional 2 orders of magnitude.[56] In particular, the maximum differentiation ($I_{rel,TRF} \approx 50$) observed for the peptides H-WTLTGKX-$NH_2$ (**4**, Figure 3), H-XGW-OH (**11**), H-XGGW-OH (**13**) and Ac-XW-OH (**14**) reflects the limited dynamic range of the presently employed instrument, i.e., the fluorescence emission after complete cleavage led to a saturation of the photomultiplier, while the detected emission before cleavage was already entirely suppressed, i.e., it was insignificantly different from that of the neat buffer reference solution.

For most substrates, the increase in fluorescence in Nano-TRF mode was smaller than the instrumental limit of ca. 50 ($I_{rel,TRF}$ = 2-10). Nevertheless, the goodness of the assay, as judged by the *Z'* factor, which takes also the standard deviation of the substrate and product fluorescence into account,[57] was always above 0.7, which is generally considered to be satisfactory even for assays performed on HTS scale. Regardless, assay performance can be further improved by rational choice of the time gate depending on the desired performance. In particular, while the preset 150 ns delay time used in the initial set of experiments was sufficiently long to efficiently suppress all common background from fluorescent impurities (e.g. buffers, cofactors or inhibitors), the differentiation between the uncleaved and cleaved substrate can be further optimized, if required, by adjusting the time delay according to the fluorescence lifetime of the uncleaved peptide; the latter varies from peptide to peptide (see above), and so does the ideal value for the delay time.

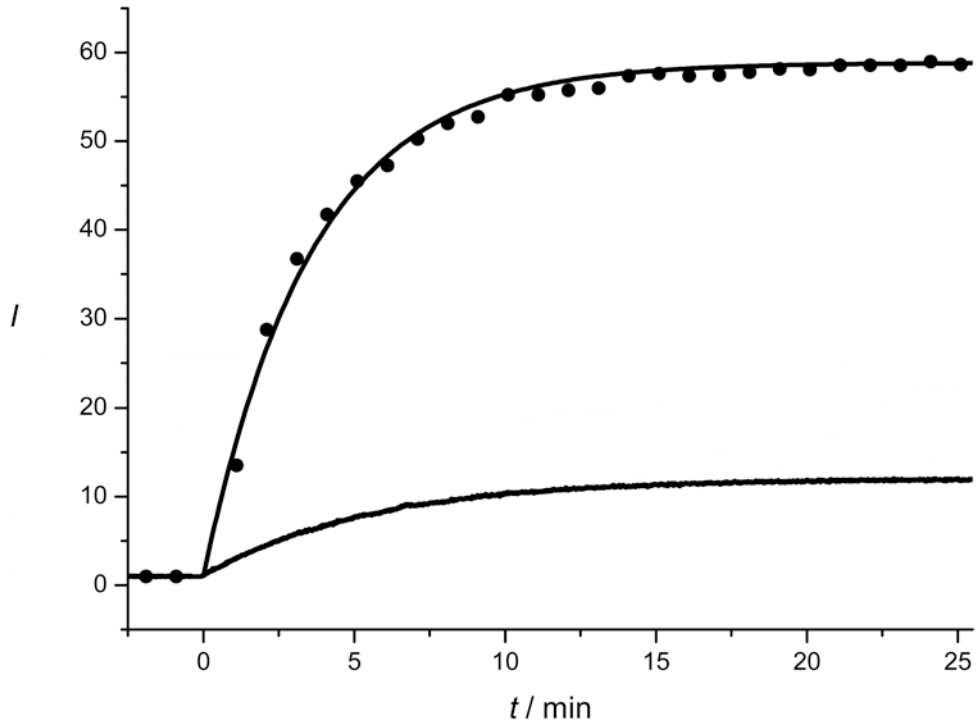


**Fig. 3**: Comparison of the fluorescence increase (initial intensity was normalized to 1) of H-WTLTGKX-$NH_2$ (20 µM) upon digestion with 300 nM trypsin at pH 8. The lower trace was recorded in steady-state mode, the upper one in Nano-TRF mode ($t_{delay}$ = 150 ns, $t_{gate}$ = 2 µs).

To illustrate, we selected the peptide H-YQIFVKX-$NH_2$, which showed the poorest increase in steady-state fluorescence of all peptides investigated ($I_{rel}$ = 1.8). The differentiation already improved significantly ($I_{rel,TRF}$ = 3.0, Table 2) by using Nano-TRF with the standard delay ($t_{delay}$ = 150 ns), but there was room for improvement. By varying the delay times, we could indeed increase the differentiation between substrate and product to a factor of 13.5 with a delay time of 750 ns; the *Z*' factor improved as well, from ca. 0.7 to ca. 0.8 (Figure 4). Although even longer delay times are theoretically expected to provide even higher values for the ratio of intensities (e.g., with a 1250 ns delay), this was not found experimentally. The stability of the assay as expressed by the *Z*' factor was also substantially diminished in this case (< 0.3). Presumably, the resulting decrease in signal intensity for long delays (note that most of the fluorescence has already decayed 1250 ns after the laser pulse, see Figure 2) and the concomitant relative increase in background emission limits the performance of the assay for long time delays. This sets a practical limitation to increasing the differentiation in Nano-TRF mode by extending the delay time, because the increased differentiation comes at the expense of a lower signal and therefore decreased signal-to-background ratio, which is nicely reflected in the deteriorated *Z*' factors.

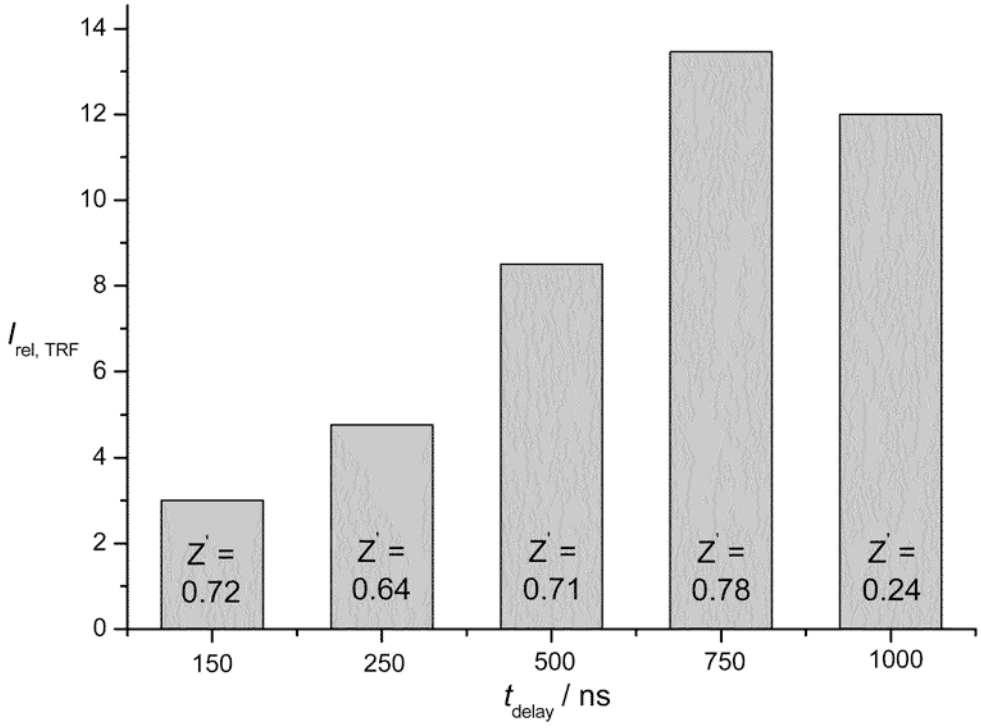


**Fig. 4**: Optimization of substrate-product fluorescence differentiation for the peptide H-YQIFVKX-$NH_2$ (in the range of 10-50 μM) by varying the delay time ($t_{delay}$) in Nano-TRF mode.

One drawback in the use of DBO as a fluorescent probe is its comparably low brightness (defined as the product of extinction coefficient $\varepsilon_{max}$ and fluorescence quantum yield $\phi_F$), which can be traced back to the low extinction coefficient of DBO ($\varepsilon_{max}$ = 50 $M^{-1}cm^{-1}$, $\phi_F$ = 0.26 in $H_2O$).[38] However, principal challenges in HTS arise not only from a weak fluorescence of the probe, but also from interferences due to strong fluorescence of library compounds. The latter can be efficiently suppressed by read-out in Nano-TRF mode, which allows the fluorescence of Dbo to be selectively sounded out even under adverse conditions (high background). In other words, the time-gated detection mode compensates for the weak brightness of Dbo. This has, in fact, already been demonstrated through a successful HTS screen for a protease on a pharmaceutical-industrial scale with 1.3 million wells.[56]

In addition, many HTS assays for proteases employ substrate concentrations in the micromolar range, which is an ideal range for detection of Dbo (detection limit: 20 nM on LF 502 NanoScan FLT plate-reader, IOM, Germany). Furthermore, determinations of proteases with high $K_M$ values become accessible with Dbo-labeled substrates, which is generally not the case for assays based on lanthanide complexes due to a non-linearity of their luminescence at high concentrations (> 1 μM).[55, 58] Such non-linear effects have also been

observed for other FRET substrates at comparably low concentrations (10 μM) and could be traced back to efficient intermolecular FRET and undesirable absorption of the acceptor.[4] This can lead to apparently lower reaction rates or may signal a faulty substrate inhibition (upward curvature in the corresponding Lineweaver-Burk plots). For Dbo/Trp and Dbo/Tyr peptides intermolecular quenching can be neglected up to 100 μM due to the collision-induced quenching mechanism as reflected in the bimolecular quenching rate constants.[20] Control experiments demonstrated that the fluorescence intensities of Dbo-labeled substrates increased indeed linearly with concentration up to 100 μM, while the fluorescence lifetimes remained also constant.

## Conclusions

Due to several complications in protease assays, there is a persistent demand for new probe-quencher pairs. An ideal assay should result, amongst others, in a large increase in fluorescence intensity upon proteolytic cleavage and have a high signal-to-noise ratio. In addition, the fluorophore (and quencher) should be hydrophilic and small to avoid unspecific binding or steric hindrance and thereby retain the biological activity.[9, 13, 14, 59] The Dbo/Trp and Dbo/Tyr probe/quencher pairs introduced herein are very promising for the design of alternative fluorescent protease substrates. The use of a natural amino acid as a quencher is advantageous from a substrate design point of view and offers the additional opportunity to investigate exopeptidases like CPA or LAP. The use of Dbo as fluorescent probe allows Nano-TRF detection, which efficiently suppresses background emission and increases the differentiation between the fluorescence of the cleaved and uncleaved peptide; the performance of Nano-TRF assays can be further fine-tuned by variation of the delay time, which has been experimentally demonstrated for the first time. Furthermore, the extraordinary chemical and photochemical stability of DBO over a wide pH-range (2-13) should allow application of Dbo-based assays to a variety of enzymes from extremophiles.[60] Additional important application areas are mutation studies and HTS assays.

## Acknowledgements

This work was supported by a research collaboration of the F. Hoffmann-La Roche Ltd. within the graduate program “Nanomolecular Science” at the International University Bremen. We thank IOM GmbH (Berlin, Germany) for determining the detection limit of DBO on the LF 502 NanoScan FLT plate-reader.

## References


[1] L. Hedstrom, Serine protease mechanism and specificity, Chem. Rev. 102 (2002) 4501-4524.

[2] F. Bordusa, Proteases in organic synthesis, Chem. Rev. 102 (2002) 4817-4868.

[3] J.C. Reed, Apoptosis-regulating proteins as targets for drug discovery, Trends Mol. Med. 7 (2001) 314-319.

[4] F. Grüninger-Leitch, D. Schlatter, E. Küng, P. Nelböck, H. Döbeli, Substrate and inhibitor profile of BACE ($\beta$-secretase) and comparison with other mammalian aspartic proteases, J. Biol. Chem. 277 (2002) 4687-4693.

[5] J.S. Rosenblum, J.W. Kozarich, Prolyl peptidases: a serine protease subfamily with high potential for drug discovery, Curr. Opin. Chem. Biol. 7 (2003) 496-504.

[6] J.-P. Goddard, J.-L. Reymond, Recent advances in enzyme assays, Trends Biotechnol. 22 (2004) 363-370.

[7] J. Neefjes, N.P. Dantuma, Fluorescent probes for proteolysis: Tools for drug discovery, Nat. Rev. Drug Discovery 3 (2004) 58-69.

[8] C.G. Knight, Fluorimetric assays of proteolytic enzymes, Methods Enzymol. 248 (1995) 18-34.

[9] A.A. Gershkovich, V.V. Kholodovych, Fluorogenic substrates for proteases based on intramolecular fluorescence energy transfer (IFETS), J. Biochem. Biophys. Methods 33 (1996) 135-162.

[10] E.D. Matayoshi, G.T. Wang, G.A. Krafft, J. Erickson, Novel fluorogenic substrates for assaying retroviral proteases by resonance energy transfer, Science 247 (1990) 954-958.

[11] P. Gribbon, A. Sewing, Fluorescence readouts in HTS: no gain without pain?, Drug Discovery Today 8 (2003) 1035-1043.

[12] A. Hennig, D. Roth, T. Enderle, W.M. Nau, Nanosecond time-resolved fluorescence protease assays, ChemBioChem 7 (2006) 733-737.

[13] C. Anne, F. Cornille, C. Lenoir, B.P. Roques, High-throughput fluorogenic assay for determination of Botulinum type B neurotoxin protease activity, Anal. Biochem. 291 (2001) 253-261.

[14] J.M. Soleilhac, F. Cornille, L. Martin, C. Lenoir, M.C. Fournié-Zaluski, B.P. Roques, A sensitive and rapid fluorescence-based assay for determination of tetanus toxin peptidase activity, Anal. Biochem. 241 (1996) 120-127.

[15] G.T. Wang, E. Matayoshi, H.J. Huffaker, G.A. Krafft, Design and synthesis of new fluorogenic HIV protease substrates based on resonance energy transfer, Tetrahedron Lett. 31 (1990) 6493-6496.

[16] B.Z. Packard, D.D. Toptygin, A. Komoriya, L. Brand, Profluorescent protease substrates: Intramolecular dimers described by the exciton model, Proc. Natl. Acad. Sci. U. S. A. 93 (1996) 11640-11645.

[17] T. Ahn, J.-S. Kim, H.-I. Choi, C.-H. Yun, Development of peptide substrates for trypsin based on monomer/excimer fluorescence of pyrene, Anal. Biochem. 306 (2002) 247-251.

[18] N. Marmé, J.P. Knemeyer, J. Wolfrum, M. Sauer, Highly sensitive protease assay using fluorescence quenching of peptide probes based on photoinduced electron transfer, Angew. Chem. Int. Ed. 43 (2004) 3798-3801.

[19] S.A. Latt, D.S. Auld, B.L. Vallee, Fluorescence determination of carboxypeptidase A activity based on electronic energy transfer, Anal. Biochem. 50 (1972) 56-62.

[20] R.R. Hudgins, F. Huang, G. Gramlich, W.M. Nau, A fluorescence-based method for direct measurement of submicrosecond intramolecular contact formation in

biopolymers: An exploratory study with polypeptides, J. Am. Chem. Soc. 124 (2002) 556-564.
[21] F. Huang, W.M. Nau, A conformational flexibility scale for amino acids in peptides, Angew. Chem. Int. Ed. 42 (2003) 2269-2272.
[22] W.M. Nau, X.J. Wang, Biomolecular and supramolecular kinetics in the submicrosecond time range: The fluorazophore approach, ChemPhysChem 3 (2002) 393-398.
[23] S.A. Latt, D.S. Auld, B.L. Vallee, Distance measurements at the active site of carboxypeptidase A during catalysis, Biochemistry 11 (1972) 3015-3022.
[24] J. Labouesse, M. Gervais, Preparation of chemically defined ε *N*-acetylated trypsin, Eur. J. Biochem. 2 (1967) 215-223.
[25] C.J. Martin, M.A. Marini, Spectral detection of the reaction of formaldehyde with the histidine residues of α-chymotrypsin, J. Biol.Chem 242 (1967) 5736-5743.
[26] J.R. Knowles, H. Sharp, P. Greenwell, The pH-dependence of the binding of competitive inhibitors to pepsin, Biochem. J. 113 (1969) 343-351.
[27] R. Misselwitz, D. Zirwer, M. Frohne, H. Hanson, Bovine lens leucine aminopeptidase number and state of tryptophyl residues, FEBS Lett. 55 (1975) 233-236.
[28] H. Du, R.-C.A. Fuh, J. Li, L.A. Corkan, J.S. Lindsey, PhotochemCAD: A computer-aided design and research tool in photochemistry, Photochem. Photobiol. 68 (1998) 141-142.
[29] U. Pischel, X.Y. Zhang, B. Hellrung, E. Haselbach, P.A. Muller, W.M. Nau, Fluorescence quenching of n,π*-excited azoalkanes by amines: What is a sterically hindered amine?, J. Am. Chem. Soc. 122 (2000) 2027-2034.
[30] W.M. Nau, U. Pischel, Photoreactivity of n,π* excited azoalkanes and ketones, in: V. Ramamurthy, K.S. Schanze (Eds.) Organic Photochemistry and Photophysics, CRC Press, Boca Raton, FL, pp. 75-129.
[31] U. Pischel, D. Patra, A.L. Koner, W.M. Nau, Investigation of polar and stereoelectronic effects on pure excited-state hydrogen atom abstractions from phenols and alkylbenzenes, Photochem. Photobiol. 82 (2006) 310-317.
[32] A.F.-P. Sonnen, H. Bakirci, T. Netscher, W.M. Nau, Effect of temperature, cholesterol content, and antioxidant structure on the mobility of vitamin E constituents in biomembrane models studied by laterally diffusion-controlled fluorescence quenching, J. Am. Chem. Soc. 127 (2005) 15575-15584.
[33] F. Huang, R.R. Hudgins, W.M. Nau, Primary and secondary structure dependence of peptide flexibility assessed by fluorescence-based measurement of end-to-end collision rates, J. Am. Chem. Soc. 126 (2004) 16665-16675.
[34] F. Huang, W.M. Nau, Photochemical techniques for studying the flexibility of polypeptides, Res. Chem. Intermed. 31 (2005) 717-726.
[35] H. Sahoo, A. Hennig, W.M. Nau, Temperature-dependent loop formation kinetics in flexible peptides studied by time-resolved fluorescence spectroscopy, Int. J. Photoenergy 2006 (2006) Article ID 89638, 9 pages, doi: 10.1155/IJP/2006/89638.
[36] W.M. Nau, F. Huang, X.J. Wang, H. Bakirci, G. Gramlich, C. Marquez, Exploiting long-lived molecular fluorescence, Chimia 57 (2003) 161-167.
[37] C. Marquez, F. Huang, W.M. Nau, Cucurbiturils: Molecular nanocapsules for time-resolved fluorescence-based assays, IEEE Trans. Nanobiosci. 3 (2004) 39-45.
[38] J. Mohanty, W.M. Nau, Refractive index effects on the oscillator strength and radiative decay rate of 2,3-diazabicyclo[2.2.2]oct-2-ene, Photochem. Photobiol. Sci. 3 (2004) 1026-1031.
[39] D.G. Smyth, Techniques in enzymic hydrolysis, Methods Enzymol. 11 (1967) 214-231.

[40] Y.-Q. Gu, L.L. Walling, Specificity of the wound-induced leucine aminopeptidase (LAP-A) of tomato: Activity on dipeptide and tripeptide substrates, Eur. J. Biochem. 267 (2000) 1178-1187.
[41] G. Yuang, R.B. Kirkpatrick, T. Ho, G.-F. Zhang, P.-H. Liang, K.O. Johanson, D.J. Casper, M.L. Doyle, J.D. Marino Jr., S.K. Thompson, W. Chen, D.G. Tew, T.D. Meek, Steady-state kinetic characterization of substrates and metal-ion specificities of the full-length and *N*-terminally truncated recombinant human methionine aminopeptidases (type 2), Biochemistry 40 (2001) 10645-10654.
[42] J. Karvinen, V. Laitala, M.-L. Mäkinen, O. Mulari, J. Tamminen, J. Hermonen, P. Hurskainen, I. Hemmilä, Fluorescence quenching-based assays for hydrolyzing enzymes. Application of time-resolved fluorometry in assays for caspase, helicase, and phosphatase, Anal. Chem. 76 (2004) 1429-1436.
[43] E.K. Kainmüller, E.P. Ollé, W. Bannwarth, Synthesis of a new pair of fluorescence resonance energy transfer donor and acceptor dyes and its use in a protease assay, Chem. Comm. (2005) 5459-5461.
[44] B.F. Le Bonniec, T. Myles, T. Johnson, C.G. Knight, C. Tapparelli, S.R. Stone, Characterization of the $P_2$' and $P_3$' specificities of thrombin using fluorescence-quenched substrates and mapping of the subsites by mutagenesis, Biochemistry 35 (1996) 7114-7122.
[45] A. Carmel, M. Zur, A. Yaron, E. Katchalski, Use of substrates with fluorescent donor and acceptor chromophores for kinetic assay of hydrolases, FEBS Lett. 30 (1973) 11-14.
[46] A.M. Edison, S.C. Barker, D.B. Kassel, M.A. Luther, W.B. Knight, Exploration of the sequence specificity of pp60$^{c\text{-}src}$ tyrosine kinase, J. Biol. Chem. 270 (1995) 27112-27115.
[47] R.S. Turner, B.E. Kemp, H.-D. Su, J.F. Kuo, Substrate specificity of phospholipid/$Ca^{2+}$-dependent protein kinase as probed with synthetic peptide fragments of the bovine myelin basic protein, J. Biol. Chem. 260 (1985) 11503-11507.
[48] W.T. Lowther, B.W. Matthews, Metalloaminopeptidases: Common functional themes in disparate structural surroundings, Chem. Rev. 102 (2002) 4581-4608.
[49] J. Grembecka, P. Kafarski, Leucine aminopeptidase as a target for inhibitor design, Mini-Rev. Med. Chem. 1 (2001) 133-144.
[50] C. Grepin, C. Pernelle, High-throughput screening - Evolution of homogeneous time resolved fluorescence (HTRF) technology for HTS, Drug Discovery Today 5 (2000) 212-214.
[51] I. Hemmilä, S. Webb, Time-resolved fluorometry: an overview of the labels and core technologies for drug screening applications, Drug Discovery Today 2 (1997) 373-381.
[52] M.K. Johansson, R.M. Cook, J. Xu, K.N. Raymond, Time gating improves sensitivity in energy transfer assays with terbium chelate/dark quencher oligonucleotide probes, J. Am. Chem. Soc. 126 (2004) 16451-16455.
[53] P.R. Selvin, J.E. Hearst, Luminescence energy transfer using a terbium chelate: Improvements on fluorescence energy transfer, Proc. Natl. Acad. Sci. U. S. A. 91 (1994) 10024-10028.
[54] P.R. Selvin, T.M. Rana, J.E. Hearst, Luminescence resonance energy transfer, J. Am. Chem. Soc. 116 (1994) 6029-6030.
[55] J. Karvinen, P. Hurskainen, S. Gopalakrishnan, D. Burns, U. Warrior, I. Hemmilä, Homogeneous time-resolved fluorescence quenching assay (LANCE) for caspase-3, J. Biomol. Screen. 7 (2002) 223-231.
[56] D. Roth, T. Enderle, unpublished results obtained with a Plate::Vision reader from Zeiss and Hoffmann-La Roche.

[57] J.-H. Zhang, T.D.Y. Chung, K.R. Oldenburg, A Simple Statistical Parameter for Use in Evaluation and Validation of High Throughput Screening Assays J. Biomol. Screen. 4 (1999) 67-73.
[58] T.M. Sadler, M. Achilleos, S. Ragunathan, A. Pitkin, J. LaRocque, J. Morin, R. Annable, L.M. Greenberger, P. Frost, Y. Zhang, Development and comparison of two nonradioactive kinase assays for I kappa B kinase, Anal. Biochem. 326 (2004) 106-113.
[59] M.K. Johansson, R.M. Cook, Intramolecular dimers: A new design strategy for fluorescence-quenched probes, Chem. Eur. J. 9 (2003) 3466-3471.
[60] S. Nee, More than meets the eye - Earth's real biodiversity is invisible, whether we like it or not, Nature 429 (2004) 804-805.

## Footnotes

[1] Abbreviations used: CPA, carboxypeptidase A; DBO, 2,3-diazabicyclo[2.2.2]oct-2-ene; Dbo, 2,3-diazabicyclo[2.2.2]oct-2-ene-labeled asparagine; FRET, fluorescence resonance energy transfer; HTS, high-throughput screening; TRF, time-resolved fluorescence; LAP, leucine aminopeptidase; CT, chymotrypsin.

[2] A static quenching mechanism was also postulated in an early hetero-double-labeling approach with an *o*-aminobenzoyl group as a probe and a *p*-nitrobenzyloxy group as quencher, *cf.* ref. [8],[9] and A. Yaron, A. Carmel, E. Katchalski-Katzir, Intramolecularly quenched fluorogenic substrates for hydrolytic enzymes, Anal. Biochem. 95 (1979) 228-235. The further development of this assay type was not recommended.[8]

[3] We also determined for each enzyme kinetics the fluorescence lifetime once no change in the fluorescence intensities was noted (plateau region in Figure 1); the observation of a monoexponential fluorescence decay confirmed in all cases that the hydrolysis of the substrate was complete. An incomplete substrate conversion could occur, for example, if the protease became inactive during the kinetic run, which would similarly result in the observation of an apparent plateau. In the latter case, a biexponential fluorescence decay would be expected with the fluorescence lifetimes of the uncleaved and partially cleaved forms as components (Table 2). This was in fact observed when lifetime measurements were performed in the rise phase before the plateau was reached, e.g., when a CT assay was intentionally stopped by addition of 1 M HCl.

[4] The smaller increase in steady-state fluorescence intensity compared to the increase in fluorescence lifetimes is presumably due to background emission and fluorescence from unknown short-lived impurities inside the sample (purity > 95 %); the contribution of the background emission may lead to a sizable increase in steady-state fluorescence of the quenched peptide, which decreases the relative increase in fluorescence intensity ($I_{rel}$), but leaves the experimental fluorescence lifetimes of Dbo unaffected, because background emission is much shorter lived and was not considered in the tail fitting of the decay traces.

## Figure Legends

**Scheme 1**: Principles of fluorescent protease assays based on a) FRET (hetero-double-labeling), b) static probe/quencher contact (either with two identical fluorophores, i.e. homo-double-labeling, or single-labeling with Trp as quencher), and c) collision-induced quenching of a probe (Dbo) by a contact quencher (Trp or Tyr).

**Fig. 1**: Representative traces (note the logarithmic intensity scale) showing the increase in relative fluorescence intensity (*I*) of the peptides H-WTLTGKX-$NH_2$ (**4**), H-XLSLSRFSWGA-OH (**7**), H-WQIFVKX-$NH_2$ (**3**) and H-YQIFVKX-$NH_2$ (**8**) (all 50 μM) during enzymatic cleavage by trypsin (300 nM), LAP (63 nM), CT (200 nM), and CT (300 nM), respectively.

**Fig. 2**: Comparison of the fluorescence lifetimes for different peptides: H-WTLTGKX-$NH_2$ (**4**, 27 ns, red), H-WQIFVKX-$NH_2$ (**3**, 90 ns, black), H-YQIFVKX-$NH_2$ (**8**, 172 ns, blue) and H-X-$NH_2$ (355 ns, green), the last one being the common cleavage product by trypsin. Note the yellow time window which reflects the standard integration window employed for Nano-TRF detection to gate out background emission (sharp peak near $t = 0$) and to increase the discrimination between uncleaved and cleaved peptide (e.g., red and green trace).

**Fig. 3**: Comparison of the fluorescence increase (initial intensity was normalized to 1) of H-WTLTGKX-$NH_2$ (20 μM) upon digestion with 300 nM trypsin at pH 8. The lower trace was recorded in steady-state mode, the upper one in Nano-TRF mode ($t_{delay}$ = 150 ns, $t_{gate}$ = 2 μs).

**Fig. 4**: Optimization of substrate-product fluorescence differentiation for the peptide H-YQIFVKX-$NH_2$ (in the range of 10-50 μM) by varying the delay time ($t_{delay}$) in Nano-TRF mode.

**Table 1:** Pseudo-first order rate constants ($k_{cat}/K_M$) of proteolytic activity for the investigated combinations of peptides and proteases.

| No. | Substrate[a] | Protease | $k_{cat}/K_M$ ($10^6$ $M^{-1}min^{-1}$)[b] |
|---|---|---|---|
| **1** | H-GSGSWR$^{\downarrow}$X-$NH_2$ | Trypsin | 5.0 |
| **2** | H-GSWR$^{\downarrow}$$(GS)_7$X-$NH_2$ | Trypsin | 12 |
| **3** | H-WQIFVK$^{\downarrow}$X-$NH_2$ | Trypsin | 5.0 |
| **4** | H-WTLTGK$^{\downarrow}$X-$NH_2$ | Trypsin | 2.5 |
| **5** | H-WRRRRRRX-$NH_2$[c] | Trypsin | 12 |
| **6** | H-WKRTLRRX-OH[c] | Trypsin | 19 |
| **7** | H-XLSLSR$^{\downarrow}$FSWGA-OH | Trypsin | 38 |
| **8** | H-YQIFVK$^{\downarrow}$X-$NH_2$ | Trypsin | 3.5 |
| **9** | H-YTLTFK$^{\downarrow}$X-$NH_2$ | Trypsin | 1.4 |
| **10** | H-AEYAAR$^{\downarrow}$GX-OH | Trypsin | 80 |
| **11** | H-XG$^{\downarrow}$W-OH[d] | CPA | 1.1 |
| **12** | H-GSGSXGS$^{\downarrow}$W-OH | CPA | 1.2 |
| **13** | H-XGG$^{\downarrow}$W-OH[d] | CPA | 0.66 |
| **14** | Ac-X$^{\downarrow}$W-OH[d] | CPA | 18 |
| **3** | H-WQIF$^{\downarrow}$VKX-$NH_2$ | Pepsin | 0.48 |
| **8** | H-YQIF$^{\downarrow}$VKX-$NH_2$ | Pepsin | 0.38 |
| **6** | H-W$^{\downarrow}$KRTLRRX-OH | LAP | 5.8 |
| **7** | H-X$^{\downarrow}$LSLSRFSWGA-OH | LAP | 24 |
| **1** | H-GSGSW$^{\downarrow}$RX-$NH_2$ | CT | 1.0 |
| **2** | H-GSW$^{\downarrow}$$R(GS)_7$X-$NH_2$ | CT | 0.6 |
| **3** | H-WQIF$^{\downarrow}$VKX-$NH_2$ | CT | 4±2 |
| **4** | H-W$^{\downarrow}$TLTGKX-$NH_2$ | CT | 0.2 |
| **5** | H-W$^{\downarrow}$RRRRRRX-$NH_2$ | CT | 0.33 |
| **6** | H-W$^{\downarrow}$KRTLRRX-OH | CT | 1.4 |
| **7** | H-XLSLSRF$^{\downarrow}$SWGA-OH | CT | 17 |
| **8** | H-YQIF$^{\downarrow}$VKX-$NH_2$ | CT | 1.4 |
| **9** | H-YTLTF$^{\downarrow}$KX-$NH_2$ | CT | 3.9 |
| **10** | H-AEY$^{\downarrow}$AARGX-OH | CT | 5.6 |

[a] Presumed cleavage site marked by an arrow. [b] 10 % error unless stated differently. [c] Several cleavage sites possible. [d] From ref. [12].

**Table 2**: Comparison of the increase in fluorescence intensity upon protease cleavage of peptides **1-14** in steady-state ($I_{rel}$) and Nano-TRF mode ($I_{rel,TRF}$); shown for comparison are the fluorescence lifetimes[a] before ($\tau_{Dbo/Q}$) and after cleavage ($\tau_{Dbo}$), the ratio of lifetimes ($\tau_{rel} = \tau_{Dbo/Q}/\tau_{Dbo}$), and the theoretically expected intensity increase in Nano-TRF mode ($I^{theo}_{rel,TRF}$).

| No. | Substrate | $\tau_{Dbo/Q}$ | $\tau_{Dbo}$ | $\tau_{rel}$ | $I_{rel}$ | $I^{theo}_{rel,TRF}$ [b] | $I_{rel,TRF}$ [c] |
|---|---|---|---|---|---|---|---|
| **1** | H-GSGSWRX-$NH_2$[d],[e] | 38 | 360 | 9.5 | 4.3 | 320 | 4.5 |
| **2** | H-GSWR$(GS)_7$X-$NH_2$[d],[e] | 50 | 227 | 4.5 | 2.5 | 47 | 2.0 |
| **3** | H-WQIFVKX-$NH_2$[d],[e],[f] | 90 | 355 | 3.9 | 3.8 | 14 | 11.4 |
| **4** | H-WTLTGKX-$NH_2$[e] | 27 | 305[g] | 11.3 | 11.9 | $1.8 \times 10^3$ | >50 |
| **5** | H-WRRRRRRX-$NH_2$[d],[e] | 108 | 330 | 3.1 | 2.4 | 7.8 | 6.7 |
| **6** | H-WKRTLRRX-OH[d],[e],[h] | 62 | 330 | 5.3 | 3.2 | 38 | 8.4 |
| **7** | H-XLSLSRFSWGA-OH[d],[e],[h] | 51 | 249 | 4.9 | 3.5 | 51 | 34 |
| **8** | H-YQIFVKX-$NH_2$[d],[e],[f] | 172 | 355 | 2.1 | 1.8 | 3.2 | 3.0 |
| **9** | H-YTLTFKX-$NH_2$[d],[e] | 110 | 360 | 3.3 | 3.1 | 8.4 | 6.7 |
| **10** | H-AEYAARGX-OH[d],[e] | 74 | 345 | 4.7 | 3.5 | 23 | 7.3 |
| **11** | H-XGW-OH[i],[j] | 5.9[k] | 342 | 58.0 | 24.8 | $4.1 \times 10^{12}$ | >50 |
| **12** | H-GSGSXGSW-OH[i] | 15 | 251 | 16.7 | | $2.0 \times 10^5$ | |
| **13** | H-XGGW-OH[i],[j] | 7.6[k] | 335 | 44.1 | 25.4 | $1.1 \times 10^{10}$ | >50 |
| **14** | Ac-XW-OH[i],[j] | 17 | 360 | 21.2 | 12.1 | $9.4 \times 10^4$ | >50 |

[a] by time-correlated single-photon counting, 10% error. [b] Calculated according to ref.[12] by assuming a standard delay time of 150 ns and a standard gate time of 2 µs. [c] Obtained with a standard delay time of 150 ns and a standard gate time of 2 µs. [d] Cleaved with trypsin. [e] Cleaved with CT. [f] Cleaved with pepsin. [g] 360 ns, if cleaved with trypsin. [h] Cleaved with LAP. [i] Cleaved with CPA. [j] From ref. [12]. [k] Re-measured data.

# APPENDIX 2

*REVISED*

# Single-Label Kinase and Phosphatase Assays for Tyrosine Phosphorylation Using Nanosecond Time-Resolved Fluorescence Detection

Harekrushna Sahoo,[†] Andreas Hennig,[†] Mara Florea,[†]
Doris Roth,[‡] Thilo Enderle,[‡] and Werner M. Nau*,[†]

Contribution from the School of Engineering and Science, Jacobs University Bremen, Campus Ring 1, D-28759 Bremen, Germany, and F. Hoffmann-La Roche AG, Grenzacherstrasse 124, CH-4070 Basel, Switzerland; E-Mail: w.nau@jacobs-university.de

## Abstract

The collision-induced fluorescence quenching of a 2,3-diazabicyclo[2.2.2]oct-2-ene-labeled asparagine (Dbo) by hydrogen atom abstraction from the tyrosine residue in peptide substrates was introduced as a single-labeling strategy to assay the activity of tyrosine kinases and phosphatases. The assays were tested for twelve different combinations of Dbo-labeled substrates and with the enzymes $p60^{c\text{-}Src}$ Src kinase, EGFR kinase, YOP protein tyrosine phosphatase, as well as acid and alkaline phosphatase, thereby demonstrating a broad application potential. The steady-state fluorescence changed by a factor of up to 7 in the course of the enzymatic reaction, which allowed for a sufficient sensitivity of continuous monitoring in steady-state experiments. The fluorescence lifetimes (and intensities) were found to be rather constant for the phosphotyrosine peptides (ca. 300 ns in aerated water) while those of the unphosphorylated peptides were as short as 40 ns (at pH 7) and 7 ns (at pH 13) as a result of intramolecular quenching. Owing to the exceptionally long fluorescence lifetime of Dbo, the assays were alternatively performed by using nanosecond time-resolved fluorescence (Nano-TRF) detection, which leads to an improved discrimination of background fluorescence and an increased sensitivity. The potential for inhibitor screening was demonstrated through the inhibition of acid and alkaline phosphatases by molybdate.

## Introduction

One of the most important regulatory mechanisms of biological signal transduction is the phosphorylation and dephosphorylation of tyrosine residues in proteins catalyzed by tyrosine kinases and phosphatases.[1,2] These enzymes play a key role in numerous diseases, such as pathogenic infections[3,4] or cancer.[5,6] In order to identify specific inhibitors and activators as potential lead structures for new drugs,[7] convenient and cost-effective kinase and phosphatase assays are required in pharmaceutical-industrial drug discovery as well as in fundamental enzymological research. While several radioimmunoassays[8] as well as laborious electrophoretic[9] or chromatographic[10] assays have been developed, homogeneous fluorescence-based assays are very attractive due to their high sensitivity, short detection times, and their possibility for an easy scale-up to high-throughput screening (HTS) format. However, the modulation of the fluorescence, i.e., the translation of the phosphorylation into a decrease or an increase of fluorescence, presents a major obstacle in the design of fluorescence-based phosphorylation assays, and requires generally the use of expensive antibodies,[11,12] phosphate binding proteins[13] or biopolymers,[14] strategies involving metal particles,[15] or metal ion-chelating sites.[16]

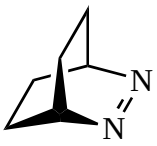


2,3-diazabicyclo[2.2.2]oct-2-ene
(DBO)

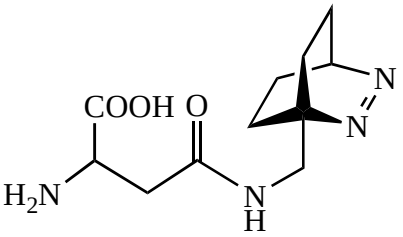


DBO-labeled asparagine
(Dbo)

Very recently, Lawrence and co-workers reported an elegant single-labeling approach to assay tyrosine kinases using originally pyrene (Pyr) and also other dyes,[17-19] which show a differential propensity to form non-fluorescent intramolecular ground-state complexes with Tyr and pTyr residues and thereby variations in static quenching (Scheme 1a). Herein, we report our results on an alternative single-label assay to follow Tyr phosphorylation (kinases) and dephosphorylation (phosphatases), which is based on the dynamic fluorescence quenching of the fluorescent amino acid Dbo (Scheme 1b), an asparagine labeled with the 2,3-diazabicyclo[2.2.2]oct-2-ene (DBO) azo chromophore.[20] Mechanistically, Dbo undergoes

efficient intrachain collision-induced quenching by Tyr,[20,21] but not with pTyr. The resulting Dbo/Tyr assays are complementary to the recently reported Pyr/Tyr assays. In particular, we employ a small hydrophilic fluorophore, which is accessible to nanosecond time-resolved detection (Nano-TRF). Nano-TRF is an attractive method for efficient background subtraction, which we have recently established for protease assays.[22,23]

**Scheme 1**

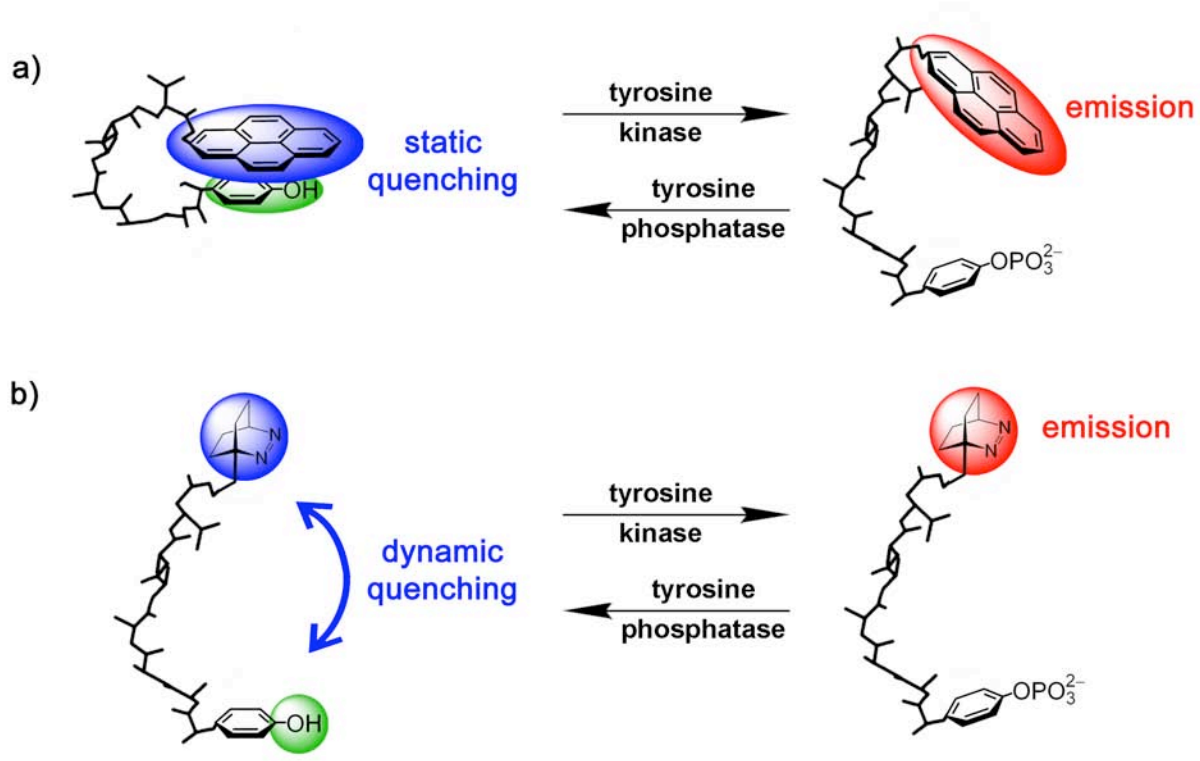


## Experimental Section

**Materials.** Fmoc-protected Dbo (available as Puretime325 dye from Assaymetrics, Cardiff, UK) was synthesized according to the literature[20] and introduced into the peptide substrates by solid-phase synthesis (Biosyntan, Berlin); the purity of the peptides was > 95%. $MgCl_2$, $MnCl_2$, EGTA, NaOAc, and Tris-HCl were purchased from Fluka or Sigma-Aldrich in highest commercial purity; glycine was from ICN Biomedicals.

**Kinase Assays.** The tyrosine kinase assays were performed in 100 mM Tris-HCl buffer (pH 7.2), containing 1.5 mM $MgCl_2$, 0.5 mM $MnCl_2$, and 0.5 mM EGTA. Peptide concentrations

were determined UV-spectrophotometrically (Varian Cary 4000) by using the molar extinction coefficient of tyrosine ($\varepsilon_{275}$ = 1400 $cm^{-1}M^{-1}$).[24] Phosphorylation was initiated by adding 10 µl of Src kinase ($p60^{c\text{-}Src}$ from Proqinase, Germany, activity 142 pmol/µg per minute for the substrate poly(Glu, Tyr) in the ratio of 4:1) or 10 µl EGFR (Sigma-Aldrich, activity 5,000-30,000 units/mg per minute for the substrate poly(Glu, Tyr) in the ratio of 4:1) to a mixture of peptide substrate and 300 µM ATP in buffer (10-50 µM, final assay volume 500 µl in semi-micro quartz glass cuvettes). The kinetic studies were carried out at 37.0 ± 0.1 °C using an external temperature controller (Peltier thermostat, Varian) and the fluorescence growth traces were recorded on a Varian Eclipse fluorometer ($\lambda_{exc}$ = 365 nm and $\lambda_{obs}$ = 430 nm).

**Phosphatase Assays.** YOP protein tyrosine phosphatase (truncated form, from *E. coli*, in buffered aqueous glycerol solution, 30,000 U/mg protein), acid phosphatase (type I from wheat germ, 0.4 U/mg), and alkaline phosphatase (from *E. coli*, suspension in 2.5 M $(NH_4)_2SO_4$, 85.4 U/mg protein) were obtained from Sigma-Aldrich. Peptide concentrations were determined by the molar extinction coefficient of phosphotyrosine ($\varepsilon_{267}$ = 652 $cm^{-1}M^{-1}$).[25] The enzyme concentrations were determined either by using a defined volume of YOP phosphatase solution, or by using an extinction coefficient of $\varepsilon_{278}$ = 1.26 $mg^{-1}cm^{-1}ml$ (for acid phosphatase), and $\varepsilon_{278}$ = 0.72 $mg^{-1}cm^{-1}ml$ (for alkaline phosphatase).[26] Dephosphorylation was initiated by adding 42 µl of the YOP phosphatase solution, 50 µl of a 1 mg/ml acid phosphatase solution, or 50 µl of a 100 µg/ml alkaline phosphatase solution to a mixture of peptide substrate (25-50 µM, final assay volume 500 µl in semi-micro quartz glass cuvettes). The assays were conducted in 50 mM NaOAc buffer at pH 5.5 containing 0.5 mM EDTA adjusted to an ionic strength of 75 mM with NaCl (for YOP phosphatase),[27] 150 mM NaOAc buffer at pH 5.0 (for acid phosphatase) or in 130 mM glycine buffer with 8.3 mM $MgCl_2$ at pH 8.8 (for acid phosphatase), respectively. The temperature was maintained at 25.0 ± 0.1 °C as described above, except for YOP phosphatase (30.0 ± 0.1 °C), and the fluorescence decay traces were recorded on a Varian Eclipse fluorometer ($\lambda_{exc}$ = 365 nm and $\lambda_{obs}$ = 450 nm). The dephosphorylation by alkaline phosphatase was additionally monitored through the absorbance changes at 283 nm on a Varian Cary 4000 UV spectrophotometer.

**Time-Resolved Fluorescence Spectroscopy.** Fluorescence lifetimes were recorded at $\lambda_{obs}$ = 450 nm on a time-correlated single photon counting (TCSPC) fluorometer (FLS 920, Edinburgh Instruments) by using 50-ps pulses from a PicoQuant diode laser LDH-P-C 375 ($\lambda_{exc}$ = 373 nm, $\lambda_{obs}$ = 450 nm, fwhm ca. 50 ps) for excitation. The lifetimes were analyzed with the instrument-specific software by means of a monoexponential or biexponential decay function (to account for short-lived impurities or scattered light) and judged on the basis of a reduced $\chi^2$ around 1.0 and a random distribution of the weighted residuals around zero. Nanosecond time-resolved fluorescence assays (final assay volume was 50 µl) were carried out in black 384-well microplates (Corning NBS) with an LF 402 NanoScan FI microplate reader (IOM, Berlin, Germany). As an instrumental modification, an external nitrogen laser (MNL 200, Laser Technik Berlin, Germany) was coupled by glass fibers to a dye laser module, which provided an excitation wavelength of $\lambda_{exc}$ = 365 nm. The experiments were performed at ambient temperature (25 °C) or at 40 °C.

## Results and Discussion

DBO has been subject to extensive photophysical investigations,[28-37] and has recently found diverse applications in supramolecular[37-45] and biomolecular chemistry,[20,21,29,35,36,40,43-57] including its use in peptides[21-23,32,38,46-53] and enzyme assays.[22,23,48,52,54] The DBO chromophore stands alone due to its exceedingly long fluorescence lifetime of up to 1 µs in gas phase and 320 ns in aerated water,[23,30,33,38,48] which enables the efficient suppression of background fluorescence[22] and an increased differentiation of product *versus* substrate by Nano-TRF detection.[23] In essence, the fluorescence can be measured after a sufficiently long time delay in the nanosecond range, e.g., after 150 or 500 ns. At this delay time, all background fluorescence (which is much shorter lived) has already decayed, while the long-lived fluorescence of DBO can still be reliably detected. In the case of protease assays,[22,23,52] we used Dbo-labeled substrates, which contained either Trp and Tyr as intramolecular quencher; the protease cleaved off probe or quencher, which led to a readily detectable fluorescence enhancement. Our conceptual approach to tyrosine kinases and phosphatases, which is shown in Scheme 1b, is based on the selective fluorescence quenching of Tyr, i.e., pTyr does not quench DBO fluorescence.

**Photophysical Characterization of Tyrosine and Phosphotyrosine Peptides**. Previous studies on the fluorescence quenching of the parent chromophore DBO by amino acids have shown that Tyr acts as an efficient fluorescence quencher ($k_q = 5.6 \times 10^8$ $M^{-1}s^{-1}$ in water at pH 7).[21] The mechanism of the collision-induced fluorescence quenching of DBO by phenols proceeds by a hydrogen atom transfer (which is aborted at a conical intersection),[29-31,55,56] as demonstrated through deuterium isotope effects,[20,21,35] and the observation of phenoxyl-type radicals.[35,57] Accordingly, the fluorescence of Dbo-labeled peptides containing Tyr is strongly quenched by intrachain collisions, the efficiency of which depends systematically on the distance between probe and quencher,[20,23,46-48] the amino acid sequence,[21,23,46,51] the temperature,[21,48] and the solvent viscosity.[20,21,46,51] The readily abstractable phenolic hydrogen of Tyr, which is responsible for the Dbo fluorescence quenching, is absent in pTyr. As a consequence, pTyr causes no significant, i.e., a more than two orders of magnitude lower, fluorescence quenching ($k_q \leq 5 \times 10^6$ $M^{-1}s^{-1}$ in pH 7 phosphate buffer, this work). Thus, Dbo-labeled peptides containing pTyr should show the fluorescence characteristic for unquenched Dbo. According to the proposed assay principle in Scheme 1b, the action of a kinase is therefore expected to increase the fluorescence of the peptide, and that of a phosphatase is expected to decrease it.

**Table 1.** Fluorescence lifetimes[a] of the unphosphorylated (**1-3**) and phosphorylated (**p1-p3**) model peptides.

| Peptide | Sequence | $H_2O$ (pH 7) | $H_2O$ (pH 13) | $D_2O$ (pD 7.4) |
|---|---|---|---|---|
| **1** | H-Y-Dbo-OH | 80 | 6.7 | 145 |
| **p1** | H-pY-Dbo-OH | 360 | 285 | 530 |
| **2** | H-AEYAARG-Dbo-OH | 74 | 26 | 150 |
| **p2** | H-AEpYAARG-Dbo-OH | 290 | 250 | 410 |
| **3** | H-Dbo-AEEEIYGE-OH | 110 (80) [b] | 58 | 180 |
| **p3** | H-Dbo-AEEEIpYGE-OH | 305 (263) [b] | 310 | 430 |

[a] At 25 °C; 5% error. [b] Values in parentheses were measured at 40 °C.

The fluorescence lifetimes of Tyr *versus* pTyr containing model peptides (independently obtained by solid-phase synthesis) under different conditions are compared in Table 1; the relative lifetimes are expected to be proportional to the relative fluorescence intensities measured in conventional steady-state measurements. As expected from the intermolecular fluorescence quenching results, the fluorescence lifetime of the phosphorylated peptides ($\tau_{pY}$) were invariably longer than those of the unphosphorylated ($\tau_{Y}$) peptides, and the expected increase in fluorescence intensity in the course of an enzymatic reaction (estimated as $\tau_{pY}/\tau_{Y}$) was sufficiently large (3-40), to ensure sufficient sensitivity for the development of the respective kinase and phosphatase assays.

The model dipeptide **1** with adjacent probe and quencher (no intervening amino acid) showed the largest difference (factor 4.5 in $H_2O$ at pH 7) in fluorescence lifetimes, but the differentiation for peptide **2** (with 4 intervening amino acids) was also quite large (factor 3.9 in $H_2O$ at pH 7), owing to the weak variations of the intrachain quenching rate for short peptides[20,47,48] and the presence of the highly flexible glycine.[20-23,46,48] Peptide **3**, with 5 intervening amino acids and one being a rigid isoleucine,[21,46] showed a slightly smaller differentiation between the phosphorylated and unphosphorylated peptide (factor 2.8 in $H_2O$ at pH 7). The differentiation in fluorescence lifetimes (and intensities) increased significantly at alkaline pH, e.g., to a factor of 40 for peptide **1**, Table 1.[58] Thus, at pH 13, the fluorescence lifetimes of the phosphorylated peptides remained similar, around the 300-ns benchmark characteristic for the parent DBO, while those of the unphosphorylated peptides dropped quite steeply, owing to the deprotonation of Tyr ($pK_a$ = 10.1).[59] The latter converts the phenol residue into a phenolate, which serves as an even more efficient quencher (with exciplex formation as presumed quenching mechanism).[20,21,31,60] Moreover, owing to the temperature dependence of intrachain fluorescence quenching,[21,48,61,62] the differentiation improved further at slightly elevated temperature (compare 40 °C values in parentheses in Table 1), which is frequently preferred for enzymatic reactions.

In addition, we determined the fluorescence lifetimes in $D_2O$ (Table 1). The use of $D_2O$ as an alternative solvent does not increase the differentiation in fluorescence lifetimes, but increases the absolute fluorescence lifetimes (by nearly 50%), which can be used to further suppress fluorescent background when measuring in the Nano-TRF mode (see below). The longer

fluorescence lifetimes are due to the reduced solvent-induced quenching in $D_2O$ compared to $H_2O$.[21,29,30,48] The variations in fluorescence lifetimes in $H_2O$ and $D_2O$ can be further used to calculate the kinetic isotope effect (*KIE*) on the intrachain quenching rate constants according to eq. 1,[28-30] where the fluorescence lifetimes of the phosphorylated peptides were taken as the respective "unquenched" lifetimes. The resulting values ranged from 1.8-2.3, which provides additional support for hydrogen atom abstraction as quenching mechanism in these peptides. The absolute *KIE* values are comparable to those previously observed for intermolecular quenching by Tyr.[20,21,35]

$$KIE = k_q^{H_2O} \Big/ k_q^{D_2O} = \frac{1}{\tau_Y^{H_2O}} - \frac{1}{\tau_{pY}^{H_2O}} \Bigg/ \frac{1}{\tau_Y^{D_2O}} - \frac{1}{\tau_{pY}^{D_2O}} \qquad (1)$$

**Enzyme Selection and Assay Performance**. With the effect of phosphorylation on the fluorescence at hand, we selected two kinases ($p60^{c\text{-}Src}$ Src and EGFR kinase) and three phosphatases (the specific YOP protein tyrosine phosphatase, and the nonspecific alkaline and acid phosphatase) to test the novel tyrosine phosphorylation assay system. The non-receptor kinase $p60^{c\text{-}Src}$ is a member of the Src family of cytoplasmic non-receptor protein tyrosine kinases. Its most important function comprises the phosphorylation of Tyr-527 at the *C*-terminal end of the Src-protein, which promotes the association of the tail region with the SH2 domain and transmits signals involved in cell movement and proliferation.[63,64] The transmembrane receptor kinase EGFR (epidermal growth receptor factor) is a member of the ErbB family receptors. The phosphorylation of *C*-terminal tyrosine motifs (Y 992, Y 1068, Y 1086, Y 1148, and Y 1173) links to the proteins containing SH2 or phosphotyrosine binding domains. EGFR activation triggers numerous downstream signaling pathways, such as, mitogenesis and apoptosis, enhanced cell motility, protein secretion, differentiation to dedifferentiation, and upregulated EGFR signaling correlated to a wide variety of tumors with progression to invasion and metastasis.[64-66]

*Yersinia* outer membrane protein (YOP) is the best characterized protein tyrosine phosphatase and is an essential virulence determinant of *Yersinia pestis* (bubonic plague or Black Death).[4,27] Acid phosphatases from wheat germ are nonspecific enzymes acting as orthophosphoric monoester and pyrophosphate phosphohydrolases under acidic environment.[67] They are

responsible for the ATP and GTP depletion during free cell translation.[68,69] Alkaline phosphatase is a homodimeric protein with nonspecific phosphoesterase activity. In contrast to the YOP and acid phosphatase, the removal of the phosphate group by alkaline phosphatase takes place at an optimum alkaline pH. Alkaline phosphatase has been widely used as an antibody label in enzyme immunoassays capable of detecting primary analytes, for example drugs and pesticides such as cocaine,[70] digoxin,[71] and 2,4-dichlorophenoxyacetic acid.[72]

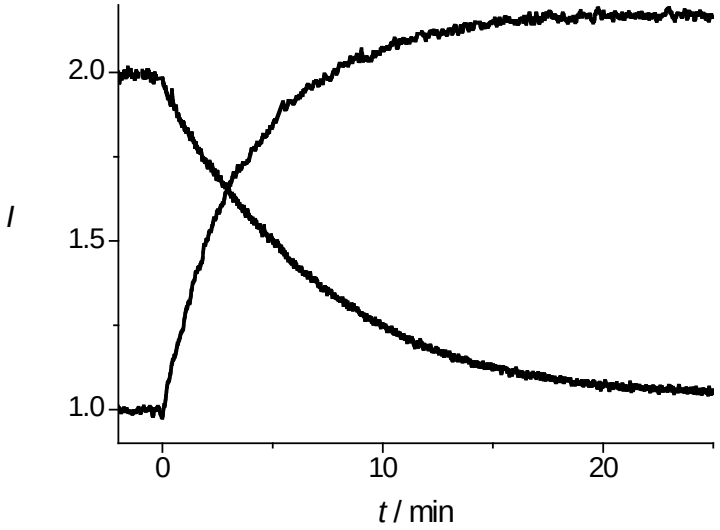


**Figure 1.** Traces of fluorescence intensity ($\lambda_{exc}$ = 365 nm) upon addition of 50 µl of a 1 mg/ml solution of acid phosphatase to 50 µM H-Dbo-AEEEIpYGE-OH (**p3**) (decrease in fluorescence, $\lambda_{obs}$ = 450 nm) and 10 µl Src kinase to 10 µM H-Dbo-AEEEIYGEFEAKKKK-$NH_2$ (**4**) (increase in fluorescence, $\lambda_{obs}$ = 430 nm).

The fluorescence response of peptides **1**-**6** (Table 2) in steady-state experiments under the enzymatic reaction conditions (Figure 1) was consistent with expectation from the photophysical parameters determined for the model peptides **1**-**3** and **p1**-**p3** (Table 1). We observed a continuous increase upon addition of kinase and a continuous decrease upon addition of phosphatase (Figure 2).[73] At the selected enzyme and substrate concentrations (*cf.* Experimental Section), the reaction times ranged from less than 30 min (acid and alkaline phosphatase) up to several hours (kinases, YOP phosphatase). The results confirmed the activity of the investigated enzymes and the feasibility of the assay principle in Scheme 1b. We also determined the

fluorescence lifetimes before addition of enzyme and after the enzymatic reaction and observed an increase or decrease in fluorescence lifetimes in the actual reaction mixture (Table 2). As expected, the fluorescence lifetimes of the phosphorylated peptides were around 300 ns, with small variations with peptide structure, pH, temperature, etc. The intensity ratios in the steady-state ($I_{pY}/I_Y$) and time-resolved ($\tau_{pY}/\tau_Y$) measurements were also in excellent mutual agreement and compared well with the values determined for the model peptides in Table 1.

**Assets of Assays Based on Single-labeled Peptide Substrates**. The Dbo/Tyr tyrosine kinase and phosphatase assays by-pass the use of antibodies[11,12] or radiolabels[8] and operate without the necessity of additional incubation steps.[8,11,12] The response of the Dbo/Tyr fluorescence assay towards addition or removal of the phosphate group is immediate and direct. This allows continuous monitoring of the enzymatic reaction in homogeneous solution and convenient measurement of enzyme kinetics (see below).[73] The (weak) near-UV absorption of Dbo ($\lambda_{max}$ ca. 365 nm, $\varepsilon$ ca. 50 $M^{-1}cm^{-1}$) is compatible with common solid-state or LED laser excitation wavelengths (355 and 375 nm); the possibility for laser excitation is critical, along with the long fluorescence lifetime of Dbo, for the refined Nano-TRF detection and background suppression discussed below.

Instructive is also a comparison with the kinase assays developed by Lawrence and co-workers.[17-19] The original assay was based on the static fluorescence quenching of pyrene (Pyr) resulting from the hydrophobic association with tyrosine in equilibrium (Scheme 1a), as confirmed by the observation of NOE enhancements.[17] The driving force for this intrachain association decreases upon phosphorylation. Both fluorescence-based methods (Scheme 1) are based on single labeling (with either Pyr or Dbo) and exploit Tyr as an intrinsic contact quencher. However, in contrast to the dynamic (collision-induced) fluorescence quenching in the Dbo/Tyr system, the fluorescence quenching in the Pyr/Tyr system is thought to be static in nature. Phosphorylation of Tyr modulates the static quenching in the latter case and switches off the collision-induced quenching in the former case. The classification of the different quenching mechanisms and their merits in assay development have recently been outlined for protease assays.[23]

**Table 2.** Fluorescence lifetimes[a] of peptides **1-6** before and after the enzymatic reaction with a kinase or phosphatase, ratios of fluorescence lifetimes, and steady-state fluorescence intensity ratios

| | Substrate | | Product | Enzyme[b] | pH | $\tau_Y$ /ns | $\tau_{pY}$ /ns | $\tau_{pY}/\tau_Y$ | $I_{pY}/I_Y$ |
|---|---|---|---|---|---|---|---|---|---|
| phosphorylation by kinases at 37 °C | | | | | | | | | |
| **2** | H-AEYAARG-Dbo-OH | **p2** | H-AEpYAARG-Dbo-OH | Src | 7.2 | 82 | --- [c] | --- [c] | --- [c] |
| | | | | EGFR | 7.2 | 82 | 290 | 3.5 | 2.0 |
| **3** | H-Dbo-AEEEIYGE-OH | **p3** | H-Dbo-AEEEIpYGE-OH | Src | 7.2 | 80 | 240 | 3.0 | 2.5 |
| **4** | H-Dbo-AEEEIYGEFEAKKKK-$NH_2$ | **p4** | H-Dbo-AEEEIpYGEFEAKKKK-$NH_2$ | Src | 7.2 | 100 | 230 | 2.3 | 2.2 |
| **5** | H-Dbo-GEYGEF-$NH_2$ | **p5** | H-Dbo-GEpYGEF-$NH_2$ | Src | 7.2 | 40 | 245 | 6.1 | 6.7 |
| dephosphorylation by phosphatases at 25 °C | | | | | | | | | |
| **p1** | H-pY-Dbo-OH | **1** | H-Y-Dbo-OH | AcP | 5.0 | 71 | 350 | 4.9 | 4.1 |
| | | | | AlkP | 8.8 | 31 | 300 | 9.6 | 6.8 |
| **p2** | H-AEpYAARG-Dbo-OH | **2** | H-AEYAARG-Dbo-OH | AcP | 5.0 | --- [c] | 285 | --- [c] | --- [c] |
| | | | | AlkP | 8.8 | 68 | 295 | 4.3 | 2.6 |
| | | | | YOP [d] | 5.5 | 70 | 285 | 4.1 | 1.5 |
| **p3** | H-Dbo-AEEEIpYGE-OH | **3** | H-Dbo-AEEEIYGE-OH | AcP | 5.0 | 100 | 365 | 3.6 | 2.0 |
| | | | | AlkP | 8.8 | 120 | 310 | 2.6 | 2.0 |
| **p6** | H-Dbo-EEEEpY-OH | **6** | H-Dbo-EEEEY-OH | AcP | 5.0 | 69 | 300 | 4.3 | 2.8 |
| | | | | AlkP | 8.8 | 86 | 290 | 3.4 | 2.1 |
| | | | | YOP [d] | 5.5 | 70 | 300 | 4.3 | 2.5 |

[a] 10% error. [b] Abbreviations used: Src: $p60^{c\text{-}Src}$ kinase, EPFR: epidermal growth receptor factor, AcP: acid phosphatase, AlkP: alkaline phosphatase, and YOP: *Yersinia* outer membrane protein. [c] No enzymatic activity detected. [d] At 30 °C.

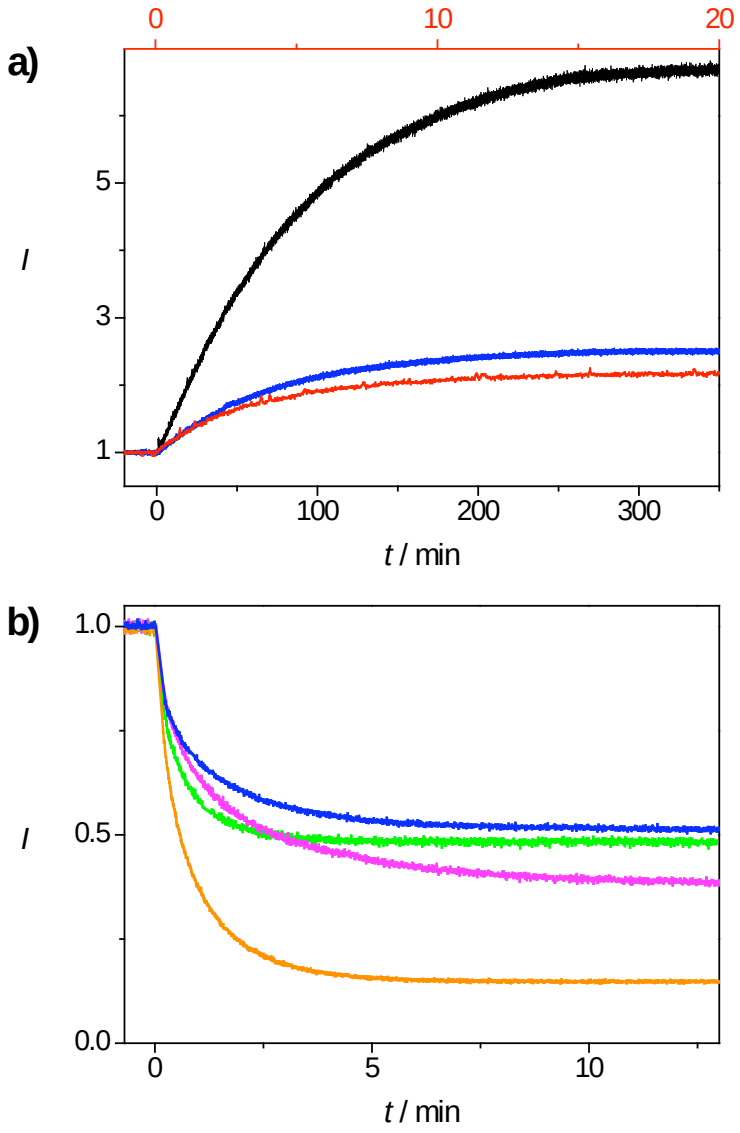


**Figure 2.** (a) Steady-state fluorescence intensity traces of Src kinase activity (normalized to the same initial fluorescence intensity). The assays were initiated by addition of 10 µl Src kinase to 10 µM of peptide **3** (blue), **4** (red), and **5** (black), all at pH 7.2 at 37 °C with $\lambda_{exc}$ = 365 nm and $\lambda_{obs}$ = 430 nm. Note the much faster time scale (upper x axis) for the enzymatic reaction of the most active peptide, **4**. (b) Steady-state fluorescence intensity traces of phosphatase activity (normalized to the same initial fluorescence intensity). The assays were initiated by addition of 50 µl of a 100 µg/ml solution of alkaline phosphatase to 50 µM of peptide **p1** (orange), **p2** (magenta), **p3** (blue), and **p6** (green), all at pH at 25 °C with $\lambda_{exc}$ = 365 nm and $\lambda_{obs}$ = 450 nm.

The two methods are highly complementary. Previous applications have illustrated, for example, the advantage of the small size (similar to Tyr) and hydrophilicity of the "noninvasive" Dbo fluorophore,[22,23,52] which broadens its application potential to assay quite different enzymes. Moreover, the fluorescent probe does not perturb the native conformation of peptides.[20,21,47,49-51,53] Although the use of Pyr is frequently prone to complications due to its higher hydrophobicity and larger size,[74-76] including a limited solubility of Pyr-appended peptides or occasionally inhibition of enzymatic activity, these problems were not encountered for the Pyr/Tyr kinase assays.[17] Moreover, Lawrence and coworkers have provided examples for the use in cellular fluorescence imaging,[18,19] applications for which the brightness of the Dbo chromophore would be presumably insufficient.

**Optimization of Fluorescence Response and Determination of Enzyme Kinetic Parameters for Kinases**. We selected the three peptides **3**-**5**, all of which derived from known recognition motifs of Src kinase,[77,78] to optimize the sensitivity, i.e., the fluorescence differentiation between product and substrate ($I_{pY}/I_Y$ or $\tau_{pY}/\tau_Y$ in Table 2), without sacrificing a high activity. Consequently, we performed the fluorescence assays in steady-state mode (Figures 1 and 2a) and compared the fluorescence lifetimes before and after phosphorylation to obtain the enhancement factors (Table 2). In peptides **3** and **4,** the fluorescent probe (Dbo) and the quencher (Tyr) are separated by same number of amino acids (AEEEI), but peptide **4** has an extended carboxy-terminal tail (FEAKKKK-$NH_2$). From a fluorescence quenching point of view, the function of this tail may be that of a dangling chain end, which slows down intrachain collisions by effectively decreasing the diffusion coefficient, in this particular case for the quencher (Tyr).[50,79] Moreover, the *C*-terminal lysine residues in peptide **4** may undergo ion pairing with the *N*-terminal glutamates, which may result in a different structural preference, e.g., a more constrained conformation. In line with these presumptions, quenching is more efficient in the shorter peptide **3** (20% shorter fluorescence lifetime than **4**), and because the fluorescence lifetime of the *phosphorylated* peptide (**p3**) remains virtually constant (no significant quenching in any case), the product/substrate differentiation increases. Compared to peptides **3** and **4**, peptide **5** has a shorter "backbone" of only two amino acids (GE) and, more importantly, incorporates a highly flexible glycine residue. As we have documented in extensive mechanistic

studies in the area of biopolymer dynamics,[20,21,32,38,46-48,50,80] the combination of the two factors (shorter separation and incorporation of a flexible amino acid) results in faster intrachain collision rates, which shortens the fluorescence lifetimes in peptide **5** and thereby leads to a very large enhancement factor of 6-7 (Table 2 and Figure 2). In addition, it needs to be considered that the kinase assays were performed at slightly elevated temperature (37 °C), which further increases the product/substrate differentiation compared to the ambient temperature data (Table 1). This is because the solvent viscosity decreases at higher temperature, which facilitates the dynamic collision-induced quenching.[21,48,61,62]

As can be seen from the foregoing, the fluorescence quenching mechanism between Dbo and Tyr is mechanistically well understood, which facilitates a rational design of the enzymatic substrate and adjustment of the temperature in order to achieve an optimal sensitivity. However, in the course of this design process, effects on the enzyme kinetic parameters require similar attention. Accordingly, we also determined for the Src kinase substrates the initial reaction rates from the normalized steady-state fluorescence traces at varying substrate concentrations. The double-reciprocal Lineweaver-Burk plots afforded the Michaelis-Menten constants $K_M$ and the maximum rates $v_{max}$ for the investigated substrate-enzyme combinations (Table 3). The $K_M$ values were found to lie in the expected range of Src kinase substrates.[17,77,78,81] For example, peptide **4** has a $K_M$ of 63 μM, while for the structurally related peptide H-AEEEIYGEFEAKKKK-OH a $K_M$ value of 33 μM has been reported.[77] The shorter peptide **5** shows a larger $K_M$ value (103 μM), and the same trend applies for the related sequence Ac-FGEYGEF-$NH_2$, with a reported $K_M$ of 479 μM.[78,81]

Peptide **4** contains an excellent recognition motif[77,78] and, accordingly, showed the highest activity. The carboxyl-terminally truncated peptide **3** displayed only a marginally improved fluorescence enhancement, but its phosphorylation proceeded more slowly, because it lacks the important phenylalanine in the Y+3 position.[77] The amino-terminal modification in peptide **5** presents a better alternative, because this substrate displayed the highest fluorescence increase (factor 6-7) upon phosphorylation, and it had an acceptable activity as well. It should be noted that the Src kinase assay was also attempted with peptide **2**, for which the constant intensity of the fluorescence traces upon addition of enzyme signaled the lack of catalytic activity. Instead,

the EGFR kinase favored peptide **2** as substrate and resulted in the expected increase in fluorescence. The combined examples for kinases and phosphatases establish Dbo/Tyr assays as a convenient tool to screen different substrates or enzymes for optimal activity by means of simple fluorescence experiments, and select the substrate with highest sensitivity for a given enzyme.

**Table 3.** Kinetic parameters of the investigated peptides in assays with Src kinase.[a]

| Peptide | Sequence | $K_M$ / μM | $v_{max}$ / (μM/min) |
|---|---|---|---|
| **3** | H-Dbo-AEEEIYGE-OH | 44 | 0.81 |
| **4** | H-Dbo-AEEEIYGEFEAKKKK-$NH_2$ | 63 | 12.1 |
| **5** | H-Dbo-GEYGEF-$NH_2$ | 103 | 1.0 |

[a] Obtained from Lineweaver-Burk plots, 10 % error.

**Determination of Inhibition for Phosphatases.** As previously demonstrated for Dbo-based protease assays,[23] the method can be implemented into HTS to search for inhibitors (or activators) of kinases and phosphatases. In HTS, the employed fluorescence detection, the direct monitoring in homogenous solution without additional incubation steps, and the possibility to apply Nano-TRF are particularly advantageous. To provide an illustrative example for inhibitor testing, we determined the inhibitory effect of $Na_2MoO_4$ on the two nonspecific phosphatases. Molybdate is known as a general inhibitor of phosphatase activity with varying potency depending on the exact type and source of the phosphatase.[67,82,83] We used the common[84] dose-response curve to determine the $IC_{50}$, which was 1.8 ± 0.3 mM and 0.09 ± 0.02 μM for alkaline (with peptide **p2** as substrate) and acid phosphatase (with peptide **p1**), respectively. This is consistent with the order of magnitude of reported inhibition constants of the two enzymes ($K_i$ = 0.32 mM for alkaline phosphatase[83] and $K_i$ = 0.07 μM for acid phosphatase[67]).

**Optimizing the Substrate/Product-Differentiation by Nano-TRF Detection**. The most appealing asset of the Dbo-based assay is the possibility of using Nano-TRF detection, which is made possible by the exceedingly long fluorescence lifetime of Dbo. Figure 3 demonstrates the principle of Nano-TRF detection. In the case of a dephosphorylation reaction, i.e., in a

phosphatase assay, the fluorescence intensity decreases (Figure 1), which is accompanied by a decrease in fluorescence lifetime. The ratio of fluorescence lifetimes is directly reflected in the ratio of the steady-state intensities before and after enzymatic conversion. However, in the Nano-TRF mode, the fluorescence is recorded after a certain delay time, $t_{delay}$, which efficiently suppresses any short-lived fluorescence as it unavoidably arises from impurities, library compounds in HTS, or sample container materials, see the initial spike in Figure 3.

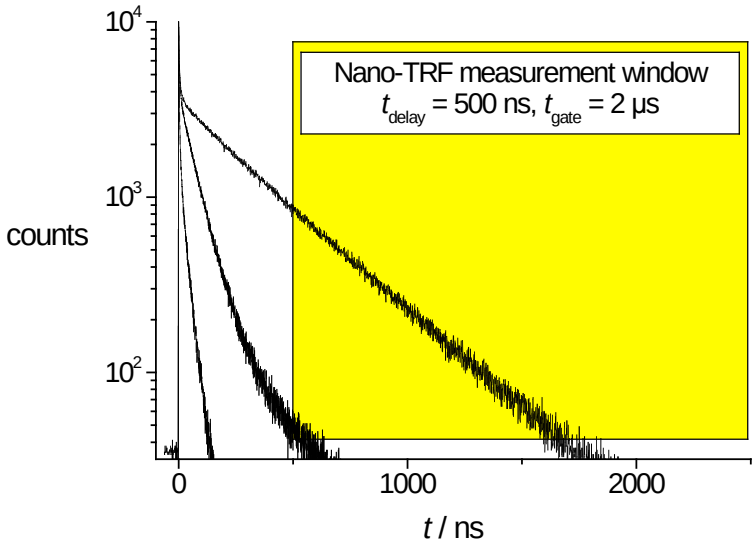


**Figure 3.** Comparison of the fluorescence lifetimes of phosphorylated and unphosphorylated peptides, obtained by single-photon counting. The long fluorescence lifetime ($\tau$ = 365 ns, peptide **p3** in 0.15 M NaOAc buffer, pH 5.0) is representative for a phosphorylated peptide. The faster decay traces were obtained for peptide **1** after dephosphorylation with acid phosphatase ($\tau$ = 71 ns, in 150 mM NaOAc buffer, pH 5.0) and with alkaline phosphatase ($\tau$ = 31 ns, in 130 mM glycine buffer with 8.3 mM $MgCl_2$, pH 8.8). The spike at $t$ = 0 ns stems from short-lived impurities in the assay mixtures.

The resulting desirable suppression of this background fluorescence is well known from TRF assays with lanthanide chelates, which have lifetimes in the millisecond time range.[85-87] However, an added value of TRF detection is the possibility to increase the differentiation of substrate and product of an enzymatic reaction (Figure 4).[23,87] The experimental feasibility of this improvement has only recently been demonstrated with lanthanide chelates for TRF assays,[87] and we have

subsequently elaborated this method with a Nano-TRF protease assay.[23] Indeed, as can be seen from Figure 4a, the enhancement factor increases (from 2.8 to 3.8) in a phosphatase assay by changing from steady-state to Nano-TRF detection. In combination with the concomitant suppression of background fluorescence, the improved substrate/product differentiation can significantly improve the sensitivity of an assay, e.g., in HTS.[54] The time-dependent change of the Nano-TRF response in Figure 4a can be further used to follow the kinetics of the enzymatic reaction, but the temporal resolution is limited compared to steady-state detection, because each Nano-TRF intensity read-out requires the accumulation of several laser pulses.

By increasing the delay times of the Nano-TRF measurement window (Figure 3), it is possible to further optimize the differentiation of substrate and product fluorescence, as can be seen from the comparison of the steady-state intensity ("0 ns delay"), the Nano-TRF intensity for a 500 ns delay, and the Nano-TRF intensity for a 750 ns delay) in Figure 4b. This characteristic dependence can be traced back to the nature of the exponential decay of the fluorescence intensity, i.e., the longer fluorescence lifetime contributes a higher fraction to the Nano-TRF intensity than the shorter lifetime at longer delay times.

To further improve the differentiation of substrate and product, we stopped the acid phosphatase assay by addition of base, which increased the pH from 5 to 12. Subsequently, we compared the Nano-TRF intensity of the product with that of the substrate. At the strongly alkaline pH, an increase in the differentiation of the fluorescence intensities of substrate and product was expected (see above and Table 2), and experimentally observed. For example, at a fixed 750 ns delay, the intensity ratio changed from 4 to 13 (Figure 4b). As can be seen from the comparison of the variation in delay times at pH 12 (from 750 to 1000 ns, Figure 4b), the differentiation decreased again at very long delays, where the signal intensity decreases and background fluorescence comes into play.[54] Measurement of the intensity ratio of substrate and product in $D_2O$ (pD 12) instead of $H_2O$ (pH 12) did not afford a significantly higher differentiation (Figure 4b). However, the longer fluorescence lifetime of the unquenched peptide allowed the application of longer delay times without sacrificing the detection limit (compare the Nano-TRF intensities for the 1000-ns delay in $H_2O$ at pH 12 and $D_2O$ at pD 12).

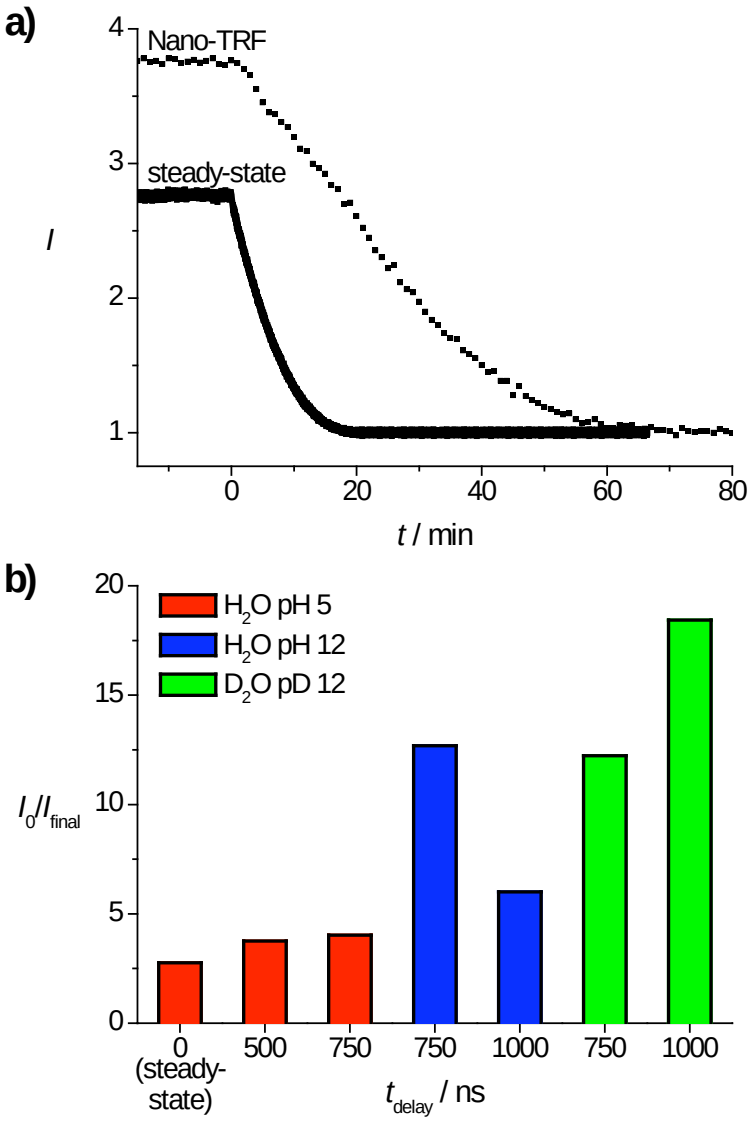


**Figure 4.** Optimization of a phosphatase assay by Nano-TRF detection (normalized to the same final fluorescence intensity). For the experiments H-Dbo-EEEEpY-OH was dephosphorylated by acid phosphatase at pH 5. (a) The steady-state trace refers to 30 µM peptide and 100 µg/ml acid phosphatase. The continuous Nano-TRF trace was recorded with 10 µM peptide and 20 µg/ml phosphatase ($t_{delay}$ = 500 ns, $t_{gate}$ = 2 µs). (b) Optimization of the substrate/product-differentiation in a Nano-TRF measurement by addition of base (pH 12), by using $D_2O$ (see text), and by varying the delay time (all measurements in the inset were recorded with 10 µM of peptide); the differentiation in a steady-state experiment (corresponding to 0 delay time) is shown for comparison.

## Conclusion

We have introduced a conceptually novel (dynamic fluorescence quenching) assay principle for kinases and phosphatases, and a mechanistically novel (hydrogen transfer as quenching mechanism) assay principle for enzyme assays in general. The fluorescence lifetime of Dbo is sufficiently long to allow mutual diffusion to Tyr, which acts as a collision-induced fluorescence quencher, thereby shortening the fluorescence lifetime up to a factor of 7. By phosphorylation it is possible to deactivate the quencher by removing the active abstractable hydrogen, and thereby switch between a short-lived, weakly fluorescent state (the Dbo/Tyr peptide) and a long-lived, strongly fluorescent state (the Dbo/pTyr peptide), which can be conveniently utilized to follow the enzymatic activity of both kinases and phosphatases. A “fine-tuning” of the fluorescence response of the Dbo/Tyr assays can be achieved by varying the pH, the solvent, and the temperature. The sensitivity can be further enhanced by making again use of the long fluorescence lifetime of unquenched Dbo, which allows the application of a time-gated fluorescence detection in the form of the recently introduced Nano-TRF technique. The assay, which allows measurement in homogeneous solution with single-labeled peptides, is complementary to recently reported assays employing static fluorescence quenching, and those involving antibodies or radioactive labels.

## Acknowledgement

This work was performed within a research collaboration of F. Hoffmann-La Roche. Financial support within the graduate program “Nanomolecular Science” at the Jacobs University Bremen, and by the Fonds der Chemischen Industrie, Frankfurt/Main, is gratefully acknowledged.

## References


[†] Jacobs University.

[‡] F. Hoffmann-La Roche AG.

(1) Hubbard, S. R.; Till, J. H. *Annu. Rev. Biochem.* **2000**, *69*, 373-398.

(2) Adams, J. A. *Chem. Rev.* **2001**, *101*, 2271-2290.

(3) Manger, M.; Scheck, M.; Prinz, H.; von Kries, J. P.; Langer, T.; Saxena, K.; Schwalbe, H.; Fürstner, A.; Rademann, J.; Waldmann, H. *ChemBioChem* **2005**, *6*, 1749-1753.

(4) McCain, D. F.; Grzyska, P. K.; Wu, L.; Hengge, A. C.; Zhang, Z.-Y. *Biochemistry* **2004**, *43*, 8256-8264.

(5) Johnson, L. N.; Lewis, R. J. *Chem. Rev.* **2001**, *101*, 2209-2242.

(6) van der Geer, P. V.; Hunter, T.; Lindberg, R. A. *Annu. Rev. Cell Biol.* **1994**, *10*, 251-337.

(7) von Ahsen, O.; Bömer, U. *ChemBioChem* **2005**, *6*, 481-490.

(8) Mallari, R.; Swearingen, E.; Liu, W.; Ow, A.; Young, S. W.; Huang, S.-G. *J. Biomol. Screen.* **2003**, *8*, 198-204.

(9) Hunter, T. *J. Biol. Chem.* **1982**, *257*, 4843-4848.

(10) Budde, R. J. A.; McMurray, J. S.; Tinker, D. A. *Anal. Biochem.* **1992**, *200*, 347-351.

(11) Karvinen, J.; Laitala, V.; Mäkinen, M.-L.; Mulari, O.; Tamminen, J.; Hermonen, J.; Hurskainen, P.; Hemmilä, I. *Anal. Chem.* **2004**, *76*, 1429-1436.

(12) Parker, G. J.; Law, T. L.; Lenoch, F. J.; Bolger, R. E. *J. Biomol. Screen.* **2000**, *5*, 77-88.

(13) Wang, Q.; Lawrence, D. S. *J. Am. Chem. Soc.* **2005**, *127*, 7684-7685.

(14) Simeonov, A.; Bi, X.; Nikiforov, T. T. *Anal. Biochem.* **2002**, *304*, 193-199.

(15) Wang, Z.; Lévy, R.; Fernig, D. G.; Brust, M. *J. Am. Chem. Soc.* **2006**, *128*, 2214-2215.

(16) Shults, M. D.; Imperiali, B. *J. Am. Chem. Soc.* **2003**, *125*, 14248-14249.

(17) Wang, Q.; Cahill, S. M.; Blumenstein, M.; Lawrence, D. S. *J. Am. Chem. Soc.* **2006**, *128*, 1808-1809.

(18) Lawrence, D. S.; Wang, Q. *ChemBioChem* **2007**, *8*, 373-378.

(19) Wang, Q.; Dai, Z.; Cahill, S. M.; Blumenstein, M.; Lawrence, D. S. *J. Am. Chem. Soc.* **2006**, *128*, 14016-14017.

(20) Hudgins, R. R.; Huang, F.; Gramlich, G.; Nau, W. M. *J. Am. Chem. Soc.* **2002**, *124*, 556-564.

(21) Huang, F.; Hudgins, R. R.; Nau, W. M. *J. Am. Chem. Soc.* **2004**, *126*, 16665-16675.

(22) Hennig, A.; Roth, D.; Enderle, T.; Nau, W. M. *ChemBioChem* **2006**, *7*, 733-737.

(23) Hennig, A.; Florea, M.; Roth, D.; Enderle, T.; Nau, W. M. *Anal. Biochem.* **2007**, *360*, 255-265.

(24) Du, H.; Fuh, R.-C. A.; Li, J.; Corkan, L. A.; Lindsey, J. S. *Photochem. Photobiol.* **1998**, *68*, 141-142.

(25) Cousins-Wasti, R. C.; Ingraham, R. H.; Morelock, M. M.; Grygon, C. A. *Biochemistry* **1996**, *35*, 16746-16752.

(26) Anderson, R. A.; Bosron, W. F.; Scott, K. F.; Vallee, B. L. *Proc. Nat. Acad. Sci. USA* **1975**, *72*, 2989-2993.

(27) Zhang, Z.-Y.; Clemens, J. C.; Schubert, H. L.; Stuckey, J. A.; Fischer, M. W. F.; Hume, D. M.; Saper, M. A.; Dixon, J. E. *J. Biol. Chem.* **1992**, *267*, 23759-23766.

(28) Nau, W. M.; Greiner, G.; Wall, J.; Rau, H.; Olivucci, M.; Robb, M. A. *Angew. Chem. Int. Ed.* **1998**, *37*, 98-101.

(29) Nau, W. M.; Greiner, G.; Rau, H.; Olivucci, M.; Robb, M. A. *Ber. Bunsen Ges. Phys. Chem.* **1998**, *102*, 486-492.

(30) Nau, W. M.; Greiner, G.; Rau, H.; Wall, J.; Olivucci, M.; Scaiano, J. C. *J. Phys. Chem. A* **1999**, *103*, 1579-1584.

(31) Sinicropi, A.; Pischel, U.; Basosi, R.; Nau, W. M.; Olivucci, M. *Angew. Chem. Int. Ed.* **2000**, *39*, 4582-4586.

(32) Nau, W. M.; Huang, F.; Wang, X.; Bakirci, H.; Gramlich, G.; Márquez, C. *Chimia* **2003**, *57*, 161-167.

(33) Mohanty, J.; Nau, W. M. *Photochem. Photobiol. Sci.* **2004**, *3*, 1026-1031.

(34) Nau, W. M.; Pischel, U. In *Organic Photochemistry and Photophysics*; Ramamurthy, V., Schanze, K. S., Eds.; CRC Press: 2006; Vol. 14, p 75-129.

(35) Pischel, U.; Patra, D.; Koner, A. L.; Nau, W. M. *Photochem. Photobiol.* **2006**, *82*, 310-317.

(36) Koner, A. L.; Pischel, U.; Nau, W. M. *Org. Lett.* **2007**, *9*, 2899-2902.

(37) Hennig, A.; Schwarzlose, T.; Nau, W. M. *Arkivoc* **2007**, (viii) 341-357.

(38) Nau, W. M.; Wang, X. *ChemPhysChem* **2002**, *3*, 393-398.

(39) Márquez, C.; Pischel, U.; Nau, W. M. *Org. Lett.* **2003**, *5*, 3911-3914.

(40) Zhang, X.; Gramlich, G.; Wang, X.; Nau, W. M. *J. Am. Chem. Soc.* **2002**, *124*, 254-263.

(41) Bakirci, H.; Koner, A. L.; Nau, W. M. *Chem. Commun.* **2005**, 5411-5413.

(42) Bakirci, H.; Koner, A. L.; Nau, W. M. *J. Org. Chem.* **2005**, *70*, 9960-9966.

(43) Bakirci, H.; Nau, W. M. *Adv. Funct. Mat.* **2006**, *16*, 237-242.

(44) Bakirci, H.; Koner, A. L.; Schwarzlose, T.; Nau, W. M. *Chem. Eur. J.* **2006**, *12*, 4799-4807.

(45) Bakirci, H.; Koner, A. L.; Dickman, M. H.; Kortz, U.; Nau, W. M. *Angew. Chem. Int. Ed.* **2006**, *45*, 7400-7404.

(46) Huang, F.; Nau, W. M. *Angew. Chem. Int. Ed.* **2003**, *42*, 2269-2272.

(47) Huang, F.; Nau, W. M. *Res. Chem. Intermed.* **2005**, *31*, 717-726.

(48) Sahoo, H.; Hennig, A.; Nau, W. M. *Int. J. Photoenergy* **2006**, DOI:10.1155/IJP/2006/89638 (OPEN ACCESS).

(49) Sahoo, H.; Roccatano, D.; Zacharias, M.; Nau, W. M. *J. Am. Chem. Soc.* **2006**, *128*, 8118-8119.

(50) Sahoo, H.; Nau, W. M. *Indian J. Radiat. Res.* **2006**, *3*, 104-112.

(51) Sahoo, H.; Nau, W. M. *ChemBioChem* **2007**, *8*, 567-573.

(52) Hennig, A.; Ghale, G.; Nau, W. M. *Chem. Commun.* **2007**, 1614-1616.

(53) Sahoo, H.; Roccatano, D.; Hennig, A.; Nau, W. M. *J. Am. Chem. Soc.* **2007**, *129*, 9762-9772.

(54) Hennig, A.; Bakirci, H.; Nau, W. M. *Nat. Methods* **2007**, *4*, 629-632.

(55) Sinicropi, A.; Pogni, R.; Basosi, R.; Robb, M. A.; Gramlich, G.; Nau, W. M.; Olivucci, M. *Angew. Chem. Int. Ed.* **2001**, *40*, 4185-4189.

(56) Sinicropi, A.; Nau, W. M.; Olivucci, M. *Photochem. Photobiol. Sci.* **2002**, *1*, 537-546.

(57) Nau, W. M. *J. Am. Chem. Soc.* **1998**, *120*, 12614-12618.

(58) The use of strongly alkaline pH sacrifices the possibility for a continuous measurement, but the addition of base could be used to deliberately terminate the enzymatic reaction ("stopped assay") and offers a unique way to dramatically enhance the differentiation of substrate and product.

(59) Sjögren, H.; Ericsson, C. A.; Evenäs, J.; Ulvenlund, S. *Biophys. J.* **2005**, *89*, 4219-4233.

(60) Pischel, U.; Nau, W. M. *J. Am. Chem. Soc.* **2001**, *123*, 9727-9737.

(61) In contrast, for assays based on static fluorescence quenching (Scheme 1a), increased temperature should reduce the substrate/product differentiation, owing to the entropy loss accompanying probe/quencher aggregation.

(62) Roccatano, D.; Sahoo, H.; Zacharias, M.; Nau, W. M. *J. Phys. Chem. B* **2007**, *111*, 2639-2646.

(63) Haskell, M. D.; Slack, J. K.; Parsons, J. T.; Parsons, S. J. *Chem. Rev.* **2001**, *101*, 2425-2440.

(64) Thomas, S. M.; Brugge, J. S. *Annu. Rev. Cell Dev. Biol.* **1997**, *13*, 513-609.

(65) Wells, A. *Int. J. Biochem. Cell Biol.* **1999**, *31*, 637-643.

(66) Oda, K.; Matsuoka, Y.; Funahashi, A.; Kitano, H. *Mol. Syst. Biol.* **2005**, *1*, E1-E17.

(67) Verjee, Z. H. M. *Eur. J. Biochem.* **1969**, *9*, 439-444.

(68) Shen, X.-C.; Yao, S.-L.; Terada, S.; Nagamune, T.; Suzuki, E. *Biochem. Eng. J.* **1998**, *2*, 23-28.

(69) Kawarasaki, Y.; Nakano, H.; Yamane, T. *Plant Sci.* **1996**, *119*, 67-77.

(70) Eremenko, A. V.; Bauer, C. G.; Makower, A.; Kanne, B.; Baumgarten, H.; Scheller, F. W. *Anal. Chim. Acta* **1998**, *358*, 5-13.

(71) Nistor, C.; Emnéus, J. *Anal. Commun.* **1998**, *35*, 417-419.

(72) Bauer, C. G.; Eremenko, A. V.; Ehrentreich-Förster, E.; Bier, F. F.; Makower, A.; Halsall, H. B.; Heineman, W. R.; Scheller, F. W. *Anal. Chem.* **1996**, *68*, 2453-2458.

(73) In order to provide an independent quantitfication of the degree of conversion in the Dbo-based assays, we developped an independent UV assay, in which the dephosphorylation of peptide p**6** by alkaline phosphatase was directly monitored through the distinct changes in the UV spectra of the tyrosine residue. Accordingly, dephosphorylation converts a phosphotyrosine residue ($\lambda_{max}$ = 273 nm, $\varepsilon$ ca. 650 $cm^{-1}M^{-1}$, ref. 25) to a tyrosine group ($\lambda_{max}$ = 273 nm, $\varepsilon$ ca. 1400 $cm^{-1}M^{-1}$, ref. 24), which results in a characteristic bathochromic and hyperchromic shift of the tyrosine absorption band. The conversion time profile as obtained by monitoring the UV absorbance of tyrosine at 283 nm, where the absolute variations in absorbance were largest, was the same, within error, as that obtained by monitoring the fluorescence of Dbo at 450 nm, which confirmed that the fluorescence changes depend linearly on the degree of conversion.

(74) Daugherty, D. L.; Gellman, S. H. *J. Am. Chem. Soc.* **1999**, *121*, 4325-4333.

(75) Soleilhac, J. M.; Cornille, F.; Martin, L.; Lenoir, C.; Fournié-Zaluski, M. C.; Roques, B. P. *Anal. Biochem.* **1996**, *241*, 120-127.

(76) Anne, C.; Cornille, F.; Lenoir, C.; Roques, B. P. *Anal. Biochem.* **2001**, *291*, 253-261.

(77) Songyang, Z.; Carraway III, K. L.; Eck, M. J.; Harrison, S. C.; Feldman, R. A.; Mohammadi, M.; Schlessinger, J.; Hubbard, S. R.; Smith, D. P.; Eng, C.; Lorenzo, M. J.; Ponder, B. A. J.; Mayer, B. J.; Cantley, L. C. *Nature* **1995**, *373*, 536-539.

(78) Edison, A. M.; Barker, S. C.; Kassel, D. B.; Luther, M. A.; Knight, W. B. *J. Biol. Chem.* **1995**, *270*, 27112-27115.

(79) Hyeon, C.; Thirumalai, D. *J. Chem. Phys.* **2006**, *124*, 104905 (1-14).

(80) Wang, X.; Nau, W. M. *J. Am. Chem. Soc.* **2004**, *126*, 808-813.

(81) A direct comparison of the $v_{max}$ values was not attempted, because of the unknown absolute concentrations of active kinase in the commercial samples, and because of the different mutants of the proteins used throughout the literature, which contain different domains of the human Src kinase. For example, the employed Proqinase sample was a GST fusion protein with a His-tag and a thrombin cleavage site.

(82) Pappas, P. W.; Leiby, D. A. *J. Cell. Biochem.* **1989**, *40*, 239-248.

(83) Stankiewicz, P. J.; Gresser, M. J. *Biochemistry* **1988**, *27*, 206-212.

(84) Copeland, R. A. *Anal. Biochem.* **2003**, *320*, 1-12.

(85) Hemmilä, I.; Webb, S. *Drug Discov. Today* **1997**, *2*, 373-381.

(86) Grepin, C.; Pernelle, C. *Drug Discov. Today* **2000**, *5*, 212-214.

(87) Johansson, M. K.; Cook, R. M.; Xu, J.; Raymond, K. N. *J. Am. Chem. Soc.* **2004**, *126*, 16451-16455.

# APPENDIX 3

W. M. Nau, M. Florea, H. Sahoo, H. Bakirci, A. Hennig, D. M. Bailey, “Nano-TRF und Tandem Assays für Multiparameteranalitik” in “Multiparameteranalitik, Methoden, Applikationen, Perspektiven”, K. Conrad, W. Lehnmann, U. Sack, U. Schedler, Eds., Pabst Verlag, Lengerich, **2008**, 147-162. Reprinted with permission from Pabst Science Publishers. The published version may be found at:

http://gfid-ev.com/formulare/IDBIB5_MPA.pdf

**Titel**: Nano-TRF und Tandem Assays für HTS und Multiparameteranalytik

**Kurztitel**: Nano-TRF und Tandem Assays

**Autoren**: Werner M. Nau, Mara Florea, Harekrushna Sahoo, Huseyin Bakirci, Andreas Hennig, David Bailey

**Institution**: Jacobs University Bremen

**Adresse**: School of Engineering and Science, Campus Ring 1, D-28759 Bremen, Germany

**E-mail**: w.nau@jacobs-university.de

**Schlagwörter**: HTS, Enzymassays, TRF, Fluoreszenz, Proteasen, Phosphatasen, Kinasen, Decarboxylasen, Sensoren, Aminosäuren

**Abstract**

Der Beitrag beschreibt zwei neuartige Ansätze für die Fluoreszenzdetektion, die für High-Throughput Screening (HTS), Enzymassays, Sensorik, und die Multiparameteranalytik von großem Interesse sind. Die Techniken werden anhand von Beispielen von Enzymassays beschrieben, sind allerdings auf allgemeinere analytische Detektionsprobleme übertragbar. Die *erste Technik* (Nano-TRF) macht von der Möglichkeit der zeitaufgelösten anstelle einer stationären, also lediglich auf Intensitätsmessungen basierenden, Fluoreszenzdetektion Gebrauch. Während sich die Fluoreszenzabklingzeiten von üblichen Fluorophoren üblicherweise im Bereich von einigen Nanosekunden bewegen, sind Fluoreszenzabklingzeiten von mehr als 100 Nanosekunden extrem selten. Durch eine spezielle Detektionstechnik, die mittlerweile auch in kommerziellen Mikroplattenlesern verfügbar ist, kann diese langlebige Fluoreszenz durch eine im Nanosekundenbereich angelegte zeitaufgelöste Fluoreszenzmessung (nanosecond time-resolved fluorescence = Nano-TRF) separat von der gesamten Fluoreszenzintensität ausgelesen werden. Dies ermöglicht je nach Bedarf die Unterdrückung kurzlebiger Hintergrundfluoreszenz (z.B. im HTS) oder, im Sinne der Multiparameteranalytik, die parallele Auslesung zweier Fluoreszenzparameter (Intensität der gesamten und der langlebigen Komponente), die somit Aufschluss über verschiedene Analyten geben kann. Nano-TRF wurde mittlerweile für Assays für Proteasen, Phosphatasen und Kinasen beschrieben. Die *zweite Technik* (Tandem Assays) verwendet zur Modulation der Fluoreszenzeigenschaften geeigneter Farbstoffe sogenannte makrozyklische Wirtmoleküle. Dies sind große zyklische organische Moleküle, die in ihrem

Inneren kleinere Gast-Moleküle einschließen und somit “erkennen” können. Durch die Komplexierung des Gastes und Analyten wird der Fluoreszenzfarbstoff aus dem Makrozyklus verdrängt und ändert seine Fluoreszenzeigenschaften (Intensität, Lebensdauer, Spektrum), wodurch eine sensitive Detektion des Analyten erfolgt. Derartige auf Indikatorverdrängung beruhende Verfahren sind in der Biologie bereits umfassend für Antikörper-Farbstoffkonjugate beschrieben, die allerdings Analyten wesentlich spezifischer binden. Makrozyklen binden Analyten weniger selektiv, wodurch sich Möglichkeiten für die Multiparameteranalytik ergeben, da mehrere strukturell verwandte Moleküle mit dem gleichen “Reporterpaar” (also demselben Markozyklus und Farbstoff) verfolgt werden können. Eine hohe Spezifität kann durch die Kopplung der Detektion des Analyten mit einer enzymatichen Reaktion erreicht werden (Tandem Assay). Diese ermöglicht beispielsweise die Detektion verschiedener Aminosäuren, biogener Amine, oder der entsprechenden Decarboxylasen.

**1 Einführung in die Nano-TRF-Detektion**

Auf Fluoreszenz basierende Detektionsverfahren sind alternativen Verfahren, die auf Radioaktivität oder Absorption beruhen, aus Gründen der allgemeinen Laborsicherheit bzw. der Sensitivität überlegen (1-3). Dies gilt sowohl im biochemischen Labormaßstab als auch im pharmazeutischen High-Throughput Screening (HTS), und insbesondere auch in der Multiparameteranalytik. Eine wichtige neuere Entwicklung ist die Verwendung von Methoden, die auf zeitaufgelöster Fluoreszenz (time-resolved fluorescence = TRF) basieren (4,5). Hierbei wird eine lange Fluoreszenzlebensdauer eines Fluorophors zur Unterscheidung von einer kurzlebigen Hintergrundfluoreszenz ausgenutzt. Etablierte TRF-Assays wurden bis vor kurzem mit auf Lanthaniden (Seltenerdmetallen) basierenden Metallkomplexen in Verbindung gebracht, da diese sehr lange Fluoreszenzen (um genau zu sein Lumineszenzen, da die Emission nicht von einem Singulett-Spinzustand herrührt) im Millisekundenbereich aufweisen (4,5), sofern geeignete Additive (Detergentien und Chelatbildner) anwesend sind. Derartig lange Lumineszenzen können auch ohne aufwendige schnelle elektronische Detektionsverfahren sehr leicht von der viel kürzeren Hintergrundfluoreszenz differenziert werden, wie dies unvermeidlich durch Streulicht, Probenmaterialien, Verunreinigungen, andere Additive (relevant für HTS) oder anwesende weitere Analyte (relevant für die Multiparameteranalytik) hervorgerufen wird.

Gemeinhin ist allerdings die Verwendung von organischen Chromophoren gegenüber der Verwendung von Metallionen oder Metallkomplexen bevorzugt, da diese problemlos als Labels und Markierungen an biologische Analyten, insbesondere Peptide, kovalent angebunden werden können, z.B. im Laufe der Festphasen-Peptidsynthese. Organische Chromophore zeigen allerdings kürzere

Fluoreszenzlebensdauern, so dass eine Detektionselektronik im Nanosekundenbereich erforderlich ist. Wir bezeichnen diese kürzlich von uns in Zusammenarbeiten mit Partnern entwickelte Technik als Nano-TRF (6-8), die mittlerweile mit kommerziellen Mikroplattenlesern leicht realisiert werden kann (siehe hierzu auch Beiträge anderer Autoren im vorliegenden Werk). Als Anregungslichtquelle dienen hierbei insbesondere gepulste Laser, die die Proben mit 10-100 hochintensiven Laserpulsen pro Sekunde zur Fluoreszenz anregen, die dann mit einer hochsensitiven Elektronik zeitaufgelöst registriert wird. Als organischen Fluorophor, der sich aufgrund seiner langen Lebensdauer von bis zu 1 Mikrosekunde besonders für Nano-TRF eignet, haben wir verschiedene Derivate des 2,3-Diazabicyclo[2.2.2]octans (DBO, Abb. 1) eingeführt (9-11), die sich auch als besonders biokompatibel erwiesen haben. Speziell das Asparaginderivat ("Dbo") kann sehr einfach in Peptide eingebaut werden; auf DBO basierende Farbstoffe sind kommerziell als Puretime™ 325 Farbstoffe verfügbar.

– Abb. 1 hier einfügen –

Für das Design von Enzymassays kommt vereinfachend hinzu, dass die Fluoreszenz von Dbo durch einige wenige natürliche Aminosäuren (Tryptophan, Tyrosin, Cystein und Metionin) gelöscht wird (11). Auf diese Weise können gezielt Peptidsubstrate synthetisiert werden, die neben dem Dbo-Baustein einen Löscher, meist Tryptophan oder Tyrosin enthalten. In derartigen Peptidsubstraten kommt es zu einer effizienten Fluoreszenzlöschung, die durch die Diffusion des Löschers zur Sonde ausgelöst wird. Diese Fluoreszenzlöschung führt zu einer stark verkürzten Fluoreszenzlebensdauer, die in der Nano-TRF-Messung zu keinem oder nur einem sehr geringen Signal führt. Durch enzymatisch-chemische Modifikation des Peptidsubstrates kann der Löschmechanismus unterdrückt werden, so dass die langlebige Fluoreszenz des ungelöschten Dbo-Fluorophors wiederhergestellt wird. Dies kann beispielsweise dadurch hervorgerufen werden, dass eine *Protease* das Peptidsubstrat (12,13) spaltet und somit den Löscher abtrennt (Abb. 2), oder dass eine Tyrosin-*Kinase* (14,15) den Löscher phosphoryliert und somit deakiviert (Abb. 3, die Löschung erfolgt in diesem Fall durch Übertragung des phenolischen Wasserstoffatoms, welches durch Phophorylierung verloren geht). Auf diese Weise kann die jeweilige enzymatische Reaktion durch die Bildung einer langlebigen Fluoreszenzkomponente hochselektiv im Nano-TRF-Modus detektiert werden. Derartige auf Dbo und Nano-TRF basierende Protease-Assays wurden bereits erfolgreich im pharmazeutisch-industriellen HTS eingesetzt, wobei hierbei die Detektion mit dem Ziel durchgeführt wird, durch Zugabe von z.B. hunderttausenden von verschiedenen Verbindungen Inhibitoren (in seltenen Fällen Aktivatoren) für das entsprechende Enzym zu identifizieren. Hierbei sei vermerkt, dass neben der Entwicklung einer langlebigen Fluoreszenz auch der Verlust dieser mittels Nano-TRF verfolgt

werden kann. So konnte z.B. gezeigt werden, dass nicht nur die Phosphorylierung von Peptidsubstraten durch Kinasen, sondern auch die Umkehrreaktion, also die Dephosphorylierung durch Phosphatasen (16), verfolgt werden kann, wobei es im letzteren Fall zu einer Abschwächung des Nano-TRF-Signals im Verlauf der enzymatischen Reaktion kommt, da der Löscher aktiviert wird.

– Abb. 2 hier einfügen –

– Abb. 3 hier einfügen –

**2 Vorteile der Nano-TRF-Detektion**

Die Vorteile der Nano-TRF-Detektion werden besonders deutlich, wenn man das Messfenster der zeitaufgelösten Messung (gelb markiert in Abb. 4) unter Berücksichtigung des exponentiellen Fluoreszenzabfallverhaltens einer kurzlebigen (blau) und einer langlebigen (rot) Komponente vergleicht. Die langlebige Komponente wird hochselektiv detektiert, da die kurzlebige Komponente zu Beginn der Nano-TRF-Messung (nach 150 ns) bereits komplett zerfallen ist, selbst wenn sie tausend- oder zehntausendmal intensiver als die langlebige Komponente wäre. Im Falle einer stationären Fluoreszenzintensitätsmessung, die das Gesamtintegral unterhalb der Fluoreszenzzerfallskurve erfasst, wird die kurzlebige Komponente stets mitdetektiert, und dies ist insbesondere dann unerwünscht, wenn diese entweder auf unspezifische Hintergrundfluoreszenz zurückzuführen ist oder aber so stark ist, dass die informative langlebige Komponente als „Rauschen“ in Gegenwart einer viel zu starken kurzlebigen Fluoreszenzkomponente untergeht. Aber auch in Fällen, in denen keine Hintergrundfluoreszenz oder die Fluoreszenz weiterer Analyten (siehe Multiparameteranalytik unten) interferiert, gewinnt man durch Nano-TRF-Detektion von enymatischen Reaktionen eine verbesserte Differenzierung zwischen der Fluoreszenz von Substrat und Produkt. Das in Abb. 4 dargestellte Beispiel zeigt in der Tat das Beispiel einer proteolytischen Substratspaltung eines in unserem Labor untersuchten Dbo-markierten Peptidsubstrates (siehe oben).

– Abb. 4 hier einfügen –

Die Elimination kurzlebiger Fluoreszenzen im Nano-TRF-Modus hängt formelmäßig mit der exponentiellen Zerfallskinetik zusammen. Es kann gezeigt werden, dass sich das im Nano-TRF-Modus gemessene Signal eines langlebig fluoreszierenden Analyten ($I_{\text{Nano-TRF}}$) zum im Nano-TRF-Modus beitragenden Restsignal einer kurzlebigen Fluoreszenz ($I_{\text{Background}}$) gemäß Gleichung 1 verhält. Dementsprechend steigt die Differenzierung (Verhältnis zwischen Signal und Rauschen) mit zunehmender Messverzögerung ($t_{\text{delay}}$) an und ist dann besonders groß, wenn sich die Lebensdauern der Komponenten ($\tau_{\text{long}}$ und $\tau_{\text{short}}$) stark unterscheiden. Zum Vergleich nimmt das Verhältnis der stationär erwarteten Fluoreszenzintensitäten ($I_{\text{rel}}$) einen Wert von $\tau_{\text{long}}/\tau_{\text{short}}$ an.

$$I_{rel}^{TRF} = \frac{I_{\text{Nano-TRF}}}{I_{\text{Background}}} = \int_{t_{\text{delay}}}^{t_{\text{delay}}+t_{\text{gate}}} A \cdot \exp\left(-\,t/\tau_{\text{long}}\right) dt \Big/ \int_{t_{\text{delay}}}^{t_{\text{delay}}+t_{\text{gate}}} A \cdot \exp\left(-\,t/\tau_{\text{short}}\right) dt \quad (1)$$

Tabelle 1 zeigt anhand von in unserem Labor tatsächlich vermessenen Lebensdauern von Peptidsubstraten die Zunahme der Differenzierung von Intensitätsverhältnissen in der stationären ($I_{\text{rel}}$) und Nano-TRF-Messung. Dementsprechend erhält man eine Verbesserung um bis zu 16 Größenordnungen! Auch wenn diese experimentell durch Beschränkungen in der Detektionselektronik in diesem Ausmaß nicht realisierbar sind, erreicht man dennoch durch die Nano-TRF-Detektion stets eine merkliche Verbesserung, sofern eine Lebensdauer „lang genug“ ist, was praktisch eine Lebensdauer von mehr als 100 Nanosekunden erfordert. Die Vorteile der Nano-TRF-Detektion im Vergleich zur Steady-State-Messung sind leicht aus den Anwendungsbeispielen in Abb. 5 erkennbar, in denen Enzymkinetiken mit beiden Methoden verfolgt wurden; die relative Signalintensität ist in beiden Fällen im Nano-TRF-Modus wesentlich höher. Allerdings bringt Nano-TRF auch den Nachteil mit sich, dass weniger Datenpunkte in der gleichen Zeit aufgenommen werden können, da die Messung auf der Akkumulation von Daten mehrerer Laserpulse basiert, welche jeweils einige Sekunden benötigt, begrenzt durch die Pulswiederholrate der betrffenden Laser (maximal 100 Hz).

– Tabelle 1 hier einfügen –

– Abb. 5 hier einfügen –

**3 Anwendungen der Nano-TRF-Detektion in der Multiparameteranalytik**

Abb. 6 zeigt Fluoreszenzmessungen von Mischungen von 7-Amino-4-methylcoumarin (AMC) und DBO in verschiedenen Mischverhältnissen, wobei die Konzentration von AMC konstant und diejenige von DBO variiert wurde. Beide Farbstoffe absorbieren im nahen UV bei ca. 375 nm und haben ein Emissionsmaximum um 430 nm, können also nicht mit konventionellen spektralen Differenzierungsmethoden der Multiparameteranalytik separat erfasst werden. Die stationäre Fluoreszenzintensität (links) bleibt von der Zugabe von DBO innerhalb der Fehlergrenze unbeeinflusst, da AMC einen etwa hundertfach stärkeren Absorptionskoeffizienten als DBO aufweist; somit hängt auch die stationär gemessene Fluoreszenzintensität lediglich von der AMC-Konzentration ab (außer bei sehr verdünnten AMC-Konzentrationen), so dass die Konzentration dieses analytischen Parameters über stationäre Fluoreszenz ausgelesen werden kann. Die langlebige Fluoreszenz des DBO-Analyten kann, auch wenn sie im Vergleich zu der von AMC schwach ist, über das Fluoreszenzsignal im Nano-TRF-Modus ausgelesen werden (rechts), welches eine lineare Abhängigkeit von der DBO-Konzentration aufweist und somit ein zuverlässig auslesbares Maß für diesen analytischen Parameter bietet.

– Abb. 6 hier einfügen –

Das angeführte Beispiel zeigt, wie die Nano-TRF-Detektion in Kombination mit der stationären Fluoreszenzintensitätsmessung in der Multiparameteranalytik Einsatz finden kann. Die in unserem Modellbeispiel verwendeten Analyten stehen hier stellvertretend für zwei Analyten, deren Fluoreszenzlebensdauer sich deutlich unterscheidet, und die somit selektiv durch die Anwendung unterschiedlicher Messverzögerungen, namentlich einer von 0 Nanosekunden (entspricht stationäre Fluoreszenzmessung) und einer deutlich längeren (z.B. 150 Nanosekunden, zur Detektion langlebiger Fluoreszenzen), ausgelesen werden können. Hierbei ist es bevorzugt, dass beide Messungen in nur einem Instrument durchgeführt werden, da die Messverzögerung kommerzieller Nano-TRF-Mikroplattenleser variabel ist. Es ist auch vorstellbar, falls beide Analyten signifikant zur Absorption bei der Anregungswellenlänge beitragen, dass die stationäre Fluoreszenzintensität die Summe beider Analyten wiederspiegelt, und die Einzelkonzentrationen durch Berücksichtigung der separat messbaren Nano-TRF-Komponente zugänglich werden. Somit ergeben sich durch Nano-TRF-Messungen neue Möglichkeiten in der Multiparameteranalytik, die momentan an Anwendungsbeispielen untersucht werden.

**4 Einführung in Tandem Assays**

Die Detektion biomolekularer Analyte, und insbesondere von Produkten enzymatischer Reaktionen, wird üblicherweise – die oben beschriebene Nano-TRF-Methode eingeschlossen – durch kovalente Anbindung von Fluoreszenzmarkern an den Analyten oder Substraten oder die Einführung radioaktiver Isotope erreicht (3,17). Zudem finden häufig noch Antikörper Verwendung, die eine hochspezifische Erkennung ermöglichen (18). Wir haben kürzlich eine einfache Methode entwickelt (19), die es erlaubt die Produkte enzymatischer Reaktionen „label-frei“, also ohne derartige Marker, zu detektieren. Hiermit können auch verschiedene Substrate für unterschiedliche zugegebene Enzyme zuverlässig und sensitiv detektiert werden, was wiederum neue Möglichkeiten für die Multiparameteranalytik eröffnet.

Das Prinzip der Messmethode (Abb. 7) basiert auf der Zugabe eines sogenannten Reporterpaars, welches aus einem makrozyklischen Molekül und einem Fluoreszenzfarbstoff besteht, die überwiegend beide kommerziell erhältlich sind. Makrozyklische Moleküle, z.B. Cyclodextrine als bekannteste Vertreter, weisen einen Hohlraum auf, der sich für den Einschluss kleinerer sogenannter Gastmoleküle eignet. Hieraus resultiert ein sogenannter Wirt-Gast-Komplex, beispielsweise mit einem Fluoreszenzfarbstoff. Auch wenn die Makrozyklen verschiedene Moleküle und potentielle Analyten nur mit teilweise geringen Affinitätsunterschieden und somit mäßiger Selektivität binden – dies steht im strikten Gegensatz zur hochspezifischen Bindung durch Antiköper – kann durch geeignete Wahl des Reporterpaars sichergestellt werden, dass das

Produkt einer enzymatischen Reaktion stärker gebunden wird als das Substrat. Mit Hilfe des Reporterpaares können also enzymatische Reaktionen verfolgt werden, wobei die Selektivität der Detektion alleine durch die Spezifität des Enzyms bewirkt wird (20), nicht jedoch durch den Makrozyklus.

– Abb. 7 hier einfügen –

Das enzymatisch gebildete Produkt verdrängt somit im Reaktionsverlauf den Fluoreszenzfarbstoff aus dem makrozyklischen Komplex, wodurch sich die Fluoreszenzeigenschaften des Farbstoffes (Intensität, Lebensdauer, Spektrum, Polarisation, etc.) im allgemeinen stark ändern, da molekulare Fluoreszenz eine stark umgebungsabhängige photophysikalische Eigenschaft darstellt. Die Zunahme (oder Abnahme) der Fluoreszenz kann somit zur wahlweisen Detektion des Substrates, Produktes, oder des betreffenden Enzyms verwendet werden. Vorteilhaft für die Multiparameteranalytik ist hierbei, dass aufgrund der mäßigen Selektivität des Makrozyklus ganze Substratklassen (z.B. verschiedene Aminosäuren), Produktklassen (z.B. biogene Amine), und Enzymklassen (z.B. Decarboxylasen) erschlossen werden können, ohne dass das Detektionssystem, also das Reporterpaar, angepasst werden muss. Dies reduziert die Kosten in Enzymassays bzw. biochemischer Analysen um Größenordnungen, da die Herstellung der spezifischen Antikörper und verschiedener radioaktiv markierter oder kovalent modifizierter Substrate mit enormen Arbeits- und Zeitaufwand verbunden ist.

Als Anwendungsbeispiel ist die Decarboxylierung von *L*-Arginin durch Arginin-Decarboxylase in Abb. 8 dargestellt. Duch die Abspaltung der negativ geladenen Carboxylatgruppe ($-CO_2^-$) entsteht ein Amin als Produkt, welches bei pH 6 als zweifach positiv geladenes Kation vorliegt. Entsprechend wurden als Makrozyklen sogenannte Kationen-Rezeptoren gewählt, namentlich Cucurbit[7]uril (CB7) und *p*-Sulfonatocalix[4]aren (CX4), beide kommerziell erhältlich. CB7 und CX4 binden das Amin-Produkt stark, das Aminosäure-Substrat jedoch schwach. Als Fluoreszenzfarbstoffe im Reporterpaar wurden Dapoxyl und DBO verwendet, die sich dahingehend unterscheiden, als dass sie bei der Verdrängung durch das Produkt eine Erniedrigung („switch-off“) bzw. Erhöhung („switch-on“) der Fluoreszenz zeigen. Das Tandem-Assay-Prinzip ist hierbei flexibel einsetzbar und kann auf mehrere andere Aminosäuren (z.B. Lysin, Tyrosin, Tryptophan, Histidin, Ornitin) übertragen werden (19).

– Abb. 8 hier einfügen –

**5 Vorteile von Tandem Assays**

Die Vorteile von Tandem-Assays können wie folgt zusammengefasst werden:

• breite Anwendbarkeit – ganze Enzymklassen zugänglich
• hohe Variabilität – Reporterpaare können frei gewählt werden
• Echtzeitdetektion – Untersuchung von Enzymkinetiken möglich
• Detektion in homogener Lösung – keine weiteren Inkubationsschritte

• label-frei – keine kovalente Bindung von Fluoreszenzmarkern erforderlich
• Umgehung von radioaktiven Markierungen – Fluoreszenzdetektion
• antikörperfrei – somit ökonomisch und rasch umsetzbar

Besonders interessant ist der Vergleich mit auf Antikörpern basierenden Detektionsverfahren, da wir Makrozyklen sozusagen als preiswerten Ersatz für diese verwenden. Makrozyklen sind im Vergleich zu Antikörpern „kleine" Moleküle und naturgemäss weniger spezifisch in Bezug auf ihre Bindungseigenschaften verschiedener Analyte. Der verwendete Makrozyklus Cucurbit[7]uril, zum Beispiel (CB7, siehe Abb. 8), fungiert als allgemeiner Kationenrezeptor, und nicht als ein spezifischer Rezeptor für ein bestimmtes biogenes Amin, beispielsweise Cadaverin, Agmatin, Histamin, Putrescin, Tyramin, oder Tryptamin. Dieser scheinbare Mangel an Selektivität verbessert allerdings das Anwendungspotential von Makrozyklen, da hiermit gleichzeitig mehrere Enzyme, oder mehrere Analyten zugänglich werden. Letzteres ist für die Multiparameteranalytik von grossem Interesse.

**6 Anwendungen von Tandem Assays in der Multiparameteranalytik**

Anhand des Beispiels einer Mischung verschiedener Aminosäuren können die Einsatzmöglichkeiten von Tandem-Assays für die Multiparameteranalytik illustriert werden. Hier gibt es neben klassischen chromatographischen Trennungsmethoden oder der Kernresonanzspektroskopie kaum einfache Detektions- und Quantifizierungsmöglichkeiten für die verschiedenen Analyten. Spezifische Antikörper für die Aminosäuren selbst oder deren enzymatische Produkte sind nicht bevorzugt, da deren Herstellung aufwendig ist, und jeweils für jeden Antikörper ein Ausleseverfahren, z.B. über eine Verdrängungsreaktion mit einem wiederum aufwendig zu synthetisierenden fluoreszenzmarkiertem Kompetitor, entwickelt werden müsste. Der Einsatz eines aus Makrozyklus und Farbstoff bestehenden gemeinsamen Reporterpaars in Kombination mit einem für die Aminosäure spezifischen Enzyms ist hierbei vorteilhaft, da auf diese Weise mehrere Analyte mit demselben Ausleseverfahren erfasst werden können.

Im Fall einer Mischung aus Histidin, Arginin, Lysin und Tyrosin kann beispielsweise gezeigt werden, dass Histidindecarboxylase nur in Gegenwart von Histidin aktiv ist und in das entsprechende Amin überführt; letzteres verdrängt den Farbstoff aus dem Komplex und liefert somit ein positives Signal (Abb. 9). Genauso liefert Tyrosindecarboxylase nur in Gegenwart von Tyrosin das gewünchte Fluorezenzsignal nach dem Tandem-Assay-Prinzip. Auf diese Weise können mit einem Reporterpaar unter identischen instrumentellen Auslesebedingungen 4 oder mehr Aminosäuren detektiert werden. Da der zeitliche Verlauf des Fluoreszenzsignals (der den Umsatz der enzymatischen Reaktion widerspiegelt) im übrigen auch von der Konzentration des Substrates abhängt, können des weiteren auch die vorliegenden Konzentrationen bestimmt

werden, im Fall der Decarboxylasen bis zu einem Detektionslimit von 1 mikromolar. Tandem-Assays können also sehr bequem eingesetzt werden, um in Gemischen mehrere verwandte Analyten zu bestimmen. Voraussetzung ist hierbei allerdings, dass es sich um biomolekulare Metaboliten handelt, die mit entsprechenden enzymatischen Reaktionen modifiziert werden können.

– Abb. 9 hier einfügen –

**7 Schlussfolgerungen, Ausblick**

Die rasche und zuverlässige Bestimmung von mehreren Substanzen in der gleichen Laborprobe stellt eine aktuelle analytische Herausforderung dar. Dies gilt insbesondere für medizinisch, biochemisch oder umwelttechnisch relevante Analyten. Von besonderer technischer Bedeutung sind hierbei auf Fluoreszenz basierende Verfahren, die eine hohe Empfindlichkeit mit einer breiten Akzeptanz beim Anwender verbinden. Die Fluorezenzlebensdauer eines Analyten stellt hierbei ein bisher vernachlässigter Ausleseparameter dar. Im Zusammenspiel mit Fluorezenzintensitätsmessungen können somit in einem stationären Fluoreszenz-Modus und einem zeitaufgelösten Fluoreszenzmodus (z.B. Nano-TRF) mindestens 2 Analyten separat ausgelesen werden, sofern sich deren Fluorezenzlebensdauern deutlich unterscheiden. Kommerzielle Mikroplattenleser für Nano-TRF und entsprechende langlebige Fluorophore (z.B. Dbo, Puretime 325 Farbstoffe) sind mittlerweile verfügbar, so dass deren vermehrte Einbindung in die Multiparameteranalytik bevorsteht.

Auf Antikörper basierende Messverfahren spielen bislang in der Multiparameteranalytik eine untergeordnete Rolle, da diese aufgrund ihrer hohen Spezifität nur für die Bestimmung einzelner Analyten geeignet sind. Die Verwendung von Makrozyklen als unselektive Antikörperersatzstoffe eröffnet neue Möglichkeiten für die Multiparameteranalytik, da im Wechselspiel mit spezifischen Enzymen und Fluoreszenzfarbstoffen, mehrere strukturell verwandte Analyten über das hier beschriebene Tandem-Assay-Messprinzip zugänglich werden. Erste Anwendung zur Aminosäureanalytik wurden bereits erfolgreich abgeschlossen, und die Übertragung auf weitere Enzymklassen ist in Planung.

**Literatur**


(1) Niemeyer CM. Nanopartikel, Proteinen und Nucleinsäure: Die Biotechnologie begegnet den Materialwissenschaften. Angew Chem 2001; 113:4254-87

(2) Goddard J-P, Reymond J-L. Recent advances in enzyme assays. Trends Biotechnol 2004; 22:363-70

(3) Gribbon P, Sewing A. Fluorescence readouts in HTS: no gain without pain. Drug Discov Today 2003; 8:1035-43

(4) Karvinen J, Laitala V, Mäkinen M-L, Mulari O, Tamminen J, Hermonen J, Hurskainen P, Hemmilä I. Fluorescence quenching-based assays for hydrolyzing enzymes. Application of time-resolved fluorometry in assays for caspase, helicase, and phosphatase. Anal Chem 2004; 76:1429-36
(5) Johansson MK, Cook RM, Xu J, Raymond KN. Time gating improves sensitivity in energy transfer assays with terbium chelate/dark quencher oligonucleotide probes. J Am Chem Soc 2004; 126:16451-55
(6) Hennig A, Roth D, Enderle T, Nau WM. Nanosecond time-resolved fluorescence protease assays. ChemBioChem 2006; 7:733-7
(7) Hennig A, Florea M, Roth D, Enderle T, Nau WM. Design of peptide substrates for nanosecond time-resolved fluorescence assays of proteases: 2,3-Diazabicyclo[2.2.2]oct-2-ene as a noninvasive fluorophore. Anal Biochem 2007; 360:255-65
(8) Sahoo H, Hennig A, Florea M, Roth D, Enderle T, Nau WM. Single-label kinase and phosphatase assays for tyrosine phosphorylation using nanosecond time-resolved fluorescence detection. J Am Chem Soc 2007; 129:15927-34
(9) Nau WM, Huang F, Wang XJ, Bakirci H, Gramlich G, Marquez C. Exploiting long-lived molecular fluorescence. Chimia 2003; 57:161-7
(10) Wang X, Nau WM. Kinetics of end-to-end collision in short single-stranded nucleic acids. J Am Chem Soc 2004; 126:808-13
(11) Hudgins RR, Huang F, Gramlich G, Nau WM. A fluorescence-based method for direct measurement of submicrosecond intramolecular contact formation in biopolymers: an exploratory study with polypeptides. J Am Chem Soc 2002; 124:556-64
(12) Neefjes J, Dantuma NP. Fluorescent probes for proteolysis: tools for drug discovery. Nat Rev Drug Discov 2004; 3:58-69
(13) Knight CG. Fluorimetric assays of proteolytic enzymes. Methods Enzymol 1995; 248:18-34
(14) Mallari R, Swearingen E, Liu W, Ow A, Young SW, Huang S-G. A generic high-throughput screening assay for kinases: protein kinase A as an example. J Biomol Screen 2003; 8:198-204
(15) Wang Q, Lawrence DS. Phosphorylation-driven protein-protein interactions: a protein kinase sensing system. J Am Chem Soc 2005; 127:7684-5
(16) McCain DF, Grzyska PK, Wu L, Hengge AC, Zhang Z–Y. Mechanistic studies of protein tyrosine phosphatases YopH and Cdc25A with *m*-nitrobenzyl phosphate. Biochemistry 2004; 43:8256-64
(17) Matayoshi ED, Wang GT, Krafft GA, Erickson J. Novel fluorogenic substrates for assaying retroviral proteases by resonance energy transfer. Science 1990; 247:954-8

(18) Geymayer P, Bahr N, Reymond J–L. A general fluorogenic assay for catalysis using antibody sensors. Chem Eur J 1999; 5:1006-12
(19) Hennig A, Bakirci H, Nau WM. Label-free continuous enzyme assays with macrocycle-fluorescent dye complexes. Nat Methods 2007; 4:629-32
(20) Das G, Matile S. Substrate-independent transduction of chromophore-free organic and biomolecular transformations into color. Chem Eur J 2006; 12:2936-44

**8 Danksagungen**

Die hier beschriebenen und veröffentlichten Nano-TRF-Arbeiten wurden im Rahmen einer Forschungskollaboration mit F. Hoffmann-La Roche (Basel) durchgeführt; wir danken Dr. T. Enderle und Dr. D. Roth für zahlreiche Diskussionen und die Durchführung der HTS-relevanten Messungen. Wir danken der Firma IOM GmbH (Berlin) für die Bestimmung des Detektionslimits von DBO auf dem Nano-TRF-Mikroplattenleser des Typs LF 502 NanoScan FLT. Das Tandem-Assay-Projekt wird durch das Graduiertenprogramm “Nanomolecular Science” an der Jacobs University Bremen, den Fonds der Chemischen Industrie (Frankfurt/Main) und die BIG Bremer Investitions-Gesellschaft mbH aus dem Ökologiefonds des Landes Bremen (in Zusammenarbeit mit Molzym GmbH & Co.KG) finanziell gefördert.

## Tabellen

**Tabelle 1:** Fluoreszenzlebensdauern von Substraten vor und nach der enzymatischen Umsetzung mit einer Carboxypeptidase, die den Löscher (Trp) vom Substrat abspaltet.

| Peptidsubstrat | $\tau_{short}$ [ns] | $\tau_{long}$ [ns] | $I_{rel}$ [a] | $I_{rel}^{TRF}$ [b] |
|---|---|---|---|---|
| Ac-Dbo-Trp-OH | 16.8 | 360 | 21.4 | $1.1 \times 10^{5}$ |
| H-Dbo-Gly-Trp-OH | 4.0 | 342 | 85.5 | $1.1 \times 10^{18}$ |
| H-Dbo-Gly-Gly-Trp-OH | 6.4 | 335 | 52.3 | $5.2 \times 10^{11}$ |

[a] Theoretisches Verhältnis der stationären Fluoreszenzintensitäten nach und vor der Spaltung. [c] Theoretisches Intensitätsverhältnis im Nano-TRF-Modus gemäß Gleichung 1 mit $t_{delay}$ = 150 Nanosekunden und $t_{gate}$ = 2 Mikrosekunden. Gemäß Literatur 6.

**Abbildungen**

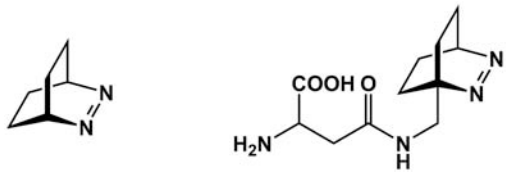


**Abb. 1**. Chemische Strukturen des Fluorophors 2,3-Diazabicyclo[2.2.2]oct-2-en (links) und seines Asparagin-Derivates Dbo (rechts), die unter dem Markennamen „Puretime 325“ Farbstoffe vertrieben werden. Die beiden Verbindungen zeigen die Fluoreszenz mit der längsten Lebensdauer (bis zu 1 Mikrosekunde) innerhalb von rein organischen Spezies.

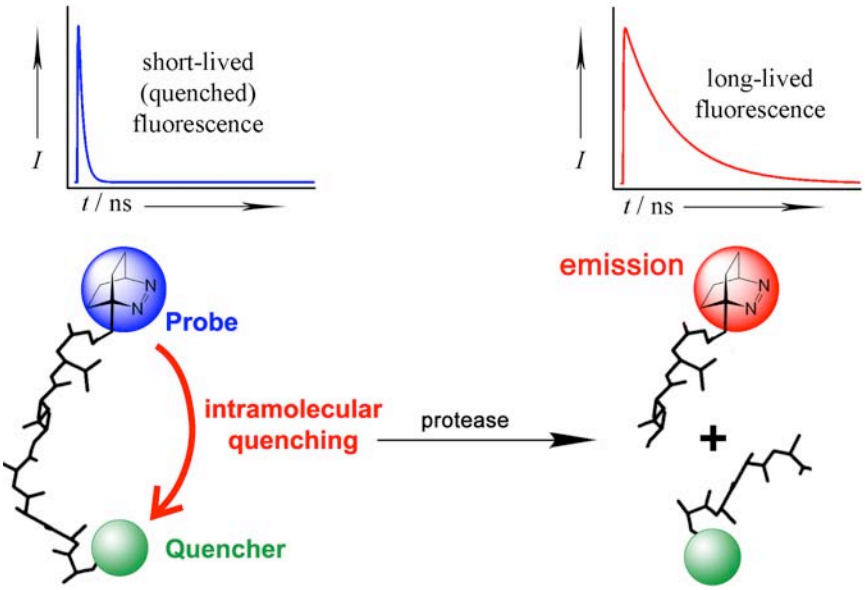


**Abb. 2:** Prinzip eines Nano-TRF-Assays am Beispiel von Proteasen. Im ungespaltenen Substrat (links unten) kommt es durch Anwesenheit des Löschers zu einer effizienten Fluoreszenzlöschung, die zu einer kurzlebigen Fluoreszenz führt (links oben). Durch die enzymatische Spaltung wird der Löscher abgetrennt (rechts unten), so dass keine Fluoreszenzlöschung mehr erfolgt, und somit die langlebige Fluoreszenz einer geeigneten Fluoreszenzsonde (z.B. Dbo, siehe Abb. 1) wiederhergestellt wird (rechts oben). Die langlebige Fluoreszenz liefert ein starkes Nano-TRF-Signal. Gemäß Literatur 6.

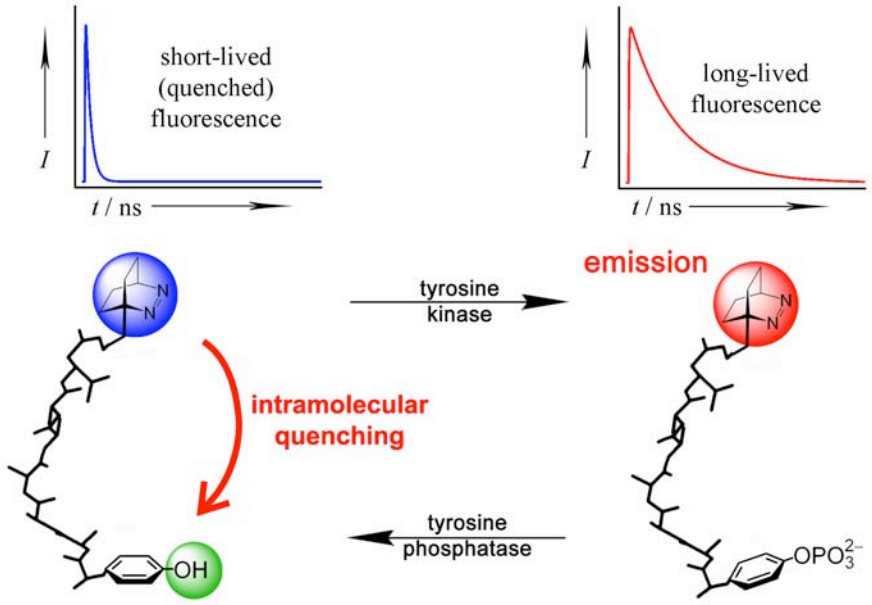


**Abb. 3:** Prinzip eines Nano-TRF-Assays am Beispiel von Tyrosin-Kinasen und Phosphatasen. Im unphosphorylierten Substrat (links unten) kommt es durch Anwesenheit des Löschers Tyrosin zu einer effizienten Fluoreszenzlöschung, die zu einer kurzlebigen Fluoreszenz führt (links oben). Durch die enzymatische Phosphorylierung wird der Löscher deaktiviert (rechts unten), so dass keine Fluoreszenzlöchung mehr erfolgt, und somit die langlebige Fluoreszenz einer geeigneten Fluoreszenzsonde (z.B. Dbo, siehe Abb. 1) wiederhergestellt wird (rechts oben). Die langlebige Fluoreszenz liefert ein starkes Nano-TRF-Signal. Im Falle der umgekehrten Reaktion (Phosphatasen) wird eine Abschwächung des Nano-TRF-Signals im Verlauf der enzymatischen Reaktion beobachtet. In Anlehnung an Literatur 8, Copyright 2007, mit Erlaubnis der American Chemical Society.

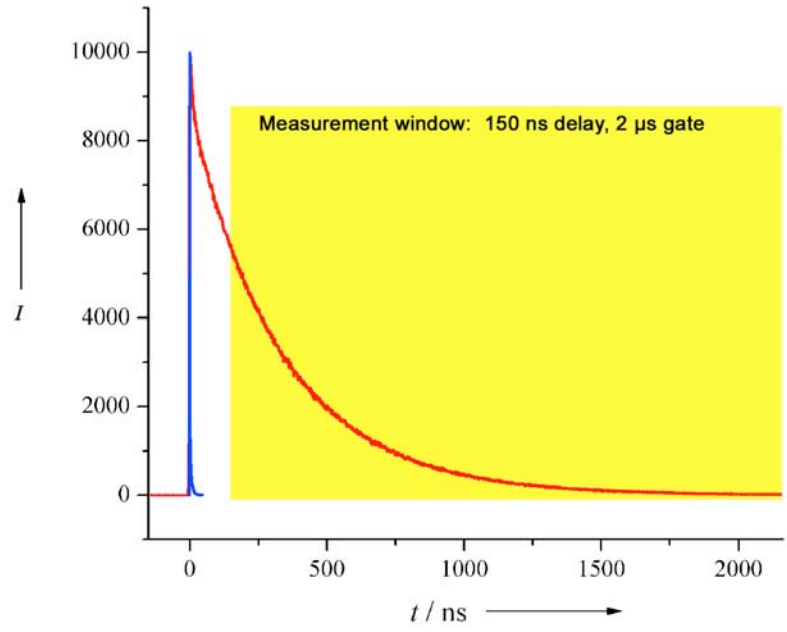


**Abb. 4:** Experimentelle Fluoreszenzzerfallskurven von H-Dbo-Gly-Trp-OH vor (Lebensdauer 4 ns, blau) und nach (Lebensdauer 340 ns, rot) enzymatischer Verdauung. Zu beachten ist die hochselektive Fluoreszenzdetektion der langlebigen Fluoreszenz bei Nano-TRF-Detektion (gelbes Zeitfenster). Gemäß Literatur 6.

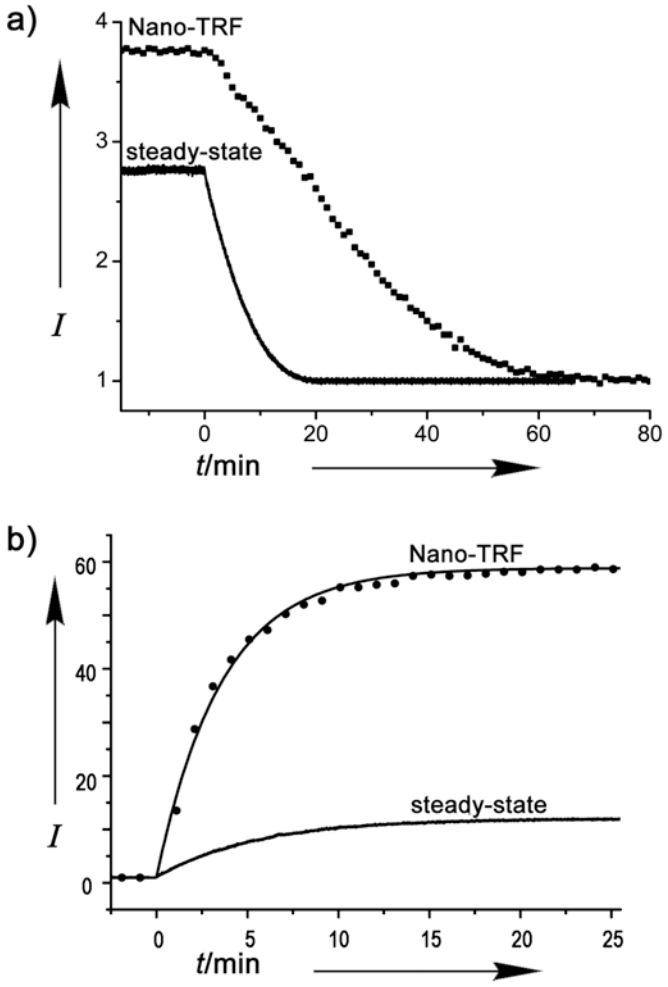


**Abb. 5:** Vergleich der Substrat/Produkt-Differenzierung von stationärer und Nano-TRF-Fluoreszenzdetektion. a) Optimierung eines Phosphatase-Assays (Dephosphorylierung von H-Dbo-EEEEpY-OH durch saure Phosphatase) mittels Nano-TRF-Detektion (normiert auf eine Endintensität von 1); in Anlehnung an Literatur 8, Copyright 2007, mit Erlaubnis der American Chemical Society. b) Optimierung eines Protease-Assays (Spaltung von H-WTLTGKX-$NH_2$ durch Trypsin) mittels Nano-TRF-Detektion (normiert auf eine Ausgangsintensität von 1); in Anlehnung an Literatur 7, Copyright 2007, mit Erlaubnis von Elsevier.

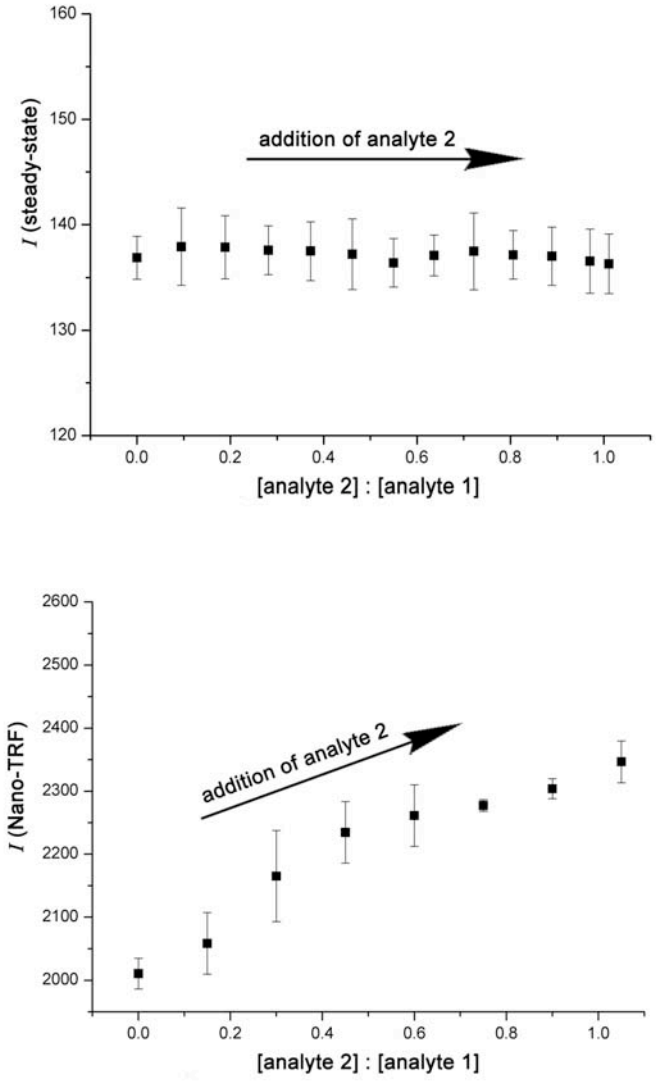


**Abb. 6**: Fluoreszenzmessungen von Mischungen von 7-Amino-4-methylcoumarin (AMC) und DBO (0 entspricht einer reinen AMC-Lösung, 1 entspricht einer äquimolaren DBO/AMC-Lösung). Die Abb. oben zeigt die stationäre Fluoreszenzintensität, die Abb. unten das Nano-TRF-Signal, gemessen mit dem in Abbidung 4 gezeigten Zeitfenster.

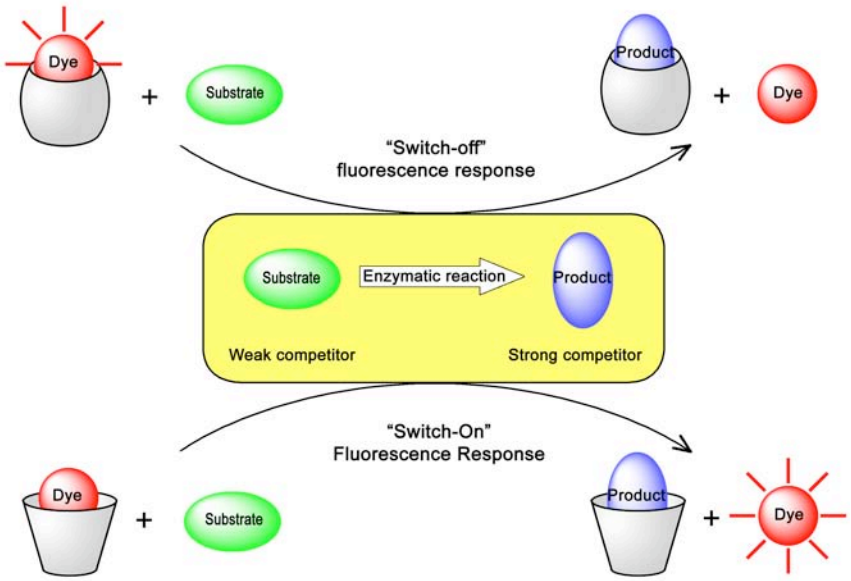


**Abb. 7**: Detektionsprinzip von Tandem-Asasays. Das im Verlauf der enzymatischen Reaktion gebildete Produkt verdrängt den Fluorezenzfarbstoff aus dem Makrozyklus, wodurch es zu einer Erniedrigung („switch-off“, oben) oder einer Erhöhung („switch-on“, unten) der Fluorezenz kommt. Gemäß Literatur 19.

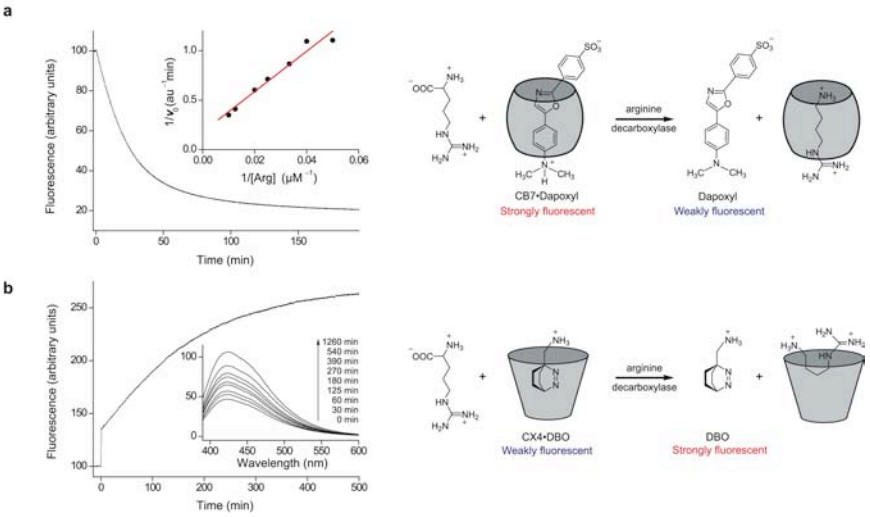


**Abb. 8**: Kontinuierlicher Fluoreszenz-Enzymassay nach dem Tadem-Assay-Prinzip für Arginin-Decarboxylase (a) mit dem CB7/Dapoxyl-Reporterpaar (8 Mikrogramm/ml Enzym, 100 mikromolar Arginin, 2.5 mikromolar Dapoxyl, 10 mikromolar CB7, Anregungswellenlänge 336 nm, Emissionswellenlänge 380 nm) und (b) mit dem CX4/DBO-Reporterpaar (40 Mikrogramm/ml Enzyme, 500 mikromolar Arginin, 100 mikromolar DBO, 200 mikromolar CX4, Anregungswellenlänge 365 nm. Emissionswellenlänge 450 nm). Der eingelegte Graph in (a) zeigt einen Lineweaver-Burk-Plot. Der eingelegte Graph in (b) zeigt die Veränderung der Fluoreszenzspektren im Verlauf der enzymatischen Reaktion. Gemäß Literatur 19.

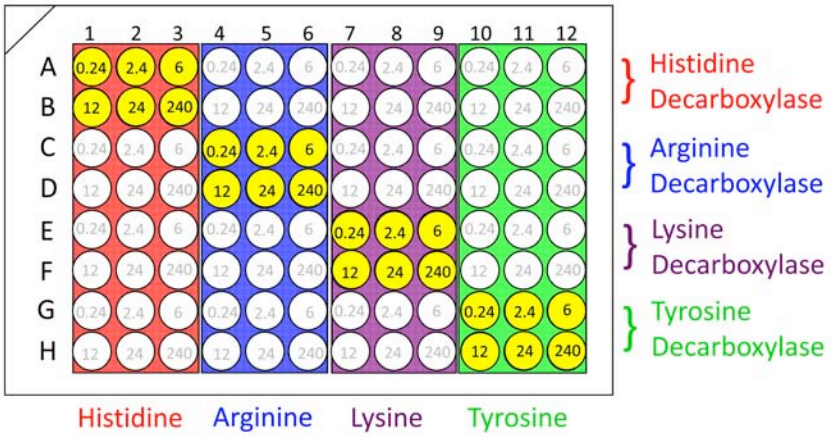


**Abb. 9:** Multiparameterassay von verschiedenen Aminosäuren im Mikrotiterplattenformat. Alle Wells enthalten dasselbe Reporterpaar (Cucurbit[7]uril und Dapoxyl) und verschiedene Aminosäuren mit der jeweiligen Decarboxylase. Gelb markiert sind die positiven Auslesewerte bei den verschiedenen mikromolaren Konzentrationen (angegebene Zahlenwerte).

# APPENDIX 4

M. Florea and W. M. Nau, "Implementation of Anion-Receptor Macrocycles in Supramolecular Tandem Assays for Enzymes Involving Nucleotides as Substrates, Products, and Cofactors", *Organic & Biomolecular Chemistry*, **2010**, *8*, 1033-1039. Reproduced by permission of the Royal Society of Chemistry. Publisher's version may be found at:
http://pubs.rsc.org/en/content/articlelanding/2010/ob/b925192h

# Implementation of anion-receptor macrocycles in supramolecular tandem assays for enzymes involving nucleotides as substrates, products, and cofactors†

**Mara Florea and Werner M. Nau***

***Received 28th September 2009, Accepted 5th December 2009***
***First published as an Advance Article on the web 7th January 2010***
**DOI: 10.1039/b925192h**

A supramolecular tandem assay for direct continuous monitoring of nucleotide triphosphate-dependent enzymes such as potato apyrase is described. The underlying principle of the assay relies on the use of anion-receptor macrocycles in combination with fluorescent dyes as reporter pairs. A combinatorial approach was used to identify two complementary reporter pairs, *i.e.* an amino-γ-cyclodextrin with 2-anilinonaphtalene-6-sulfonate (ANS) as dye (fluorescence enhancement factor of 17 upon complexation) and a polycationic cyclophane with 8-hydroxy-1,3,6-pyrene trisulfonate (HPTS) as dye (fluorescence decrease by a factor of more than 2000), which allow the kinetic monitoring of potato apyrase activity at different ATP concentration ranges (μM and mM) with different types of photophysical responses (switch-ON and switch-OFF). Competitive fluorescence titrations revealed a differential binding of ATP (strongest competitor) *versus* ADP and AMP, which constitutes the prerequisite for monitoring enzymatic conversions (dephosphorylation or phosphorylation) involving nucleotides. The assay was tested for different enzyme and substrate concentrations and exploited for the screening of activating additives, namely divalent transition metal ions ($Ni^{2+}$, $Mg^{2+}$, $Mn^{2+}$, and $Ca^{2+}$). The transferability of the assay could be demonstrated by monitoring the dephosphorylation of other nucleotide triphosphates (GTP, TTP, and CTP).

## Introduction

Numerous supramolecular receptors for nucleotides have already been introduced with the general aim to achieve a high selectivity and the ultimate goal to construct highly specific biological chemosensors.[1–19] But applications to actual biological systems have remained scarce. With the tandem assay strategy, we have recently developed a supramolecular application, which reduces the key requirement for a receptor from the specificity for a single analyte to the mere necessity to show a differential binding between two analytes: the substrate and the product of an enzymatic reaction.[20–23] This affords convenient label-free enzyme assays, in which the enzymatic conversion is monitored through a reporter pair composed of a fluorescent dye and a macrocycle, which responds to the concentration changes affected by the enzymatic reaction. This involves, drawing inspiration from the indicator-displacement principle,[24,25] either a continuous displacement of the dye from the macrocycle by the higher affinity product (product-selective assay), or its uptake into the host, facilitated by the depletion of the competing substrate (substrate-selective assay).

At least two designed chemosensors with covalently incorporated chromophores have been previously demonstrated to be principally suitable for following enzymatic reactions in a non-continuous manner.[1,2] But in order to monitor an enzymatic reaction, it is in fact not required to employ a highly specific receptor with a covalently attached fluorophore, because the specificity of the reaction is determined through the enzyme itself. This principal insight is similar to that reached by Matile and coworkers, who have followed enzymatic reactions by using multifunctional synthetic pores embedded in vesicles,[26,27] with the difference that supramolecular tandem assays allow direct continuous monitoring in homogeneous solution.

While our previous examples of tandem assays were limited to cationic analytes in combination with cation-receptors,[20–23] the investigation of anionic metabolites such as nucleotides, and particularly ATP, requires the use of macrocycles with anion-receptor properties,[28] which we have now investigated.

## Results and discussion

We have first screened a combinatorial library consisting of a set of 10 water-soluble anion receptors, which in part were already known to bind to nucleotides,[11–15] in combination with a set of 9 anionic and neutral water-soluble fluorescent dyes (Charts 1 and 2). To develop practical tandem assays, our aim was to obtain *i*) a large fluorescence response upon dye complexation, *ii*) a strong macrocycle-dye binding, and *iii*) a large differentiation in binding between nucleotide tri- and monophosphates. Our best (and new) reporter pair consists of the amino-γ-cyclodextrin **1** (the amino groups of which are positively charged near neutral pH) in combination with 2-anilinonaphtalene-6-sulfonate (ANS) as dye. A complementary reporter pair, originally suggested for the selective recognition of GTP,[10,11] consists of the cyclophane **2** with 8-hydroxy-1,3,6-pyrene trisulfonate (HPTS) as dye.

*School of Engineering and Science, Jacobs University Bremen, Campus Ring 1, D-28759, Bremen, Germany. E-mail: w.nau@jacobs-university.de; Fax: +494212003229; Tel: +494212003233*

† Electronic supplementary information (ESI) available: Additional experimental results. See DOI: 10.1039/b925192h

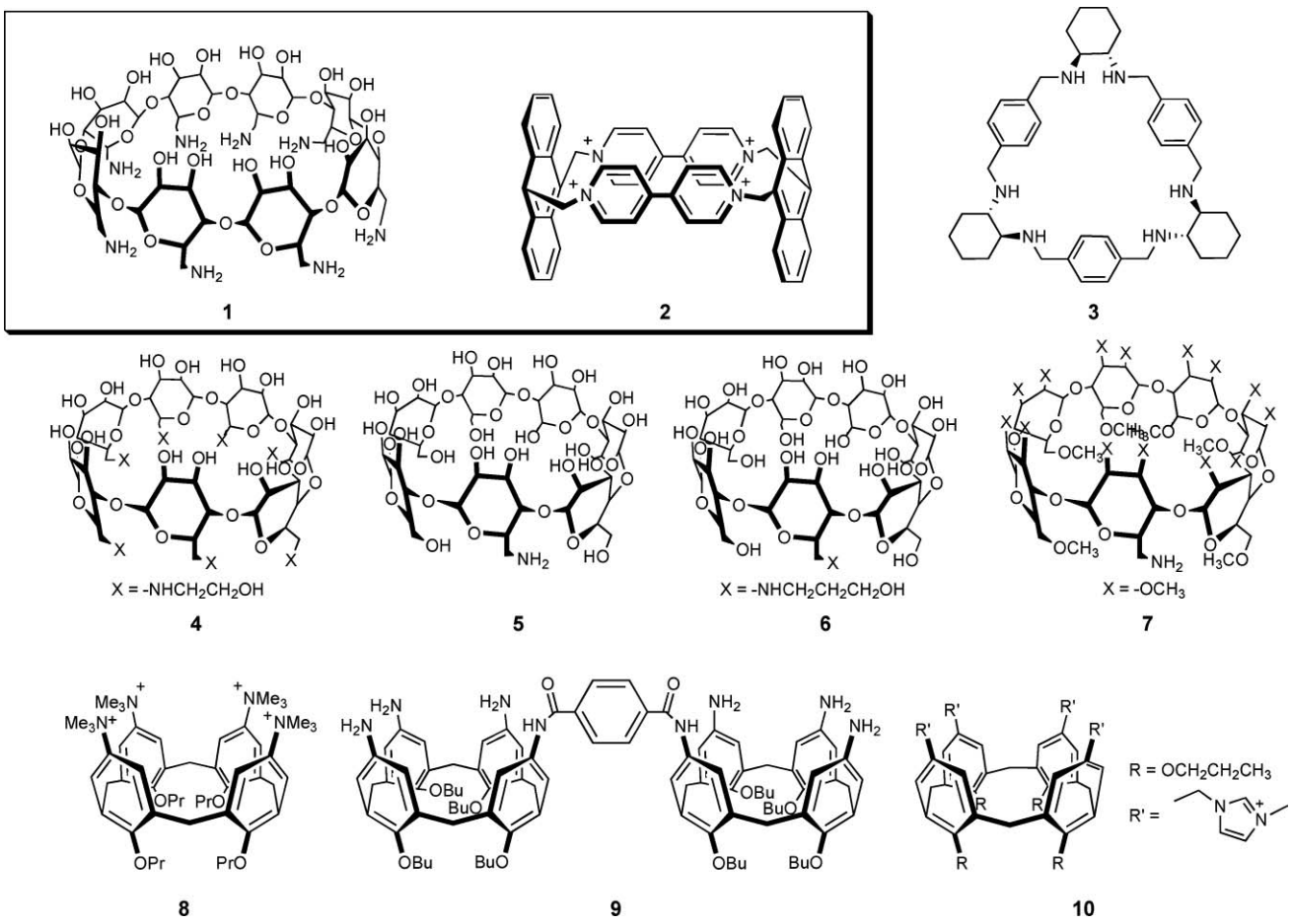


**Chart 1** Investigated library of macrocycles with anion-receptor properties.

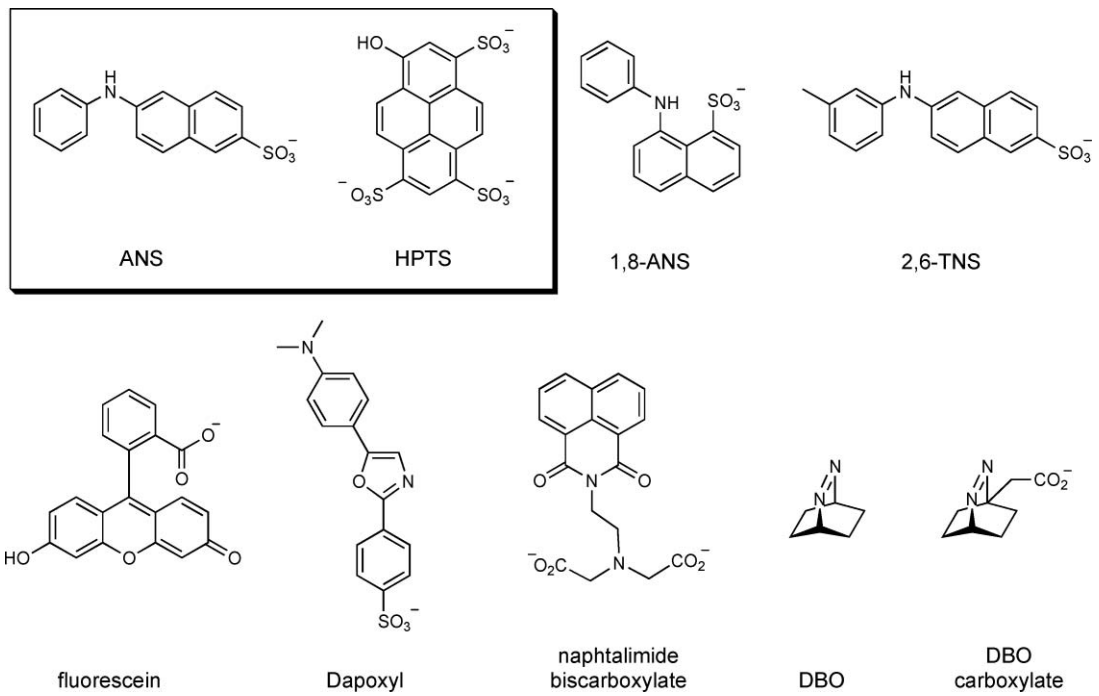


**Chart 2** Investigated library of anionic and neutral fluorescent dyes studied in combination with the macrocycles in Chart 1.

 

**Table 1** Binding constants of **1** and **2** with the substrate as well as intermediary and final enzymatic products

| Guest | $K/10^6$ $M^{-1}$ (**1**)[a] | $K/10^3$ $M^{-1}$ (**2**)[b] |
|---|---|---|
| ATP | 100 ± 60 | 4.5 ± 1.0 |
| ADP | 2.8 ± 0.8 | < 1 |
| AMP | 0.011 ± 0.003 | < 1 |
| Orthophosphate | 0.05 ± 0.01 | < 0.1 |

[a] Determined by competitive fluorescence titration using **1**/ANS in 50 mM NaOAc buffer, pH 5.5, *cf.* Fig. 2a. The binding constant of **1**/ANS is $(1.7 \pm 0.1) \times 10^4$ $M^{-1}$ *cf.* Fig. 1a. [b] Determined by competitive fluorescence titration using **2**/HPTS in 10 mM phosphate buffer, pH 7.4. The binding constant of **2**/HPTS was determined as $(7 \pm 3) \times 10^6$ $M^{-1}$, *cf.* Fig. 1b.

Successive addition of macrocycle to dye solutions resulted in a strong fluorescence enhancement by a factor of 17 ($\lambda_{exc}$ = 318 nm, $\lambda_{obs}$ = 462 nm, for **1**/ANS) or quenching by a factor of more than 2000 ($\lambda_{exc}$ = 425 nm, $\lambda_{obs}$ = 512 nm, for **2**/HPTS), from which dye binding constants of $1.7 \times 10^4$ and $7 \times 10^6$ $M^{-1}$ were determined (Fig. 1). Addition of different nucleotides reversed these fluorescence changes due to competitive binding (Fig. 2 and Fig. 3). Both systems showed a charge-dependent differentiation of nucleotides (*e.g.*, between ATP, ADP, AMP, and orthophosphate),[10] which is the sufficient and necessary criterion for our presently explored application (*cf*. binding constants in Table 1). Specifically, we implemented the **1**/ANS and **2**/HPTS

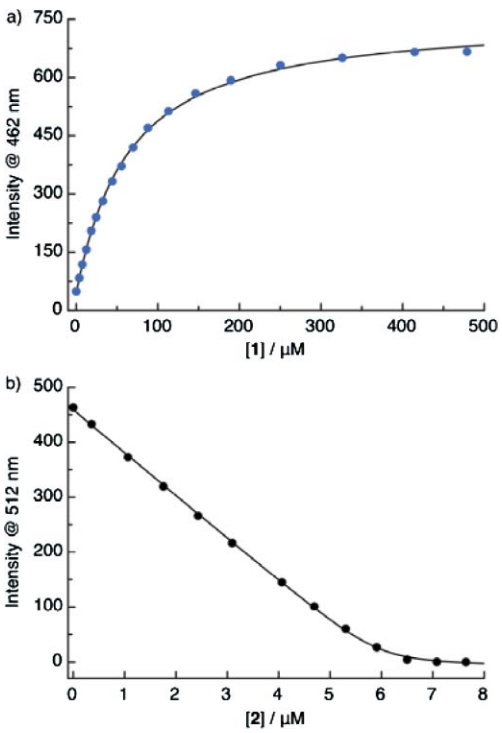


**Fig. 1** Plots of the fluorescence intensity of a) 10 μM ANS with increasing concentrations of **1** in 50 mM NaOAc buffer, pH 5.5 ($\lambda_{exc}$ = 318 nm, $\lambda_{obs}$ = 462 nm) and b) 6.3 μM HPTS with increasing concentrations of **2** in 10 mM phosphate buffer, pH 7.4 ($\lambda_{exc}$ = 425 nm, $\lambda_{obs}$ = 512 nm). The nonlinear fittings were made by assuming the formation of a 1 : 1 complexation model. It should be noted that the fluorescence of HPTS increased again slightly at higher macrocycle (**2**) concentrations, suggesting the formation of higher-order complexes. An equimolar mixture of **2** and HPTS was consequently employed as reporter pair.

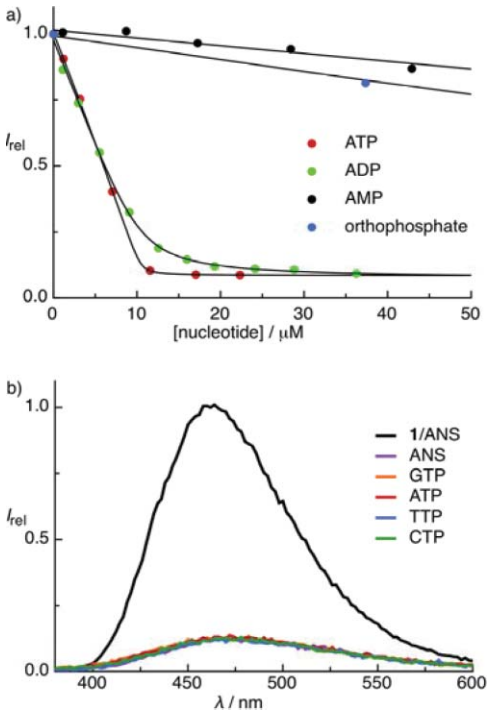


**Fig. 2** Changes in fluorescence intensity and spectra of the **1**/ANS reporter pair (10 μM **1** and 25 μM ANS, $\lambda_{exc}$ = 318 nm) upon displacement by a) varying concentrations of ATP, ADP, AMP, and orthophosphate ($\lambda_{obs}$ = 462 nm) and b) different nucleotide triphosphates (16 μM), in NaOAc buffer, pH 5.5.

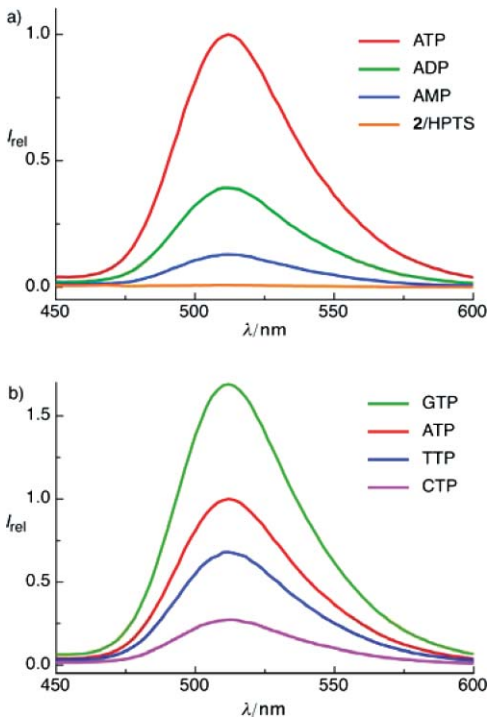


**Fig. 3** Changes in fluorescence spectra of the **2**/HPTS reporter pair (both 6.3 μM) upon addition of a) ATP, ADP, and AMP (each 4 mM) and b) different nucleotide triphosphates (4 mM), in succinate buffer, pH 6.5; $\lambda_{exc}$ = 403 nm.

reporter pairs into supramolecular tandem assays for potato apyrase, an ectoenzyme of the class of ATP-diphosphohydrolases (E.C. 3.6.1.5) which convert ATP to AMP through a stepwise dephosphorylation with ADP as an intermediate.[29–32] Apyrases regulate extracellular nucleotide levels (in animal tissues) and the biosynthesis of starch and cell walls (in plants).

The working principle is illustrated in Scheme 1. Our assay is based on the propensity of the highly positively charged hosts **1** and **2** to form self-assembled complexes with negatively charged guest molecules, particularly ANS and HPTS, as well as ATP. The dye ANS is weakly fluorescent in its uncomplexed form, but experiences an efficient fluorescence enhancement upon complexation with **1**, due to its sensitivity towards environmental polarity.[33] In contrast, the dye HPTS is highly fluorescent in its free form, but suffers from a strong fluorescence quenching when complexed with **2**, presumably by charge-transfer-induced quenching.[10]

Behaving as a strong competitor, ATP displaces the dyes from the complexes, which results in a low or high initial fluorescence intensity, respectively (Fig. 2 and Fig. 3). Upon enzymatic dephosphorylation, AMP and orthophosphate are formed as final products, which behave as weak competitors (due to their lower net negative charge) and thereby allow a successive complexation of the fluorescent dyes with the macrocycles. This results in a switch-ON (for **1**/ANS) or switch-OFF (for **2**/HPTS) fluorescence response,[20] which allows a highly sensitive monitoring of the enzymatic activity. Moreover, since the guest-macrocycle exchange equilibria are much faster than the enzymatic reactions, the response of the system to concentration changes is immediate and allows for real-time continuous kinetic monitoring. It is thus possible to follow the ATP depletion as a result of an enzymatic reaction or, conversely, the enzymatic reaction through the depletion of ATP. Conceptually, the resulting tandem assays can be qualified as substrate-selective assays because the substrate binds more strongly than the product.[22]

The two reporter pairs are complementary in the sense that they show μM or mM affinities to the different nucleotides, respectively (Fig. 2 and Fig. 3). This determines the substrate concentration range of the tandem assays, which were run with 25 μM ATP for **1**/ANS and 2.3 mM for **2**/HPTS. Addition of ATP to the pre-formed reporter pair partially recovered the fluorescence of the uncomplexed dyes through competitive displacement and an approximately 10-fold fluorescence reduction (for **1**/ANS) or more than 100-fold enhancement (for **2**/HPTS) was observed. Addition of apyrase to a solution containing ATP as substrate along with one of the reporter pairs led to a time-resolved rise (factor of 4 for **1**/ANS) or decay (factor of 12 for **2**/HPTS) of the fluorescence intensity with a plateau being reached within 1–2 h (black traces, Fig. 4). In accordance with Scheme 1, we assigned the time-resolved fluorescence response to the enzymatic conversion, thereby establishing a convenient supramolecular tandem assay for apyrases, and generally, for the conversion of ATP. The occurrence of the enzymatic reaction on the same time scale was independently monitored by $^{31}$P NMR (Fig. S1 in ESI†). The assay could also be conducted with ADP as substrate (see Fig. S2 in ESI†), but for AMP no significant fluorescence change was noticed, as no dephosphorylation is possible (negative control, data not shown).

Enzyme assays are employed in pharmaceutical-industrial high-throughput screening. Previously, we have demonstrated the potential of tandem assays in the screening of inhibitors,[22] and the apyrase assay offered the complementary opportunity to screen for activators, namely, divalent metal ions ($Ni^{2+}$, $Mg^{2+}$, $Mn^{2+}$, and $Ca^{2+}$). In all cases, we observed rate enhancements between a factor of 1.3 to 17, with $Ca^{2+}$ and $Mn^{2+}$ being the most potent activators of potato apyrase (Fig. 4),[34] consistent with literature findings obtained by more laborious and complex multi-step colorimetric and radioisotope-based assays.[30–32] Consequently, all enzymatic reactions were subsequently performed with $Mn^{2+}$ (for **1**/ANS) or $Ca^{2+}$ (for **2**/HPTS), which reduced the assay times typically to 10–20 min.

One could argue that the **1**/ANS pair is 2 orders of magnitude more "sensitive" since it allows the conversion of μM instead of mM amounts of ATP to be followed. However, one has to recall that the substrate (or cofactor) concentration range is not the limiting factor for an assay, as it could be for a sensor. Rather, the substrate concentration can be adjusted at will to the desired time and the specific activity of the enzyme, such that even assays with mM substrate concentrations are common.[26] For example, the reported $K_M$ values of potato apyrase ranges

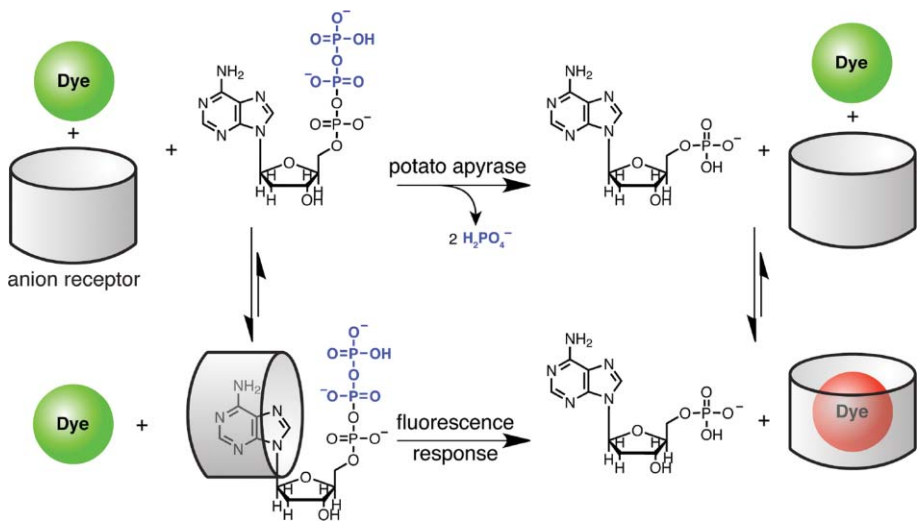


**Scheme 1** Working principle of a supramolecular tandem assay for monitoring dephosphorylation of ATP.

 

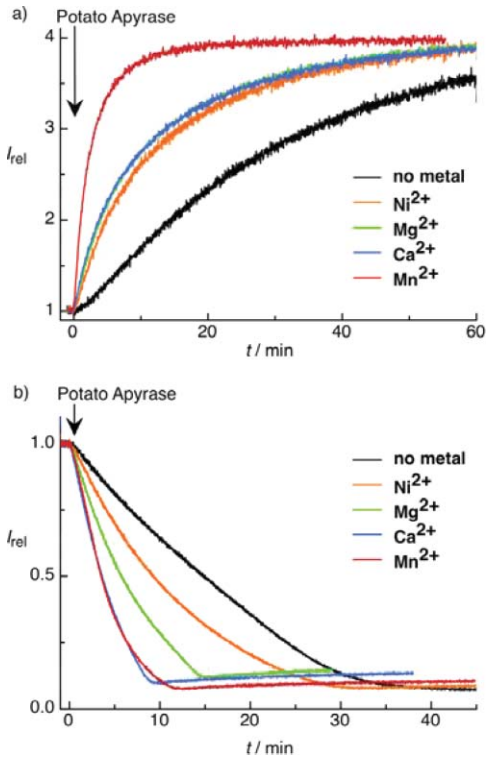


**Fig. 4** Evolution of normalized fluorescence intensity monitoring potato apyrase activity with and without activating metal ions (1.7 mM). Assays were initiated by addition of a) 25 μg ml$^{-1}$ enzyme to ATP (25 μM) with the **1**/ANS reporter pair (25 μM both) and b) 100 μg ml$^{-1}$ enzyme to ATP (2.3 mM) with the **2**/HPTS reporter pair (6.3 μM both).

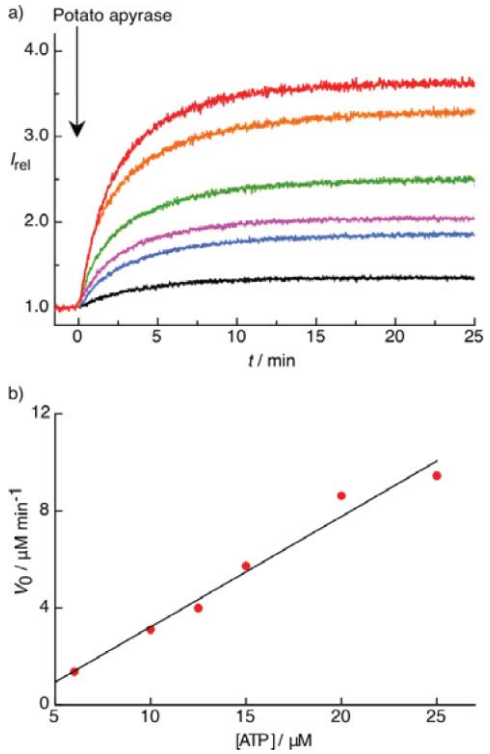


**Fig. 5** a) Evolution of normalized fluorescence intensity monitoring potato apyrase activity (25 μg ml$^{-1}$) at different substrate (ATP) concentrations with the **1**/ANS reporter pair (both 25 μM, in NaOAc buffer, pH 5.5, with 1.8 mM $Mn^{2+}$, $\lambda_{exc}$ = 318 nm, $\lambda_{obs}$ = 462 nm). ATP concentrations (in μM) are, from bottom to top trace: 6, 10, 12.5, 15, 20, 25. b) Plot of the initial rates, $v_0$, *versus* substrate concentration and linear correlation line. The initial rates were obtained by linear fits of the normalized intensities (assuming a conversion linear with the fluorescence intensity and full conversion at the plateau region).

from 24 to 200 μM,[31,32] suggesting that the **1**/ANS and **2**/HPTS reporter pairs operate either below or above the $K_M$ value. For the **1**/ANS reporter pair, the initial rates do in fact increase linearly with the substrate concentration (Fig. 5). A more detailed analysis of the enzyme kinetics is, however, not possible because the complexation of the substrate by the host lowers the effective substrate concentration, which presents a peculiarity of substrate-selective assays.[22] This was possible, however, for the **2**/HPTS reporter pair, for which a large excess of substrate was used and where the enzyme kinetics was expected to be zero-order with respect to the substrate. Indeed, determination of the initial reaction rates from the fluorescence decays at a fixed enzyme concentration (50 μg ml$^{-1}$) and 4 varying substrate concentrations (0.5–3.2 mM) afforded the same rate, within 10% error (0.17 μmol min$^{-1}$, expected from reported commercial activity: 0.19 μmol min$^{-1}$). This rate was assigned to the $v_{max}$ value when working far above the $K_M$ value. Finally, as shown for both reporter pairs (Fig. S3 in ESI†), the initial rates of ATP dephosphorylation increased linearly with the enzyme concentration.

Important to note, all nucleotide triphosphates caused a fluorescence decrease for the **1**/ANS reporter pair and a fluorescence enhancement of the **2**/HPTS reporter pair, by competitive displacement (see Fig. 2b and Fig. 3b). This shows that hosts **1** and **2** are actually unselective or at best moderately selective anion receptors, at least in the investigated concentration range. In tandem assays, such a "sloppy" molecular recognition[24,27] presents actually an advantage, because dephosphorylation of both nucleotide di- and triphosphates can be monitored quite generally (for example also GTP, TTP and CTP, Fig. 6), which opens screening possibilities in many directions.

## Conclusions

In conclusion, we have introduced convenient supramolecular tandem assays for monitoring biocatalytic ATP dephosphorylation. The assay principle relies on the addition of an anion-receptor macrocycle and a fluorescent dye setting up a reporter pair. It is the high specificity of the enzyme itself which reduces selectivity considerations in the choice of a receptor to a minimum, bypasses the necessity to utilize designed chemosensors, but instead allows the use of simple, even if moderately selective, macrocycles. We demonstrated applications in the screening of activators and a broader applicability for other nucleotides and complementary reporter pairs. Our dephosphorylation assays should be transferable to other nucleotide-dependent enzymes.

This work was supported by the Deutsche Forschungsgemeinschaft (DFG grant NA-686/5-1), the Fonds der Chemischen Industrie, and the BIG Bremer Investitions-Gesellschaft mbH (Ökologiefonds des Landes Bremen). The authors also thank Dr A. Hennig for helpful discussions.

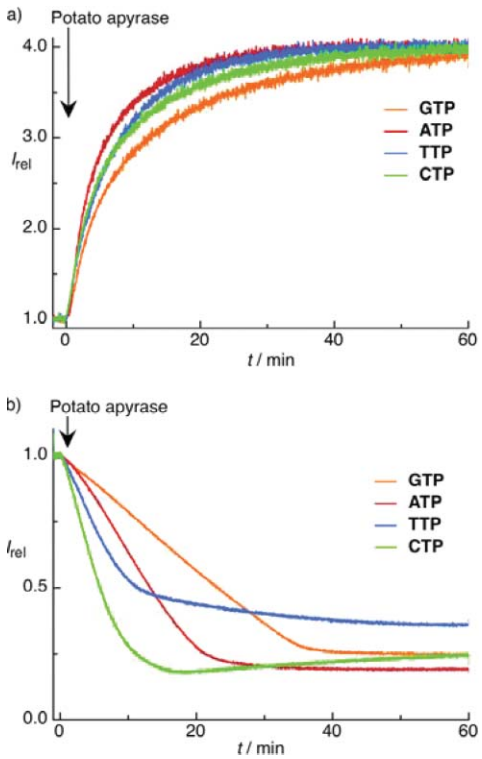


**Fig. 6** Evolution of normalized fluorescence intensity monitoring dephosphorylation of various nucleotide triphosphates. Assays were initiated by addition of a) 12.5 μg ml$^{-1}$ potato apyrase in the presence of **1**/ANS (25 μM both) to nucleotides (25 μM), and b) 100 μg ml$^{-1}$ potato apyrase in the presence of **2**/HPTS (6.3 μM both) to nucleotides (4 mM).

## Experimental

### Materials

The macrocycles and dyes employed in the initial screening are shown in Charts 1 and 2. 2-Anilinonaphtalene-6-sulfonic acid (ANS), and Dapoxyl were obtained from Molecular Probes. 8-Anilinonaphtalene-1-sulfonic acid (1,8-ANS), 8-hydroxy-1,3,6-pyrene trisulfonic acid (HPTS), 6-(*p*-toluidino)-2-naphtalene-sulfonic acid (2,6-TNS), fluorescein sodium, GTP, and ADP were purchased from Fluka. The naphtalimide biscarboxylate, 2,3-diazabicyclo[2.2.2]oct-2-ene (DBO), and DBO carboxylate were synthesized according to the literature.[35–37] ATP, AMP, CTP, TTP, and apyrase (grade I, from potato, 7.7 U/mg) were from Sigma-Aldrich. The cyclodextrin samples octakis(6-amino-6-deoxy)-γ-cyclodextrin (**1**), heptakis(6-deoxy-6-*N*-(2-hydroxy)ethylamino)-β-cyclodextrin (**4**), 6-monoamino-6-monodeoxy-β-cyclodextrin (**5**), 6-monodeoxy-6-mono(3-hydroxy)propylamino-β-cyclodextrin (**6**), heptakis(2,3-di-*O*-methyl)-hexakis(6-*O*-methyl)-6-monodeoxy-6-monoamino-β-cyclodextrin (**7**) were obtained as hydrochloride salts from CycloLab, Hungary. The synthesis of the cyclophane (**2**) was performed according to the literature with minor modifications.[11] Trianglamine (**3**) was kindly supplied by Prof. N. Kuhnert, Jacobs University Bremen, Germany. The bis-calixarene (**9**) was synthesized according to the literature,[15] whereas calixarenes (**8**) and (**10**) were kindly supplied by Prof. J. Schatz, Universität Erlangen-Nürnberg, Germany.

### Instrumentation

Fluorescence spectra, intensities, and time courses were recorded on a Varian Eclipse fluorometer at ambient temperature (for the titrations) or at 25.0 ± 0.1 °C (using an external Peltier thermostat, only for the enzyme assays). UV measurements were performed with a Varian Cary 4000 UV-Vis spectrophotometer. The dephosphorylation of nucleotides was additionally monitored by $^{31}$P NMR using a Jeol JNM-ECX 400 spectrometer.

### Fluorescence titrations

All fluorescence titrations were performed in 1.4 mL quartz cuvettes (Starna, Typ 29-F/Q/10 mm). The titration of host with fluorophore was performed by keeping the dye concentration constant. Accordingly, the titrant contained the same concentration of dye, and a much higher host concentration (approximately 10–100 times higher). The competitive titrations using different nucleotides were carried out similarly to the host-guest titrations, ensuring a constant host and dye concentration during the titration. Therefore, the titrant contained, besides a high concentration of competitor, host and dye in concentrations equal to those in the cuvette solution. All titrations were performed in 50 mM sodium acetate buffer, pH 5.5 when the **1**/ANS reporter pair was employed, and in 10 mM sodium phosphate buffer, pH 7.4, or 10 mM sodium succinate buffer, pH 6.5, when using the **2**/HPTS reporter pair.

### Supramolecular tandem assays

Stock solutions of substrate (nucleotides), host (**1** or **2**), fluorescent dye (ANS or HPTS), and enzyme were required for performing the enzyme assays. The stock solutions were prepared in 50 mM sodium acetate buffer, pH 5.5, with 1.6–1.8 mM $MnCl_2$ (when using **1**/ANS reporter pair) and in 10 mM sodium succinate buffer, pH 6.5, with 1.6–1.8 mM $CaCl_2$ (when **2**/HPTS was employed). Careful control of the pH was required to obtain reproducible fluorescence intensities. The required volumes of all stock solutions were calculated to afford the final concentrations in 1 mL total assay volume. All assays were conducted using equimolar mixtures of host and fluorescent dye (25 μM for **1**/ANS and 6.3 μM for **2**/HPTS). The volumes of nucleotide stock solutions were calculated to obtain the respective concentrations. The enzymatic reactions were initiated by adding an aliquot from a stock solution of 1 mg mL$^{-1}$ enzyme.

## Notes and references

1 D. H. Vance and A. W. Czarnik, *J. Am. Chem. Soc.*, 1994, **116**, 9397–9398.
2 J. Wongkongkatep, Y. Miyahara, A. Ojida and I. Hamachi, *Angew. Chem., Int. Ed.*, 2006, **45**, 665–668.
3 J. Y. Kwon, N. J. Singh, H. N. Kim, S. K. Kim, K. S. Kim and J. Yoon, *J. Am. Chem. Soc.*, 2004, **126**, 8892–8893.
4 M. T. Albelda, M. A. Bernardo, E. Garcia-España, M. L. Godino-Salido, S. V. Luis, M. João Melo, F. Pina and C. Soriano, *J. Chem. Soc., Perkin Trans. 2*, 1999, 2545–2549.
5 S. E. Schneider, S. N. O'Neil and E. V. Anslyn, *J. Am. Chem. Soc.*, 2000, **122**, 542–543.
6 C. Bazzicalupi, S. Biagini, A. Bencini, E. Faggi, C. Giorgi, I. Matera and B. Valtancoli, *Chem. Commun.*, 2006, 4087–4089.
7 J. L. Sessler, H. Furuta and V. Král, *Supramol. Chem.*, 1993, **1**, 209–220.

 

8 V. Král, A. Andrievsky and J. L. Sessler, *J. Chem. Soc., Chem. Commun.*, 1995, 2349–2351.
9 N. Marcotte and A. Taglietti, *Supramol. Chem.*, 2003, **15**, 617–625.
10 P. P. Neelakandan, M. Hariharan and D. Ramaiah, *J. Am. Chem. Soc.*, 2006, **128**, 11334–11335.
11 P. P. Neelakandan, M. Hariharan and D. Ramaiah, *Org. Lett.*, 2005, **7**, 5765–5768.
12 A. V. Eliseev and H.-J. Schneider, *J. Am. Chem. Soc.*, 1994, **116**, 6081–6088.
13 Y. H. Shi and H.-J. Schneider, *J. Chem. Soc., Perkin Trans. 2*, 1999, 1797–1804.
14 P. Schwinté, R. Darcy and F. O'Keeffe, *J. Chem. Soc., Perkin Trans. 2*, 1998, 805–808.
15 R. Zadmard and T. Schrader, *Angew. Chem., Int. Ed.*, 2006, **45**, 2703–2706.
16 M. Sirish and H.-J. Schneider, *J. Am. Chem. Soc.*, 2000, **122**, 5881–5882.
17 R. Moreno-Corral and K. O. Lara, *Supramol. Chem.*, 2008, **20**, 427–435.
18 A.-S. Delépine, R. Tripier, N. L. Bris, H. Bernard, A. Honraedt and H. Handel, *Inorg. Chim. Acta*, 2009, **362**, 3829–3834.
19 A.-S. Delépine, R. Tripier and H. Handel, *Org. Biomol. Chem.*, 2008, **6**, 1743–1750.
20 A. Hennig, H. Bakirci and W. M. Nau, *Nat. Methods*, 2007, **4**, 629–632.
21 D. M. Bailey, A. Hennig, V. D. Uzunova and W. M. Nau, *Chem.–Eur. J.*, 2008, **14**, 6069–6077.
22 W. M. Nau, G. Ghale, A. Hennig and D. M. Bailey, *J. Am. Chem. Soc.*, 2009, **131**, 11558–11570.
23 A. Praetorius, D. M. Bailey, T. Schwarzlose and W. M. Nau, *Org. Lett.*, 2008, **10**, 4089–4092.
24 S. L. Wiskur, H. Ait-Haddou, J. J. Lavigne and E. V. Anslyn, *Acc. Chem. Res.*, 2001, **34**, 963–972.
25 J.-P. Goddard and J.-L. Reymond, *Curr. Opin. Biotechnol.*, 2004, **15**, 314–322.
26 G. Das, P. Talukdar and S. Matile, *Science*, 2002, **298**, 1600–1602.
27 G. Das and S. Matile, *Chem.–Eur. J.*, 2006, **12**, 2936–2944.
28 R. Martínez-Máñez and F. Sancenón, *Chem. Rev.*, 2003, **103**, 4419–4476.
29 J. Molnar and L. Lorand, *Arch. Biochem. Biophys.*, 1961, **93**, 353–363.
30 P. A. Lanzetta, L. J. Alvarez, P. S. Reinach and O. A. Candia, *Anal. Biochem.*, 1979, **100**, 95–97.
31 A. Traverso-Cori, H. Chaimovich and O. Cori, *Arch. Biochem. Biophys.*, 1965, **109**, 173–184.
32 M. A. Valenzuela, A. M. Kettlun, M. Mancilla, V. Calvo, N. Fanta and A. Traverso-Cori, *Phytochemistry*, 1988, **27**, 1981–1985.
33 B. D. Wagner and S. J. Fitzpatrick, *J. Inclusion Phenom. Macrocyclic Chem.*, 2000, **38**, 467–478.
34 The fact that $Ca^{2+}$ is less activating than $Mn^{2+}$ at low substrate concentration (for **1**/ANS), but becomes equally effective at high substrate concentration (for **2**/HPTS), is presumably related to different $K_M$, but comparable $v_{max}$ values of the respective metalloenzyme complexes.
35 A. L. Koner, J. Schatz, W. M. Nau and U. Pischel, *J. Org. Chem.*, 2007, **72**, 3889–3895.
36 R. Askani, *Chem. Ber.*, 1965, **98**, 2551–2555.
37 A. Hennig, T. Schwarzlose and W. M. Nau, *ARKIVOC*, 2007, **8**, 341–357.

# APPENDIX 5

W. M. Nau, M. Florea, K. I. Assaf, "Deep Inside Cucurbiturils: Physical Properties and Volumes of their Inner Cavity Determine the Hydrophobic Driving Force for Host-Guest Complexation", *Israel Journal of Chemistry*, **2011**, *51* (5-6), 559-577. doi: 10.1002/ijch.201100044. 

Review

Israel Journal of Chemistry

DOI: 10.1002/ijch.200((full DOI will be filled in by the editorial staff))

# Deep Inside Cucurbiturils: Physical Properties and Volumes of their Inner Cavity Determine the Hydrophobic Driving Force for Host-Guest Complexation

Werner M. Nau,*[a] Mara Florea,[a] and Khaleel I. Assaf [a]

*Dedication in memoriam of the Geheime Regierungsrat Professor Dr. Robert Behrend on the occasion of his 155th birthday anniversary.*

**Abstract:** Cucurbit[*n*]urils (CB*n*) bind guest molecules through a combination of electrostatic interactions with the carbonyl rims and hydrophobic interactions with the inner cavity. Investigations with solvatochromic probes in CB7 reveal that the polarity of the cavity resembles that of alcohols (e.g., *n*-octanol), while its polarizability ($P$ = 0.12) and apparent refractive index ($n_D$ = 1.10±0.12) are extremely low, close to the gas phase. The calculated molecular quadrupole moments of CBs are extremely large ($\Theta_{zz}$ = –120 to –340 Buckingham). A survey of reported binding constants of neutral guests, as well as hydrophobic residues, which form 1:1 inclusion complexes with CB6, reveals a preferential inclusion of C3-C5 residues in its cavity. The largest guests which show non-negligible binding contain 7 heavy atoms (excluding hydrogen). For CB7, the strongest binding is observed for guests with adamantyl (10 heavy atoms) and ferrocenyl groups (11 heavy atoms), while the largest guests known to be complexed are carborane and the adduct of two pyridine derivatives (12 heavy atoms). The evaluation of different volumes shows that the most meaningful cavity, namely that responsible for binding of hydrophobic residues, is confined by the planes through the oxygen carbonyls. The volume of this inner cavity follows the formula $V/Å^3$ = 68 + 62($n$–5) + 12.5($n$–5)$^2$, affording representative cavity volumes of 68 Å$^3$ for CB5, 142 Å$^3$ for CB6, 242 Å$^3$ for CB7, and 367 Å$^3$ for CB8. The volume of the 2 bond dipole regions is comparably smaller, amounting, for example, to 2 × 35 Å$^3$ for CB6. The analysis of packing coefficients for representative sets of known guests with clearly defined hydrophobic binding motifs reveals average values of 47% for CB5, 58% for CB6, 52% for CB7, and 53% for CB8, which are well in line with the preferred packing ("55% solution", see S. Mecozzi, J. Rebek, *Chem. Eur. J.* **1998**, *4*, 1016-1022) in related supramolecular host-guest assemblies. The driving force for binding of hydrophobic guests and residues by CBs is interpreted in terms of the unimportance of dispersion interactions (owing to the low polarizability of their cavity) and the dominance of classical and nonclassical hydrophobic effects related to the removal of very-high-energy water molecules (2 for CB5, 4 for CB6, 8 for CB7, and 12 for CB8) from the cavity.

**Keywords:** supramolecular chemistry • host-guest systems • macrocycles • cucurbiturils • packing coefficients • solvatochromic probes

## 1. Introduction

Cucurbit[*n*]urils (CB*n*) are highly symmetric, rigid macrocycles with two identical carbonyl-lined portals and a hydrophobic cavity. Written documents reveal that the first CB sample (presumably containing mostly CB6, Figure 1, its structure being unknown by then) was most likely synthesized by Rusche under the supervision of Behrend around the year 1900. The first published study dealing with the characterization of some physical properties of this CB sample is the doctoral thesis of Meyer, handed in at the University of Heidelberg.[1] He had started his PhD thesis at the end of 1901 and finished his thesis at the Technical University of Hannover in 1903, again under the supervision of Behrend. These efforts have led to the joint publication in *Justus Liebigs Annalen der Chemie* in 1905.[2] Meyer has characterized in his thesis already several "addition products" of the CB compound with $KMnO_4$, $HgNO_3$, $K_2Cr_2O_7$, $NaAuCl_4$, as well as several cationic dyes such as methylene blue and fuchsine.

[a] Prof. Dr. Werner M. Nau, Mara Florea, Khaleel I. Assaf
School of Engineering and Science, Jacobs University Bremen, Campus Ring 1, 28759 Bremen, Germany
phone: +49 421 2003233
fax: +49 421 2003229
e-mail: w.nau@jacobs-university.de

Supporting information for this article is available on the WWW under http://dx.doi.org/10.1002/ijch.201xxxxxx.

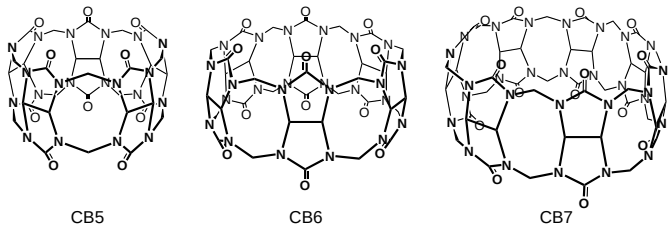


**Figure 1.** Molecular structures of cucurbit[*n*]urils (*n* = 5-7).

Nowadays, initiated by the structural and mechanistic investigations by Mock,[3] we know that these adducts can be mostly described as host-guest complexes between CB6 and cations, either inorganic ones or ammonium-based organic ones. CBs have subsequently become available in different sizes ($n$ = 5-8 and 10) due to the work of Kim,[4,5] Day,[6,7] as well as Isaacs,[8,9] and detailed procedures for their preparation, e.g., for CB7, have been reported.[10-13] CBs are nowadays well recognized in supramolecular chemistry as macrocycles with cation-receptor properties owing to their two carbonyl portals, which establish natural docking sites for positively charged residues. CBs are, on the other hand, also well known to host hydrophobic residues in the confined space between the carbonyl portals, which we refer to, herein, as their *inner cavity* (Figure 2). Although it is well recognized that the extraordinarily high binding affinities of CBs[14] are due to a *combination* of ion-dipole interactions with the portals and hydrophobic forces inside their inner cavity,[4,15-23] the fascinating properties of the latter have remained comparably unexploited and poorly understood, if not neglected. This is unquestionably due to the fact that relatively few host-guest complexes with neutral uncharged guests have been characterized;[24-31] for CB5, CB8, and CB10 binding constants with neutral guests are elusive.[32-35] Interestingly, although CB6 has been found to exhibit a *higher* affinity than the size-complementary $\alpha$-cyclodextrin[36] towards alcohols as neutral guests,[25] the conception that CBs bind preferentially cations, while cyclodextrins have an intrinsic propensity to complex neutral (or anionic) guests persists in the literature.[9,37] The propensity of CBs to complex neutral guests by hydrophobic interactions deserves, therefore, the attention it receives in the present review.

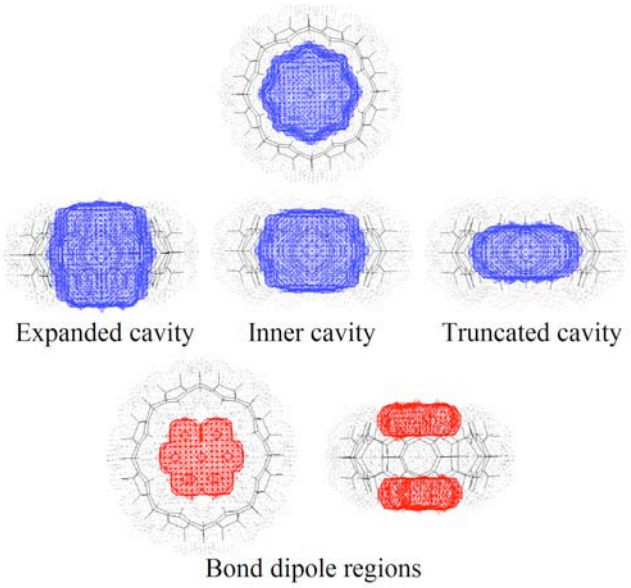


**Figure 2.** Top and side views of the distinct cavities and of the bond dipole regions. See Section 4.1. for method of calculation.

## 2. Physical Properties of the Inner Cavity

The supramolecular encapsulation of guest molecules by molecular containers is well known to provide a partial or complete protection of the guest from the outer environment. Cucurbiturils, together with other prototypal classes of water-soluble macrocycles, namely cyclodextrins and calixarenes, have been routinely described in the literature as supramolecular hosts possessing an internal hydrophobic cavity capable of encapsulating neutral molecules and/or organic residues. While the notion of a hydrophobic cavity has been broadly accepted, we will first raise the question of what exactly renders and defines an environment as *hydrophobic*, specifically the one corresponding to the interior of CBs.


Werner M, Nau was born in Fulda, Germany, in 1968. He started his chemistry studies in 1987 at the University of Würzburg, Germany, obtained his MSc in 1991 at St. Francis Xavier University, Canada, in spectroscopy, and his PhD at the University of Würzburg in 1994 with Waldemar Adam in organic chemistry. Following his postdoc at the University of Ottawa, Canada, in 1994/95 with J.C. "Tito" Scaiano in photochemistry, he completed his habilitation in physical chemistry with J. Wirz at the University of Basel, Switzerland, where he became Assistant Professor in 2000. Since 2002, he is Professor of Chemistry at Jacobs University Bremen, Germany. He has held visiting professorships at St. Francis Xavier University, the University of Wisconsin–Madison, USA, the University of Cambridge, UK, and the Institute of Chemical Research of Catalonia (ICIQ), Spain. His research combines principles of supramolecular chemistry and organic photochemistry with spectroscopy and is directed towards applications in bioanalytical chemistry, specializing on fluorescent dyes and probes.

Mara Florea was born in Alba-Iulia, Romania, in 1984. She obtained her MSc degree from Jacobs University Bremen, Germany, in 2008 and is currently pursuing her PhD studies with Werner Nau at the same university. Her research interests lie in the areas of supramolecular and physical organic chemistry, with emphasis on the use of macrocycles and dyes in the design of fluorescence-based enzyme assays and sensors for biologically and environmentally relevant analytes.

Khaleel Ibrahim Assaf was born in Amman, Jordan, in 1985. He obtained his MSc degree from the Hashemite University, Jordan, in 2009, working on molecular dynamics simulations of cucurbiturils and their inclusion complexes in aqueous solution under the supervision of Musa El-Barghouthi. Since 2010, he is pursuing his PhD studies with Werner Nau at Jacobs University Bremen, Germany. His research interests lie in the areas of computational and supramolecular chemistry.


A qualitative assessment can be made on the basis of the electrostatic potential map of this class of macrocycles (Figure 3). Such illustrations immediately visualize the excess electron density at the carbonyl oxygens and thereby rationalize the cation-receptor properties of CBs, but they bear little information on the hydrophobicity of the microenvironment inside the inner cavity, set aside the piece of information that the equatorial regions are electron deficient. For CBs, the situation is distinct from that of cyclodextrins, where C–H bonds are known to point towards the inside of the cavity and thus characterize it as "alkane-like", or that of calixarenes, where aryl π systems are known to frame the cavity and thus naturally qualify it as electron-rich and "aromatic". For CBs, there are neither bonds, nor

lone electron pairs pointing towards the inside, and the ureido π system is strongly polarized towards the oxygens. This leads to an overall electron-deficient situation, which can hardly be approximated by a known condensed phase.

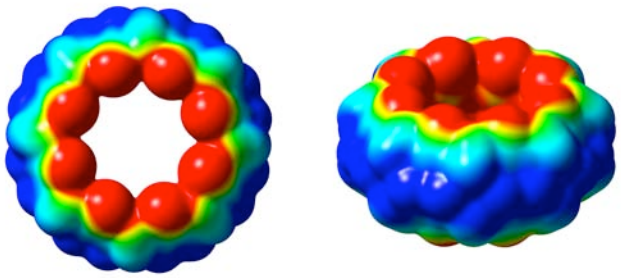

**Figure 3.** Electrostatic potential map (top and side view) of CB8 revealing the negatively charged carbonyl regions (in red) and the electron-deficient equatorial region (in blue).

To explore unknown, peculiar microenvironments, solvatochromic probes have proven useful. They can be used as molecular spies to sound out physical properties of bulk as well as molecular cavities through changes of their photophysical properties (absorption and emission). Of particular interest are the polarity and polarizability of different macrocyclic cavities and their comparison with common solvents. The polarity determines the effective hydrophobicity, while the polarizability is an important denominator of intermolecular interactions, prominently dispersion interactions, which affect the binding strengths of host-guest complexes. The hydrophobic effect and dispersion interactions jointly define the driving force for complexation of neutral guest molecules with CBs.[38]

### 2.1. Polarity

Due to the well established trends in their absorption, fluorescence, or phosphorescence spectra, solvatochromic molecular probes have been employed to determine the polarity of solvents, or that of the inner cavity of molecular containers, as well as to study hydrogen-bond donor properties. The seminal study in this context is the development of the $E_T(30)$ parameter and related scale for solvent polarity by Reichardt.[39] Several polarity-sensitive probes have already been tested with CBs in order to estimate the polarity of their inner cavity.[15,40] The fluorescence properties of curcumin pointed to a polarity lower than water, but much higher than ethanol.[40] Encapsulation of various fluorescent dyes by CB7 results in most cases in a bathochromic shift in the fluorescence and absorption bands, which characteristically signals immersion of the probes in a less polar environment. Specifically, the absorption maximum of Rh6G complexed by CB7 signals a microenvironmental polarity similar to that of *n*-octanol ($\varepsilon$ = 10.3).[41] Additionally, differential characteristic Stokes shifts, observed for laser dyes such as xanthenes or coumarin C102, also suggest a less polar environment than water.[15]

Table 1 shows a comparison in polarity of different supramolecular environments and common solvents. The microenvironment of CBs, sensed by the different dyes, is similar to that of alcohols or alcohols:water mixtures. In fact, very similar polarities have also been established for other macrocycles such as cyclodextrins and calixarenes where anilinonaphthalenesulfonate as polarity-sensitive probe has been utilized.[42-44] In conclusion, the interior of CBs is less polar than that of water and therefore by trend hydrophobic in nature.

Geometrical confinement effects and specific complexations of certain regions of the dyes present a source of uncertainty in such polarity estimates. It must also be kept in mind that the investigated polarity-sensitive probes are relatively large and mostly elongated in nature and therefore not fully immersed in the CB cavity. They consequently report on a mixed environment, being partially inside the host and partially still exposed to the aqueous bulk. It is relatively safe to predict that a solvatochromic probe, which could be fully immersed in the inner CB cavity would report an even less polar and certainly less protic microenvironment than the alcoholic one presently determined.

**Table 1.** Polarity, refractive index, and polarizability inside macrocyclic host molecules and different solvents.

| environment | $P$[a] | $n_D$[b] | $E_T(30)$[c] |
|---|---|---|---|
| gas phase | 0.000 | 1.000 | 27.1 |
| **cucurbit[7]uril (CB7)** | **0.12**[d] | **1.10±0.12**[e] | **≈ 48**[f] |
| perfluorohexane | 0.159 | 1.252 | n.a.[g] |
| *β*-cyclodextrin (*β*-CD) | 0.20 | 1.33 | ≈ 55[h] |
| water | 0.206 | 1.333 | 63.1 |
| acetonitrile | 0.212 | 1.344 | 45.6 |
| *n*-hexane | 0.229 | 1.375 | 31.0 |
| isopropanol | 0.231 | 1.377 | 48.4 |
| *p*-sulfonatocalix[4]arene (CX4) | 0.25[i] | 1.41 | ≈ 54[j] |
| dichloromethane | 0.255 | 1.424 | 40.7 |
| chloroform | 0.267 | 1.446 | 39.1 |
| carbon tetrachloride | 0.274 | 1.460 | 32.4 |
| benzene | 0.295 | 1.501 | 34.3 |
| carbon disulfide | 0.355 | 1.627 | 32.8 |
| diiodomethane | 0.404 | 1.742 | 36.5 |
| hemicarcerand | 0.45[k] | 1.86 | - - - |

[a] Value obtained using DBO as solvatochromic probe, see text. [b] Refractive index, converted from polarizability values using $P = (n_D^2 - 1)/(n_D^2 + 2)$. [c] All $E_T(30)$ values corresponding to the different solvents or solvent-like environments were taken from ref. [39]. $E_T(30)$ was introduced as an empirical parameter for assessing solvent polarity by using a pyridinium *N*-phenolate betaine dye as solvatochromic probe. [d] From ref. [45]. [e] From ref. [15]. [f] Polarity similar to that of *n*-octanol, according to ref. [41] [g] The low solubility of solvatochromic dyes in perfluoroalkanes prevents $E_T(30)$ determinations, *cf.* ref. [46]. [h] Polarity similar to that of methanol, according to ref. [42]. [i] From ref. [47]. [j] Polarity similar to that of 80% ethanol, according to ref. [44]. [k] Value obtained using biacetyl as solvatochromic probe (see ref. [45]).

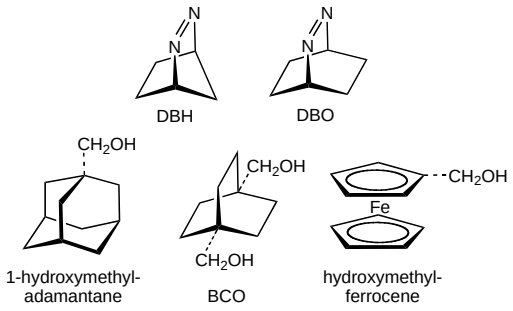


**Figure 4**. Bicyclic and tricyclic recognition motifs for CBs; the portions considered not to be encapsulated in the inner cavity are shown as dashed bonds.

### 2.2. Polarizability

The inner cavity of CBs shows an exceedingly low polarizability. We have detected this astounding property by studying the UV absorption and fluorescence of 2,3-diazabicyclo[2.2.2]oct-2-ene (DBO, Figure 4) in depth.[45,48] DBO is a neutral azoalkane with an extremely long-lived (up to 1 μs) fluorescence. In contrast to the solvatochromic probes employed to determine polarity, the bicyclic structure of DBO results in a spherical shape, which along with its small size (111 Å$^3$),[31] allow it to be entirely immersed inside the size-complementary cavity of CB7 (no binding with CB6 could be detected). The full immersion ensures that a genuine property of the inner cavity is being explored, not only for CB7, but also for closely related macrocycles with similarly large cavities,[49] such as *β*-cyclodextrin[50] and *p*-sulfonatocalix[4]arene.[47,51] The good match of the CB7•DBO complex is reflected in a strong binding ($K$ = 5.8 × 10$^6$ M$^{-1}$),[52] and can be visualized from a crystal structure (Figure 5).

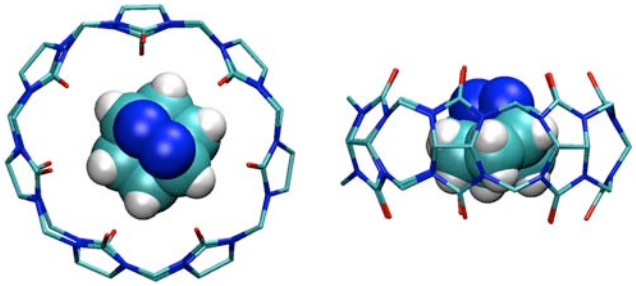

**Figure 5.** Crystal structure (from the corresponding $AgNO_3$ complex, *cf*. ref.[52]) showing the deep immersion of the spherical DBO inside CB7; the actual co-conformation of the azo group may differ in the absence of ligating metals.

DBO, as well as selected other n,$\pi^*$-excited states such as biacetyl, undergo environmentally dependent changes in their absorption spectra. Specifically, in order to assess the polarizability of CB7, the oscillator strength, *f*, of the near-UV band of DBO was measured in the gas phase, as well as in different solvents and supramolecular environments. An empirical linear correlation was established between the inverse of the oscillator strength and bulk polarizability of the environment *P* ($1/f$ = 3020 – 8320 *P*, Figure 6), which is directly related to the refractive index (Table 1).[45]

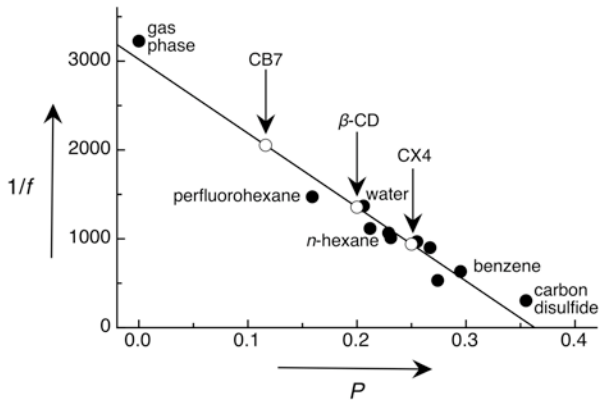


**Figure 6.** Linear correlation of the inverse oscillator strength of DBO and the polarizability of the environment. White circles mark interpolated values for macrocyclic cavities. For values and abbreviations see Table 1.

The most striking feature is the low polarizability/refractive index measured inside the CB7 cavity, which is close to that of the gas phase,[53] and falls even below that of the least polarizable solvent, perfluorohexane (Figure 6). The extremely low and high polarizabilities and refractive indices inside the supramolecular complexes of CBs and hemicarcerands (independently established with biacetyl as guest),[45] respectively, provided the first experimental confirmation of Cram's daring postulate that the inside of molecular containers represents a completely new phase of matter.[54,55] For comparison, the polarizabilities of cyclodextrins and calixarenes are "normal", i.e., lie somewhat below or above those of alkanes, respectively.

The characteristic molecular structure of CBs (electron-deficient cavity, no bonds or lone pairs inside, see above) nicely rationalizes its very low polarizability. Guests which are fully entrapped in the inner cavity of CBs experience therefore an extreme environment, which is more similar in nature to the gas phase than to solution. The low polarizability of CBs is not just a curiosity. There are immediate important consequences, one line is spectroscopic and photophysical in nature, the other one supramolecular and thermodynamic, and these will be separately addressed, the first here and the second in Section 5. Note that a low polarizability or refractive index affects directly the radiative decay rate ($k_r$) of fluorescent states, given as the ratio of the fluorescence quantum yield ($\phi_f$) and lifetime ($\tau_f$). The Einstein coefficient for spontaneous emission is directly related to the square of the refractive index of the environment, $n_D^2$, and this results, other things being equal, in longer fluorescence lifetimes of chromophores in low-polarizability environments (Strickler-Berg equation 1).[56]

$$k_r = \frac{\phi_f}{\tau_f} = 0.668 \langle \tilde{\nu} \rangle_{av}^2 n_D^2 f \qquad (1)$$

Indeed, many fluorescent dyes (rhodamines, coumarins, pyronins, oxazines, and cyanines) display their longest fluorescence lifetimes ever recorded (note here that large polyaromatic dyes cannot be vaporized) in the inside of the CB cavity.[15,41,48,57] This is surprising for some of the fluorescent dyes, which are clearly too large to be fully immersed, but where the influence of the cavity nevertheless leaves its signature on their spectroscopic properties. The CB7 complex of DBO, fully immersed and capped with sodium ions, holds presently the world record for "slow-fluorescing", displaying a fluorescence lifetime above 1 μs in aqueous solution.[48] While the correlation of the oscillator strength with polarizability constitutes an empirical measure, the exceptionally long fluorescence lifetimes provide direct spectroscopic evidence for the low refractive index of the inner cavity of CBs,[10,48,58] resulting in a projected value of 1.10 ± 0.12, well below that of perfluorohexane (1.25).[15]

For the fluorescence lifetime enhancing effect of CBs, we have coined the name 'supramolecular radiative decay engineering',[57] a term inspired by Lakowicz for the apparent increase of radiative decay rates near metal surfaces and nanoparticles.[59] Supramolecular radiative decay engineering can be generically understood as the combined beneficial effects, which the encapsulation of CBs has on the performance of fluorescent dyes. These are not limited to longer fluorescence lifetimes, but also refer to a higher brightness,[15,60] an enhanced photostability,[41,53,57] resistance toward (photo)oxidation,[61] and a reduced tendency towards aggregation as well as unspecific absorption.[15,41,62] They have jointly led to numerous practical applications of CBs, particularly CB7, for the construction of (tunable) water-

based dye lasers[63,64] and for confocal microscopy,[15,65] potentially even information storage. Today, the most photostable water-soluble fluorescent dye is Rhodamine 6G encapsulated by CB7.[41] These applications demonstrate nicely how an initially innocuous effect, such as the observed low polarizability, can have an immediate impact.

### 2.3. Quadrupole Moments

Owing to their high symmetry, CBs do not possess a permanent monopole (charge), dipole, or octupole moment. However, they do possess a molecular (electric) quadrupole moment. Experimentally, these are challenging to assess, but our density-functional theory calculations have revealed exceedingly high (negative) quadrupole moments (Table 2), which will certainly contribute to the intermolecular electrostatic stabilization of the complexes with encapsulated dipolar or quadrupolar guests. Although the absolute values may be subject to a significant error, the values are 10-40 times larger than largest values known for small molecules such as benzene or carbon dioxide (ca. 10 B). Equatorially alkylated CBs have an even larger quadrupole moment (values in square brackets in Table 2), which is expected to enhance the electrostatic contributions to host-guest binding.

**Table 2.** Molecular electric quadrupole moments of CBs.

| CB*n* | $\Theta_{zz}$/B [a] |
|---|---|
| CB5 | –120 [–128] [b] |
| CB6 | –155 [–168] [b] |
| CB7 | –194 |
| CB8 | –237 |
| CB9 | –284 |
| CB10 | –334 |

[a] 1 B (Buckingham) = 1 D (Debye) × 1 Å = 3.3356 × $10^{-40}$ $Cm^2$. Obtained by electrostatic analysis of CB structures geometry-optimized under the highest $D_{nh}$, ($n$ = 5-10) symmetry constraints at the B3LYP/6-311G** level of theory with the Gaussian 03 software package,[66] see Supporting Information. [b] Values for permethylated derivatives given in square brackets.

Calculations in the gas phase have revealed a 3-4 kcal $mol^{-1}$ higher binding energy for the orthogonal arrangement of the ferrocene axis with that of CBs,[67] in which quadrupolar interactions are maximized; note that ferrocene has a large quadrupole moment (–9±2 Buckingham, similar to that of benzene).[68] The isosteric (see below) adamantane anchor, however, has a vanishing quadrupole moment due to its spherical charge distribution, but binds similarly strongly with CB7;[69] this reveals that the enthalpic contribution of quadrupole interactions cannot be large. The contribution is sufficient, however, to serve as a structure-determining element. In fact, the screening of crystal structures (see below) reveals that CBs frequently adapt a "T-type" stacking in the solid state,[4,70-73] with the wall of one CB topping the portal of another, thereby achieving optimal quadrupolar interactions. The molecular quadrupole moment of CBs has also been implicated to account for the equatorial alignment of (dipolar) ketones in these hosts, which would maximize dipole-quadrupole interactions.[74,75]

## 3. Binding of Neutral Guests in the Inner Cavity

The complexation of neutral guests with CBs is interesting because it eliminates interferences from charge-dipole interactions, which otherwise become readily dominant, and therefore allows the isolation of the hydrophobic driving force for complexation. Moreover, neutral guests will tend to fill partially or completely the inner cavity, which allows not only for the size, but also for the intermolecular interactions of guests with the inner CB cavity to be explored in detail. Known binding constants of neutral guests with CB6 and CB7 (the only homologues for which extended data sets are at hand) are compiled in Tables 3 and 4. Note in advance that the binding constants for CB6 and CB7 cannot be directly compared, even for an identical guest: Binding constants for CB7 can be readily measured by a variety of titration techniques, including NMR, because of the high water solubility of this host (ca. 5 mM).[45] CB6 is intrinsically less water-soluble (ca. 30 μM)[31] such that binding constants have, until recently, routinely been obtained in either mixed solvents (commonly formic acid)[25] or in the presence of salts (e.g., 50-200 mM $Na_2SO_4$).[24,26,28-31,76] Such conditions modulate (reduce) the affinity markedly;[24,31,77] for example, the binding constant of cyclohexylmethylammonium decreases from 1.1 × $10^5$ $M^{-1}$ in neat water (estimated from the solubilization of CB6 in the presence of excess guest, by $^1$H NMR) to 170 $M^{-1}$ in the presence of 200 mM $Na_2SO_4$.[31] This competitive binding effect is largest for ammonium ions, where the docking of cations to the carbonyl rims causes a Coulombic repulsion of the guest, but it is also significant for neutral guests, as can be implied from the only available data set for xenon binding to an alkylated CB6 derivative (decrease from 3400 to 180 $M^{-1}$).[30]

**Table 3.** Binding constants of selected neutral guests with CB6 in water/formic acid mixtures or in salt solutions.

| guest | $K$/$M^{-1}$ | guest | $K$/$M^{-1}$ |
|---|---|---|---|
| **alcohols** | | | |
| ethanol | 90[a,b] | butanol | 1200[a,b] |
| | 26[a,c] | | 340[d] |
| | 440[d] | pentanol | 410[a,b] |
| propanol | 710[a,b] | | 540[d] |
| | 490[a,e] | hexanol | 510[d] |
| | 120[a,f] | heptanol | 440[d] |
| | 410[d] | | |
| **carboxylic acids** | | | |
| acetic acid | 150[a,g] | hexanoic acid | 590[d] |
| TFA | 11[h,i] | heptanoic acid | 590[d] |
| propionic acid | 590[d] | octanoic acid | 560[d] |
| pentanoic acid | 500[d] | nonanoic acid | 620[d] |
| **miscellaneous** | | | |
| propionitrile | 200[d] | 1-hexane nitrile | 370[d] |
| THF | 1700[h,i] | $SF_6$ | 31000[h,j] |
| furan | 7100[h,k] | Xe | 210[h,i] |
| benzene | 27[h,k] | | 180[h,l] |
| cyclopentanone | 2200[h,k] | | 3400[l,m] |
| cyclohexylmethylamine | 10[h,n] | DBH | 1300[h,n] |

[a] From ref. [24]. [b] In 50 mM NaCl. [c] In 50 mM CsCl. [d] In 50% (v/v) formic acid, from ref. [25]. [e] In 50 mM KCl. [f] In 50 mM RbCl; value in 50 mM CsCl is < 5 $M^{-1}$. [g] In 50 mM sodium citrate, pH 3.1. [h] In 200 mM $Na_2SO_4$. [i] From ref. [26]. [j] From ref. [28]. [k] From ref. [29]. [l] Data for an alkylated, water-soluble CB6 derivative from ref. [30]. [m] In neat water. [n] From ref. [31].

Besides water molecules, which have been identified early in the crystal structures of CBs (see Section 5.1.),[3,4,37,78-80] the first neutral guests to form inclusion complexes with CBs in general, and CB6 in particular, were tetrahydrofuran (THF),[18,29] tetrahydrothiophene,[18] cyclopentane,[18] and the bicyclic 2,3-diazabicyclo[2.2.1]hept-2-ene (DBH, Figure 4).[31] The first neutral guest to form a very stable host-guest inclusion complex with CB7 was the bicyclic DBO.[45] Note that bicyclic (and polycyclic) binding motifs have subsequently become very popular for CB7 due to their ultrahigh affinity.[69,81] Binding of small neutral guests is especially instructive because they are fully immersed in the inner cavity of the two CBs. This allows, for example, the additional docking of cations in the dipolar regions of the CB hosts under formation of ternary complexes,[10,52,82] i.e., without displacement of the guest as is commonly observed for alkylammonium salts.[31]

**Table 4.** Binding constants of selected neutral guests with CB7, in water.

| guest | $K/(10^3\ M^{-1})$ | guest | $K/(10^3\ M^{-1})$ |
|---|---|---|---|
| **ketones**[a] | | | |
| $Me_2CO$ | 0.58 | PhMeCO | 9.6 |
| MeEtCO | 3.1 | BnEtCO | 4.6[b] |
| $Et_2CO$ | 2.1 | Bn(*t*Bu)CO | 270[b] |
| Me(*t*Bu)CO | 6.7 | cyclopentanone | 420[c] |
| **dyes (neutral forms)** | | | |
| DBH[d] | 380[d] | neutral red | 6.5[e] |
| DBO[d] | $5.8 \times 10^3$ [d] | acridine orange | 0.95[f] |
| **benzimidazoles**[g] | | | |
| benzimidazole | 1.5 | thiabendazole | 0.15 |
| albendazole | 65 | fuberidazole | 0.05 |
| carbendazim | 24 | HPBI[h] | < 1.0 |
| **alcohols ($RCH_2OH$)**[i] | | | |
| R = 1-adamantyl | $2.3 \times 10^7$ | BCO[j] | $6.1 \times 10^6$ |
| R = ferrocenyl | $3.2 \times 10^6$ | | |
| **carboxylic acids (RCOOH)** | | | |
| R = adamantyl | $3.2 \times 10^5$ [k] | R = $Me_3SiCD_2CD_2$ | $1.8 \times 10^4$ [k] |
| R = ferrocenyl | ---[l] | | |
| **solvents**[a] | | | |
| methylacetate | 1.0 | dimethylformamide | 1.0 |
| dimethylsulfoxide | 0.14 | acetonitrile | 0.0011 |
| **miscellaneous** | | | |
| ranitidine | 1.2[m] | melamine | 39[n] |

[a] From ref. [74]. [b] From ref. [83]. [c] From ref. [14]. [d] See Figure 4, from ref. [52]. [e] In aqueous solution, pH 11, from ref. [84]. [f] In aqueous solution, pH 14, from ref. [85]. [g] Determined at pH 10.5, except for albendazole (pH 8.4), from ref. [86]. [h] 2-(2'-hydroxyphenyl)benzimidazole, from ref. [87]. [i] From ref. [69]. [j] 1,4-(dihydroxymethyl)bicyclo[2.2.2]octane, see Figure 4. [k] In 50 mM $CD_3CO_2Na$, pH 4.74, from ref. [81]. [l] From ref. [88]; no binding constant was extracted, but the inclusion of the guest was evidenced by NMR. [m] From ref. [89]. [n] From ref. [90].

Alcohols are known to bind with CB6, but with low binding constants ($\leq 10^3\ M^{-1}$).[24,25] Carboxylic acids, up to 1-nonanoic acid, have also been reported to be included by CB6 with small binding constants ($\leq 600\ M^{-1}$), and in these cases it is clear that it is the neutral protonated form of the acid, and not the anionic form, which is encapsulated. The action of trifluoroacetic acid (TFA) on the dissociation of the "sodium-lidded" CB6•THF has in fact been initially interpreted as a proton-induced release of THF from the complex,[29] but was later reinterpreted to a genuine competitive binding of protonated TFA inside CB6.[26] The larger homologue CB7 is known to bind acids in their neutral form when they possess a strong hydrophobic recognition motif, such as ferrocenyl, adamantyl, or trimethylsilyl.[81] Interestingly, binding constants of CB8 with (single) neutral guests appear to be unavailable. For CB10, the complex with CB5 has been well characterized.[7,35] CB5, in contrast, has been found early to form inclusion complexes with neutral guests, in particular small gases such as He, Ne, $H_2$, Kr, Xe, $CH_4$, $N_2$, $O_2$, Ar, $N_2O$, NO, CO, $CO_2$, acetylene,[32] as well as with solvent molecules such as acetonitrile and methanol.[33] The crystal structures of CB5 reveal even binding with *anionic* guests such as $Cl^-$ or $NO_3^-$.[7,91-94] The binding of small gases with CB6 has also been studied by Kim and coworkers who characterized inclusion complexes with Xe,[26,27] and, more recently, $CO_2$.[95] Also $SF_6$ has been reported to bind to CB6.[28] Finally, several binding constants of ketones and organic solvents with CB7 have been determined.[74,83]

The trends of the binding constants in Tables 3 and 4 are not in all cases systematic. For example, while the increased binding constant of butan-2-one ($K$ = 3100 $M^{-1}$) *vs*. 3,3-dimethylbutan-2-one (6700 $M^{-1}$) could be interpreted in terms of a better fitting of the neopentyl motif with CB7, the selectivity appears to be small and could be similarly due to differential desolvation effects of the uncomplexed guests. The selectivity of CB6 towards alcohols as well as carboxylic acids is also poorly pronounced, displaying essentially no significant dependence on the chain length upon going from C2 to C9 homologues.[24-26] A simple explanation for such a constancy in binding constants would be that the complexation of all homologues is driven by the removal of a constant number of, presumably all, water molecules from the cavity. Why the smaller furan has a larger binding constant (7100 $M^{-1}$)[29] than THF and cyclopentanone (ca 2000 $M^{-1}$)[26,27] is a similarly unanswered question, especially since dispersion interactions do not drive the binding to CBs (see Section 5). The tiny, but non-negligible binding of cyclohexylmethylamine is important, because for this guest the maximum capacity of CB6 (cyclohexyl residue included in inner cavity) is reached. Guests with more than 6 heavy (non-hydrogen) atoms can only be accommodated if the structures are spherical, and the maximum is reached for 7 heavy atoms, a prediction originally made for DBH.[31] This was later matched by $SF_6$, although fluorine is effectively not much larger than hydrogen and may thus not be considered as a "heavy" atom in this context.[28] In contrast, for CB7, the maximum affinity coincides with a guest size of 10-11 heavy atoms for adamantane[81] and ferrocene,[14,88] while the maximum capacity appears to be approached for 12 heavy atoms, i.e., for carborane ($C_2H_{12}B_{10}$)[96] or the product derived from photocycloaddition of 2 pyridine rings (here, the 2-amino groups are considered to be located in the bond dipole regions, see below).[97]

Also pertinent in the context of size considerations for included residues are the reported binding constants of tetraalkylammonium, tetraalkylphosphonium, and trialkylsulfonium ions.[98,99] Although these guests are cationic, their binding topology is special because the cationic

sites do not interact with the dipolar regions of CB7, but they are fully or partially immersed in the inner cavity, thus revealing an overall hydrophobic driving force. The variations of the alkyl substituents have revealed maxima of the binding constants on the order of $10^6$ $M^{-1}$ for tetraethyl ammonium (9 heavy atoms), triethylsulfonium, and tetramethylphosphonium. Tetrapropyl- (13 heavy atoms, i.e., 1 too many, see above) and tetrabutylammonium guests were found to be too large to be fully included in the cavity of CB7, with two alkyl 'arms' residing outside the cavity.

Neopentylammonium associates weakly to CB6, but the complex is of the exclusion type, i.e., *no inclusion* in the cavity.[16,18] This can be readily deduced from the complexation-induced $^1$H NMR shifts, which are up-field for included protons, negligible for protons in the portal planes, and down-field for protons positioned outside the CB and above the rim. Consequently, the neopentyl group (even though it is composed of only 5 heavy atoms) is too large to be included inside CB6,[16,18] a fact which has been exploited by using them as stoppers in the construction of rotaxanes.[100] Another clear-cut hole-size exclusion effect is that DBO (8 heavy atoms, 1 too many) cannot be included inside CB6 while binding of the smaller homologue DBH is feasible with a non-vanishing binding constant (1300 $M^{-1}$, Table 3).[31] DBO binds, however, more than one order of magnitude stronger than DBH inside the larger cavity of CB7 (Table 4).[52]

Recently, it has been recognized that the complexation of basic guest molecules with CBs causes shifts in their p$K_a$ values,[53,84-86,101] which allows the determination of binding constants of neutral guests from the corresponding experimental binding constants of the higher-affinity protonated counterparts even in cases where direct measurements are not possible, namely through a thermodynamic cycle. This method is limited to optically active guests, particularly fluorescent dyes for which accurate pH titrations of their UV-Vis and fluorescence spectra can be performed. These binding constants are also included in Table 4 (neutral red, acridine orange, and benzimidazoles). They confirm in all cases a 1 to 5 orders of magnitude larger binding constant of the protonated forms of the guests, which can be used to dissect the contributions of hydrophobic binding (as reflected by the affinity of the neutral guests) from the synergetic ion-dipole interactions in the protonated forms.[53,84-86,101] In general, the introduction of a positive charge accounts for an increase by a factor of 10-100000 in binding constant (the absolute enhancement factor appears to depend critically on the "correct" positioning of the emerging charge).

The state of the art of the thermodynamics of binding of neutral guests with CBs is therefore such that more than one clear-cut binding motif has been recognized for CB7, namely quarternary and spherical polycyclic guests as well as ferrocene (Figure 4 and Table 4), but that a binding motif for CB6 can only be indirectly inferred from studies with alkyl(di)ammonium[16,18,24,76,102] and alkylimidazolium[103,104] salts as guests. These have shown a pronounced chain-length dependence, and affinity maxima appear to be reached for C3-C5 residues included in the *inner* cavity (the ammonium methyl groups are located in the bond dipole region, i.e., they do not occupy the inner cavity, as established by single-crystal structures and complexation-induced chemical shifts, see also Section 4.1.).[18,76] For (polar) neutral guests, such a trend is less obvious and can at best be inferred from the slightly larger binding constant of butanol compared to those of the other alcohols (Table 3).

In order to predict binding preferences in more detail, knowledge of the inner cavity volumes is indispensable because it sets an upper limit to the size of potential guests and allows simple predictions based on the goodness of fit, in a simplistic approximation according to the key-lock principle.[31,73] A more refined method rests on existing knowledge of preferred packing coefficients (*PC*s) in conceptually related capsule complexes, according to which guests with ideal volumes can be identified.[105-111] Also conclusions regarding the potential presence of residual water molecules in the cavity can be drawn.

## 4. Volumes of the Inner Cavity and Packing Coefficients for Guest Binding

### 4.1. Methodology for Calculations of Cavity Volumes

All cavities reported herein were computed and graphically represented (see Figure 2) by using the DeepView/Swiss-Pdb Viewer software.[112] In contrast to self-assembling capsules,[105,107-109] hemicarcerands,[110] and cryptophanes,[106,111] for which cavity volumes have been frequently reported, CBs possess 2 open portals which need to be "sealed" in order to evaluate the cavity volumes from computed structures. For this purpose, two identical blocking groups were introduced, which served as hypothetical lids to artificially seal the cavity. Specifically, we have employed a cyclic graphene-like section (Figure 7) and chose it to be sufficiently large to cover all CB portals, up to CB10. We have evaluated three different cavities for each CB (Figure 2), one in which the blocking group approaches with its own van der Waals (vdW) surface the vdW radius of the oxygens (expanded cavity, Figure 7), another in which it penetrates to the plane defined by the portal oxygen nuclei (inner cavity), and another one in which it is forced near the vdW radius of the carbonyl carbons (truncated cavity). The bond dipole regions (Figure 2) were visualized by first defining an expanded cavity with 2 blocking groups, and then placing a blocking group into the equator.

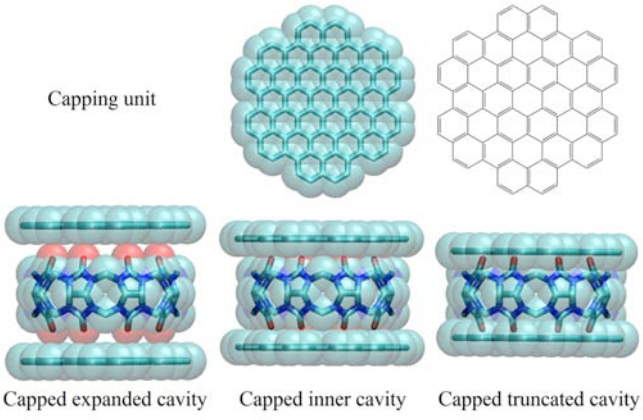


**Figure 7**. Capping unit (top) and its positioning (side view, for CB8 as an example) utilized in the calculation of the different cavities. To define the expanded and truncated cavities the capping unit was positioned at the vdW radius of the carbonyl oxygens and carbons, respectively. To define the inner cavity, it was placed to reach the plane defined by the oxygen atoms.

The calculated volumes for the differently defined cavities are shown in Table 5. As illustrated in Figure 8, the inner cavity volumes increase rapidly, in a parabola-like fashion, when going along the homologous CB*n* series.

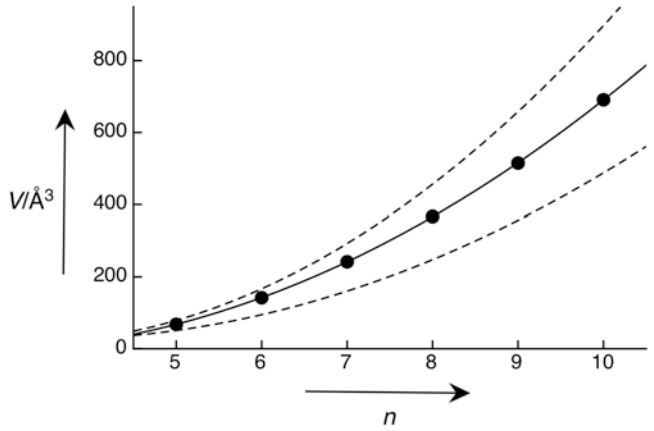


**Figure 8.** The increase of the inner cavity volume (*V*) of CBs obeys exactly (±1Å$^3$, solid line) the functional relationship $V/Å^3 = 68 + 62(n–5) + 12.5(n–5)^2$, where *n* presents the number of glycoluril units. The dashed lines show the corresponding fits for the expanded (top) and truncated (bottom) cavity volumes; data from Table 5.

**Table 5.** Calculated volumes of differently defined cavities and the bond dipole regions of CBs. Recommended values are shown in **boldface**.

| | calculated cavity volume/Å$^3$ [a] | | | | bond dipole regions[c] |
|---|---|---|---|---|---|
| CB*n* | expanded | **inner** | truncated | X-ray[b] | |
| CB5 | 81 (82)[d] | **68** | 51 | 43 ± 7[e] | 30 |
| CB6 | 164 (164)[d] | **142** | 93 | 119 ± 21[f] | 71 |
| CB7 | 282 (279)[d] | **242** | 158 | 205 ± 18[g] | 124 |
| CB8 | 479 (479)[d] | **367** | 263 | 356 ± 16[h] | 216 |
| CB9 | 642 | **515** | 339 | - - - | 303 |
| CB10 | 901 (870)[i] | **691** | 494 | - - - | 407 |

[a] See text as well as Figures 2 and 7 for definition and method of calculation; for the volume calculations with capping groups, the CBs were geometry-optimized under the highest $D_{nh}$, (*n* = 5-10) symmetry constraints at the B3LYP/6-311G** level of theory with the Gaussian 03 software package,[66] see Supporting Information. [b] Determined from experimental crystal structures by removing atoms with coordinates within the inner cavity, i.e., between the planes defined by the carbonyl oxygens; error refers to standard deviation. [c] Taken as difference of the expanded and truncated cavities. [d] Values in parentheses were estimated (no details provided) from crystal structures of pure CBs, i.e., without guests except crystal water, from ref. [4]. [e] Value derived from 35 distinct cavities of 29 different CB5 crystal structures from the CCDC database, see Table S1 of Supporting information. [f] Value derived from 88 distinct cavities of 67 different CB6 crystal structures from the CCDC database, see Table S2 of Supporting information. [g] Value derived from 7 distinct cavities of 6 different CB7 crystal structures from the CCDC database, see Table S3 of Supporting information. [h] Value derived from 7 distinct cavities of 7 different CB8 crystal structures from the CCDC database, see Table S4 of Supporting information. [i] From ref. [8].

Additionally, cavity volumes have also been estimated from a statistical analysis of various single-crystal X-ray diffraction structures contained in the database of the Cambridge Crystallographic Data Centre (CCDC). For this purpose, all different CB complexes in the asymmetric units were identified, the atoms with coordinates inside the planes defined by the carbonyl oxygens were removed to create the unfilled cavity, and atoms outside the portals (frequently belonging to the outer walls of another CB or inorganic ions) were retained as "real" lids. It should be noted that this strategy produced in most, but not all cases cavities which were recognizable by the software,[112] and the negative results were discarded without introducing "artificial" boundaries to force the cavity to become closed. The volumes of the recognized cavities in the different structures are reported as average values with standard deviation in Table 5.

### 4.2. The Cavity Relevant for Hydrophobic Binding

The calculated *expanded* cavity volumes (Table 5) are, surprisingly, in excellent agreement with previous estimates (no detailed methodology was described)[4] based on crystal structures of neat, guest-free CBs. However, these volumes do not provide the preferred measure for the "effective" volume of the hydrophobic space, because they include the bond dipole regions (Table 5). These are fully or partially occupied by atoms and residues carrying positive charges, commonly inorganic ions or ammoniummethyl fragments, as well as water. The bond dipole regions possess no intrinsic affinity for hydrophobic residues or guests, certainly not for the smaller CB homologues. In fact, the experimental cavity volumes (X-ray values in Table 5) fall *far* below the volumes calculated for the expanded cavities.

The calculated truncated cavity volumes are, on the other hand, unreasonably small in comparison with the crystallographic data (with the exception of that for CB5, Table 5). As can be deduced from several crystal structures, many guests have atoms, which protrude from the inside into the planes defined by the vdW radii of the carbonyl oxygens. This is structurally viable, because the lone pair electron density of the oxygen atoms points, as a consequence of the macrocyclic topology and concave geometry, towards the poles of the CB axes,[67] and not towards the inside of the cavity (where it would disfavor hydrophobic guest binding). In other words, hydrophobic guests or residues can penetrate partially into the portal regions without interfering with the propensity of the oxygens to engage in electrostatic interactions with the solvent or cations.

Consequently, the most useful measure to estimate the space available for hydrophobic interactions is that of the inner cavity. It provides the best match with the volumes derived from the X-ray analyses, and the two volumes, calculated and experimental, tend to converge for the larger CBs. Closer inspection reveals that the computed values of the inner cavities tend to be larger than the experimental ones, presumably because they do not include complexing cations or water residues electrostatically bound to the portals, which may partially protrude with their vdW volumes below the plane defined by the carbonyl oxygen. However, the experimentally found upper limits (see standard deviations of the crystallographic volumes) reveal nicely that in principle the entire volume of the inner cavity can become accessible to a hydrophobic guest, when it adapts a space-filling structure. We therefore recommend the volumes of the inner cavity to be used in the evaluation of the capacity of the respective CBs and for goodness-of-fit considerations.

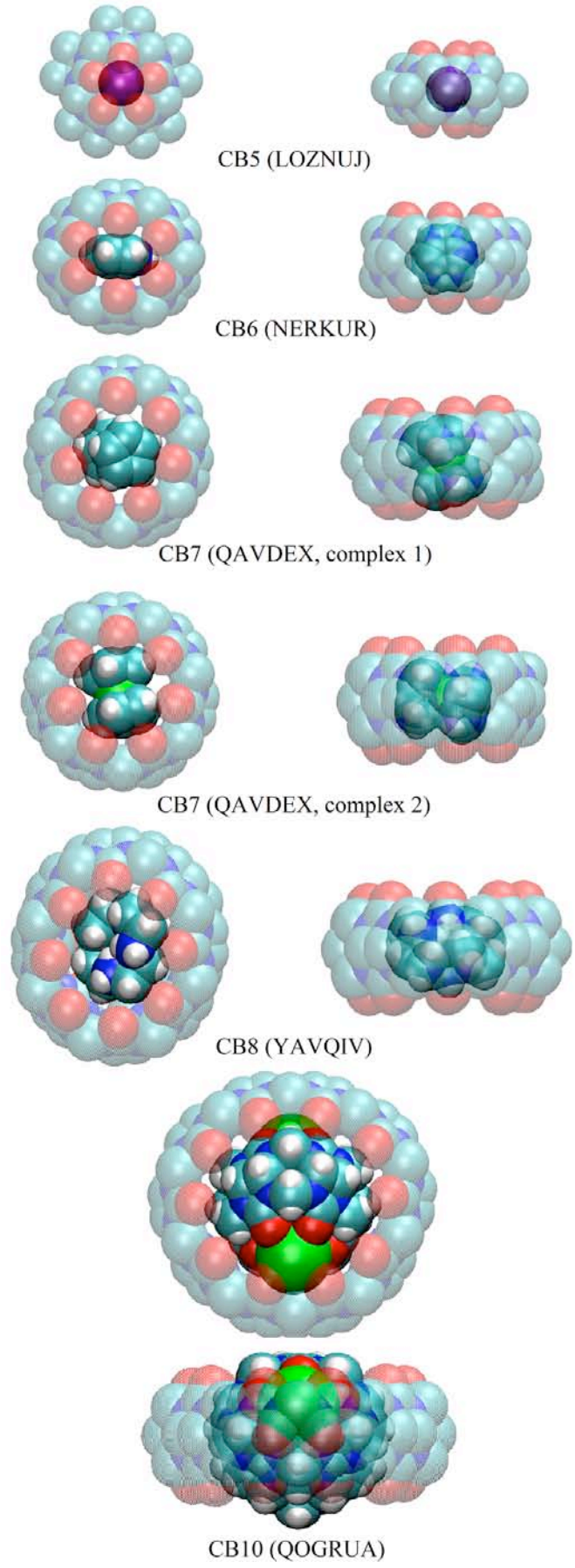


**Figure 9.** Visualization of crystal structures (codes from CCDC data base) of the complexes of different CBs showing deep immersion and ideal fitting with selected hydrophobic guests, namely Xe in LOZNUJ from ref. [32] (note that the host is a decamethyl-CB5 derivative), pyridine in NERKUR from ref. [113], ferrocene in QAVDEX (two distinct complexes in unit cell are shown) from ref. [88], cyclam in YAVQIV from ref. [34], and CB5 in QOGRUA (with $K^+$ ions at each CB5 portal) from ref. [35].

### 4.3. Packing Coefficients (*PC*s)

Cavity volumes are not equivalent with capacities; any phase tends to retain a characteristic void space in order to maximize entropy. Leaning on what was known for packing in different phases, Rebek has proposed a relationship (the "55% solution"),[105] which predicts an optimum packing coefficient (*PC*, volume of the guest divided by the volume of the host cavity), generally associated with highest binding affinity. This rule has been developed for self-assembling capsules,[105,107-109] later transferred to other hosts with closed cavities,[106,110,111] and there is no lucid reason why it should not be applicable, with variations, to the cavities offered by CBs. Recall that the underlying reason for the void space, which remains in such host-guest complexes (typically 45%), lies in the retention of vibrational degrees of freedom of both host and guest, and rotational, eventually even translational ones of the guest, which would be lost for a compressed packing. Important to keep in mind, the ideal *PC* provides only information on the *preferred* packing; smaller and larger values are tolerated, at the expense of lower binding constants.[105,106] The latter can only be determined in solution, such that solid-state structures provide less meaningful information on the preferred packing *inside* the host-guest complex, and too large or too small *PC*s inside the cavity could well be overcome by the stability of the crystal as a whole; moreover, *PC*s in the solid state are larger than 55% (typically larger than 68%), which in fact characterizes this phase (see below). This explains why some guests, such as diethyl ether, which have a low affinity for CB6 in solution may nevertheless crystallize as their host-guest complexes.[114]

We have therefore computed the volumes for a representative set of guest molecules with the QSAR module of HyperChem,[115] after geometry optimization with the AM1 semiempirical method. The selected guests (Table 6) are known from crystal structures or characteristic $^1$H NMR shifts to be either fully immersed in the cavity of a particular CB, or to be immersed in a well defined manner with a single residue. Some representative examples of essentially perfect inclusion complexes of the different CBs are shown in Figures 5 and 9. Most immersed residues are hydrophobic, except for CB5, where also simple anions were considered;[94] these would certainly not bind to the carbonyl rims and can therefore be assumed to be deeply included.[7,91-93]

Only guest atoms positioned with their nuclei within the *truncated* cavity must be taken into account because only these are expected not to protrude with their vdW radii outside the limits of the *inner* cavity (recall that the definitions of these two cavities differ by the vdW radius, Figure 7). This was judged from molecular models or, where available, crystal structures. In particular, cationic (amino or ammoniummethyl) or neutral (hydroxy or hydroxymethyl) pendant groups were removed in the hydrophobic guest volume calculations, because they occupy space above the carbonyl oxygen plane, i.e., outside the inner cavity. In those cases, the portions of the guests, which were considered to be hydrophobic and deeply immersed, are indicated in the structure charts in Figures 4 and 10 as regular bonds. For the

same reason (atoms outside the inner cavity), no calculation was performed for the CB10•CB5 complex (see CB10 structure in Figure 9). For CB7, only guests with reported binding constants higher than $10^3$ $M^{-1}$ were incorporated in the data set, while both aromatic ketones[74] and peralkylated onium ions[98] were excluded because of their incomplete immersion in CB7.

**Table 6.** Guest volumes and packing coefficients (*PC*s) with CBs; guests listed in approximate order of increasing volumes in the following sequence of categories: gases, solvents, aliphatic, aromatic, bicyclic, and miscellaneous guests.

| host | guest | Volume/Å$^3$ | *PC*/%[a] |
|---|---|---|---|
| CB5 | $O_2$ [b] | 19 | 28 |
| | $N_2$ [b] | 24 | 35 |
| | $CO_2$ [b] | 31 | 46 |
| | Xe[b] | 43 | 63 |
| | $CH_3OH$[c] | 36 | 53 |
| | $CH_3CN$[c] | 47 | 69 |
| | $Cl^-$ [d] | 23 | 34 |
| | $NO_3^-$ [e] | 34 | 50 |
| CB6[f] | Xe | 43 | 30 |
| | $SF_6$ | 52 | 37 |
| | 2 × $CO_2$[g] | 62 | 44 |
| | $Me_2CO$, propionitrile | 64 | 45 |
| | furan | 67 | 47 |
| | THF | 77 | 54 |
| | diethyl ether[h] | 88 | 62 |
| | cyclopentanone | 87 | 61 |
| | butane-1,4-diamine[i] | 76 | 54 |
| | pentane-1,5-diamine[i] | 93[j,k] | 65 |
| | hexane-1,6-diamine[i] | 110[j,l] | 77 |
| | cyclopropylmethylamine[m] | 56[m] | 39 |
| | cyclobutylmethylamine[m] | 74[m] | 52 |
| | cyclopentylmethylamine[m] | 86[m] | 61 |
| | cyclohexylmethylamine | 104[m] | 73 |
| | benzene[n] | 89[m] | 63 |
| | pyridine[o] | 82 | 58 |
| | DBH | 96 | 68 |
| | [DBO] [p] | [111] [p] | [78] [p] |
| CB7[q] | $Et_2CO$ | 98 | 40 |
| | Me(*t*Bu)CO | 114 | 47 |
| | cyclopentanone | 87 | 36 |
| | trimethylsilyl propionic acid | 107 | 44 |
| | **1**[r,s] | 132 | 55 |
| | DBH | 96 | 40 |
| | DBO | 111 | 46 |
| | bicyclo[2.2.2]octane (BCO) | 121 | 50 |
| | adamantane | 147 | 61 |
| | **2** (cycloadduct)[r,t] | 151 | 62 |
| | 2 × 2-aminopyridine (dimer)[t] | 161 | 67 |
| | carborane[u] | 147 | 61 |
| | *cis*-$SnCl_4(H_2O)_2$ [v] | 136 | 56 |
| | ferrocene[w,x] | 141 | 58 |
| CB8 | cyclen[y] | 217 | 59 |
| | cyclam[y] | 265 | 72 |
| | **3**[r,z] | 132 | 36 |
| | 2 × *p*-cyanopyridine (dimer)[aa] | 161 | 44 |
| | 2 × **1** (dimer)[r,s] | 265 | 72 |
| | *trans*-$[Ni(en)_2(H_2O)_2]^{2+}$ [w,aa] | 158 | 43 |
| | *trans*-$[Co(en)_2Cl_2]^+$ [w,bb] | 171 | 47 |

[a] Packing coefficient. [b] See ref. [32]. [c] See ref. [33]. [d] See ref. [7,92] [e] See ref. [91,93]. [f] Same references as in Table 3, unless stated differently. [g] See ref. [95]. [h] See ref. [114]. [i] See ref. [18,76]. [j] The included methylene groups were identified from $^1$H NMR shifts in ref. [18], which up to hexane-1,6-diamine coincide with the included portions in crystal structures, *cf.* ref.[76]. [k] Same volume determined for heptane-1,7-diamine, see Figure 10. [l] Same volume determined for octane-1,8-diamine, see Figure 9. [m] From ref. [31]. [n] Same included volumes for 4-methyl-benzylamine (ref. [31]), *p*-xylylenediamine (ref. [116]), *p*-phenyldiamine (ref. [117]), and 1,4-dihydroxybenzene (ref. [118], CB6 derivative), see Figure 10. [o] See ref. [119]. [p] This guest is not included in CB6 even after 1 year, negative control, *cf.* ref. [31]. [q] Same references as in Table 4, unless stated differently. [r] Structures depicted in Figure 10. [s] See ref. [4]. [t] See ref. [97]. [u] Structure from ref. [96]. [v] See ref. [120]. [w] Volume of guest calculated directly from the crystal structure. [x] See ref. [88]. [y] See ref. [34]. [z] See ref. [121]. [aa] See ref. [122]. [bb] See ref. [123].

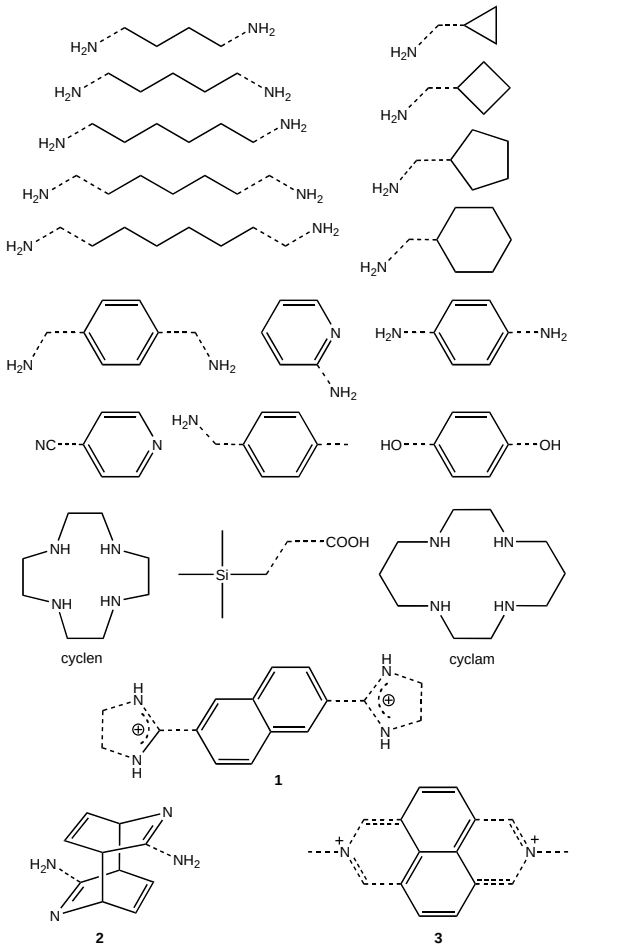


**Figure 10.** Chemical structures of selected guests investigated for volume calculations; the portions considered not to be encapsulated in the inner cavity are shown as dashed lines.

It should be noted that arguments related to guest volumes have already been occasionally used to rationalize binding phenomena in CB chemistry. In an own early study, we concluded that the "capacity" or "effective volume" of CB6 is 105 Å$^3$, based on the volume of the cyclohexyl group,[31] the largest one encapsulated. But we could then not reconcile this value in view of the reported volume (164 Å$^3$),[4] which we see now (Table 5) corresponds to that of the expanded cavity. The same cavity volume has been employed for the calculation of the *PC* for $SF_6$ (48%),[28] for which a guest volume of 78 Å$^3$ has been assumed, based on a "diameter" of

5.3 Å rather than the actual volume. The latter should be principally calculated with a comparable method to that of the cavity volume calculations, and we do in fact find a much smaller volume for $SF_6$ (52 $Å^3$, *PC* = 37%, Table 6). Finally, the guest volume of the ferrocene core was specified as 154 $Å^3$ (no details of calculation given),[14] which with the reported[4] (expanded) cavity volume of 279 $Å^3$ gives 55%. While this provides an exact match with Rebek's rule, the size estimates for the ferrocene core vary (our own value amounts to 141 $Å^3$, Table 6) and the choice of the expanded cavity volume would, for consistency, require the volumes of the attached hydroxymethyl and (trimethylammonium)methyl groups to be counted fully or partially into the guest volume. It transpires that large uncertainties in the *PC*s can result depending on how the included guest and cavity volumes are defined and calculated.

Guest *versus* cucurbituril cavity volumes were also estimated with the Voronoi-Dirichlet method, which defines confinements with molecular polyhedra rather than vdW surfaces;[124] this approach produces cavity volumes which are similar to that of the inner cavity for CB5 (Table 5), but only slightly larger than that of the truncated cavity for the larger homologues. In fact, the volume produced for CB6 (113 ± 10 $Å^3$) appears to resemble more the capacity or effective volume of CB6 estimated previously (105 $Å^3$).[31] The guest volumes produced by this method cannot be directly compared with (are larger than) the volumes in Table 6. It also predicts molecules to serve as ideal guests, which are very unlikely to be encapsulated on the basis of their molecular size (e.g., several molecules with 6 heavy atoms for CB5), which calls for refinement of this method.

Due to the largely different methods, in particular for calculating the guest volumes, and the previous restriction to a single known volume as parameter (that approximated for the expanded cavity), it was desirable to analyze larger data sets of *PC*s to draw better conclusions. We have thus calculated *PC* values for the known inclusion complexes of selected guest and residues with different CBs by using the volume of the inner cavity as reference point (Table 6). In all cases the calculated volumes of the guests fell below the calculated volume of the inner cavity, which was sensible to expect.

The *PC*s for molecules, which are included in CB5 range from 28 – 69%, suggesting that a sizable amount of void space remains in the case of smaller guests. Unfortunately, no accurate solution-phase binding constants for CB5 complexes are available, but when the data set in Table 6 is being taken as representative, a value of 47±14% is obtained as average and standard deviation. This is reasonable, especially because the data for CB5 include several gases, for which smaller *PC*s than 55% have also been reported for other host-guest complexes.[106,109,110] For example, methane complexed with a hemicarcerand[110] and cryptophane-A[106] exhibits *PC*s as low as 18% and 35%, respectively. In fact, the low *PC*s in the case of gaseous guests are in line with predictions for phase behavior.[125] When the occupancy factor, *k*, is above 0.68, the phase of matter is associated with the solid state; liquids tend to exhibit a sharp drop, to approximately 0.58. Lower values than 0.5 are characteristic for the gaseous phase of matter. Condensed phases with such low *PC*s, including the inside of host-guest complexes, resemble the environment of supercritical fluids,[106] where the gaseous guests behave as small spheres colliding with the cavity walls.

For CB6, the average *PC* was found to be 58±13%, in nice agreement with Rebek's rule. The two investigated gases (Xe and $SF_6$) have, again as expected, *PC*s at the lower end (30% and 37%). In the case of CB6, it is also known that the binding constants frequently reach a maximum when C4-C5 residues are encapsulated. This has been found to be the case for the series of alkylammonium, diammoniumalkyl, and cycloalkylammonium salts. The determined *PC*s for these C4 groups (e.g., 52% for the cyclobutyl ring group) are in fact close to 55% and rationalize this experimental finding. In contrast, some guests are sufficiently small to be included inside CB6, but too large to be comfortably bound, at least in solution. Interestingly, the benzene group is with 6 carbons already somewhat too large (*PC* = 63%) to be ideally bound, and, not surprisingly, it is a poor recognition motif for CB6.[16,126] For the cyclohexyl group, the *PC* increases even to 73%, and the corresponding cyclohexylmethylamine has indeed a hardly detectable binding (10 $M^{-1}$, Table 3).[31] The azoalkane DBH has a *PC* of 68%; it binds somewhat more strongly (1300 $M^{-1}$, Table 3), but clearly more weakly than smaller guests. The *PC* of DBO (78%) becomes ultimately too large to allow it to bind, although in this case a kinetic hindrance towards binding cannot be ruled out either.[31]

For CB7, many groups are known to bind inside the cavity, but for the smaller ones, particularly alkyl chains, the co-existence of residual water in the cavity cannot be excluded.[127-130] We have therefore entered in Table 6 only neutral guests, which have 6 or more heavy atoms included, and residues, which give rise to large binding constants (see Table 4). The resulting average *PC* (52±10%) agrees with what is expected for guests immersed in such cavities, although the maximum affinity appears to peak at 60% packing (values for ferrocene and adamantane); however, the "potential" appears to be rather shallow since guests with *PC*s of only 45-50% (DBO and BCO) bind also very strongly with CB7 (Table 4). The same agreement holds for the representatively selected guests for CB8 (*PC* = 53±15%), although this appears to be a coincidence in view of the error, which is expected to become larger as the size of the host increases and its rigidity decreases.

While the agreement with the ideal *PC* between these largely different host molecules (cucurbiturils and capsules) may come as a surprise, the associated analysis is extremely valuable to rationally design guests with maximum binding,[14] to modulate binding constants by structural modifications, and to predict whether a guest can be at all included. The consistency between the determined *PC*s and the anticipated one, regardless of the investigated CB homologues, demonstrates also that the choice of the inner cavity as the one relevant for binding of hydrophobic residues is self-consistent. The use of the expanded or truncated cavities would have led to *average PC*s quite different from 55% (e.g., 44% for the expanded cavity of CB7), and for some combinations far too large (e.g., 88%, for the truncated cavity of CB6) when compared with the accepted range of typical *PC*s in host-guest complexes (45%-65%).[105]

#### 4.4. Bond Dipole Regions

The bond dipole regions (Table 5) can be fully occupied by added inorganic ions or cationic pendant groups of the guests. Also water molecules can be centered in the portal region, as seen in one polymorphous crystal structure of CB6.[80] The bond dipole regions of CB5 are very small, only 15 $Å^3$ per side, and this value is very likely to be insufficient to allow atoms to be permanently positioned in this "bottleneck", although a breathing motion of the portals can be imagined to

allow the entry of guests into the interior. In fact, there is only a single report in which a guest molecule has been presumed to be threaded through the CB5 portal.[131]

The bond dipole regions for CB6 are more than twice as large (ca. 35 Å$^3$ on each side), while a very early prediction has placed this volume as 30 Å$^3$.[31] This is sufficiently large for threading, a property which has been abundantly employed in the construction of rotaxanes.[132-135] The isobutyl group is still sufficiently small to thread through the portal,[136] while the neopentyl group serves as a permanent stopper in rotaxane architectures.[100] Commonly, methylene groups, firstly the size-matching ammonium-methyl groups, are the ones found to occupy the bond dipole region in many CB6 complexes;[18,76] already a 1-ammonium-ethyl group is too large to fit in.[18] The bond dipole regions for the larger homologues become ultimately so spacious (> 100 Å$^3$, Table 5) that the permanent positioning of larger fragments such as phenyl rings becomes spatially viable,[23,137-139] and has in fact been observed in crystal structures, e.g., for CB8.[140] Hydrophobic regions of guests positioned in the bond dipole region of the larger CBs may still not be favorable, though, because they prevent or decrease synergetic electrostatic interactions.

## 5. The Hydrophobic Driving Force for Complexation

It is well established that the complete immersion of organic guests inside macrocyclic hosts, or their partial immersion, namely of certain residues of larger organic molecules, is driven by "hydrophobic interactions". These have already given rise to ample discussions in the biological[141-143] as well as supramolecular communities,[144,145] starting from their definition to how they can be characterized both conceptually and experimentally. They are routinely considered, in combination with electrostatic interactions as well as specific topological interactions, such as C–H---π or π-π interactions,[38] to present the driving force for complexation of most organic molecules or residues inside the cavities of cyclodextrins, calixarenes, resorcinarenes, cavitands, and self-assembling capsules. CBs present no exception in this respect. The statement that "the encapsulation of alkyl chains of ammonium or diammonium salts into CB6, or of adamantyl or ferrocenyl residues into CB7 is driven by hydrophobic interactions" will accordingly meet no opposition.

But what are exactly the hydrophobic interactions with CBs, and why are they fundamentally different from those with cyclodextrins and calixarenes? Most importantly, hydrophobic interactions are frequently lumped together with dispersion interactions. These two intermolecular interactions are often difficult to dissect, because they are both thought to reach their maximum for "hydrophobic" guests in aqueous solution.[38] This conjecture, however, turns out to be incorrect for CBs, because the polarizability of their cavity is actually lower than that of water, such that dispersion interactions of hydrophobic guests or residues will actually slightly favor immersion in water over that in the CB cavity. Consequently, the immersion of neutral guests or organic residues in CBs is the result of "pure" hydrophobic interactions (assuming that the electrostatic interactions with the carbonyl rim are either negligible or have been corrected for).

### 5.1. Release of Water Molecules from the Cavity

The driving force, which leads to the encapsulation of hydrophobic guests inside CBs, will be largely determined by the *number* of water molecules contained in their cavity (mainly an entropic contribution according to the Frank-Evans effect)[38] and the height of *their energy* (nonclassical effect with predominant enthalpic contribution).[146] Estimates for the number of water molecules are found in Table 7. Three methods were employed: 1) Crystal structures of CBs with or without cations complexed to the carbonyl portals, but always without encapsulated guests, were inspected. 2) Molecular dynamics (MD) calculations in explicit water were carried out. 3) Predictions were made from the calculated inner cavity volumes, the volume of a water molecule (17 Å$^3$) and by assuming an ideal *PC* of 55%. The entirely independent approaches afforded values in very good agreement, especially if one considers that some water molecules in the crystal structures of the smaller CBs may have escaped detection due to disorder. We recommend the values derived from the *PC*s as best estimates of the number of water molecules contained in the inner cavity of the different CBs. They have the added advantage that they can be directly compared with the guest volumes in Table 6, which allows estimates on how many water molecules a particular guest can expel at the minimum. Note that predictions on the number of water molecules occupying the bond dipole regions near the portals are more challenging, because specific dipole-dipole interactions are expected to become dominant, and those may differ strongly in the solid phase *versus* solution.

**Table 7.** Occupancy of the inner cavities of CBs with water molecules (recommended values shown in **boldface**).

| CB*n* | number of water molecules in inner cavity | | |
|---|---|---|---|
| | X-ray [a] | MD simulations [b] | ***PC* analysis [c]** |
| CB5 | 1-2 [d] | 2 | **2** |
| CB6 | 3-4 [e] | 4 [3] [f] | **4** |
| CB7 | - - - | 7 | **8** |
| CB8 | 11-12 [g] | 10 | **12** |
| CB9 | - - - | 14 | **16** |
| CB10 | - - - | 20 | **22** |

[a] Number of water molecules found in the cavity in the absence of encapsulated guests; disordered molecules were counted according to their occupancy, where available. [b] Determined from MD simulations with the Amber8 software,[151] see Supporting Information for details. [c] Determined by assuming an ideal *PC* of 55%, a volume per water molecule of 17 Å$^3$, and the inner cavity volumes from Table 5. [d] The following three CB5 structures were analyzed (CCDC codes): LIRTEL, BOHXEC, and TANJEY from refs [4,78,79]. [e] The following three CB6 structures were analyzed (codes from CCDC database): BEBDOB, RIPKUX, and KOBNEV from refs [3,78,80]. [f] Value in square brackets from ref. [152]. [g] The following two CB8 structures were analyzed (codes from CCDC database): RIPKOR and LIRTOV from refs [4,78].

Accordingly, the cavity of CB5 houses 2 water molecules, that of CB6 4, that of CB7 8, and that of CB8 12 (see Table 7). The comparison with cyclodextrins (CDs) is interesting, where the $\alpha$ homologue accommodates also 2 water molecules, the $\beta$ homologue 6 to 7, and the $\gamma$ one 12.[147,148] Thus, even though $\alpha$-CD is frequently compared with CB6 due to its similar dimensions,[149] it presents a better match with CB5 in terms of the number of water molecules released upon guest binding. CB7, in turn, may have a slightly higher

"water content" than $\beta$-CD, to which it is frequently compared.[49,84] Only for CB8 and $\gamma$-CD the common conception in terms of identical cavity sizes works out perfectly.[5] The largest isolated CB, CB10, seems to contain a similar amount of water as the large-ring $\varepsilon$-CD (22 to 26).[150]

For CB7, the adamantyl, ferrocenyl, and bicyclic bicyclo[2.2.2]octyl groups (DBO and BCO, Table 4) are good examples of large hydrophobic groups, which are capable of removing all water molecules from the inner cavity (Figure 4). Their inclusion should result in a comparable nonclassical, i.e., enthalpic, hydrophobic effect due to removal of very-high-energy water. The modulation in binding constants for these guests must consequently be due to differential desolvation of the hydrophobic residues, which presents an important factor in the thermodynamics of binding to any macrocycle, not only CBs. Instructive is the comparison of equally large residues. While the ferrocenyl/adamantyl couple is discussed below, among the neutral bicyclo[2.2.2]octyl derivatives, the ca. 3 orders of magnitude lower binding constant of DBO relative to BCO (Table 4) can be accounted for in terms of the strongly dipolar azo group in DBO, which renders this residue highly water-soluble even in the absence of auxiliary hydroxyl groups. The bicyclic hydrocarbon anchor in BCO has, however, a smaller solvent-accessible surface than the tricyclic adamantyl core, which results in a comparably smaller desolvation and, therefore, lower affinity to CB7. Only if the desolvation of both host *and* guest remain rather constant, similar affinities are expected. This has been found to be the case for longer chains with hydrophilic heads such as alcohols and carboxylic acids, which always penetrate with the same head group and approximately the same depth into CB6, and consequently afford very small variations in binding constants (Table 3).

If one assumes that the number of released very-high-energy water molecules dominates the driving force of CB complexation (this should hold best for the smaller homologues, up to CB7), one expects a strong increase in maximal binding constant for neutral cavity binders with increasing size of the host.[153] Indeed, such a trend becomes very obvious when comparing the binding constants of CB6 (Table 3) with those of CB7 (Table 4).

Unfortunately, few homologous series of binding constants of neutral guests with different CBs are available to further test these predictions, while the available calorimetric data are yet too heterogeneous to draw rigorous conclusions.[14,24,25,76,88,102,130,139,154] The ultrahigh affinity guests for CB7,[69] for example, differ in their pendant groups, e.g., one *versus* two hydroxymethyl groups or an aminomethyl *versus* a trimethylammoniummethyl one. Discussions of calorimetric data have frequently focused on enthalpy-entropy compensations (or the lack of them), mainly for organic ammonium salts.[14,69,139,154] These are interesting to be contrasted to the findings for other macrocycles such as cyclodextrins, but allow limited conceptual understanding, which would facilitate to pin-point the peculiarities of the inner-cavity binding of neutral guests with CBs. In fact, the value of enthalpy-entropy correlations in the context of supramolecular binding mechanisms has been questioned.[155-162]

### 5.2. The Unimportance of Dispersion Interactions

The discussion on the unimportance of dispersion interactions, which we have started early,[31] and continue here is not a semantic one. A famous example of a CB host-guest complex is that of 1,1'-bis(trimethylammoniummethyl)ferrocene, which achieves avidin-biotin affinity with CB7.[14,69] Optimal vdW contacts have been held responsible for the high affinity, which would imply that dispersion interactions between the ferrocene core and CB7 are an important contributor. We contend that the complexation of ferrocene is not driven by dispersion (i.e., attractive vdW) interactions, but solely by the complete removal of very-high-energy water from the CB cavity (which can be achieved by many other, also slightly smaller residues) *and* the concomitant desolvation of the large ferrocenyl core. Recall that the dispersion energy, within London's theoretical framework of dispersion interactions,[38,141,145,163] increases linearly with the product of the polarizabilities of the interacting partners, and decreases steeply with increasing distance ($R^{-6}$ dependence). However, the most recent affinity data (see alcohols in Figure 4 and Table 4)[69] reveal that the saturated and less polarizable adamantane anchor and even the considerably smaller (*cf.* Table 6) bicyclo[2.2.2]octane scaffold have larger or similar affinities to CB7 than ferrocene, respectively. It appears that the ferrocenyl group is better "solvated" in water than the isosteric adamantyl one (*cf.* Table 6), in line with the notion that a polarizable residue will experience a larger microenvironmental polarizability (Table 1) and, thus, dispersive stabilization in bulk water. It transpires that dispersion interactions inside the CB cavity do not present an overall enthalpic driving force for guest inclusion.

Further in-depth scrutiny of the literature reveals that there is not a single experimental or theoretical indication that dispersion interactions drive the complexation of CBs in aqueous solution. On the opposite – experimental evidence speaks against it. Dispersion interactions are always larger for aromatic molecules and those containing heavy atoms than for saturated hydrocarbons. However, such molecules do not possess a particularly high affinity for CBs. The exchange of methylene groups by sulfur in alkylammonium guests causes no systematic increase in affinity with CB6.[18] The benzene *versus* cyclopentyl rings as well as the toluene *versus* cyclohexyl rings have comparable volumes (are approximately "isosteric", Table 6) and are both sufficiently large to efficiently remove all water molecules from the CB6 cavity. However, as previously noticed, it is the less polarizable cyclopentyl ring, which binds strongly with CB6, not the benzene ring:[31] The gain in dispersion interaction of a benzene ring with water is larger than the gain of a cycloalkyl residue with water, such that it shows a weak affinity for CBs in general.[164] There is also no experimental indication that aryl rings would bind more strongly to CB7 than cyclohexyl rings, and the example of ferrocene *versus* the isosteric adamantane has already been elaborated on.[14,81] The accurate theoretical evaluation of dispersion interactions in CB complexes would, on the other hand, require MP2 calculations at high levels instead of the popular DFT calculations.[165] To the best of our knowledge, these have not yet been performed.

The observed trend towards a preferential binding of saturated over unsaturated hydrocarbons with CBs is *opposite* to that observed for the formation of complexes with porphyrins, where dispersion interactions are in fact dominant.[38] It is also in contrast to the binding preferences of cyclodextrins and calixarenes, for which the dispersion interactions are presumed to be largest between aryl rings and the cavities.[38] This "inverted" selectivity establishes CBs as macrocycles with highly distinctive binding preferences.

## 6. Outlook

Cucurbit[*n*]urils stand out among macrocyclic hosts with respect to their high affinities for cationic guests and the low polarizability of their cavity, which gives rise to interesting selectivities, e.g., a preferential binding of aliphatic *versus* aromatic guests. This intrinsic selectivity has still not been fully exploited. The study of neutral guest binding, in particular, is still in its early stages, but essential to understand the hydrophobic driving force for complexation by cucurbiturils. (*i*) The interplay between repulsive and attractive van der Waals interactions (the latter being dispersion), (*ii*) between the classical and nonclassical hydrophobic effect (the latter being related to the release of the very-high-energy water molecules from the inner cavities), (*iii*) the contribution of quadrupole interactions, and (*iv*) the packing coefficients discussed herein are all *desiderata* which deserve more detailed attention in future studies. These may include experimentally in the solution phase the systematic investigation of homologous series of *neutral* guests, also by calorimetric methods, and mass spectrometry with *neutral* guests in the gas phase to eliminate the influence of the solvent (ionization could be achieved either by docked metal ions or, for CB8, by employing a charged first guest). High in demand are also quantum-chemical calculations at sufficiently high levels (e.g., MP2) to quantify dispersion contributions and quantum mechanics/molecular mechanics hybrid calculations with explicit water molecules in order to evaluate their release from the cavity.

## Acknowledgements

The authors thank the Deutsche Forschungsgemeinschaft (DFG), the Fonds der Chemischen Industrie, the Deutscher Akademischer Austausch Dienst (DAAD), and the Center for Functional Materials and Nanomolecular Science (NanoFun) for their continued support, including graduate fellowships for MF and KIA. WMN thanks Pablo Ballester (ICIQ, Tarragona, Spain) for his advice on cavity volume calculations.

## References

[1] E. Meyer, **1904**, Inaugural-Dissertation, Heidelberg, Germany.
[2] R. Behrend, E. Meyer, F. Rusche, *Justus Liebigs Ann. Chem*. **1905**, *339*, 1-37.
[3] W. A. Freeman, W. L. Mock, N. Y. Shih, *J. Am. Chem. Soc*. **1981**, *103*, 7367-7368.
[4] J. Kim, I. S. Jung, S. Y. Kim, E. Lee, J. K. Kang, S. Sakamoto, K. Yamaguchi, K. Kim, *J. Am. Chem. Soc.* **2000**, *122*, 540-541.
[5] J. W. Lee, S. Samal, N. Selvapalam, H. J. Kim, K. Kim, *Acc. Chem. Res.* **2003**, *36*, 621-630.
[6] A. Day, A. P. Arnold, R. J. Blanch, B. Snushall, *J. Org. Chem*. **2001**, *66*, 8094-8100.
[7] A. I. Day, R. J. Blanch, A. P. Arnold, S. Lorenzo, G. R. Lewis, I. Dance, *Angew. Chem.* **2002**, *114*, 285-287; *Angew. Chem. Int. Ed*. **2002**, *41*, 275-277.
[8] S. M. Liu, P. Y. Zavalij, L. Isaacs, *J. Am. Chem. Soc.* **2005**, *127*, 16798-16799.
[9] J. Lagona, P. Mukhopadhyay, S. Chakrabarti, L. Isaacs, *Angew. Chem*. **2005**, *117*, 4922–4949; *Angew. Chem. Int. Ed*. **2005**, *44*, 4844-4870.
[10] C. Márquez, F. Huang, W. M. Nau, *IEEE Trans. Nanobiosci*. **2004**, *3*, 39-45.
[11] W.-H. Huang, S. Liu, L. Isaacs, in *Modern Supramolecular Chemistry* (Eds.: F. Diederich, P. J. Stang, R. R. Tykwinski), Wiley-VCH, Weinheim, **2008**, pp. 113-142.
[12] D. Jiao, N. Zhao, O. A. Scherman, *Chem. Commun*. **2010**, *46*, 2007-2009.
[13] Note that CBs have little, if not negligible cellular and *in vivo* toxicity, *cf*. V. D. Uzunova, C. Cullinane, K. Brix, W. M. Nau, A. I. Day, *Org. Biomol. Chem*. **2010**, *8*, 2037-2042, and G. Hettiarachchi, D. Nguyen, J. Wu, D. Lucas, D. Ma, L. Isaacs, V. Briken, *PLoS ONE* **2010**, *5*, e10514. doi:10.1371/journal.pone.0010514.
[14] M. V. Rekharsky, T. Mori, C. Yang, Y. H. Ko, N. Selvapalam, H. Kim, D. Sobransingh, A. E. Kaifer, S. Liu, L. Isaacs, W. Chen, S. Moghaddam, M. K. Gilson, K. M. Kim, Y. Inoue, *Proc. Natl. Acad. Sci. U.S.A.* **2007**, *104*, 20737-20742.
[15] W. M. Nau, J. Mohanty, *Int. J. Photoenergy* **2005**, *7*, 133-141.
[16] W. L. Mock, N. Y. Shih, *J. Org. Chem*. **1983**, *48*, 3618-3619.
[17] H.-J. Buschmann, E. Cleve, K. Jansen, A. Wego, E. Schollmeyer, *J. Inclusion Phenom. Macrocyclic Chem.* **2001**, *40*, 117-120.
[18] W. L. Mock, N. Y. Shih, *J. Org. Chem*. **1986**, *51*, 4440-4446.
[19] W. L. Mock, N. Y. Shih, *J. Am. Chem. Soc*. **1988**, *110*, 4706-4710.
[20] W. L. Mock, N. Y. Shih, *J. Am. Chem. Soc*. **1989**, *111*, 2697-2699.
[21] K. Moon, A. E. Kaifer, *Org. Lett.* **2004**, *6*, 185-188.
[22] F. Wei, S. Liu, L. Xu, G. Z. Cheng, C. T. Wu, Y. Q. Feng, *Electrophoresis* **2005**, *26*, 2214-2224.
[23] M. I. El-Barghouthi, K. I. Assaf, A. M. M. Rawashdeh, *J. Chem. Theory Comput*. **2010**, *6*, 984-992.
[24] M. V. Rekharsky, Y. H. Ko, N. Selvapalam, K. Kim, Y. Inoue, *Supramol. Chem*. **2007**, *19*, 39-46.
[25] H.-J. Buschmann, K. Jansen, E. Schollmeyer, *Thermochim. Acta* **2000**, *346*, 33-36.
[26] M. El Haouaj, Y. H. Ko, M. Luhmer, K. Kim, K. Bartik, *J. Chem. Soc., Perkin Trans. 2* **2001**, 2104-2107.
[27] M. El Haouaj, M. Luhmer, Y. H. Ko, K. Kim, K. Bartik, *J. Chem. Soc., Perkin Trans. 2* **2001**, 804-807.
[28] L. Fusaro, E. Locci, A. Lai, M. Luhmer, *J. Phys. Chem. B* **2008**, *112*, 15014-15020.
[29] Y. M. Jeon, J. Kim, D. Whang, K. Kim, *J. Am. Chem. Soc.* **1996**, *118*, 9790-9791.
[30] B. S. Kim, Y. H. Ko, Y. Kim, H. J. Lee, N. Selvapalam, H. C. Lee, K. Kim, *Chem. Commun*. **2008**, 2756-2758.
[31] C. Márquez, R. R. Hudgins, W. M. Nau, *J. Am. Chem. Soc.* **2004**, *126*, 5806-5816.
[32] Y. Miyahara, K. Abe, T. Inazu, *Angew. Chem*. **2002**, *114*, 3146–3149; *Angew. Chem. Int. Ed*. **2002**, *41*, 3020-3023.
[33] K. A. Kellersberger, J. D. Anderson, S. M. Ward, K. E. Krakowiak, D. V. Dearden, *J. Am. Chem. Soc.* **2001**, *123*, 11316-11317.
[34] S. Y. Kim, I. S. Jung, E. Lee, J. Kim, S. Sakamoto, K. Yamaguchi, K. Kim, *Angew. Chem*. **2001**, *113*, 2177–2179; *Angew. Chem. Int. Ed*. **2001**, *40*, 2119-2121.
[35] J. X. Liu, R. L. Lin, L. S. Long, R. B. Huang, L. S. Zheng, *Inorg. Chem. Commun.* **2008**, *11*, 1085-1087.
[36] H. Fujiwara, H. Arakawa, S. Murata, Y. Sasaki, *Bull. Chem. Soc. Jpn.* **1987**, *60*, 3891-3894.
[37] K. Kim, N. Selvapalam, D. H. Oh, *J. Inclusion Phenom. Macrocyclic Chem*. **2004**, *50*, 31-36.
[38] H.-J. Schneider, *Angew. Chem.* **2009**, *121*, 3982-4036; *Angew. Chem. Int. Ed*. **2009**, *48*, 3924-3977.
[39] C. Reichardt, *Solvents and Solvent Effects in Organic Chemistry*, Wiley-VCH, Weinheim, **1988**.
[40] M. A. Rankin, B. D. Wagner, *Supramol. Chem*. **2004**, *16*, 513-519.
[41] J. Mohanty, W. M. Nau, *Angew. Chem*. **2005**, *117*, 3816-3820; *Angew. Chem. Int. Ed*. **2005**, *44*, 3750-3754.
[42] B. D. Wagner, P. J. MacDonald, *J. Photochem. Photobiol. A* **1998**, *114*, 151-157.

[43] B. D. Wagner, P. J. MacDonald, M. Wagner, *J. Chem. Educ.* **2000**, *77*, 178-181.
[44] T. Arimura, T. Nagasaki, S. Shinkai, T. Matsuda, *J. Org. Chem.* **1989**, *54*, 3766-3768.
[45] C. Márquez, W. M. Nau, *Angew. Chem.* **2001**, *113*, 4515-4518; *Angew. Chem. Int. Ed.* **2001**, *40*, 4387-4390.
[46] C. Reichardt, M. Eschner, G. Schäfer, *J. Phys. Org. Chem.* **2001**, *14*, 737-751.
[47] H. Bakirci, W. M. Nau, *Adv. Funct. Mater.* **2006**, *16*, 237-242.
[48] J. Mohanty, W. M. Nau, *Photochem. Photobiol. Sci.* **2004**, *3*, 1026-1031.
[49] Y. Liu, C. J. Li, D. S. Guo, Z. H. Pan, Z. Li, *Supramol. Chem.* **2007**, *19*, 517-523.
[50] W. M. Nau, X. Zhang, *J. Am. Chem. Soc.* **1999**, *121*, 8022-8032.
[51] H. Bakirci, A. L. Koner, W. M. Nau, *J. Org. Chem.* **2005**, *70*, 9960-9966.
[52] A. L. Koner, C. Márquez, M. H. Dickman, W. M. Nau, *Angew. Chem.* **2011**, *123*, 567-571; *Angew. Chem. Int. Ed.* **2011**, *50*, 545-548.
[53] A. L. Koner, W. M. Nau, *Supramol. Chem.* **2007**, *19*, 55-66.
[54] D. J. Cram, *Nature* **1992**, *356*, 29-36.
[55] D. J. Cram, M. E. Tanner, R. Thomas, *Angew. Chem.* **1991**, *103*, 1048–1051; *Angew. Chem. Int. Ed.* **1991**, *30*, 1024-1027.
[56] S. J. Strickler, R. A. Berg, *J. Chem. Phys.* **1962**, *37*, 814-822.
[57] W. M. Nau, A. Hennig, A. L. Koner, in *Springer Ser Fluorescence Vol. 4* (Ed.: M. N. Berberan-Santos), Springer, **2008**, pp. 185-211.
[58] W. M. Nau, F. Huang, X. Wang, H. Bakirci, G. Gramlich, C. Márquez, *Chimia* **2003**, *57*, 161-167.
[59] J. R. Lakowicz, *Anal. Biochem.* **2001**, *298*, 1-24.
[60] R. L. Halterman, J. L. Moore, K. A. Yakshe, J. A. I. Halterman, K. A. Woodson, *J. Inclusion Phenom. Macrocyclic Chem.* **2010**, *66*, 231-241.
[61] H.-J. Buschmann, *Vom Wasser* **1995**, *84*, 263-269.
[62] R. L. Halterman, J. L. Moore, L. M. Mannel, *J. Org. Chem.* **2008**, *73*, 3266-3269.
[63] J. Mohanty, H. Pal, A. K. Ray, S. Kumar, W. M. Nau, *ChemPhysChem* **2007**, *8*, 54-56.
[64] J. Mohanty, K. Jagtap, A. K. Ray, W. M. Nau, H. Pal, *ChemPhysChem* **2010**, *11*, 3333-3338.
[65] T. A. Martyn, J. L. Moore, R. L. Halterman, W. T. Yip, *J. Am. Chem. Soc.* **2007**, *129*, 10338-10339.
[66] M. J. Frisch, G. W. Trucks, H. B. Schlegel, G. E. Scuseria, M. A. Robb, J. R. Cheeseman, J. A. Montgomery, T. V. Jr., K. N. Kudin, J. C. Burant, J. M. Millam, S. S. Iyengar, J. Tomasi, V. Barone, B. Mennucci, M. Cossi, G. Scalmani, N. Rega, G. A. Petersson, H. Nakatsuji, M. Hada, M. Ehara, K. Toyota, R. Fukuda, J. Hasegawa, M. Ishida, T. Nakajima, Y. Honda, O. Kitao, H. Nakai, M. Klene, X. Li, J. E. Knox, H. P. Hratchian, J. B. Cross, V. Bakken, C. Adamo, J. Jaramillo, R. Gomperts, R. E. Stratmann, O. Yazyev, A. J. Austin, R. Cammi, C. Pomelli, J. W. Ochterski, P. Y. Ayala, K. Morokuma, G. A. Voth, P. Salvador, J. J. Dannenberg, V. G. Zakrzewski, S. Dapprich, A. D. Daniels, M. C. Strain, O. Farkas, D. K. Malick, A. D. Rabuck, K. Raghavachari, J. B. Foresman, J. V. Ortiz, Q. Cui, A. G. Baboul, S. Clifford, J. Cioslowski, B. B. Stefanov, G. Liu, A. Liashenko, P. Piskorz, I. Komaromi, R. L. Martin, D. J. Fox, T. Keith, M. A. Al-Laham, C. Y. Peng, A. Nanayakkara, M. Challacombe, P. M. W. Gill, B. Johnson, W. Chen, M. W. Wong, C. Gonzalez, J. A. Pople, *Gaussian 03 Revision E.01*, Gaussian, Inc., Wallingford CT, 2004.
[67] R. V. Pinjari, S. P. Gejji, *J. Phys. Chem. A* **2008**, *112*, 12679-12686.
[68] G. L. D. Ritchie, M. K. Cooper, R. L. Calvert, G. R. Dennis, L. Phillips, J. Vrbancich, *J. Am. Chem. Soc.* **1983**, *105*, 5215-5219.
[69] S. Moghaddam, C. Yang, M. Rekharsky, Y. H. Ko, K. Kim, Y. Inoue, M. K. Gilson, *J. Am. Chem. Soc.* **2011**, *133*, 3570–3581.
[70] D. G. Samsonenko, A. V. Virovets, J. Lipkowski, O. A. Gerasko, V. P. Fedin, *Journal of Structural Chemistry* **2002**, *43*, 664-668.
[71] Y. Ling, J. T. Mague, A. E. Kaifer, *Chem. Eur.J.* **2007**, *13*, 7908-7914.
[72] I. Hwang, W. S. Jeon, H.-J. Kim, D. Kim, Hyunuk Kim, N. Selvapalam, N. Fujita, S. Shinkai, K. Kim, *Angew. Chem. Int. Ed.* **2007**, *46*, 210-213.
[73] L. Isaacs, *Chem. Commun.* **2009**, 619-629.
[74] I. W. Wyman, D. H. Macartney, *Org. Biomol. Chem.* **2008**, *6*, 1796-1801.
[75] X. L. Ni, Y. Q. Zhang, Q. J. Zhu, S. F. Xue, Z. Tao, *J. Mol. Struct.* **2008**, *876*, 322-327.
[76] Y. Kim, H. Kim, Y. H. Ko, N. Selvapalam, M. V. Rekharsky, Y. Inoue, K. Kim, *Chem. Eur. J.* **2009**, *15*, 6143-6151.
[77] W. Ong, A. E. Kaifer, *J. Org. Chem.* **2004**, *69*, 1383-1385.
[78] D. Bardelang, K. A. Udachin, R. Anedda, I. Moudrakovski, D. M. Leek, J. A. Ripmeester, C. I. Ratcliffe, *Chem. Commun.* **2008**, 4927-4929.
[79] S. Liu, Z. Huang, X. Wu, F. Liang, C. Wu, *Chin. J. Chem.* **2004**, *22*, 1208-1210.
[80] S. Lim, H. Kim, N. Selvapalam, K. J. Kim, S. J. Cho, G. Seo, K. Kim, *Angew. Chem.* **2008**, *120*, 3400–3403; *Angew. Chem. Int. Ed.* **2008**, *47*, 3352-3355.
[81] S. Liu, C. Ruspic, P. Mukhopadhyay, S. Chakrabarti, P. Y. Zavalij, L. Isaacs, *J. Am. Chem. Soc.* **2005**, *127*, 15959-15967.
[82] D. Whang, J. Heo, J. H. Park, K. Kim, *Angew. Chem.* **1998**, *110*, 83-85; *Angew. Chem. Int. Ed.* **1998**, *37*, 78-80.
[83] E. Mezzina, F. Cruciani, G. F. Pedulli, M. Lucarini, *Chem. Eur. J.* **2007**, *13*, 7223-7233.
[84] J. Mohanty, A. C. Bhasikuttan, W. M. Nau, H. Pal, *J. Phys. Chem. B* **2006**, *110*, 5132-5138.
[85] M. Shaikh, J. Mohanty, P. K. Singh, W. M. Nau, H. Pal, *Photochem. Photobiol. Sci.* **2008**, *7*, 408-414.
[86] A. L. Koner, I. Ghosh, N. Saleh, W. M. Nau, *Can. J. Chem.* **2011**, *89*, 139-147.
[87] M. Shaikh, S. D. Choudhury, J. Mohanty, A. C. Bhasikuttan, W. M. Nau, H. Pal, *Chem. Eur. J.* **2009**, *15*, 12362 – 12370.
[88] W. S. Jeon, K. Moon, S. H. Park, H. Chun, Y. H. Ko, J. Y. Lee, E. S. Lee, S. Samal, N. Selvapalam, M. V. Rekharsky, V. Sindelar, D. Sobransingh, Y. Inoue, A. E. Kaifer, K. Kim, *J. Am. Chem. Soc.* **2005**, *127*, 12984-12989.
[89] R. Wang, D. H. Macartney, *Org. Biomol. Chem.* **2008**, *6*, 1955-1960.
[90] Y. Y. Zhou, J. Yang, M. Liu, S. F. Wang, Q. Lu, *J. Lumin.* **2010**, *130*, 817-820.
[91] A. Flinn, G. C. Hough, J. F. Stoddart, D. J. Williams, *Angew. Chem.* **1992**, *104*, 1550–1551; *Angew. Chem. Int. Ed.* **1992**, *31*, 1475-1477.
[92] Y. Q. Zhang, Q. J. Zhu, S. F. Xue, Z. Tao, *Molecules* **2007**, *12*, 1325-1333.
[93] J. X. Liu, L. S. Long, R. B. Huang, L. S. Zheng, *Inorg. Chem.* **2007**, *46*, 10168-10173.
[94] CB5 has a much higher tendency to include anions than other CBs, at least in the solid state. This tendency is not understood. While in the case of cyclodextrins dispersion interactions are considered to be largest (*cf.* V. Rüdiger, A. Eliseev, S. Simova, H. J. Schneider, M. J. Blandamer, P. M. Cullis, A. J. Meyer, *J. Chem. Soc., Perkin Trans. 2* **1996**, 2119-2123 and ref. 38) for the smallest homologue ($\alpha$-cyclodextrin), this reason appears to be unlikely for CB5, owing to the low polarizability of CBs in general. Alternative reasons could include (*i*) a particularly high driving force for the removal of the two very-high-energy water molecules from the cavity (see Section 5), (*ii*) favourable ion pairing with cations docked to the upper rim, and/or (*iii*) geometrically more favorable electrostatic interactions of the anions with the electron-

deficient carbonyl carbons. The latter are well known to drive anion binding to the structurally related macrocycles termed hemicucurbit[6]uril, *cf.* H. J. Buschmann, E. Cleve, E. Schollmeyer, *Inorg. Chem. Commun.* **2005**, *8*, 125-127, and phrased bambus[6]uril, *cf.* J. Svec, M. Necas, V. Sindelar, *Angew. Chem.* **2010**, *122*, 2428-2431; *Angew. Chem. Int. Ed.* **2010**, *49*, 2378-2381.

[95] H. Kim, Y. Kim, M. Yoon, S. Lim, S. M. Park, G. Seo, K. Kim, *J. Am. Chem. Soc.* **2010**, *132*, 12200-12202.

[96] R. J. Blanch, A. J. Sleeman, T. J. White, A. P. Arnold, A. I. Day, *Nano Lett.* **2002**, *2*, 147-149.

[97] R. Wang, L. Yuan, D. H. Macartney, *J. Org. Chem.* **2006**, *71*, 1237-1239.

[98] A. D. St-Jacques, I. W. Wyman, D. H. Macartney, *Chem. Commun.* **2008**, 4936-4938.

[99] I. W. Wyman, D. H. Macartney, *Org. Biomol. Chem.* **2010**, *8*, 253-260.

[100] D. Tuncel, O. Özsar, H. B. Tiftik, B. Salih, *Chem. Commun.* **2007**, 1369-1371.

[101] N. Saleh, A. L. Koner, W. M. Nau, *Angew. Chem.* **2008**, *120*, 5478–5481; *Angew. Chem. Int. Ed.* **2008**, *47*, 5398-5401.

[102] C. Meschke, H.-J. Buschmann, E. Schollmeyer, *Thermochim. Acta* **1997**, *297*, 43-48.

[103] V. Kolman, R. Marek, Z. Strelcova, P. Kulhanek, M. Necas, J. Svec, V. Sindelar, *Chem. Eur. J.* **2009**, *15*, 6926-6931.

[104] N. Zhao, L. Liu, F. Biedermann, O. A. Scherman, *Chem. Asian J.* **2010**, *5*, 530-537.

[105] S. Mecozzi, J. Rebek, Jr., *Chem. Eur. J.* **1998**, *4*, 1016-1022.

[106] L. Garel, J.-P. Dutasta, A. Collet, *Angew. Chem.* **1993**, *105*, 1249-1251; *Angew. Chem. Int. Ed.* **1993**, *32*, 1169-1171.

[107] N. Branda, R. Wyler, J. Rebek, Jr., *Science* **1994**, *263*, 1267-1268.

[108] B. W. Purse, J. Rebek, Jr., *Proc. Natl. Acad. Sci. U.S.A.* **2006**, *103*, 2530-2534.

[109] A. Shivanyuk, A. Scarso, J. Rebek, Jr., *Chem. Commun.* **2003**, 1230-1231.

[110] A. V. Leontiev, A. W. Saleh, D. M. Rudkevich, *Org. Lett.* **2007**, *9*, 1753-1755.

[111] O. Taratula, P. A. Hill, N. S. Khan, P. J. Carroll, I. J. Dmochowsky, *Nat. Commun.* **2010**, *1*, 148, DOI: 10.1038/ncomms1151.

[112] N. Guex, M. Pleitsch, T. Schwede, A. Diemand, DeepView, Swiss-Pdb Viewer, Ver. 4.0.1, Swiss Institute of Bioinformatics.

[113] E. A. Mainicheva, O. A. Gerasko, L. A. Sheludyakova, D. Y. Naumov, M. I. Naumova, V. P. Fedin, *Russ. Chem. Bull.* **2006**, *55*, 267-275.

[114] L. Liu, N. Nouvel, O. A. Scherman, *Chem. Commun.* **2009**, 3243-3245.

[115] HyperChem, Ver. 7.01, Hypercube, Inc., Gainesville, FL.

[116] W. A. Freeman, *Acta Cryst.* **1984**, *B40*, 382-387.

[117] W. H. Huang, P. Y. Zavalij, L. Isaacs, *Acta Cryst.* **2007**, *E63*, o1060-o1062.

[118] L. B. Lu, Y. Q. Zhang, Q. J. Zhu, S. F. Xue, Z. Tao, *Molecules* **2007**, *12*, 716-722.

[119] A. A. Tripolskaya, O. A. Gerasko, D. Y. Naumov, V. P. Fedin, *J. Struct. Chem.* **2007**, *48*, 949-953.

[120] S. Lorenzo, A. Day, D. Craig, R. Blanch, A. Arnold, I. Dance, *Cryst. Eng. Comm.* **2001**, *49*, 1-7.

[121] V. Sindelar, M. A. Cejas, F. M. Raymo, W. Chen, S. E. Parker, A. E. Kaifer, *Chem. Eur. J.* **2005**, *11*, 7054-7059.

[122] T. V. Mitkina, D. Y. Naumov, N. V. Kurat´eva, O. A. Gerasko, V. P. Fedin, *Russ. Chem. Bull., Int. Ed.* **2006**, *55*, 26-35.

[123] T. V. Mitkina, M. N. Sokolov, D. Y. Naumov, N. V. Kuratieva, O. A. Gerasko, V. P. Fedin, *Inorg. Chem.* **2006**, *45*, 6950-6955.

[124] A. V. Virovets, V. A. Blatov, A. P. Shevchenko, *Acta Cryst. B* **2004**, *60*, 350-357.

[125] A. I. Kitaigorodsky, Academic Press, New York, **1973**, pp. 18-19.

[126] C. Klöck, R. N. Dsouza, W. M. Nau, *Org. Lett.* **2009**, *11*, 2595-2598.

[127] V. Wintgens, L. Biczók, Z. Miskolczy, *Supramolecular Chemistry* **2010**, *22*, 612-618.

[128] Z. Miskolczy, L. Biczók, M. Megyesi, I. Jablonkai, *J. Phys. Chem. B* **2009**, *113*, 1645-1651.

[129] A. Hennig, H. Bakirci, W. M. Nau, *Nature Methods* **2007**, *4*, 629-632.

[130] D. M. Bailey, A. Hennig, V. D. Uzunova, W. M. Nau, *Chem. Eur. J.* **2008**, *14*, 6069-6077.

[131] H.-J. Buschmann, E. Cleve, K. Jansen, E. Schollmeyer, *Anal. Chim. Acta* **2001**, *437*, 157-163.

[132] H.-J. Buschmann, A. Wego, E. Schollmeyer, D. Döpp, *Supramol. Chem.* **2000**, *11*, 225-231.

[133] K. Kim, *Chem. Soc. Rev.* **2002**, *31*, 96-107.

[134] M. W. Ambrogio, T. A. Pecorelli, K. Patel, N. M. Khashab, A. Trabolsi, H. A. Khatib, Y. Y. Botros, J. I. Zink, J. F. Stoddarrt, *Org. Lett.* **2010**, *12*, 3304-3307.

[135] Y. Liu, C. F. Ke, H. Y. Zhang, W. J. Wu, J. Shi, *J. Org. Chem.* **2007**, *72*, 280-283.

[136] X. Ling, E. L. Samuel, D. L. Patchell, E. Masson, *Org. Lett.* **2010**, *12*, 2730-2733.

[137] W. Ong, M. Gómez-Kaifer, A. E. Kaifer, *Org. Lett.* **2002**, *4*, 1791-1794.

[138] H. J. Kim, W. S. Jeon, Y. H. Ko, K. Kim, *Proc. Natl. Acad. Sci. U.S.A.* **2002**, *99*, 5007-5011.

[139] G. A. Vincil, A. R. Urbach, *Supramol. Chem.* **2008**, *20*, 681-687.

[140] H. J. Kim, J. Heo, W. S. Jeon, E. Lee, J. Kim, S. Sakamoto, K. Yamaguchi, K. Kim, *Angew. Chem.* **2001**, *40*, 1574-1577; *Angew. Chem. Int. Ed.* **2001**, *40*, 1526-1529.

[141] G. I. Makhatadze, P. L. Privalov, *Adv. Protein Chem.* **1995**, *47*, 307-425.

[142] J. A. Schellman, *Biophys. J.* **1997**, *73*, 2960-2964.

[143] L. R. Pratt, A. Pohorille, *Chem. Rev.* **2002**, *102*, 2671-2692.

[144] I. O. Sutherland, *Chem. Soc. Rev.* **1986**, *15*, 63-91.

[145] W. Blokzijl, J. B. F. N. Engberts, *Angew. Chem.* **1993**, *105*, 1610-1644; *Angew. Chem. Int. Ed.* **1993**, *32*, 1545-1579.

[146] W. P. Jencks, *Catalysis in Chemistry and Enzymology*, McGraw Hill, New York, **1989**.

[147] K. A. Connors, *Chem. Rev.* **1997**, *97*, 1325-1358.

[148] W. Saenger, in *Inclusion Compounds, Vol. 2* (Eds.: J. L. Atwood, J. E. Davies, D. D. McNicol), Adademic Press, New York, **1984**.

[149] H.-J. Buschmann, E. Schollmeyer, L. Mutihac, *Thermochim. Acta* **2003**, *399*, 203-208.

[150] O. Nimz, K. Imamura, J. Jacob, D. Myles, S. A. Mason, S. Kitamura, T. Aree, W. Saenger, *Acta Cryst. B* **2001**, *57*, 833-841.

[151] D. A. Case, T. A. Darden, T. E. Cheatham, C. L. Simmerling, J. Wang, R. E. Duke, R. L. Luo, K. M. Merz, B. Wang, D. A. Pearlman, M. Crowley, S. Brozell, V. Tsui, H. Gohlke, J. Mongan, V. Hornak, G. Cui, P. Beroza, C. Schafmerister, J. W. Caldwell, W. S. Ross, P. A. Kollman, AMBER 8 (2004), University of California, San Francisco, USA.

[152] K. B. Tarmyshov, F. Müller-Plathe, *J. Phys. Chem. B* **2006**, *110*, 14463-14468.

[153] If one assumes naively that the enthalpic contribution related to the release of each very-high-energy water molecule is constant ($\Delta H_w$) and increases linearly with their number ($m$) in the cavity (ignoring that the water molecules inside the smallest cavities must have the highest energies), and that it dominates the free energy (negligible entropic effect, similar to the 1,1'-bis(trimethylammoniummethyl)ferrocene complex with CB7, *cf.* ref. 14), one expects the affinity of neutral cavity binders to increase with $\exp(-m\,\Delta H_w/RT)$. By assuming a maximal binding constant of $10^{10}$ $M^{-1}$ with CB7 (see value for 1-(hydroxymethyl)adamantane in Table 4), and with $m$ = 8 from Table 7, one can estimate $-2.0$ kcal $mol^{-1}$ for $\Delta H_w$. This allows us to project maximal binding constants of $10^6$ $M^{-1}$ for CB6 and $10^3$

$M^{-1}$ for CB5. For CB6, this value has not yet been reached for neutral guests (Table 3), which may be due to the use of salt-containing solutions (see above), while for CB5 no absolute binding constants with neutral guests have yet been reported.

[154] J. J. Reczek, A. A. Kennedy, B. T. Halbert, A. R. Urbach, *J. Am. Chem. Soc.* **2009**, *131*, 2408-2415.

[155] O. Exner, *Prog. Phys. Org. Chem.* **1973**, *10*, 411-482.

[156] R. Lumry, S. Rajender, *Biopolymers* **1970**, *9*, 1125-1227.

[157] W. Linert, *Chem. Soc. Rev.* **1994**, *23*, 429-438.

[158] K. Sharp, *Protein Science* **2001**, *10*, 661-667.

[159] Y. Inoue, Y. Liu, L. H. Tong, B. J. Shen, D. S. Jin, *J. Am. Chem. Soc.* **1993**, *115*, 10637-10644.

[160] M. Rekharsky, Y. Inoue, *J. Am. Chem. Soc.* **2000**, *122*, 4418-4435.

[161] A. Cornish-Bowden, *J. Biosci.* **2002**, *27*, 121-126.

[162] D. M. Ford, *J. Am. Chem. Soc.* **2005**, *127*, 16167-16170.

[163] M. M. Taddei, T. N. C. Mendes, C. Farina, *Eur. J. Phys.* **2010**, *31*, 89-99.

[164] The fact that CB8 forms numerous 2:1 complexes with aromatic molecules (*cf.* for example, refs 139 and 140) provides no indication for significant dispersion interactions either, because one of the included guests (e.g., methylviologen) is always held in place by (two) ion-dipole interactions, while the inclusion of a second, electron-rich aromatic neutral guest (e.g., 2,6-dihydroxynaphthalene or 1,4-dihydroxybenzene) is, arguably, driven by dispersion and charge-transfer interactions with the first guest rather than with the cavity, in addition to hydrophobic interactions, see also U. Rauwald, F. Biedermann, S. Deroo, C. V. Robinson, O. A. Scherman, *J. Phys. Chem. B* **2010,** *114*, 8606-8615.

[165] D. Quiñonero, C. Garau, A. Frontera, P. Ballester, A. Costa, P. M. Deyà, *J. Phys. Chem. A* **2005**, *2005*, 4632-4637.

# APPENDIX 6

M. Florea and W. M. Nau, "Strong Binding of Hydrocarbons to Cucurbituril Probed by Fluorescent Dye Displacement: A Supramolecular Gas-Sensing Ensemble", *Angewandte Chemie International Edition*, **2011**, *50* (40), 9338-9342. doi: 10.1002/anie.201104119. 

DOI: 10.1002/anie.200((will be filled in by the editorial staff))

# Strong Binding of Hydrocarbons to Cucurbituril Probed by Fluorescent Dye Displacement: A Supramolecular Gas-Sensing Ensemble**

*Mara Florea and Werner M. Nau**

The inclusion of small hydrocarbons into molecular container compounds in solution has received considerable attention.[1-9] It allows for a puristic understanding of the solvophobic driving force for the formation of discrete host-guest complexes,[10] and has additional potential for gas storage, uptake, and separation, thus complementing solid-state applications of porous materials[11,12] or surface-immobilized macrocycles.[13] Studies on the precipitation of complexes between the smallest alkanes with $\alpha$-cyclodextrin date back to the 1950's.[14] Subsequently, synthetic hosts such as cryptophanes[1], self-assembling capsules,[2-5] and hemicarcerands[6,7] have been investigated for their potential to entrap small hydrocarbons. Herein, we describe a highly sensitive fluorescence-based method for the quantification of volatile hydrocarbons binding with cucurbituril. We observe exceptionally strong, highly selective, and reversible binding in aqueous solution.

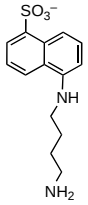


**1**

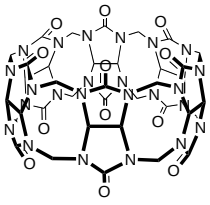

CB6

Cucurbit[*n*]urils (CB*n*) are water-soluble, highly symmetrical pumpkin-shaped synthetic macrocycles,[15,16] and their unique supramolecular chemistry is presently unfolding.[17,18] They are well established to bind organic ammonium ions through a combination of hydrophobic interactions inside the nonpolar inner cavity and ion-dipole interactions with the carbonyl portals. While a CB5 derivative has been reported to bind very small guests such as methane and acetylene,[12,19] the homologue which holds most promise for hydrocarbon binding is CB6,[20] the original cucurbituril, which possesses an intermediary size to allow inclusion of guests with up to 7 heavy atoms into its inner cavity.[18,21] Unfortunately, CB6 has an intrinsically low water solubility of about 30 μM, which complicates the determination of actual binding constants.[21,22] In particular, it prevents $^1$H NMR titrations, which have been routinely employed in all previous studies on solution-phase gas binding by molecular containers.[1-9] The binding of xenon with CB6 has been studied by $^{129}$Xe NMR in the presence of 0.2 M $Na_2SO_4$,[23] where the solubility is increased (but where also the binding strength suffers, see below). Alternatively, an alkylated CB6 derivative with higher water solubility has been employed, which was also investigated by isothermal titration calorimetry, to afford a binding constant of 3400 $M^{-1}$ with xenon.[24] The binding constants, which we report herein for several simple hydrocarbons, are much larger than those observed for xenon, and, in fact, the largest ones reported for neutral guests with CB6.[18] In several cases, they exceed those previously observed for any molecular container.[1-9]

In the quest for a convenient method to monitor volatile hydrocarbon binding to CB6, we selected an indicator displacement strategy[25] based on our recently developed anchor dye approach.[26] In detail, compound **1** possesses a putrescine anchor for strong binding with CB6,[27] and a microenvironmentally highly sensitive 1-naphtylamine-5-sulfonic acid chromophore to ensure a robust fluorescence response upon binding. Complexation of **1** by CB6 increases its locally excited fluorescence band ($\lambda_{exc}$ = 283 nm, $\lambda_{obs}$ = 334 nm) by a factor of 50-1000, depending on pH; the binding constants were extracted from direct host-dye fluorescence titrations (see Supporting Information) to afford values of 4.3 × $10^7$ $M^{-1}$ in 1 mM HCl (pH 3.0) and 2.5 × $10^3$ $M^{-1}$ in 50 mM NaOAc (pH 5.5).

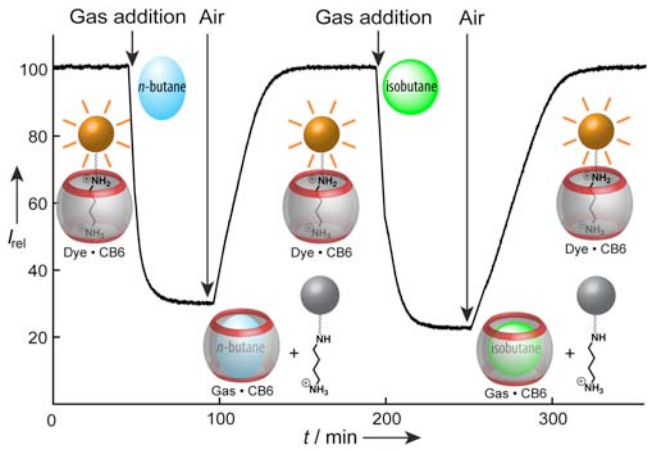


***Figure 1.*** Fluorescence-based approach for gas sensing in aqueous solution. The trace refers to actual experiments with sequential uptake and release of *n*-butane and isobutane.

The working principle for gas sensing is depicted in Figure 1. Starting from the pre-assembled highly fluorescent host-dye complex (4 μM CB6 and **1**), the addition of gas results (with an immediate onset signaling fast exchange on the time scale of the experiment) in a continuous displacement of the dye until the saturation limit has been achieved. As can be seen from Figures 1 and 2, the different hydrocarbons showed sizable effects and markedly different fluorescence responses. From the final plateau of the fluorescence intensity and the accurately known (owing to their importance for fossil energies) aqueous solubility of the

[*] M. Florea, Prof. Dr. W. M. Nau
School of Engineering and Science
Jacobs University Bremen
Campus Ring 1, 28759 Bremen, Germany
Fax: (+49) 421-200-3229
E-mail: w.nau@jacobs-university.de

[**] This work was supported by the Deutsche Forschungsgemeinschaft (DFG grant NA-686/5-1), the COST Action CM1005 "Supramolecular Chemistry in Water", and the Fonds der Chemischen Industrie (doctoral stipend for M. F.). We thank Prof. D. Klapstein and K. I. Assaf for preliminary calculations, and Dr. H.-J. Buschmann for providing us with an independently prepared reference sample of CB6.

Supporting Information for this article is available on the WWW

volatile hydrocarbons, the binding constants were directly calculated by assuming a 1:1 complexation stoichiometry (see Supporting Information), akin to competition experiments carried out, for example, by $^1$H NMR.[28] Higher-order complexes were not expected in the solution phase on the basis of packing arguments (see below) and since even xenon (volume 42 Å$^3$) shows only 1:1 binding with CB6.[23,29] Moreover, representative titrations at different gas pressures (and assuming Henry's law, Supporting Information) showed 1:1 binding isotherms and afforded the same binding constants, within error, as those obtained from repeated end-point measurements of the fluorescence intensity of gas-saturated solutions. The accuracy of the fluorescence-based method for measuring binding constants was also cross-checked for other neutral guests such as Xe, $SF_6$, tetrahydrofuran, furan, cyclopentanone, and benzene (Supporting Information), which had been previously studied by NMR in saline solution. Finally, the inclusion nature of the complexes was established by $^1$H NMR up-field shifts (in the presence of salts to achieve sufficient solubility of CB6 (Supporting Information).

***Table 1.*** Binding constants of hydrocarbons with CB6.

| | Hydrocarbon [Volume / Å$^3$] [b] | PC[c] [%] | $K$ [10$^3$ M$^{-1}$] [a] Water, pH 3.0[d] | NaOAc, pH 5.5 |
|---|---|---|---|---|
| C1 | methane [29] | 20 | < 2 | < 0.05 |
| C2 | ethane [45] | 32 | 24 [e] | 2.6 ± 0.7 |
| | ethene [41] | 29 | 3.9 | 0.25 [e] |
| | acetylene [35] | 25 | 0.11 [e] | 0.047 [e] |
| C3 | propane [63] | 44 | 180 [e] | 10 |
| | propane-$d_8$ [63] | 44 | 160 [f] | - - - |
| | propene [58] | 41 | 25 [e] | 1.4 |
| C4 | *n*-butane [80] | 56 | 280 | 4.4 |
| | 1-butene [75] | 53 | 79 | 1.3 |
| | *cis*-butene [74] | 52 | 150 | 2.1 |
| | *trans*-butene [74] | 52 | 21 | 0.32 |
| | isobutane [79] | 56 | 850 | 23 |
| | isobutane-$d_{10}$ [79] | 56 | 910 [f] | - - - |
| | isobutene [75] | 53 | 84 | 1.9 |
| C5 | *n*-pentane [96] | 68 | 9 ± 4 | 0.14 |
| | isopentane [96] | 68 | 15 ± 5 | 0.30 |
| | neopentane [96] | 68 | < 2 | < 0.05 |
| | cyclopentane [86] | 61 | 1300 ± 300 | 25 ± 10 |
| ≥C6 | higher alkanes[g] [> 102] | > 72 | < 2 | < 0.05 |

[a] Determined by competitive fluorescence displacement with the **1**·CB6 reporter pair at 298 K; error in data is 20% unless specified differently. [b] Obtained from AM1-optimized geometries. [c] Packing coefficient, obtained by dividing the guest volume by the inner cavity volume of CB6 (142 Å$^3$, from ref. [18]). [d] Adjusted with 1 mM HCl. [e] 10% error. [f] Measurement relative to protiated form. [g] *n*-hexane, isohexane, 2,3-dimethylbutane, cyclohexane, *n*-heptane.

The binding constants for the different hydrocarbons are shown in Table 1. Most important, because the fluorescence-based method allows the use of very low CB6 concentrations (0.1-4 μM), well below its solubility limit, measurements could not only be performed in 50 mM NaOAc (pH 5.5), but also in salt-free solution at pH 3.0 (1 mM HCl was employed in order to exclude pH fluctuations in the course of the measurements). The first surprise from the data in Table 1 is that the affinity of simple hydrocarbons to CB6 in water is exceptionally high, contrasting the common conception of CBs as cation-receptor macrocycles.[30] The selectivity of CB6 towards hydrocarbon binding stands out also when compared to previously investigated molecular containers.[1,2,4,9] Figure 3 shows DFT-optimized structures of the corresponding inclusion complexes, which nicely illustrate the hole-size and cavity-height matching of some representative gases.

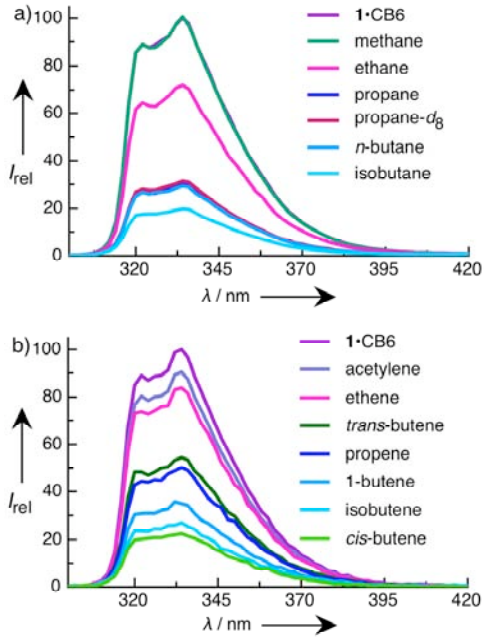


***Figure 2.*** Displacement of dye **1** (4 μM) from CB6 (4 μM) monitored by fluorescence after saturation of aqueous solutions with different gaseous a) alkanes and b) alkenes and acetylene. Measurements in water at pH 3.0, $\lambda_{exc}$ = 283 nm. Note that hydrocarbons showing similar displacements may exhibit different binding constants due to varying solubilities (cf. Supporting Information).

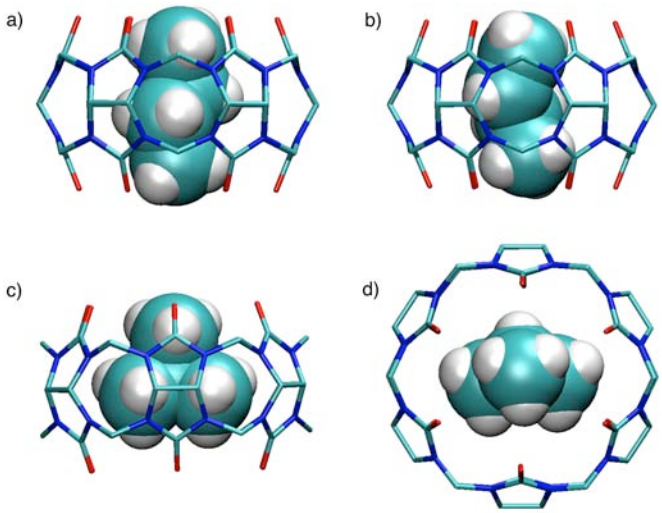


***Figure 3.*** Optimized geometries of the CB6 complexes with a) *n*-butane, b) 1-butene, c) isobutane (side view), and d) isobutane (top view) at the B3LYP/6-31G** level of theory (gas phase).

Gases, which were known to bind – although with unknown affinity – to CB5,[12] ($CH_4$, but also Ar, Kr, $N_2$, and $O_2$) did not show any detectable binding with CB6. Isobutane is bound strongest, with a binding constant approaching $10^6$ M$^{-1}$. Different hexanes and larger alkanes caused no fluorescence displacement at all, suggesting a more than 2 orders of magnitude lower affinity, which is consistent with the previously measured very low binding of a neutral cyclohexane derivative (10 M$^{-1}$).[21] As might be expected from the spherical void, CB6 preferentially includes branched and cyclic hydrocarbons (isobutane > *n*-butane and cyclopentane >> *n*-pentane), which reveals an interesting constitutional selectivity.

The size selectivity can be illustrated by considering the packing coefficients (PCs) of the different gases (Table 1).[18] As can be seen, a maximum is reached for isobutane and cyclopentane with guest volumes of 79-86 Å$^3$, corresponding to a packing coefficient of 56-

61%, in good agreement with Rebek´s "55% solution".[2,3,31] The affinity drops expectedly for smaller and larger guests, corresponding to a too loose or too tight packing. CB6 also differentiates well between saturated and unsaturated hydrocarbons: alkenes show a 4-10 times weaker binding. This drop is unlikely to be due to the minimal size variation (5-10%, Table 1), but rather to the 3-5 times higher water solubility of alkenes, which reduces the driving force for inclusion. The same trend applies for acetylene, which has not only a factor of 9 higher water solubility than ethylene, but also a more than a factor of 30 lower affinity to CB6. Stereoselective binding is also observed, as revealed by the 7 times larger binding of *cis*-butene *versus* its *trans* form, a stereochemical effect which manifests itself on the larger-molecule scale in the preferential binding of a *cis*-azobenzene with the homologous CB7.[32] The comparison of the four butene isomers is particularly intriguing. They display virtually the same water solubilities and volumes, and are consequently capable of displacing the same number of very-high-energy water molecules from the cavity of CB6.[18] Also attractive van der Waals interactions are expected to be comparable due to their comparable polarizability, which leaves the observed order (*cis*-butene > isobutene ≈ 1-butene > *trans*-butene) presently unaccounted for.

Neopentane is equally large as isopentane and 2,3-diazabicyclo[2.2.1]hept-2-ene (all 96 Å$^3$) and shows additionally an essentially perfect shape fitting. Nevertheless, only the latter two guests show sizable binding with CB6 (Table 1 and ref. [21]). The absence of binding of neopentane must consequently be due to a kinetic effect, i.e., the tight cucurbituril portals block the ingression of the most bulky guest (constrictive binding).[6,21,33] Indeed, already Mock and Shih have shown that neopentylammonium does not form inclusion complexes with CB6.[34]

Alkali cations affect the thermodynamics and kinetics of binding of guest molecules to cation-receptor macrocycles in an adverse fashion.[22,27,35,36] Nevertheless, the addition of salts is routinely applied when working with CB6 to increase solubility and enable NMR measurements.[15,21,28,35] Even though salts are not expected to interact with the inert nonpolar hydrocarbons investigated herein, they destabilize the resulting host-guest complexes. In detail, the binding constants dropped by 1-2 orders of magnitude in the presence of 50 mM $Na^+$ ions, which are known to bind to the carbonyl portals, and thereby compete with the binding of guests. Our data also reveal a guest-size dependence: The C4 and C5 hydrocarbons show the most pronounced drop in binding constant in the presence of salt. This is well in line with a steric hindrance, where the sodium ions bound to the portals interfere strongly with the binding of large guests (Figure 3), and only weakly with smaller ones such as the C2 hydrocarbons. From a conceptual viewpoint, the differential salt effects set precedent that cations do not only lead to much smaller absolute binding constants, but that they also adulterate the intrinsic selectivity of CB6. For example, in the presence of sodium, ethane, *cis*-butene, and isobutene *appear* to have the same affinity for CB6, while in its absence the true selectivity order emerges, with *cis*-butene > isobutene > ethane. The different gases do therefore not only show different absolute fluorescence responses, but also exhibit characteristic salt effects towards the fluorescent sensing ensemble. The possibility to modulate the binding constant by simple addition of salts (or other competitors for CB6 such as cadaverine) offers, on the other hand, the possibility to effectively trigger the release of an encapsulated analyte.[21,26]

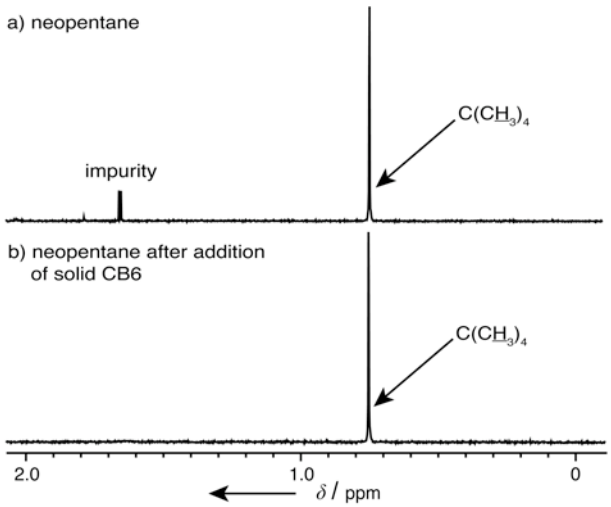


**Figure 4.** $^1$H NMR spectra of neopentane-saturated $D_2O$ before and after addition of CB6.

The apparent isotope effects for complexation of perdeuterated propane and perdeuterated isobutane with CB6 were determined by relative measurements. The resulting values ($K'_H/K'_D$, assuming identical solubilities of the isotopomers)[37] were 1.1±0.1 and 0.9±0.1 (Table 1) and are therefore negligible within experimental error. Significant deuterium isotope effects have been occasionally observed on host-guest complexation equilibria (0.98–0.58),[38] but in all previously investigated cases the binding was driven by C–H---π interactions between the aromatic guest and aromatic host, which respond sensitively, through variations of the partition function caused by changes of the C–H *versus* C–D vibrational energies, to deuterium isotope effects. The complexation of hydrocarbons by CB6 does not involve specific interactions of the C–H and C–D bonds, such that the observed absence of a sizable deuterium isotope effect can be well accounted for.

In conclusion, we have applied for the first time a fluorescent dye displacement approach to the real-time monitoring of gas binding. Volatile hydrocarbons bind very tightly and selectively to cucurbituril in water. The set of binding constants is the most extensive one so far obtained for binding of nonpolar neutral guests with a cucurbituril, and the largest one for complexation of gaseous hydrocarbons to macrocycles in general. They will serve as a benchmark, in particular since the measurements refer to aqueous solution, for the choice of force fields and solvation models in MD simulations in an effort to reproduce hydrophobic effects in supramolecular host-guest binding phenomena. The affinity data provide the thermodynamic foundation for patented claims,[20] and practical applications of the differential binding of CB6 towards different gases are indeed not far-fetched. For example, even though commercial neopentane is already highly pure (99%), it contained traces of an unknown impurity at approximately 1.66 ppm (Figure 4), which accumulated upon prolonged bubbling. Addition of solid CB6 to a $D_2O$ solution of neopentane resulted in the selective removal of the impurity. Neopentane is too large to be encapsulated and, hence, very effectively purified.

## *Experimental Section*

Gases of highest commercial purity (≥ 99%) were purchased from Air Liquide, Germany, except for *cis*- and *trans*-butene (Sigma-Aldrich, Germany), neopentane (ChemSampCo, USA), propane-$d_8$ (ISOTEC™, USA), and 2-methylpropane-$d_{10}$ (CDN Isotopes, Canada). Liquid hydrocarbons were from Sigma-Aldrich, Germany. CB6 was synthesized as reported[15,16] and an independently prepared sample

(which afforded the same results) was kindly provided by Dr. H.-J. Buschmann. Fluorescence measurements were done with a Varian Eclipse fluorometer at 25.0 ± 0.1 °C (using an external Peltier thermostat). Experiments for the sensing of gaseous hydrocarbons and noble gases were performed in a rubber-sealed long-neck quartz cuvette. The different gases were administered to the aqueous mixture containing the **1**·CB6 complex by purging with a needle. For the on-line monitoring of the uptake of volatile liquid analytes, we employed $N_2$ as carrier gas for transferring the hydrocarbon of interest through the gas phase into the aqueous solution containing the reporter pair until the solubility limit was reached. Experiments at varying gas pressures were performed by deaerating a home-built cuvette by three freeze-pump-thaw cycles and subsequently dosing different gas pressures on a vacuum manifold, as detailed in our previous gas-phase work.[39] Acetylene was also dosed in this manner (instead of bubbling) to avoid the accumulation of acetone, an ubiquitous stabilizer in acetylene samples. For those hydrocarbons, which showed no immediate effect on the fluorescence signal, the solutions were exposed for a prolonged time (several hours) to exclude the possibility of a slower guest exchange kinetics being responsible for the absence of binding.

Received: ((will be filled in by the editorial staff))
Published online on ((will be filled in by the editorial staff))

**Keywords:** supramolecular chemistry · host-guest systems • cucurbiturils · gas sensing · fluorescence · hydrocarbons

[1] L. Garel, J.-P. Dutasta, A. Collet, *Angew. Chem.* **1993**, *105*, 1249-1251; *Angew. Chem. Int. Ed.* **1993**, *32*, 1169-1171.
[2] N. Branda, R. Wyler, J. Rebek, Jr., *Science* **1994**, *263*, 1267-1268.
[3] A. Shivanyuk, A. Scarso, J. Rebek, Jr., *Chem. Commun.* **2003**, 1230-1231.
[4] C. L. D. Gibb, B. C. Gibb, *J. Am. Chem. Soc.* **2006**, *128*, 16498-16499.
[5] D. Ajami, J. Rebek, Jr., *Angew. Chem.* **2008**, *120*, 6148-6150; *Angew. Chem. Int. Ed.* **2008**, *47*, 6059-6061.
[6] D. J. Cram, M. E. Tanner, C. B. Knobler, *J. Am. Chem. Soc.* **1991**, *113*, 7717-7727.
[7] A. V. Leontiev, A. W. Saleh, D. M. Rudkevich, *Org. Lett.* **2007**, *9*, 1753-1755.
[8] D. M. Rudkevich, *Angew. Chem.* **2004**, *116*, 568-581; *Angew. Chem. Int. Ed.* **2004**, *43*, 558-571. J. Nakazawa, Y. Sakae, M. Aida, Y. Naruta, *J. Org. Chem.* **2007**, *72*, 9448-9455.
[9] a) S. Tartaggia, A. Scarso, P. Padovan, O. De Lucchi, F. Fabris, *Org. Lett.* **2009**, *11*, 3926-3929. b) J. Nakazawa, J. Hagiwara, M. Mizuki, Y. Shimazaki, F. Tani, Y. Naruta, *Angew. Chem.* **2005**, *117*, 3810-3812; *Angew. Chem. Int. Ed.* **2005**, *44*, 3744-3746.
[10] H.-J. Schneider, *Angew. Chem.* **2009**, *121*, 3982-4036; *Angew. Chem. Int. Ed.* **2009**, *48*, 3924-3977.
[11] a) J. L. Atwood, L. J. Barbour, A. Jerga, *Science* **2002**, *296*, 2367-2369. b) S. Lim, H. Kim, N. Selvapalam, K. J. Kim, S. J. Cho, G. Seo, K. Kim, *Angew. Chem.* **2008**, *120*, 3400-3403; *Angew. Chem. Int. Ed.* **2008**, *47*, 3352-3355. c) H. Kim, Y. Kim, M. Yoon, S. Lim, S. M. Park, G. Seo, K. Kim, *J. Am. Chem. Soc.* **2010**, *132*, 12200-12202.
[12] Y. Miyahara, K. Abe, T. Inazu, *Angew. Chem.* **2002**, *114*, 3146-3149; *Angew. Chem. Int. Ed.* **2002**, *41*, 3020-3023.
[13] L. Pirondini, E. Dalcanale, *Chem. Soc. Rev.* **2007**, *36*, 695-706.
[14] F. Cramer, F. M. Henglein, *Chem. Ber.* **1957**, *90*, 2572-2575.
[15] R. Behrend, E. Meyer, F. Rusche, *Justus Liebigs Ann. Chem.* **1905**, *339*, 1-37.
[16] W. A. Freeman, W. L. Mock, N. Y. Shih, *J. Am. Chem. Soc.* **1981**, *103*, 7367-7368.
[17] a) K. Kim, N. Selvapalam, D. H. Oh, *J. Incl. Phenom. Macrocycl. Chem.* **2004**, *50*, 31-36. b) N. J. Wheate, A. I. Day, R. J. Blanch, A. P. Arnold, C. Cullinane, J. G. Collins, *Chem. Commun.* **2004**, 1424-1425. c) J. Lagona, P. Mukhopadhyay, S. Chakrabarti, L. Isaacs, *Angew. Chem.* **2005**, *117*, 4922-4949; *Angew. Chem. Int. Ed.* **2005**, *44*, 4844-4870. d) M. V. Rekharsky, T. Mori, C. Yang, Y. H. Ko, N. Selvapalam, H. Kim, D. Sobransingh, A. E. Kaifer, S. Liu, L. Isaacs, W. Chen, S. Moghaddam, M. K. Gilson, K. M. Kim, Y. Inoue, *Proc. Natl. Acad. Sci. U.S.A.* **2007**, *104*, 20737-20742. e) R. Wang, L. Yuan, H. Ihmels, D. H. Macartney, *Chem. Eur. J.* **2007**, *13*, 6468-6473. f) L. Liu, N. Nouvel, O. A. Scherman, *Chem. Commun.* **2009**, 3243-3245. g) M. K. Sinha, O. Reany, G. Parvari, A. Karmakar, E. Keinan, *Chem. Eur. J.* **2010**, *16*, 9056-9067. h) A. L. Koner, C. Márquez, M. H. Dickman, W. M. Nau, *Angew. Chem.* **2011**, *123*, 567-571; *Angew. Chem. Int. Ed.* **2011**, *50*, 545-548. i) D. W. Lee, K. M. Park, M. Banerjee, S. H. Ha, T. Lee, K. Suh, S. Paul, H. Jung, J. Kim, N. Selvapalam, S. H. Ryu, K. Kim, *Nat. Chem.* **2011**, *3*, 154-159. j) Y. Chen, Y.-M. Zhang, Y. Liu, *Isr. J. Chem.* **2011**, *51*, 515-524. k) D. Das, O. A. Scherman, *Isr. J. Chem.* **2011**, *51*, 537-550. l) D. H. Macartney, *Isr. J. Chem.* **2011**, *51*, 600-615. m) L. Biczók, V. Wintgens, Z. Miskolczy, M. Megyesi, *Isr. J. Chem.* **2011**, *51*, 625-633. n) G. Parvari, O. Reany, E. Keinan, *Isr. J. Chem.* **2011**, *51*, 646-663. o) A. R. Urbach, V. Ramalingam, *Isr. J. Chem.* **2011**, *51*, 664-678. p) A. C. Bhasikuttan, H. Pal, J. Mohanty, *Chem. Commun.* **2011**, *47*, DOI: 10.1039/c1cc12091c.
[18] W. M. Nau, M. Florea, K. I. Assaf, *Isr. J. Chem.* **2011**, *51*, 559-577.
[19] a) K. A. Kellersberger, J. D. Anderson, S. M. Ward, K. E. Krakowiak, D. V. Dearden, *J. Am. Chem. Soc.* **2001**, *123*, 11316-11317. b) Even if a crystal structure of decamethyl-CB5 with methane has been previously reported (ref. 12), the corresponding solution binding constants of CB5 and decamethyl-CB5, as determined by $^1$H NMR in $D_2O$, were only on the order of $10^3$ $M^{-1}$ for methane, $10^2$ $M^{-1}$ for ethylene, and $10^1$ $M^{-1}$ for ethane (R. Dsouza, W. M. Nau, unpublished results).
[20] In CsCl solution, qualitative evidence for binding of hydrocarbons to CB6 ($^1$H NMR shifts and precipitation of complexes) has been obtained, cf. A. I. Day, A. P. Arnold, R. J. Blanch, US Patent Application Publication US 2003/0140787A1. Pub. date July 31, 2003.
[21] C. Márquez, R. R. Hudgins, W. M. Nau, *J. Am. Chem. Soc.* **2004**, *126*, 5806-5816.
[22] H.-J. Buschmann, K. Jansen, C. Meschke, E. Schollmeyer, *J. Sol. Chem.* **1998**, *27*, 135-140.
[23] a) M. El Haouaj, M. Luhmer, Y. H. Ko, K. Kim, K. Bartik, *J. Chem. Soc., Perkin Trans. 2* **2001**, 804-807. b) M. El Haouaj, Y. H. Ko, M. Luhmer, K. Kim, K. Bartik, *J. Chem. Soc., Perkin Trans. 2* **2001**, 2104-2107.
[24] B. S. Kim, Y. H. Ko, Y. Kim, H. J. Lee, N. Selvapalam, H. C. Lee, K. Kim, *Chem. Commun.* **2008**, 2756-2758.
[25] a) S. L. Wiskur, H. Ait-Haddou, J. J. Lavigne, E. V. Anslyn, *Acc. Chem. Res.* **2001**, *34*, 963-972. b) T. Zhang, E. V. Anslyn, *Org. Lett.* **2007**, *9*, 1627-1629.
[26] a) A. Praetorius, D. M. Bailey, T. Schwarzlose, W. M. Nau, *Org. Lett.* **2008**, *10*, 4089-4092. b) J. Rohacova, A. I. Lazar, W. M. Nau, unpublished results.
[27] M. V. Rekharsky, Y. H. Ko, N. Selvapalam, K. Kim, Y. Inoue, *Supramol. Chem.* **2007**, *19*, 39-46.
[28] S. Liu, C. Ruspic, P. Mukhopadhyay, S. Chakrabarti, P. Y. Zavalij, L. Isaacs, *J. Am. Chem. Soc.* **2005**, *127*, 15959-15967.
[29] Two $CO_2$ molecules have been shown to be included in a slipped-parallel fashion inside porous CB6, cf. ref. 11c, which can be rationalized with the very small molecular volume of $CO_2$ (31 Å$^3$).
[30] A. G. Grechin, H.-J. Buschmann, E. Schollmeyer, *Angew. Chem.* **2007**, *119*, 6619-6621; *Angew. Chem. Int. Ed.* **2007**, *46*, 6499-6501.
[31] a) S. Mecozzi, J. Rebek, Jr., *Chem. Eur. J.* **1998**, *4*, 1016-1022. b) B. W. Purse, J. Rebek, Jr., *Proc. Natl. Acad. Sci. U.S.A.* **2006**, *103*, 2530-2534.
[32] J. Wu, L. Isaacs, *Chem. Eur. J.* **2009**, *15*, 11675-11680.
[33] D. J. Cram, M. T. Blanda, K. Paek, C. B. Knobler, *J. Am. Chem. Soc.* **1992**, *114*, 7765-7773.
[34] a) W. L. Mock, N. Y. Shih, *J. Org. Chem.* **1983**, *48*, 3618-3619. b) W. L. Mock, N. Y. Shih, *J. Org. Chem.* **1986**, *51*, 4440-4446.
[35] a) Y. M. Jeon, J. Kim, D. Whang, K. Kim, *J. Am. Chem. Soc.* **1996**, *118*, 9790-9791. b) Y. Kim, H. Kim, Y. H. Ko, N. Selvapalam, M. V. Rekharsky, Y. Inoue, K. Kim, *Chem. Eur. J.* **2009**, *15*, 6143-6151.
[36] W. Ong, A. E. Kaifer, *J. Org. Chem.* **2004**, *69*, 1383-1385.
[37] The solubility isotope effects of the particular alkanes in aqueous solution are unknown, but knowledge of the reported value for methane ($CH_4$ has a 1.016 times higher water solubility than $CD_4$ (cf. M. F. C. Gomes, J. P. Grolier, *Phys. Chem. Chem. Phys.* **2001**, *3*, 1047-1052) suggests that such a correction would fall within the error.
[38] a) D. Wade, *Chem. Biol. Interact.* **1999**, *117*, 191-217. b) T. Felder, C. A. Schalley, *Angew. Chem.* **2003**, *115*, 2360-2363; *Angew. Chem. Int. Ed.* **2003**, *42*, 2258-2260. c) Y. L. Zhao, K. N. Houk, D. Rechavi, A. Scarso, J. Rebek, Jr., *J. Am. Chem. Soc.* **2004**, *126*, 11428-11429. d) Y. Liu, R. Warmuth, *Org. Lett.* **2007**, *9*, 2883-2886. e) T. Haino, K. Fukuta, H. Iwamoto, S. Iwata, *Chem. Eur. J.* **2009**, *15*, 13286-13290. f) J. S. Mugridge, R. G. Bergman, K. N. Raymond, *Angew. Chem.* **2010**, *122*, 3717-3719; *Angew. Chem. Int. Ed.* **2010**, *49*, 3635-3637.
[39] D. Klapstein, U. Pischel, W. M. Nau, *J. Am. Chem. Soc.* **2002**, *124*, 11349-11357.

## Gas Binding

*Mara Florea and Werner M. Nau**

_____ ***Page – Page***

**Strong Binding of Hydrocarbons to Cucurbituril Probed by Fluorescent Dye Displacement: A Supramolecular Gas-Sensing Ensemle**

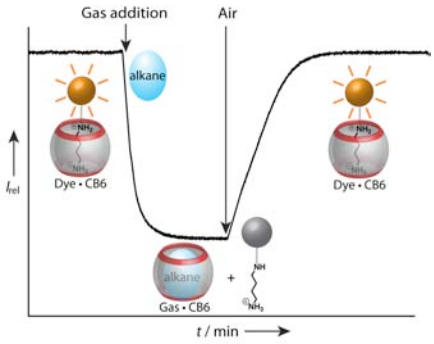


**No more hydrophobia for volatile hydrocarbons**, which can now be reversibly encapsulated by cucurbituril. Surprisingly, the pumpkin-shaped molecular container exhibits a wider array of likings as initially believed and their high affinity and selectivity towards neutral molecules have been unveiled for the first time in salt-free aqueous solution. A supramolecular sensing ensemble, composed of cucurbit[6]uril and an anchored indicator dye, is introduced as a highly sensitive fluorescence-based on-line detection tool for gas binding in solution.

# CURRICULUM VITAE

# Mara Florea

Jacobs University Bremen
Campus Ring 1
28759 Bremen, Germany
Tel: (+49) 17658862109
E-mail: m.florea@jacobs-university.de

Nationality: Romanian
Date of birth: 09/06/1984
Place of birth: Alba-Iulia, Romania

## Education

06/2008 - to date Jacobs University Bremen, Germany
PhD degree in Chemistry

07/2006 - 05/2008 Jacobs University Bremen, Germany
MSc degree in Nanomolecular Science graduate program
Master's Thesis: *"Development of Novel Fluorescent Enzyme Assays"* under the guidance of Prof. Dr. Werner Nau

08/2003 - 06/2006 Jacobs University Bremen, Germany
BSc degree in Chemistry
Bachelor's thesis entitled: *"Novel Types of Fluorescent Protease and Phosphatase Assays"* under the guidance of Prof. Dr. Werner Nau

09/1998 - 06/2003 "Elena Ghiba-Birta" National College (high school), Arad, Romania

## Practical and Research Experience

06/2008 - to date Jacobs University Bremen, Germany

Area of research:
Supramolecular, Physical-Organic, and Analytical Chemistry.

Area of expertise:
1. Use of fluorescent dyes and macrocycles as sensing systems for the detection of biologically and environmentally relevant analytes.

2. Design, development, and optimization of fluorescence-based enzyme assays.

Hands on experience with:
Steady-state and time-resolved spectrofluorometer, UV-Vis spectrophotometer, multiplate reader, $^{1}H$ and $^{13}C$ NMR spectroscopy, GC/MS.

06/2010 University of Cambridge, UK – research visit associated with the project "Strong Binding of Hydrocarbons to Cucurbiturils Probed by Fluorescent Dye Displacement"

02/2004 - 06/2008 Jacobs University Bremen, Germany - student assistant positions

- Teaching Assistant for General Organic Chemistry course and Structure Elucidation course (chemical structures are identified by analyzing spectra of several characterization techniques)
- Student job in Prof. Dr. Arnulf Materny's research group, focusing on Raman enhanced spectroscopic methods
- Worked in Prof. Dr. Thomas Nugent's laboratory for familiarization with the basic instrumentation of a synthetic organic chemistry laboratory
- Performed experiments for a project entitled "Development of Novel Heterogeneous Enantioselective Catalysts" under the guidance of Prof. Dr. Ryan Richards

06/2005 - 08/2005 Institute of Chemistry, University of Neuchâtel, Switzerland
The project I worked for was entitled "Enantioselective Oxidation with Artificial Metalloenzymes" in Prof. Thomas Ward's laboratory

## Fellowships and Distinctions

11/2011 Awarded the "A. T. Kearney scholarship" and selected for the Falling Walls – The International Conference on Future Breakthroughs in Science and Society in Berlin, Germany

10/2008 - 10/2010 PhD stipend from the Fonds der Chemischen Industrie

08/2010 Received the "Karl-Ziegler-Stiftung"/GDCh stipend, for participation in the 3rd EuCheMS Chemistry Congress in Nürnberg, Germany

06/2009 Nominated (by the Fonds der Chemischen Industrie) and selected for the 59th Meeting of Nobel Laureates dedicated to Chemistry, Lindau, Germany (Fellow of Henkel AG)

07/2006 - 05/2008 Scholarship throughout MSc studies from Jacobs University Bremen, Germany

09/2001 - 06/2003 Scholarship from "Elena Ghiba-Birta" National College for excellent academic results

## Memberships

| | |
|---|---|
| 2008 - to date | Member of the German Chemical Society (GDCh) |
| 2008 – to date | Member of the Photochemistry division of the GDCh |
| 2009 – to date | Member of the European Photochemistry Association (EPA) |

## Publications

M. Florea, S. Kudithipudi, A. Rei, M. José Gonzáles-Álvarez, A. Jeltsch, W. M. Nau, "A Fluorescence-Based Supramolecular Tandem Assay for Monitoring Lysine Methyltransferase Activity in Homogeneous Solution", *Chem. Eur. J.*, 2012, *18*, in press.

M. Florea and W. M. Nau, "Strong Binding of Hydrocarbons to Cucurbituril Probed by Fluorescent Dye Displacement: A Supramolecular Gas-Sensing Ensemble", *Angew. Chem.* 2011, *123*, 9510-9514; *Angew. Chem. Int. Ed.*, 2011, *50*, 9338-9342. (featured in ChemViews Magazine)

W. M. Nau, M. Florea, K. I. Assaf, "Deep Inside Cucurbiturils: Physical Properties, Binding Preferences, and Volumes of their Inner Cavity", *Isr. J. Chem.*, 2011, *51*, 559-577.

M. Florea and W. M. Nau, "Implementation of Anion-Receptor Macrocycles in Supramolecular Tandem Assays for Enzymes Involving Nucleotides as Substrates, Products, and Cofactors", *Org. Biomol. Chem.,* 2010, *8*, 1033-1039.

W. M. Nau, M. Florea, H. Sahoo, H. Bakirci, A. Hennig, D. M. Bailey, "Nano-TRF und Tandem Assays für HTS und Multiparameteranalytik" in: "Multiparameteranalytik – Methoden, Applikationen, Perspektiven", K. Conrad, W. Lehmann, U. Sack, U. Schedler, Eds., Pabst Verlag, Lengerich, 2008, 147-162.

H. Sahoo, A. Hennig, M. Florea, D. Roth, T. Enderle, W. M. Nau, "Single-Label Assays for Tyrosine Phosphorylation using Nanosecond Time-Resolved Fluorescence Detection", *J. Am. Chem. Soc.,* 2007, *129*, 15927-15934.

A. Hennig, M. Florea, D. Roth, T. Enderle, W. M. Nau, "Design of Peptide Substrates for Nanosecond Time-Resolved Fluorescence Assays of Proteases: 2,3-Diazabicyclo[2.2.2]oct-2-ene as a Noninvasive Fluorophore", *Anal. Biochem.*, 2007, *360*, 255-265.

Ongoing projects:

M. Florea, K. I. Assaf, D. Klapstein, W. M. Nau, "An experimental and computational investigation of the hydrophobic effect driving host-guest complexation with cucurbiturils", in preparation.

R. Sharma, M. Florea, W. M. Nau, K. Swaminathan, "An exploratory screening for inhibitors against *Mycobacterium tuberculosis* L-aspartate-$\alpha$-decarboxylase", in preparation.

## Additional Skills and Interests

Languages:

| Language | Understanding | Speaking | Reading | Writing |
|---|---|---|---|---|
| Romanian | Excellent | Excellent | Excellent | Excellent |
| English | Excellent | Excellent | Excellent | Excellent |
| French | Excellent | Excellent | Excellent | Very Good |
| German* | Good | Good | Good | Good |
| Italian | Good | Basic | Basic | |
| Spanish | Basic | Basic | Basic | |

*Level B2.2

| | |
|---|---|
| PC-Knowledge | Windows and Mac OS, MS Office, ProFit, Origin, ChemDraw, HyperChem, Adobe Photoshop, Adobe Illustrator |
| Voluntary | Animal protection, active member of the animal shelter from my home city (Arad, Romania) |
| Cultural | Interest in oriental dancing, reading, cooking |
| Community | Organization of Diwali festival and Romanian Country Information Day, Floor Representative (Jacobs University Bremen) |
| Sports | Fitness, Spinning, Bowling, Swimming |